12-2008

The development of hyaluronic acid biomaterials for vascular tissue engineering

Samir Ibrahim
Clemson University, ibrahim@clemson.edu

THE DEVELOPMENT OF HYALURONIC ACID BIOMATERIALS FOR VASCULAR TISSUE ENGINEERING

A Dissertation
Presented to
the Graduate School of
Clemson University

In Partial Fulfillment
of the Requirements for the Degree
Doctor of Philosophy
Bioengineering

---

by
Samir Ibrahim
December 2008

Accepted by:
Anand Ramamurthi, PhD, Committee Chair
Craig Beeson, PhD
Martine LaBerge, PhD
Bryan Toole, PhD

ABSTRACT

Current vascular implant materials poorly interact with smooth muscle cells (SMCs) of the media allowing the permanent loss of vascular elastin, eliminated by trauma or disease, a crucial element in maintaining the natural biomechanics of the blood vessel and overall vascular homeostasis. In addition, these materials insufficiently recruit vascular endothelial cells (ECs) to form a normally functional, confluent endothelium that acts as the interface between the blood and vascular tissue and regulates numerous vital vascular processes. As a result, the restenosis, or re-occlusion, rate within these devices has remained fairly high stimulating the investigation of numerous new materials capable of providing the necessary stimuli for the regeneration of vascular tissue. Our lab has reported extensively on hyaluronic acid (HA) as a vascular regenerative agent. We found it beneficially impact two key aspects of vascular regeneration, namely functional endothelialization and elastin matrix repair/ regeneration, and that the biologic impact is dependant on HA molecular weight. This project was initiated to investigate the size-specific ability of exogenous HA to promote endothelialization, and then attempted to utilize this, and previously acquired information on the HA-dependant upregulation of elastogenesis of vascular SMCs, for the development of HA biomaterials, in the form of surface coatings and hydrogels, for vascular tissue engineering.

Exogenous supplementation of a HA digest (D2) containing a concentrated mixture of HA oligomers (0.75–10 kDa) promoted EC proliferation and tube formation, but also enhanced platelet attachment, CAM expression, and cytokine release.

Conversely, the exogenous addition of HMW HA (HA 1500) inhibited platelet deposition on cultured ECs and limited their CAM expression and cytokine release. Upon immobilization onto a substrate through derivatization of HA without crosslinking, ECs were able to attach on D2, however HA 1500 deterred attachment. As observed with exogenous D2, ECs were able to proliferate on D2 substrates similar to cultures on fibronectin but also elicited CAM expression. Another HA digest (D1) containing a broad mixture of HA oligomers, previously shown to promote elastogenesis of vascular SMCs as an exogenous supplement, was also immobilized and stimulated SMCs to upregulate synthesis of soluble tropoelastin, and crosslinked matrix elastin similar to the levels previously observed with exogenous D1. These surfaces also enhanced elastin organization into fibrils and desmosine crosslinking to a greater degree than exogenous D1. These HA digests (D2, D1) were then separately embedded within divinyl sulfone (DVS) and glycidyl methacrylate (GM) crosslinked HA 1500 hydrogels (DVS-HA, GM-HA), respectively, and we found the mechanical and physical properties of these hydrogels can be modulated by varying the crosslinker and oligomer concentration within them. However, the mechanical properties of these gels were too weak to act as standalone vascular scaffolding biomaterials and, therefore, must be used as composite structures. DVS-HA gels were somewhat cytotoxic stimulating an inflammatory reaction *in vivo* and EC CAM expression *in vitro*. Yet, the highest amount of EC attachment and proliferation was observed on DVS-HA that contained the highest amount of D2. SMCs survived encapsulation into the more biocompatible GM-HA gels and D1 incorporation elevated elastin levels to 2× the amount within GM-HA without D1.

Overall, we showed that HA oligomers are useful to incorporate within vascular biomaterial scaffold, either as surface-immobilized coatings or as hydrogels to promote endothelialization and elastic tissue regeneration. Our studies also indicate that incorporation of HMW HA is also necessary to temper adverse cell responses to HA oligomers (e.g., CAM expression) and provide mechanical stability/ ease of handling to the gels.

ACKNOWLEDGEMENTS

Successfully accomplishing the wide scope of this project and mastering the many techniques it demanded, would not have been possible without the help of many people. First and foremost, I would like to express extreme gratitude to my advisor Dr Anand Ramamurthi for introducing me to the field of bioengineering, guiding me through the initial twists and turns of my project and finally allowing me to pursue my own interests within it. His ambition as a professor and compassion as a mentor will forever be remembered. I would also like to thank my committee members – Dr Craig Beeson, Dr Martine LaBerge, Dr Brian Toole – for their advice and support at all stages of this work. I especially appreciate their flexibility in accommodating the many meetings required by the PhD process, despite their busy schedules.

I would also like to thank the members of CTEL, especially Binata Joddar for initiating an elastin aspect to my work, Chandra Kothapali for his insight on mechanical testing techniques and mathematical modeling, and Erin Pardue for her expertise on confocal imaging. I also want to show appreciation to the other members of the CU-MUSC Bioengineering program that contributed to this work: Jonathan Kuo, of the Yao lab, for the rheology and DMA analysis; Yong Qiu, of the Wen lab, for the FTIR analysis; and Dr Qian Kang, of the Orthopedic Research lab, for performing the surgery in our animal studies. Joan Hudson of the Clemson University Electron Micoscopy facility was instrumental in our studies involving SEM and XPS. Matthew Craps, of the

Rao lab at Clemson, performed the AFM work and Richard Peppler, of the MUSC flow cytometry facility, provided us with data on EC CAM expression.

Last but not least, I would like to thank my family who have provided me with opportunities throughout my life and supported me at all levels of my education.

TABLE OF CONTENTS

Page

Table of Contents (Continued)

Page

Table of Contents (Continued)

Page

Table of Contents (Continued)

Page

Table of Contents (Continued)

Page

Table of Contents (Continued)

Page

LIST OF FIGURES

List of Figures (continued)

List of Figures (continued)

List of Figures (continued)

List of Figures (continued)

LIST OF TABLES

CHAPTER 1

INTRODUCTION

1.1 Engineering Vascular Regenerative Biomaterials

With increasing insight into the structural and functional characteristics of living organs, researchers have begun to investigate the possibility of designing and regenerating tissues, resulting in the development of tissue engineering, a field which focuses on the replacement of tissues damaged by disease and trauma. Broadly, tissue engineering may be defined as '*the use of a combination of cells, engineering materials or scaffolds, and suitable biochemical factors to improve or replace biological functions in an effort to effect the advancement of medicine*' [1] Tissue engineering technologies have the potential to regenerate nearly limitless organs and tissues, and treat a wide variety of injuries and diseases. However, to date, the successful development of tissue engineering products has been limited to relatively simple and actively regenerating tissues, such as skin; the more complex and static tissues of the vascular system, are far more difficult to regenerate and current tissue engineering techniques have shown limited success in creating replacements for such tissues. Therefore, the current strategy is to focus on regenerating specific components of the blood vessel.

An outstanding problem addressed by this study is the insufficiency of conventional vascular biomaterials to stimulate the regeneration of the luminal endothelial cell (EC) monolayer and medial elastin matrix of blood vessels. Vascular ECs are one of the most complex and sensitive components of the blood vessel in terms of

physical structure, cell signaling, and physiologic function. They serve as a semi-permeable barrier between the two vascular compartments, namely blood and vascular connective tissue, controlling the transfer of cellular and non-cellular (e.g., growth factors, proteins, cytokines) components between the compartments and thereby influencing effective vascular function. Under healthy, non-activated, conditions ECs regulate numerous processes that maintain vascular homeostasis but if diseased or physiologically injured, they initiate restorative signaling pathways that can be exaggerated and lead to further tissue impairment, if prolonged. Moreover the ECs also actively regulate smooth muscle cells (SMCs) within the underlying medial layer of the vessel wall by release of signaling biomolecules such as nitric oxide (NO) and prostacyclin [2]. While SMCs are responsible for vasoregulation, they also generate structural matrix proteins (e.g. collagen, elastin) within the media, which contributes to the structural integrity of the blood vessel. The vascular extracellular matrix (ECM) is composed primarily of collagen and elastin, which affect the mechanical behavior of blood vessels in different ways. The initial strain applied to blood vessels due to blood flow is accommodated by elastin allowing the vessel to expand with minimal resistance. Continued expansion and increased strain is eventually strongly resisted by collagen preventing overexpansion and rupture. While collagen provides rigidity, elastin allows the connective tissues in blood vessels to stretch and then recoil to their original positions [3]. Vascular SMCs routinely produce collagen throughout adulthood but their capacity for synthesizing elastin vastly decreases. In addition to blood vessel mechanics, elastin is crucial to regulating cell-signaling pathways [4-7] involved in injury response, and inflammation [8]. In light of the vital

physiologic significance of these two vascular cell types and their surrounding ECM, their injury by chemical agitation, physical trauma, or infections (e.g. bacterial, viral) can initiate and progressively lead to the pathology of life threatening complications such as atherosclerosis, aneurysm and vasospasms [9,10]. Therefore, the regeneration of these two components of blood vessels is vital to the viability of a vascular implant material for the treatment of vascular disease.

1.2 Clinical Problem and Significance

In the United States, cardiovascular disease (CVD) accounts for more annual fatalities than any other disease [2], and incurs the national health care system over $448.5 billion per year as costs for its treatment and management [11]. Atherosclerosis, or occlusive plaque development within the vessel wall resulting in gradual vessel narrowing and loss of patency, is the predominant manifestation of CVD. When severely occluded, vessel segments are routinely bypassed with conduits of natural or synthetic origin [12]. While autologous tissues (e.g., autologous saphenous veins), the current gold standard, remain patent in the long-term, they are often unavailable due to prior harvesting, or chronic systemic disease [13]. In such cases, vascular grafts fabricated from synthetic materials (e.g., Dacron; expanded-polytetrofluoroethylene or ePTFE) are implanted instead. While synthetic materials remain mostly patent (93% for Dacron and 95% for ePTFE at 5 years) when integrated into large (> 6 mm diameter) vessels, they are not as effective in smaller vessels due to the inherent pre-disposition of such sized vessels to re-occlude (43% and 45% patency, respectively) [14-16]. The details of this reocclusion

process is still poorly understood, however scientists agree it is a direct result of the failure of the graft lumens to re-endothelialize completely with functional ECs, the exaggerated response of healthy patient cells to the graft material, and a compliance mismatch between the non-elastic graft and the viscoelastic blood vessel wall. Therefore, new tools (e.g. biomolecular cues, biomaterial scaffolds) must be developed to modulate cell responses to ensure faithful functional vascular tissue regeneration and ensure long-term patency when used as small diameter vessel replacements.

1.3 Project Rationale and Objectives

To overcome the poor vascular response to synthetic materials, recent studies have developed "natural or tissue-based" materials that could likely evoke more regenerative/ healing responses by the blood vessel. The extracellular matrix (ECM), once regarded simply as a structural scaffold, is now recognized as an important modulator of cell phenotype and function. From the tissue engineering perspective, it is increasingly apparent that ECM molecules provide the necessary biomechanical and biochemical stimulation of cells to create an environment similar to native tissues. A class of ECM molecules that are increasingly studied in the context of regenerative materials are glycosaminoglycans (GAGs). One such GAG, hyaluronic acid (HA), occurs naturally in connective tissues (e.g. skin) as a simple linear molecule consisting of repeating dissacharide units of N-acetyl-D-glucosamine and D-glucuronic acid [17]. Most cells have the ability to synthesize HA at some point during their cell cycle, implicating its function in several fundamental biological processes [18].

In recent years, HA has been recognized as a potential biomaterial for effective tissue regeneration. It is now known that HA, when degraded into small fragment sizes, plays a role in wound healing by promoting angiogenesis [19]. HA fragments can, under specific circumstances, also promote early inflammation, which is critical to initiate wound healing, and then modulate later stages of the process, allowing for matrix stabilization and reduction of long term inflammation [18]. HA is also highly biocompatible and does not elicit a foreign-body response upon cross-transplantation due to the homology of the HA structure across species [18]. Although the mechanism of interaction between HA and the human body is still incompletely elucidated, its promising characteristics have assured its extensive use as a tissue engineering biomaterial, most recently for cartilage [20] and skin repair [21]. Our lab is currently investigating the potential use of HA as a regenerative vascular implant material. Since HA forms a significant (4-7% w/w) component of vascular ECM [22], we hypothesize that HA modified biomaterials will provide healthy biomechanical and biochemical signals to blood vessels.

HA has been shown to exhibit a size-specificity in modulating EC proliferation, essential to repopulating the luminal EC monolayer, and SMC elastin production. Exogenous HA oligomers (<20 kDa) have been shown to stimulate angiogenesis [23,24] and proliferation [23] of vascular ECs, while high molecular weight (HMW) HA (MW > 1000 kDa) is generally bioinert [25]. Recent studies have shown HA oligomers upregulate the activity of the EC receptor for vascular endothelial cell growth factor (VEGF) and induce VEGF release to stimulate EC proliferation and promote tube formation [26]. In the context of influencing SMC behavior, independent studies have suggested critical roles

for HA and other GAGs in elastin matrix synthesis and organization by SMCs during development [27-29] and particular disease pathologies [30]. Our laboratory, for the first time, has shown certain sized HA oligomers to stimulate inherently poor elastogenic adult SMCs to produce elastin matrix structures vital to maintenance of tissue homeostasis. We found that healthy SMCs, in the presence of exogenously supplemented HA oligomers, increased production of tropoelastin, desmosine and crosslinked elastin [31,32]. In addition, the elastin fibers were laterally aggregated and thicker than those produced by SMCs cultured with HA of higher MW. Overall, these findings encourage the utility of exogenous HA cues and HA biomaterials to promote vascular endothelialization and elastogenesis. To date, the size-specific effects of HA on EC phenotype and long-term function, and the use of HA oligomers as biomaterials for enabling EC and SMC mediated vascular tissue regeneration/ remodeling have not been thoroughly investigated. Also, the effects of HA derivatization and/or crosslinking, necessary to obtain HA scaffolds with good handling properties, and the densities at which bioactive HA fragments should be presented within such scaffolds are unknown. Such information would also be vital in designing strategies to incorporate/ present these HA cues within existing synthetic or biologic scaffolding materials which may be more appropriate from a mechanical standpoint. We hope of fill this void.

Our objective is to investigate the potential use of HA as a regenerative vascular material. Specifically, we aim to examine the size-specific ability of HA to promote vascular endothelialization and elastogenesis, as an exogenous supplement, a surface coating and a hydrogel. The results of this study will allow us to determine the optimal

fragment size (i.e. HMWHA, HA fragments, HA oligomers) and presentation modality (i.e. exogenous, surface coating, hydrogel) of HA for the regeneration of the vascular endothelium and production of an elastin rich matrix by SMCs. To investigate these issues, we propose four **specific aims**:

1.4 Specific Aims and Hypotheses

Aim 1: Investigate the impact of exogenously supplemented HMW HA, HA fragments, and HA oligomers on the phenotype and function of vascular ECs.

Hypothesis: It is now known that HA, when degraded into small fragment sizes, plays a vital role in wound healing by promoting angiogenesis [19]. In this regard, the exogenous supplementation of HA fragments and oligomers are more likely to stimulate EC proliferation and migration than HMW HA. However, under specific circumstances, these fragments may also incite early inflammation. Therefore, HA fragments and oligomers may also adversely affect ECs by inciting CAM expression and the release of cytokine/ chemokines resulting in enhanced platelet deposition.

Approach: To generate HA oligomers, HMW HA (1500 kDa) will be enzymatically digested under iteratively defined conditions, until a mixture containing a maximal yield of HA oligomers is obtained. Initially, an EC proliferation study will be conducted by exogenous supplementation of HA oligomer digests, and commercially available HMW HA and HA fragments (200 kDa, 20 KDa) to determine the most angiogenic fragment size of HA. Then the effects of HMW HA and this angiogenic HA fragment on ECs will be compared by investigating angiogenesis potential, CAM and functionality marker

expression, cytokine release, thrombomodulin expression, and platelet deposition. From this study we will determine the HA fragment capable of stimulating endothelialization and identify its potential adverse effects, if any, on ECs.

Aim 2: Prepare a surface tethered model for investigating the size specific effects of HMW HA, HA fragments, and HA oligomers on EC functionality and SMC elastin production.

Hypothesis: The biologically active group of HA (acetyl) is not used in the immobilization process. Therefore, surface tethered HA should function in the same manner as exogenously supplemented HA. However, the high negative charge of long-chain HA due to the abundance hydroxyl and carboxyl groups will deter cellular attachment to its surface. This may only allow cell adherence to surfaces composed on HA fragments and oligomers.

Approach: HA (1500 kDa, 200 kDa, 20 kDa) and oligomer mixtures (based on digests prepared in Aim 1) will be tethered onto an aminosilane (APTMS)-treated glass surfaces using a carbodiimide reaction. Immunofluorescence, SEM, AFM and XPS analysis will be used to determine the success of our immobilization technique by comparing the glass, APTMS and HA surfaces. The density of APTMS and HA will also be quantified using an amine s-SDTB assay and HA Fluorophore-Assisted Carbohydrate Electrophoresis (FACE), respectively. The stability of surface-bound HA over 21 days will be analyzed with toluidine blue. ECs and SMCs will then be cultured on these surfaces. The endothelialization potential of the surface will be based on EC morphology (Calcein AM

uptake), proliferation (MTT assay) and CAM expression (Immunofluorescence). Elastin production of SMC will be determined by an elastin assay (quantification), immunofluorescence (macro-structure), and TEM (micro-structure). From this study we will determine whether HA surfaces stimulate ECs and SMCs similarly to exogenous HA and identify surface bound HA fragments that benefit functional endothelialization and elastogenesis.

Aim 3: Investigate the impact DVS crosslinked HMW HA hydrogels containing varying concentrations (w/w) of crosslinker and bioactive HA fragments on its physical, biologic and mechanical properties and utility for achieving functional endothelialization.

Hypotheses: The incorporation of HA fragments into a HMW HA hydrogel reduces the overall bonding within the construct. Therefore, the presence of HA fragments diminishes the strength of the hydrogel and its resistance to enzymatic degradation. However, HA fragments potentially stimulate EC proliferation resulting in a surface more conducible to endothelialization. HA fragments also have the potential to elicit inflammatory CAM expression by vascular ECs but when incorporated within a bioinert HMW construct, these effects might be suppressed. Also, the use of a crosslinker may alter HA's interaction with ECs. However, we aim to use a low concentration of DVS to minimize its affect.

Approach: HMW HA and bioactive fragments (aim 1; 0, 5, 10, 20% w/w) will be incorporated into a crosslinked construct using two concentrations of DVS (1:1, 2:1 w/w HA:DVS) and the formation of crosslinks verified by FTIR. The mechanical properties of

these hydrogels will be determined by frequency sweep rheology, uniaxial compression testing, and swelling ratio. The stability of the gels will be analyzed by *in vitro* and *in vivo* degradation, and the gels will be subcutaneously implanted in a rat model to test their biocompatibility. Finally, ECs will be culture on the surface of these gels and their morphology, proliferation and CAM expression will be tested. In the event that the high concentration of HMW HA deters cell attachment, the gels will be soaked in a matrigel solution of low concentration to adsorb a minimum amount of laminin and collagen IV on the surface of the gels prior to seeding the ECs. This will force the ECs to interact with the HMW HA and bioactive fragments. The results will determine the endothelialization potential of bioactive fragments with a HMW HA construct and allow us to compare these results to pure HA surfaces and exogenously supplemented HA.

Aim 4: Investigate the impact GM crosslinked HMW HA hydrogels containing varying concentrations of HA oligomers on its physical, biologic, and mechanical properties and use as a 3D elastogenic scaffold for SMCs.

Hypotheses: The incorporation of bioactive HA fragments into a HMW HA hydrogel will reduce its strength and resistance to enzymatic degradation by lowering the overall bonding within the construct. However, HA fragments are capable of stimulating SMCs to produce elastin when supplemented exogenously and this should be replicated when the HA oligomers reside within a 3D scaffold. Also, the use of a crosslinker may alter HA's interaction with SMCs but we aim to use a low concentration of GM to minimize its affect.

Approach: Prior to crosslinking, HMW HA and oligomers will be modified with glycidyl methacrylate (GM). Then GM modified HMW HA and HA oligomers (aim 1; 0, 5, 10, 20% w/w) will be combined and treated with UV to form crosslinks; the presence of which will be verified by FTIR. The mechanical properties of these hydrogels will be determined by frequency sweep rheology, uniaxial compression testing, and swelling ratio. The stability of the gels will be analyzed by *in vitro* and *in vivo* enzymatic degradation, and the gels will be subcutaneously implanted in a rat model to test their biocompatibility. Finally, SMCs will be encapsulated within these gels and their morphology (calcein AM) and elastin production (immunolabelling) will be tested. In the event that the high concentration of HMW HA deters cell attachment, matrigel (laminin, collagen IV) will be added into the hydrogel construct prior to crosslinking. This will result in a 3D network of cell adhesion molecules (matrigel) and HA forcing the SMCs to interact with the HMW HA and HA oligomers. The results will determine the SMC elastogenic potential of HA oligomers within a 3D HMW HA construct and allow us to compare these results to pure HA surfaces and exogenously supplemented HA.

1.5 Organization of Dissertation

This dissertation was arranged into seven chapters to most effectively convey the scope, analytical progression, eventual conclusions of this project. Chapter two introduces luminal ECs and medial matrix elastin as essential components of the vasculature and also presents a comprehensive review vascular disease, the deficiencies of the current treatment options including vascular grafting materials, current tissue

engineering strategies under development, and the attractive properties of HA that make it a suitable biomaterial for the regeneration of ECs and vascular elastin when lost due to disease or injury. Chapter three examines the effects of exogenous HA and HA fragments on EC phenotype and functionality. The surface immobilization of different sized HA and their ability to provide a microenvironment conducive to ECs growth and SMC elastogenesis are presented in chapter four. Chapter five is devoted to discussion of divinyl sulfone (DVS) crosslinked HA hydrogels and the effects of crosslinker and HA bioactive fragment concentration on EC function. Chapter six includes an analysis of the incorporation of HA bioactive fragments into glycidyl methacrylate (GM) crosslinked HMW HA hydrogels and its ability to stimulate elastin production by encapsulated SMCs. Finally, chapter seven will draw overall conclusions from all the studies conducted, identify inadequacies of the present work, and suggest future directions for the continued progress of this project.

CHAPTER 2

LITERATURE REVIEW

2.1 Vascular Structure and Function

Blood vessels contain three layers, each one containing a complex bundle of cells and *extracellular matrix* (ECM) distinctly organized to serve specific functions. In addition, many different types of blood vessels exist in the body and the structural components of each are adjusted to efficiently distribute nutrients and collect waste from the tissues via the blood.

2.1.1 Components of the Blood Vessel and Their Function

Vascular walls consist of three layers, the *tunica intima*, *tunica media* and *tunica adventitia*, as displayed in Figure 2.1. The *tunica intima* is comprised of endothelial cells (ECs) resting on a basement membrane, a meshwork comprised of ECM components, mainly collagen type IV, laminin and heparin sulfate proteoglycans, and an *internal elastic lamina* (IEL) composed of elastin sheets and fibers. The ECs form a continuous single layer boundary along the lumen and act as a barrier that regulates the coagulation of plasma proteins on its surface and the entry of blood elements into the vessel wall. The tissue between the EC layer and the IEL, or sub-*intima*, may house non-striated smooth muscle cells (SMCs) and macrophages [33].

The *tunica media* extends from the IEL to the *external elastic lamina* (EEL). It consists of SMCs and elastin arranged into concentric alternating bundles. The SMCs

regulate blood flow by constricting and dilating the blood vessel. By contracting, the SMCs collectively decrease the diameter of the blood vessel inhibiting blood flow (vasoconstriction). In contrast, SMC relaxation increases blood flow by enlarging the diameter of the blood vessel (vasodilatation) [33].

The *tunica adventitia* lies beyond the EEL as the outer most layer of blood vessels and is predominantly composed of fibroblasts and collagen-rich ECM [34]. This densely fibrous layer prevents vessel over-expansion and rupture due to luminal blood pressure, and anchors the blood vessel to the surrounding tissue. The thickness of each layer is dependant on the type of blood vessel [33].

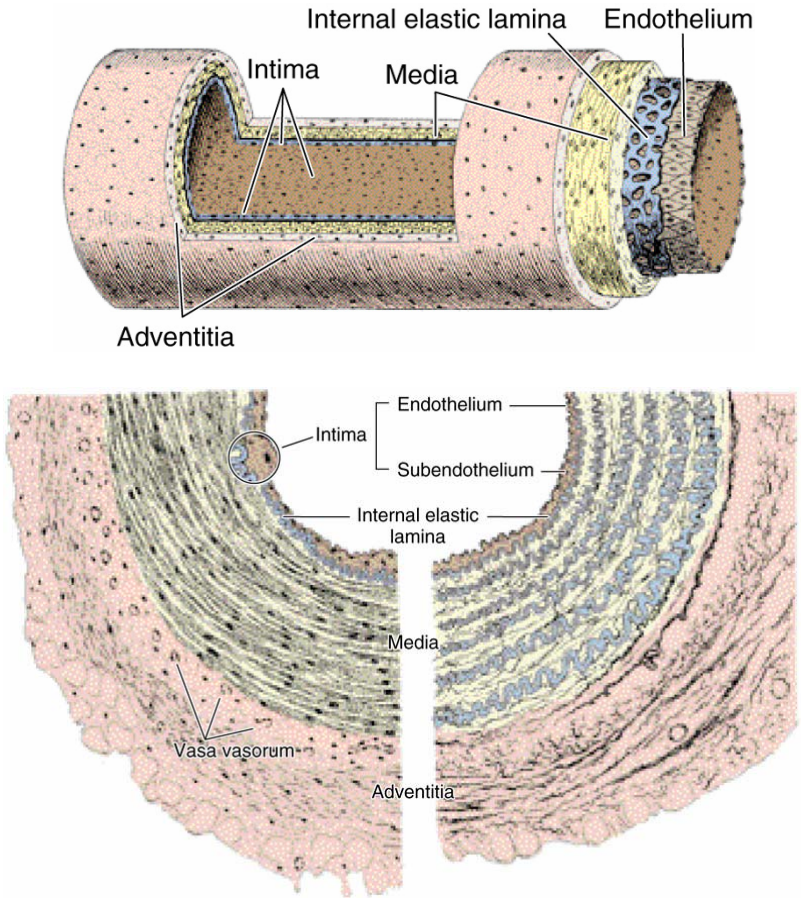

Figure 2.1 Anatomy of blood vessels [35].

2.1.2 Types of Blood Vessels

Blood leaving the heart is distributed to the tissue by the conducting arteries, distributing arteries, arterioles and finally capillaries. The conducting arteries (elastic arteries) contain a large amount of elastin, allowing them to expand and accommodate large volumes of blood flow. Distributing arteries (muscular arteries) are comprised of large numbers of medial SMCs that help control the amount of distributed blood by contracting or relaxing in response to sympathetic nerve stimulation. Arterioles have thin wall layers and regulate blood flow to specific capillary beds by the contraction and relaxation of SMCs. They are controlled by both nerve and hormonal stimulation. Capillaries possess very thin walls that provide permeability and allow the diffusion of nutrients, gases, hormones, etc. into the tissues. The blood within the capillaries also collects metabolic waste products and gases from adjacent cells [34]. The relative characteristics of these vessels are shown in Figure 2.2.

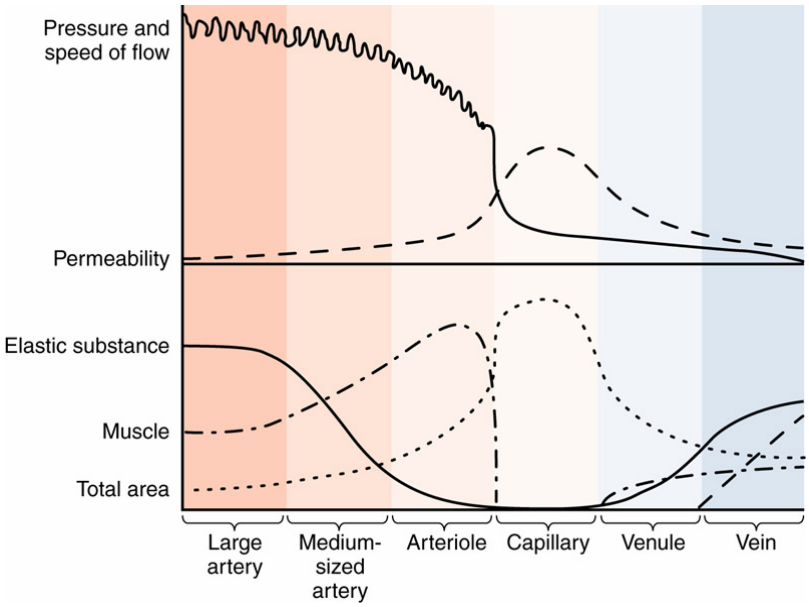

Figure 2.2 Characteristics of blood vessels [35].

Blood returns to the heart through the venules, medium veins and finally, the large veins. The venous wall is thinner than the arterial wall. The prominent layer in veins is the adventitia. Veins are much less muscular than arteries due to the lower blood pressures encountered within. For the same reason larger veins have valves that prevent backflow of blood, especially when propelled against gravity. Due to the greater pressures and hence stresses encountered in arteries then in veins, the former are more susceptible to injury or disease and even more so due to aberrations in the function of vascular SMCs that play key roles in the biochemical and biomechanical homeostasis of the vessel wall [34].

2.2 Vascular Disease: Atherosclerosis

Cardiovascular disease, an extremely prevalent disorder in the United States, is frequently characterized by the development of atherosclerotic plaques. The initiation of atherosclerosis is still debatable since the theories procured through the study of developmental animal models and advanced human atherosclerotic tissue do not coincide. But the most popular theory involves the development of a fatty streak and its transformation into a fibrous plaque.

2.2.1 Cardiovascular Disease

Cardiovascular disease (CVD) accounts for more deaths than any other disease in the United States [2]. As per the 2008 estimates of the American Heart Association, the US health care system will incur over $448.5 billion in costs for treatment and management

of CVD [11]. Research is working toward reducing this cost and saving lives by treating atherosclerosis, the causative factor in nearly three-fourths of the fatalities from cardiovascular disease [36]. Atherosclerosis, an occlusive vascular disease, is characterized by the accumulation of low density lipoprotein (LDL) cholesterol, cell debris, calcium, and extra cellular matrix to form a plaque within the vessel wall, narrowing the lumen cross-sectional area and inhibiting blood flow.

Atherosclerosis is likely triggered by damage to the endothelium. In an effort to develop therapies to limit destructive effects of the disease, physicians have identified several risk factors that can adversely impact endothelial health and viability through physical and chemical attacks. These factors include vessel morphology, hypertension, hyperlipidemia, diabetes mellitus, and free radicals caused by cigarette smoking [37]. Endothelial dysfunction as a result of aging is an additional risk factor for atherosclerosis [38-40]. The early but reversible sign of atherosclerosis is the development of fatty streaks along the lumenal wall of blood vessels.

2.2.2 Development of a Fatty Streak

Atherosclerosis has been suggested to be initiated by an increase in the content of low-density lipoprotein (LDL) or bad cholesterol in the blood. LDLs gradually deposit in the vascular wall, especially at low flow sites within the arteries, and accumulate to create an initial lesion. The amassed LDLs within the lesion may undergo modifications, including slight oxidation by exposure to oxidative vascular waste. The endothelium responds to these minimally oxidized LDLs by attracting monocytes and T-lymphocytes

with chemotactic proteins and adhesion molecules, known as vascular cell adhesion molecule-1 (VCAM-1) and intercellular adhesion molecule-1 (ICAM-1). The monocytes and T-lymphocytes migrate between the tight junctions of the ECs into the intima where the monocytes differentiate into macrophages and consume the minimally oxidized LDL, forming foam cells [41]. The accumulation of foam cells within the sub-*intima* results in the formation of fatty streaks, which appear as yellow strips along the vascular wall. These fatty streaks appear in children as young as 10 – 14 years old and are completely reversible by reducing or eliminating the LDL content within the blood.

2.2.3 Development of a Fibrous Plaque

The continued accumulation of LDL within the sub-*intima* eventually triggers ECs, foam cells, and T-lymphocytes to produce pro-inflammatory growth factors, such as platelet derived growth factor (PDGF), basic fibroblast growth factor (bFGF), transforming growth factor α (TGF-α), transforming growth factor β (TGF-β) and endothelial growth factor (EGF), resulting in exuberant intimal SMC proliferation and the migration of medial SMCs towards the *intima*, seen in Figure 2.3, a phenomenon termed *hyperplasia*. Hyperplasic SMCs, which now exhibit an unnatural synthetic phenotype, produce a hefty matrix comprised of collagen, elastin and proteoglycans. Extracellular lipids and debris accumulate as the foam cells die and release oxidized LDL and cellular structures into the subendothelium. The accumulation of all these products within the *intima* results in the formation of an uncomplicated fibrous plaque which has the potential to transform to a complicated fibrous plaque and become life threatening, as

shown in Figure 2.4 [42].

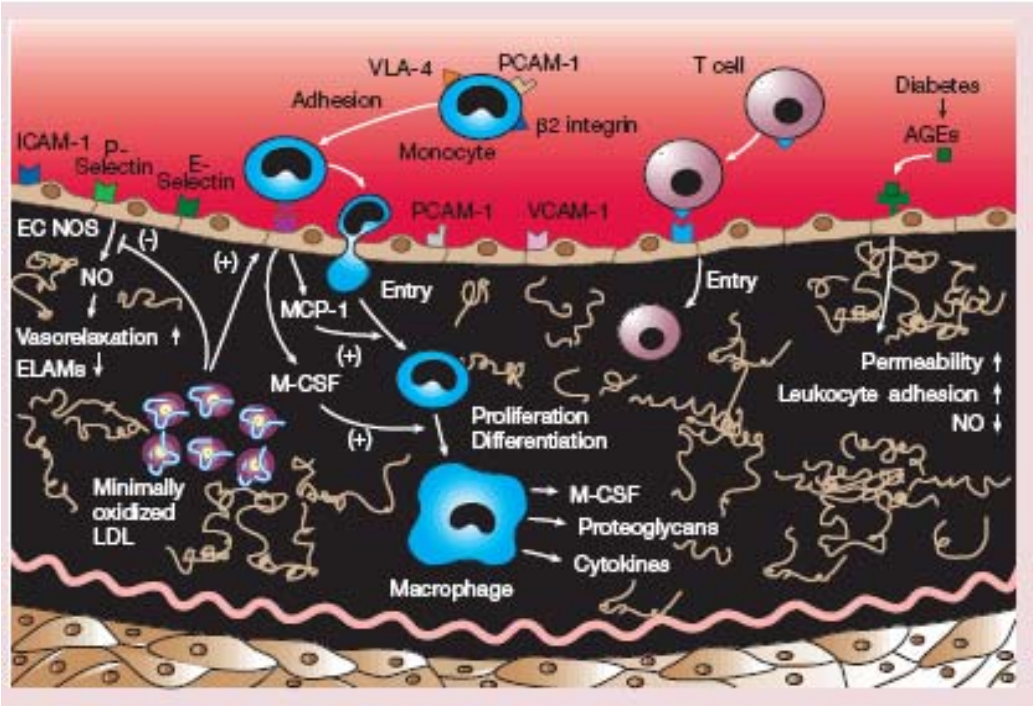

Figure 2.3 Cascade of events during atherosclerosis [43].

2.2.4 Complicated Fibrous Plaques

Complicated fibrous plaques are generated through two mechanisms, fibrous plaque calcification and thrombus/ emboli production. The deposition of calcium phosphate from the blood results in calcification of the fibrous plaque and degradation of the vascular elastic matrix causing reduced vascular elasticity. These brittle segments are prone to rupture, possibly resulting in an aneurysm.

Plaques enclosed by a thin fibrous cap are considered vulnerable and at risk for rupture, which commonly occurs at the edges of the plaque, a foam cell rich region [43].

The growing fibrous plaque may occlude the blood vessel or cause the EC layer to denude resulting in platelet adherence to the exposed subendothelial matrix. These platelets release PDGF, TGF-α, TGF-β, EGF and platelet-derived EC growth factor (PD-ECGF) to further stimulate SMC proliferation and migration. If a sufficient number of platelets deposit, a thrombus or embolus may form, which can occlude blood flow [42]. The blockage of coronary arteries, peripheral arteries and cerebrovascular arteries can result in myocardial infarction (heart attack), peripheral tissue necrosis and a stroke, respectively. These are very serious and potentially fatal complications that can be prevented through clinical treatment.

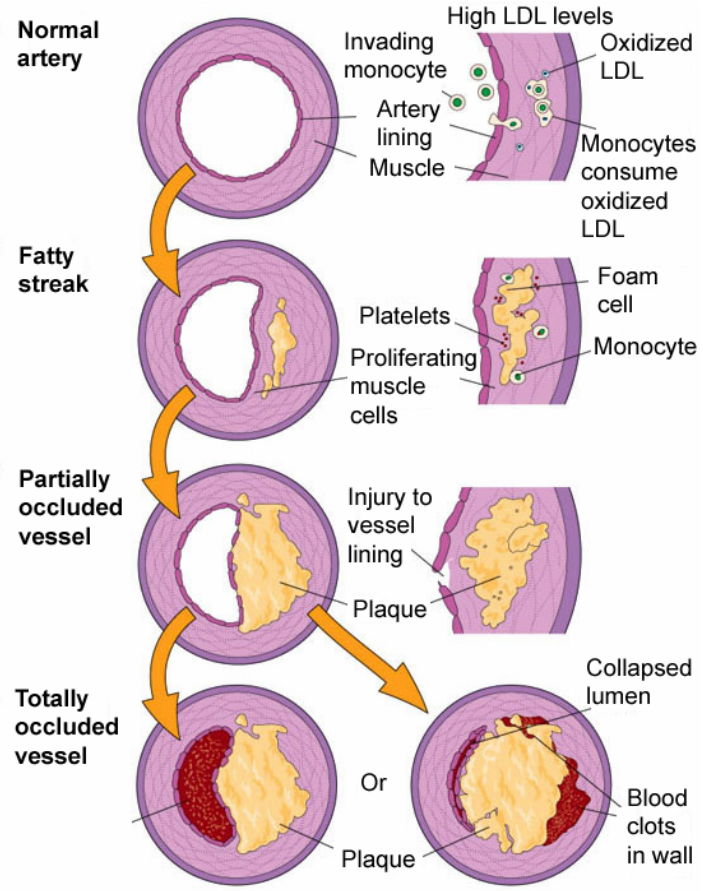

Figure 2.4 Etiology of atherosclerotic plaque development [44].

2.3 Treatment of Atherosclerosis

To determine the mode of vascular treatment a patient requires, a physician must compare the risk of occlusion and amount/ type of tissue the occlusion would affect. If the diseased blood vessels exhibit a low risk of occlusion and the affected tissue is insignificant, noninvasive treatment is pursued. Surgical treatment is necessary when the vessel has a high risk of occlusion and a large portion of a vital organ is in danger. In most other situations, minimally invasive treatment is used.

2.3.1 Non-Invasive Treatment Modalities

Treatment of atherosclerosis can begin before manifestation of the symptoms, usually through lifestyle management to restrict risk factors and behaviors. These include cessation of smoking, diet alterations, exercise enhancement, and drug therapies (e.g. to decrease serum cholesterol levels, or control hypertension). When atherosclerosis progresses to a state wherein significant occlusion of the vessels is caused, physicians must use more invasive treatments to correct these complications.

2.3.2 Surgical Treatment

Currently, the prevalent surgical method for treating vascular occlusions is bypass surgery, shown in Figure 2.5. During this procedure, the patient is completely sedated. In coronary bypass surgery (the most common bypass operation), the surgeon makes an incision down the center of the sternum. The ribcage is spread open using a retractor to expose the heart. In most instances, the heart is stopped for 90 minutes of the 5 hour

bypass procedure using a cardioplegic solution while a heart-lung machine takes over the blood circulation and breathing functions of the body. The surgeon uses a graft to re-route the blood passed the plaque occluded segment of the coronary vessel [12]. Peripheral bypass surgery is also available for arterial blockages within the arms and legs.

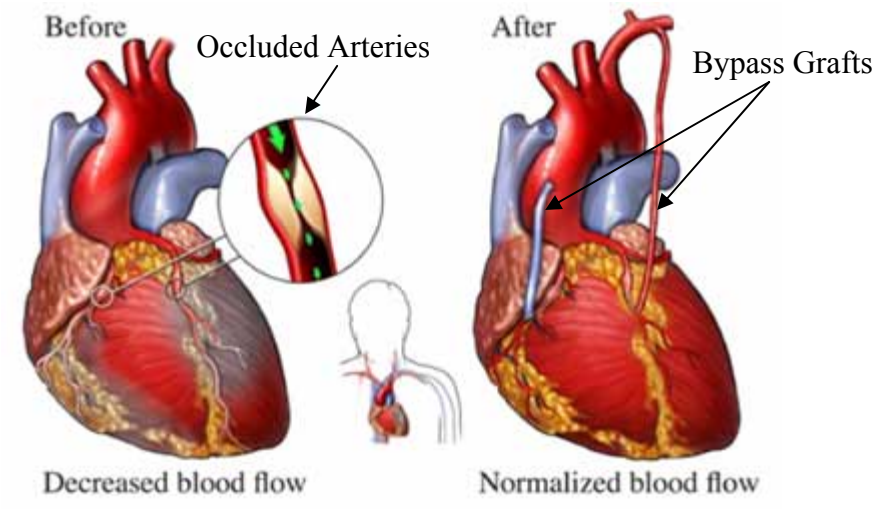

Figure 2.5 Bypass surgery. Occluded coronary arteries require a bypass graft to re-rout the blood passed the blockage and supply oxygen to the cardiac tissue dependant on these arteries for blood. The proximal end of the graft is attached to a major artery (aorta) and the distal end is fastened to the occluded artery down stream of the blockage [45].

Coronary bypass surgery is capable of treating multiple coronary vessels with little increase in risk of complication. Most complications that arise from coronary bypass surgery are short-term including difficulty breathing, bleeding, infection, hypertension and arrhythmias. More serious complications, such as myocardial infarction, stroke and death, are usually the result of stopping the heart and using the heart-lung machine. Graft occlusion may also occur resulting in the need for a second bypass surgery; a procedure that presents a greater risk. Other risk factors include diabetes and age, though patients

older than 80 years of age have benefited from coronary bypass surgery [12]. In addition, bypass procedures are extremely expensive (~$10,000 for coronary bypass surgery) and highly invasive, often causing a great deal of trauma and requiring lengthy hospital stays with plenty of pain medication [46]. Moreover, calcium channel blockers frequently need to be administered during the procedure to reduce vasospasms of denervated vessels, which can by themselves induce further complications [47]. Nevertheless, bypass surgery may be the only option in cases of severe and almost total occlusions, especially if blood supply to a vital organ is directly and immediately threatened.

2.3.3 Minimally-Invasive Treatment

Alternative to bypass techniques are percutaneous vascular intervention (PI) procedures, depicted in Figure 2.6. PI patients are only administered a mild sedative and remain conscious throughout the procedure. Initially, a guide wire is inserted into the vasculature, usually through the femoral artery, and directed through the vasculature to the region of occlusion. Guide wires are shaped and designed to percutaneously navigate through complicated vascular paths that a catheter would not otherwise be able to traverse and hence provide a path enabling the catheter to reach the site of occlusion. The guide wire and catheter are visualized traversing the vasculature on an x-ray imager by radio-opaque markings on the tips and the injection of a radio-opaque contrast medium (usually an iodine derivative).

Through a procedure called *percutaneous transluminal angioplasty* (PTA), a deflated balloon-tipped catheter is inserted into the luminal space of the occluding plaque,

as seen in Figure 2.6. The balloon is then inflated with saline or contrast media at pressures averaging 5-17 atm, to enlarge the vessel diameter and compress the plaque against the blood vessel wall increasing blood flow capacity [48]. The balloon is also radio-opaque and its expansion is seen on the x-ray imager. The balloon is then deflated, and the catheter removed. Catheters are provided with variable expanded balloon diameters. The appropriate expanded balloon diameter must be chosen to prevent over dilation and rupture of the vessel.

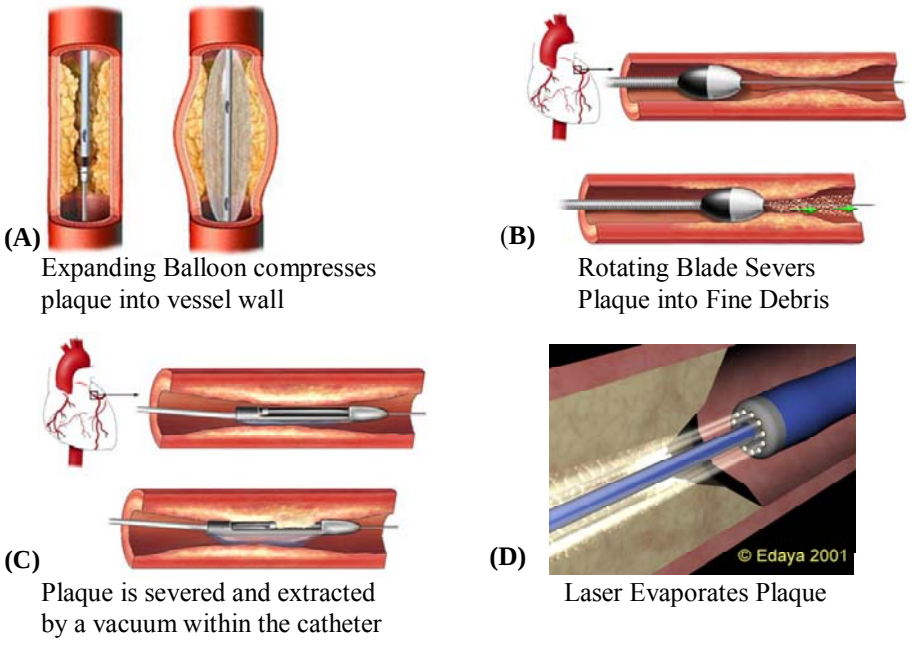

Figure 2.6 PI Treatments: (A) Balloon angioplasty [49], (B) rotational atherectomy [50], (C) transluminal extraction atherectomy [51], (D) laser angioplasty [52].

PTA procedures are much less expensive than bypass surgery (~$6,000 for percutaneous transluminal coronary angioplasty; PTCA) and far less invasive [46]. Patients usually spend one night in the hospital and return home the following day. They are

typically able to walk within 2 – 6 hours and return to their normal routine within a week. However, balloon catheters are incapable of re-vascularizing chronic total occlusions or highly calcified occlusions due to their inability to penetrate into such plaques. Highly thrombotic occlusions are also a concern for PTA operations because the expanding balloon may dislodge a piece of the thrombus ridden plaque (embolus) allowing it to flow downstream causing distal vascular occlusion (embolism). Atherectomy has been developed to address some of these concerns.

Atherectomy is another PI procedure capable of removing highly calcified or thrombotic plaque and chronic total occlusions. Atherectomy catheters exist in two different forms (e.g. rotational, transluminal extraction) and incorporate a catheter tip fitted with rotating blades that sever the plaque into small debris, depicted in Figure 2.6. Rotational atherectomy generates extremely fine debris, while transluminal extraction requires the incorporation of a catheter fitted vacuum to remove the large particles that have the potential to occlude a smaller blood vessel downstream [53]. An additional method to re-vascularize a completely occluded vessel is laser angioplasty, seen in Figure 2.6, in which a laser catheter emits pulsating beams of light from its tip that vaporize the plaque [54]. Yet, advances in PI treatment have not completely eliminated bypass surgery as a re-vascularization technique. PI operations presently have a high risk of re-occlusion and the need for repeat procedures. Therefore, they are not recommended for patients with more than two occluded vessels, or occlusions that surpass the collateral blood supply in vessels that act as the major blood supply to a vital organ. In order to prevent re-occlusion, a metal mesh tube graft called a stent (further discussed in Section 2.4.4) may

be deployed after PI treatment.

2.4 Vascular Grafting

Vascular grafts are blood vessel substitutes or implants that maintain the structural integrity of blood vessels. Many graft designs are currently under development, but only four are commonly used clinically: tissue autografts, synthetic grafts (Dacron; Teflon), and stents.

2.4.1 Autografts

Autografts (i.e. greater saphenous vein, internal mammary artery) are considered the gold standard for vascular grafting due to their long-term patency relative to synthetic grafts (discussed in Sections 2.4.2 and 2.4.3). This stems from its inherent antigenic nature and favorable mechanical properties. Studies indicate that the saphenous vein is capable of remodeling in the arterial environment, transforming into a more artery-like structure [55]. Therefore, autografts are the most viable clinical option but they are limited by a lack of quality and availability. Many patients simply do not have enough appropriate blood vessels for use as grafts; either the blood vessels are systemically diseased or the blood vessels are unavailable due to prior explantation for use as bypass grafts [56,57]. In such cases, readily available synthetic conduits made of Dacron (polyethylene terepthalate, PET) or Teflon (expanded Polytetrafluoroethylene, ePTFE) are used.

2.4.2 Dacron Grafts

Dacron is a robust material with a tensile strength of 170-180 MPa and tensile modulus of 1.4×10^4 MPa [58]. These properties contribute to its resistance to mechanical failure, but also reduce its compliance relative to native tissue. Dacron is produced in either woven or knitted forms. Woven Dacron grafts are stronger, while knitted grafts are more compliant and have larger pores that promote greater tissue in-growth. The high porosity of knitted Dacron necessitates the use of a biological sealant such as gelatin, collagen, or albumin to plug the pores and prevent the leakage of blood. The porous nature of knitted Dacron grafts also increases their susceptibility to infiltration of hyperplasic medial SMCs. This is initiated by abnormal mechanical signals sourced from a compliance mismatch between the graft and blood vessel. Upon implantation into the body, proteins immediately adsorb to the luminal surface followed by platelets, macrophages, ECs and SMCs. Over the course of 18 months, this cellular mixture forms a three layer neointima consisting of a fibrin luminal layer, macrophage middle layer and connective tissue outer layer. Although Dacron has been shown to remain intact for more than 10 years in large diameter vessels, studies have also shown that they tend to dilate in the arterial environment increasing their susceptibility to mechanical failure [59].

2.4.3 Expanded Polytetrofluoroethylene Grafts

ePTFE is a highly crystalline material. The material exhibits a stiffness of 0.5 GPa and tensile strengths on the order of 14 MPa [58]. It has an electronegative surface that inhibits protein adsorption and thrombus formation improving its biostability. The pore

size of ePTFE can range from 20 – 90 μm but the most common pore size in ePTFE vascular grafts is 35 μm. A pore size of approximately 60 μm would enhance the tissue interaction with the graft. Upon implantation, ePTFE elicits a mild inflammatory response that results in the formation of a neointima, over the course of 18 months, similar to Dacron, and is a viable option for large diameter vessels.

2.4.4 Stents

Autografts, Dacron grafts and ePTFE grafts are commonly used to bypass occluded blood vessel segments. However when the occlusive plaque is subtotal and not diffuse, PI techniques are performed. In such cases, stents are deployed at the site of occlusion in order to maintain the luminal diameter of the revascularized blood vessel and prevent reocclusion, a stent may be positioned at the PI-operated plaque site, as shown in Figure 2.7. A stent is a metal mesh tube that maintains the structural integrity and dimensions of the re-vascularized vessel. Angioplasty with stenting involves the deployment of a self-expanding or balloon expandable metal stent at the re-vascularized site of vessel constriction in an effort to prevent vessel collapse and to ensure its patency. Balloon expandable stents consist of collapsed stents placed over angioplasty balloon catheters. After balloon angioplasty, the stent is expanded to the appropriate diameter and provides a firm support to the vessel wall, ensuring that it remains patent. Self-expanding stents are delivered in the collapsed form and when released from the catheter expand to a pre-determined diameter. Memory alloy stents such as nickel or nickel-cadmium plated stents are processed to be in a collapsed state under cool temperatures and expand when

exposed to heat. Immediately following balloon angioplasty, the memory alloy stents are expanded with hot saline. Matching the expanded stent and blood vessel diameters is important when choosing an appropriate stent. Expansion and pressure profiles, stent strut design, and material all influence the success of stented PI treatments.

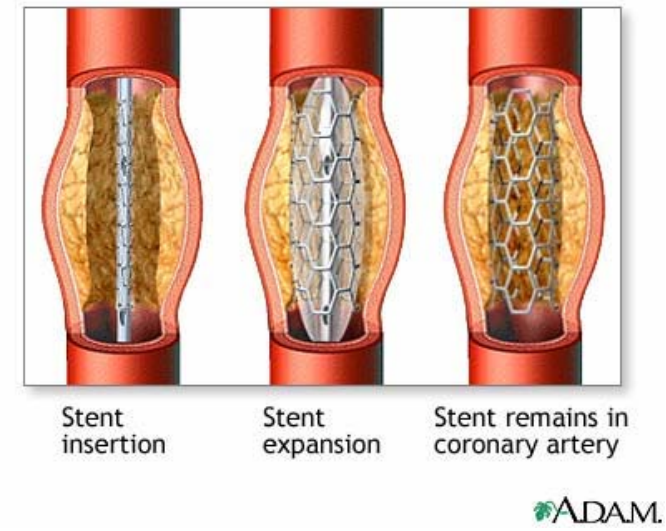

Figure 2.7 Percutaneous stenting of a blood vessel [60].

Stenting is now commonly adopted, comprising 70-90% of re-vascularization procedures [61]. Stent use is determined by parameters such as location and size of the vessel, blood flow patterns and the disease state. Although advances in device technology have been significant, the utility of interventional strategies such as stents is still compromised by re-occlusion.

2.5 Restenosis

To date, a vascular graft capable of long-term patency, especially in small-diameter vessels, is not available due to re-occlusion, or restenosis. The mechanism of

restenosis of vascular substitute grafts and PI treated vessels with and without stent deployment are similar but differ slightly. Therefore, they are discussed separately in this section.

2.5.1 Restenosis of Dacron and ePTFE Grafts

Endovascular grafts must mediate a two-front attack involving the graft-tissue and graft-blood interfaces. The interaction of all three species involves highly complex microenvironments that are ultimately responsible for the graft patency. Immediately upon implantation, serum proteins (albumin, fibrinogen, IgG) adsorb onto the graft surface and eventually re-distribute according to the Vroman effect. The Vroman effect predicts small proteins adsorb first followed by less mobile larger proteins. The larger proteins are more strongly bound to surfaces and displace the smaller proteins resulting in a rearrangement that depends on the concentration of proteins within the blood. Depending on the type and concentration of protein adsorbed, these protein constructs attract the cellular components of the blood (platelets, neutrophils, monocytes) through receptor mediated interactions. Adherent platelets eventually degrade, releasing bioactive molecules that activate additional platelets, recruit monocytes, and stimulate SMCs within the vascular wall. These receptors also govern neutrophil (acute inflammatory response) and monocyte (chronic inflammatory response) adherence to the adsorbed protein layer and activated/ damaged ECs surrounding the graft. The monocytes differentiate into macrophages and release degradative agents (proteases, oxygen free radicals) and bioactive molecules (PDGF, FGF, TGF-β). These bioactive molecules

released by platelets, macrophages and damaged/ activated ECs trigger medial SMCs to become hyperplasic and migrate toward the lumen, and deposit an exuberant and unnaturally fibrous matrix.

Early graft failure can occur due to a compliance mismatch between the non-elastic graft and the viscoelastic blood vessel wall, and the development of SMC hyperplasia at the anastomosis site due to EC damage caused by sutures that tether the graft to adjoining healthy vessel segments. These events incite proliferation and migration of medial SMCs towards the intima and onto the lumenal surface of the graft, with subsequent synthesis of matrix proteins and other extracellular material. Direct exposure of these matrix components to blood, in the absence of a complete endothelium, initiates platelet adhesion followed by the infiltration of inflammatory cells and the eventual formation of an occlusive plaque [62]. Even though extensive research has been carried out on intimal hyperplasia, its causes are still poorly understood; however, the development of atherosclerosis is known to be very strongly associated with disturbed flow and injury to the vessel wall. A majority of prosthetic vascular grafts fail within five years due to severe occlusion of the vessel immediately distal to the graft caused by intimal hyperplasia [63]. Grafts can be limited by one or more parameters including (1) large pore size/high porosity as with Dacron grafts that permit lumenal infiltration by hyperplasic SMCs, (2) thrombogenicity, mediated by a surface conducive to deposition of adhesive proteins and platelets, (3) mechanical failure induced by a poor compliance mismatch between the graft and vessel, and (4) exaggerated cell responses and healing due to unnatural stimuli imparted by synthetic graft materials to contacting vascular cells

[64]. A successful graft must thus optimize tissue-biomaterial interactions to elicit non-hyperplasic responses, exhibit inherent mechanical properties similar to that of host vascular tissues and be intrinsically non-thrombogenic at the lumenal surface.

2.5.2 Restenosis of PI-Treated Vessels

The rate of restenosis, or re-occlusion, within PI treated vessels is 30% – 40% after 6 months [8]. Restenosis may occur through elastic recoil, negative remodeling or neointimal hyperplasia. Elastic recoil is almost immediate, resulting within 1 hour of PI. Balloon angioplasty stretches the elastic fibers within the vessel wall. The stretched elastic fibers respond by recoiling back to their original size resulting in a loss of luminal diameter [65]. Negative remodeling occurs within 1 to 6 months. Balloon angioplasty often damages the vessel adventitia. This activates fibroblasts causing them to begin fibrotic remodeling. Such remodeling ultimately results in adventitial thickening and a reduction of luminal diameter [66]. Neointimal hyperplasia, which is exuberant proliferation of medial SMCs towards the vessel lumen, is a common response to vascular injury and inflammation and also results in the reduction of luminal diameter [67,68]. The expanding balloon can cause damage to the intima resulting in the accumulation of inflammatory cells, remodeling and cellular proliferation. As in atherosclerosis, this may result in repeated plaque-induced occlusion of the vessel.

2.5.3 Restenosis in Stented Vessels

A bare metal stent is also prone to restenosis since it is a foreign material and may

cause mechanical damage to the intima, which will incite an inflammation response. While it does inhibit elastic recoil and negative remodeling, a stent is also capable of promoting neointimal hyperplasia and thrombosis [69]. Stent struts often protrude into the lumen altering the natural hemodynamics, and thus promote thrombosis [70]. Since stenting also damages or denudes lumenal ECs, platelets bind to the sub-endothelial matrix and degranulate, to release bioactive molecules that can stimulate underlying SMCs to become hyperplasic and move towards the vessel lumen through gaps between the stent struts, to form an occlusive plaque.

Studies suggest that the mechanisms leading to in-stent restenosis differ from those associated with restenosis caused by balloon-induced injury. Stent injury-induced restenosis shows a higher degree of neointimal growth and higher levels of neutrophil recruitment. Anatomical and pathological investigations show that coronary stenting associated with medial damage or penetration of the stent into a lipid core induces increased arterial inflammation accompanied by increased neointimal growth [71]. Device design, material, pore size, surface roughness and charge, hemodynamics, and vessel type (i.e. artery, vein), location (i.e. coronary, peripheral), and size are strong determinants of restenosis in stented or grafted vessels [70].

2.6 Blood Vessel Size as a Risk Factor for Restenosis

The conventional techniques of revascularization described above for large vessels, are not as effective in small diameter vessels (< 5 mm), due to their particular pre-disposition to re-occlusion after intervention [14-16]. One major problem with the

treatment of small vessels is the fact that the area decreases in proportion to the radius squared. Hence, the plaque required to occlude smaller diameter vessels is drastically decreased in comparison to larger vessels. Small vessels also have lower shear rates than larger vessels due to sluggish flow, which favor platelet deposition and plaque accumulation. The development of long, diffuse plaque accumulations increases the difficulty of treating small vessels [72]. These factors make small-diameter vessels prone to occlusion and difficult to treat.

2.6.1 Dacron and ePTFE Grafts in Small-Diameter Vessels

In large conduits where high pressures are encountered, such as in the aorta, stiffer and stronger polymeric grafts are desireable. However, in smaller grafts, compliance is more important than strength. While inert polymer grafts such as Dacron and ePTFE perform reasonably well in the high flow and low resistance conditions of large peripheral arteries, they are not quite suitable for deployment in small diameter vessels [58,73]. To illustrate, Dacron has a five-year patency rate of 93% for aortic bifurcation grafting [74], but only 43% for above-knee femoropopliteal bypass grafts [17]. One of the major flaws is their compliance mismatch with vascular tissues in small diameter vessels limit their applicability to such vessels [74]. Furthermore, when exposed to relatively sluggish blood flow in small-diameter vessel, coagulation and platelet deposition is much enhanced on Dacron grafts. The addition of heparin has somewhat reduced coagulation in femoropopileteal bypass grafts, as shown by a three year study [75], but the duration of the heparin is yet to be determined [76]. ePTFE similarly has a reported

5-year patency of 91% and 95% [74,77] when used as an aortic graft but exhibits much lower patencies (61% and 45%) when deployed as femoropopliteal bypass grafts [17].

2.6.2 Stents in Small-Diameter Vessels

Performing interventional procedures on small vessels presents a number of technical challenges for the interventional cardiologist. Negotiating a stent to a given lesion in a small vessel may be hampered by distal location, vessel tortuosity and intra-vascular calcification. An additional technical problem is that distal lesions are more frequently diffuse, thus requiring longer, less flexible stents to fully cover the diseased segment. There are also fewer stenting options (i.e. type, diameter, length) available for vessels < 3 mm [78]. Another important issue is that the small vessel lumen leaves little room for error in sizing and stent expansion.

The average extent of in-stent *late lumen loss* (radial lumen reduction; LLL) after implantation of a bare metal stent is 0.8 - 1 mm, regardless of vessel size. This has vital implications for small diameter vessels. To illustrate, a 4 mm diameter vessel with 1 mm of LLL experiences a 44% reduction in lumen area, while a 2 mm diameter vessel with the same LLL, suffers a 75% lumen area loss. Therefore, the impact of 1 mm LLL is far greater in small diameter vessels than large diameter vessels [79]. Bare metal stents (BMS) have reduced the rate of restenosis to 19.9% in large arteries (≥ 3 mm diameter) but only 32.6% in small arteries (< 3 mm) after 6 months which is drastically insufficient [80].

2.7 Vascular Tissue Engineering

Despite the progress in vascular engineering, scientists have still not created a viable vascular substitute that possesses the necessary complex mechanical properties and mimics the biological function of a native artery. A recent approach called tissue engineering, appears to have the most promise in developing a suitable blood vessel replacement. The field of tissue engineering encompasses both therapeutic and diagnostic applications. Diagnostic tissue engineering uses tissues or cells excised from the body and grown *in vitro* to test their drug uptake, metabolism, cytotoxicity and pathogenicity. The diagnostic form of tissue engineering also serves as an easily accessible and characterizable model to understand combinational interactions between cells, their ECM and exogenous or endogenous bio-signaling molecules. Therapeutic tissue engineering involves manufacturing a tissue and transplanting it into the body. Therefore, tissue engineering is defined as, '*the use of a combination of cells, engineering materials or scaffolds, and suitable biochemical factors to improve or replace biological functions in an effort to effect the advancement of medicine*' [1]. This definition clearly highlights the three key ingredients to successfully engineer tissues: cells, a scaffold or matrix, and regulatory-biomolecules.

Tissue engineered vascular biomaterials have specific advantages over traditional materials (i.e. Dacron, ePTFE, Stents) since they are designed to be biologically active and mechanically responsive. A tissue-engineered vascular construct may contain synthetic materials, biological materials, biomolecules and/or cells but must integrate with the target tissue and eventually function as a native blood vessel. However the

challenges facing tissue engineered biomaterials include sufficient strength and elasticity, matched compliance with native vessels, and immediate functionality on implantation [86-90].

2.7.1 Biodegradable Synthetic Materials

Some designers are investigating the use of biodegradable synthetic polymer scaffolds, as vascular biomaterials. Since the conditions used to create these polymers are too harsh for the cells to survive, cells cannot be directly encapsulated into the polymer prior to implantation. Therefore, if cellularization is desired, it must be accomplished by pressure-driven cell infiltration or dynamic cell seeding techniques [81]. The concept underlying this approach is to generate a scaffold that initially acts as a mechanical support until infiltrating cells, from the target tissue or seeded *in vitro*, are able to produce a significant amount of ECM to maintain mechanical stability. Once implanted, the polymer will be re-absorbed at the same rate that tissue regenerates, ideally. A challenge however, is to tailor the degradation rate of these polymers so as to exhibit extended degradation times, since the failure of the cells to properly infiltrate and rapidly produce the requisite amount of ECM can result in implant failure.

The most commonly used synthetic, bio-degradable polymer for tissue engineering is polyglycolic acid (PGA). When unmodified, PGA is rapidly resorbed by the body causing premature weakening of the material. Therefore, it is copolymerized with other degradable polymers such as poly-L-lactic acid [81], polyhydroxyalkanoate [82], poly-4-hydroxybutyrate [83], polycaprolactone-co-polylactic acid [84] and polyethylene

glycol [85] to improve its long-term mechanical stability. In addition, cell interaction with such constructs can be enhanced by incorporating adhesion peptides (RGD [86]), proteins (fibronectin) or growth factors (TGF-β [29]) such as RGD peptides.

One co-polymer tested as a vascular prosthesis was PGA-polyhydroxyalkanoate (PHA). The polymer conduit was seeded with autologous fibroblasts, SMCs and ECs, and implanted in the abdominal aortic segments of lambs for 5 months. All the implants remained patent and no aneurysms developed at the time of sacrifice [82]. Co-polymeric scaffolds of PGA and polycaprolactone-co-polylactic acid have also been seeded with a mixed population of autologous ECs and SMCs derived from the canine femoral vein. In canines, this implant completely degraded after 3 months while the vessel remained patent for 13 months with no evidence of dilation or stenosis. The first successful clinical application of a tissue engineered vascular implant was accomplished using this material formulation in a 4-year -old. After 7 months, no sign of aneurysms or stenosis was evident [84]. Subsequent clinical trials using this degradable polymer with bone marrow cells resulted in 100% patency rate with no evidence of thrombotic or obstructive complications [87]. Bio-degradable polymer have shown much promise in animals as vascular implant materials but these results must be replicated in the more complex human anatomy to establish these biomaterials as a viable option.

2.7.2 Biological Tissues

In the past, vascular tissues explanted from a member of the same species (allogenic) or another species (xenogenic), and then decellularized to yield non-cellular

matrix scaffolds, have shown little success due to the generation of an immune response in the host and a loss of mechanical properties after processing in vitro [88-90]. Decellularization is usually accomplished by treating tissues with a combination of detergents, enzyme inhibitors and buffers that ideally remove the cells and epitopes from the vascular tissue [91]. This process typically results in shrinkage due to the removal of proteoglycans [92]. The lack of cells and proteoglycans can adversely impact the vessel, reducing the ultimate tensile strength and compliance [93]. Yet, recent studies suggest that decellularized xenogenic vascular tissues are less susceptible to thromboembolism [94] and cryopreserved allogenic vascular tissues reduce aneurysm formation [95]. An *in vitro* investigation also found decellularized human saphenous veins contain an intact ECM and exhibit mechanical properties adequate for implanting within small vessels [96]. Small intestinal submucosa (SIS) has also been decellularized to create matrix conduits composed of primarily collagen with additional fibronectin, growth factors, glycosaminoglycans, proteoglycans, and glycoproteins [97]. The patency rates for these decellularized autogenic and xenogenic vascular implants were comparable to that obtained with the saphenous vein, in canines [98]. Therefore, in the near future such methods may prove to be clinically applicable.

2.7.3 Cell-Based Vascular Constructs

Some researchers also attempted to create a completely cell based vascular constructs. The most impressive to date has been designed by Auger *et al.* [72]. His approach involved culturing sheets of SMC layers in the presence of ascorbic acid to

induce sufficient collagen production and wrapping them around a porous mandrel to form a media. The porosity of the mandrel allows the transport of nutrients to the lumenal cells. Subsequently, fibroblast layers were produced in a similar fashion and wrapped around the media to create an adventitia. After several weeks in culture these layers fused into a single cohesive unit. During this incubation period, the constructs were removed from the mandrels, the ends were cannulated and the lumenal surface was endothelialized by filling the lumen with a solution of ECs. The resulting blood vessels had distinct multilayer organization, contained abundant ECM deposition and a normally functional endothelium. This structure sustained burst pressures greater than the saphenous vein and a compliance greater than ePTFE but far lower than the small diameter vessels it was designed to replace. It was hypothesized that the lack of compliance was due to insufficient elastic fiber deposition. Also, the manufacture of these vessels takes at least three weeks and longer if the patients own cells are used [72]. A major difficulty with any organ developed in an *ex vivo* culture is that, over time, the cells alter their phenotype as well as their immunogenic responses [99-101].

2.7.4 Biopolymers

Some groups have attempted to tissue engineer a hybrid vascular constructs by combining biopolymers (i.e. collagen) with synthetic biomaterials. The first attempt at tissue engineering a hybrid vascular biomaterial involved Dacron impregnated with collagen but was unable to withstand physiologic pressure conditions [102]. Since then, blood vessel engineering has been successful at developing biomaterials that can

withstand arterial pressure for up to 6 weeks [103,104]. Such hybrid vascular prostheses were developed using SMCs and collagen reinforced with a knitted, segmented polyester mesh to create compliance similar to the native tissue. The mechanical properties of these materials were improved by using SMCs and/ or fibroblasts with ascorbic acid to produce a three dimensional ECM similar to that observed *in vivo*, but requires 56 days of culture [72]. The biomaterial was successfully seeded with ECs and examined under pulsatile flow [105].

More recently, scaffolds comprised exclusively of biopolymer were constructed. The most popular biopolymer in vascular engineering is collagen I since it is the most abundant protein in the human body and a major component in the ECM wall, making it a natural cell substrate. Bovine collagen I has also been approved by the Food and Drug Administration for clinical [106]. Fibrin is another commonly used biopolymer, which is the major structural material in blood clots and plays a major role in wound healing by being remodeled by cells into ECM post-injury. Clinically, it is used as common wound sealant. Both collagen and fibrin scaffolds are constructed in the form of a hydrogel within a hollow cylindrical mold and the mild fabrication conditions allow direct cellularization by cell entrapment during gelation. Collagen monomers spontaneously polymerize at body temperature while fibrin monomers require thrombin for polymerization [107,108]. The mechanical properties of these gels are improved by cross-linking using ribose [109], lysyl oxidase [110] and Factor XIII [111]. Yet, when fabricated into a tubular form, it was found that collagen fibers do not organize properly and its mechanical properties do not match that of native vessels. The strength of these collagen conduits and fiber organization within

were improved by subjecting them to dynamic contraction around a mandrel. However, the mechanics of the construct still fell short of the native vessel [104,112-115]. It was reasoned that entrapped cells must be stimulated to produce their own ECM, align the fibers, and compact the fiber bundles by traction.

Continued study of SMCs and fibroblasts entrapped within collagen gels found ECM production to be suppressed relative to monolayer cultures [116]. Conversely, fibroblasts entrapped in a fibrin gel were stimulated to produce ECM in comparison to collagen-entrapped fibroblasts [117]. Neonatal rat aortic SMCs cultured within fibrin gels were shown to compact and align the gel fibers and deposit collagen fibers in the same circumferential direction potentially improving the mechanical properties [118].

In order to promote desirable cellular activities, growth factors can be provided to cells within the tissue-engineered constructs. Incorporation of TGF-β1 and insulin were shown to increase SMC collagen production by 20-fold within fibrin gels, as compared to collagen gels. These constructs also exhibited uniaxial tensile strengths similar to rat abdominal aorta. Also, a significant amount of elastin production was observed when SMCs were cultured on fibrin gels, which does not occur on collagen gels [114]. When implanted into a canine vasculature, endothelialized fibrin-based vascular constructs remained patent for up to 15 weeks [119].

A new generation of biomimetic materials is being developed in terms of fibrillar structure. The electrospinning technique is capable of producing fibers with diameters similar to those found in natural ECM from collagen [120] and fibrinogen [121]. It is capable of aligning the fibers in a pre-described pattern but cells cannot be entrapped during the

electrospinning process and must be seeded post-fabrication. Other potential approaches to create small diameter fibers are based on self-assembly techniques [122] although to date it has not been truly successful.

2.7.5 Role of Mechanical Transduction in Tissue-Engineering Vascular Constructs

Recently, several groups have attempted to use mechanical conditioning to influence vascular cell behavior, and thus improve the structure and mechanics of tissue-engineered vascular constructs. Blood vessels experience four hemodynamic forces including: (1) shear stress, (2) luminal pressure, (3) radial stretch and (4) longitudinal stretch. These mechano-transduction forces act independently and synergistically to control the behavior of vascular cells [123-125]. Thus, subjecting cells in culture to these forces can induce more native cell responses, such as cell-matrix interactions.

2.7.6 Pulsatile Distention Conditioning

SMCs are primarily affected by the pulsatile distention forces mentioned above. The mechanical stretching of SMCs cultured on substrates or with a collagen gel has shown to extensively affect SMC behavior in terms of phenotype [126], orientation [127], ECM deposition [128], growth factor production [129], proliferation [130] and vascular tone [131]. As a result, investigators utilize the application of these mechanical forces to enhance the development of cell-embedded tissue engineered vascular biomaterials. Cyclically loading SMCs within a collagen construct altered the SMCs to a more contractile phenotype [132] and increased both the ultimate tensile strength and tensile tangent modulus

of the construct by approximately three fold [113]. In another study, blood vessels were created using biodegradable scaffolds made of PGA with embedded SMCs for 8 weeks under pulsatile conditions then seeded with ECs. These pulsed constructs proved to have a thicker vascular wall, better suture retention, greater SMC and collagen densities, and be patent longer than similar non-pulsed constructs. Average burst pressures of 2150 mm Hg were observed with these constructs but the compliance was low resulting in possible creep and aneurysm formation. These cultured vessels also showed contractile responses to pharmacological agents [133].

2.7.7 Shear Stress Mechanical Conditioning

Shear stress directly affects the function of lumenal endothelial cells and can also indirectly modulate behavior of underlying SMCs through secondary signals released by the ECs. In this manner, the entire vessel can respond to changes in shear stress. Normal levels of shear stress reduce thrombogenicity, maintain proper vascular tone and inhibit SMC proliferation. Low levels of shear stress increase thrombus formation on the luminal surface and induce SMC proliferation and intimal thickening [123]. The function, orientation and morphology of ECs are considerably affected by laminar flow while turbulent flow is incapable of inducing such changes [134]. This process of mechanotransduction is not well understood but evidence suggests that the actin filaments of the cytoskeleton play a central role [135]. Shear stress has shown to align ECs in the direction of flow with significant changes in cytoskeletal and subendothelial matrix formation altering the ability of ECs to transmit mechanical stresses [136]. In addition, shear

stress regulates the transport of fluid and biomolecules across the vessel wall by affecting EC permeability in a time dependant manner [137].

2.8 Vascular Endothelial Cells

Vascular ECs are one of the most complex and sensitive components of the blood vessel in terms of physical structure and cell signaling. They act as a wall between the blood and vascular tissue and therefore, are capable of communicating with both blood and tissue -based elements. Under healthy non-activated conditions these cells regulate numerous processes to maintain homeostasis but if damaged or diseased, ECs initiate restorative signaling pathways that can lead to further tissue impairment if prolonged. As a result, the ability to populate vascular biomaterials with functional cells is an important facet of its design.

2.8.1 Endothelial Cell Structure

A monolayer of ECs lines the lumen of all blood and lymph vessels. They have a simple squamous morphology with a central nucleus and are arranged either in a cobble stone pattern or aligned depending on the species and vessel type. On average, ECs are 1-2 μm thick and 10-20 μm in diameter. *In vivo*, vascular ECs act as a semi-permeable layer that controls the transfer of cellular and fluid blood elements into the vessel wall. The surfaces of these cells are highly specialized. The apical surface interacts directly with the blood, the basal surface contains adhesion junctions that attach the EC to the basal lamina and the lateral surfaces are comprised of junctions responsible for joining

ECs together and allowing communication between ECs, as portrayed in Figure 2.8. The basal and lateral surfaces are referred to as a single unit; the basolateral surface. ECs are in close apposition and use these specialized junctions to create sheets that act as barriers.

Adjacent ECs connect and communicate with each other via three types of cell junctions: tight junctions, anchoring junctions and gap junctions, depicted in Figure 2.8. Tight junctions form a seal between ECs to prevent apical proteins and cells from moving to the basolateral surface and vice versa [138]. Gap junctions are composed of connexons or hemichannels which connect the cytoplasm of one cell to another across the intracellular space. They allow rapid communication between cells by permitting small molecules to pass from one cell to another [23,139]. Anchoring junctions enable groups of cells to function as robust structural units by connecting the cytoskeletal elements of a cell either to those of another cell or to the ECM. Anchoring junctions occur in three structurally and functionally different forms. Adheren junctions attach the actin filaments of ECs to each other or the subendothelial matrix in a Ca^{+} dependant manner and are involved in contractile mediated permeability functions [140,141]. Desmosomes are specialized for cell-cell adhesion linking the cytoskeleton and distributing tensile or shearing forces through the endothelium and underlying connective tissue [142]. Hemidesmosomes anchor ECs to the underlying basal lamina [143]. In all anchoring junctions, the specialized proteins involved in cell-cell and cell-subendothelial matrix interactions are cadherin and integrin, respectively [144]. ECs also act as a selectively permeable and thromboresistent barrier, regulate vasodilatory response and blood flow and control platelet activation, adhesion and aggregation, leukocyte adhesion and SMC migration and proliferation as one

component of Virchow's triad [145]. Virchow's triad describes the factors involved in the pathogenesis of thrombosis: alterations in blood flow (haemostasis), injury to the vascular endothelium, and alterations in blood constitution (hyper-coagulability).

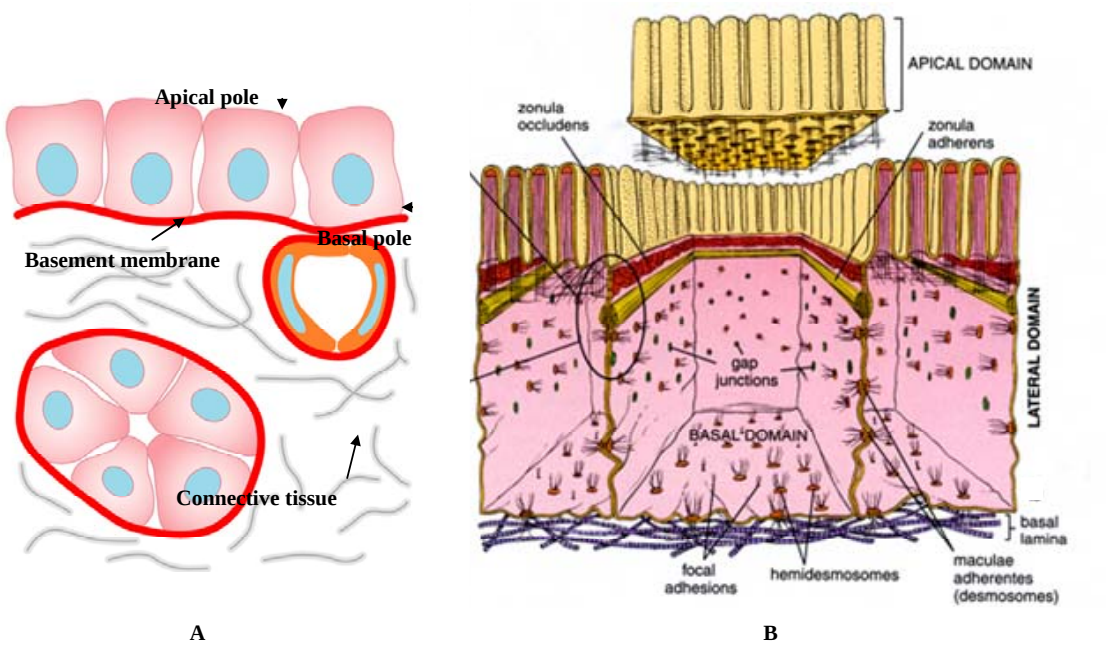

Figure 2.8 Endothelial cell structure. (A) Position of ECs on the basement membrane, (B) EC junctions.

2.8.2 Anti-Thrombotic Properties of Endothelial Cells

ECs are essential to maintaining haemostasis by inhibiting the activation platelets. On the lumenal surface of ECs lies the *glycocalyx*, a negatively charged 0.5 µm-thick hydrated mesh of proteoglycns, GAGs and glycoproteins, bound directly or indirectly to the endothelial plasma membrane. Since most of these molecules are negatively charged, the glycocalyx prevents thrombogenic proteins from depositing on the lumenal vessel surfaces. This relatively thick layer also physically masks cellular adhesion molecules

(CAM) on the EC surface from signaling leukocytes under healthy, non-inflammatory conditions [146].

Nitric oxide (NO, previously called endothelial-derived relaxing factor or EDRF) is produced by ECs and is a very potent inhibitor of platelet adhesion to ECs [147,148] and platelet aggregation [149,150]. Prostacyclin (PGI_2), also produced by ECs, inhibits platelet recruitment and activation [151,152] by raising cAMP levels in the plasma [153]. Endothelial ecto-ADPase destroys ADP released upon platelet activation and degranulation [154].

2.8.3 Endothelial Cells Regulate Coagulation of Blood

ECs regulate haemostasis and thrombosis through anti- and pro-thrombotic mechanisms that involve coagulation factors and fibrinolysis, as shown in Figure 2.9. The intact endothelium inhibits the coagulation of blood through control of circulating levels of thrombin, a product involved in the last step of the coagulation process. Antithrombin III slowly inactivates thrombin by forming a covalent thrombin-antithromin complex that is cleared by the liver [155]. This process is accelerated in the presence of heparin and heparin sulfate found on the apical EC surface [156,157]. Thrombomodulin, an integral surface membrane protein of ECs, binds thrombin and activates protein C in the plasma. Protein C in conjunction with protein S, produced by endothelial cells, inhibits the activation of factor V and VIII preventing thrombin formation [158,159]. ECs also secrete protease nexin I which inhibits thrombin formation by forming a covalent complex with thrombin. This complex then binds to ECs, is internalized and degraded by lysosomes [160].

Continued inhibition of thrombus formation occurs through fibrinonolysis by

activation of soluble plasma plasminogen to a serine protease called plasmin. Local endothelial secretion of tissue plasminogen activator (t-PA) and subsequent endothelial assembly of fibrinolytic factors (plasminogen, t-PA) leads to plasmin generation and accelerated fibrinolysis [161]. Plasmin also inactivates clotting factors involved in thrombin generation.

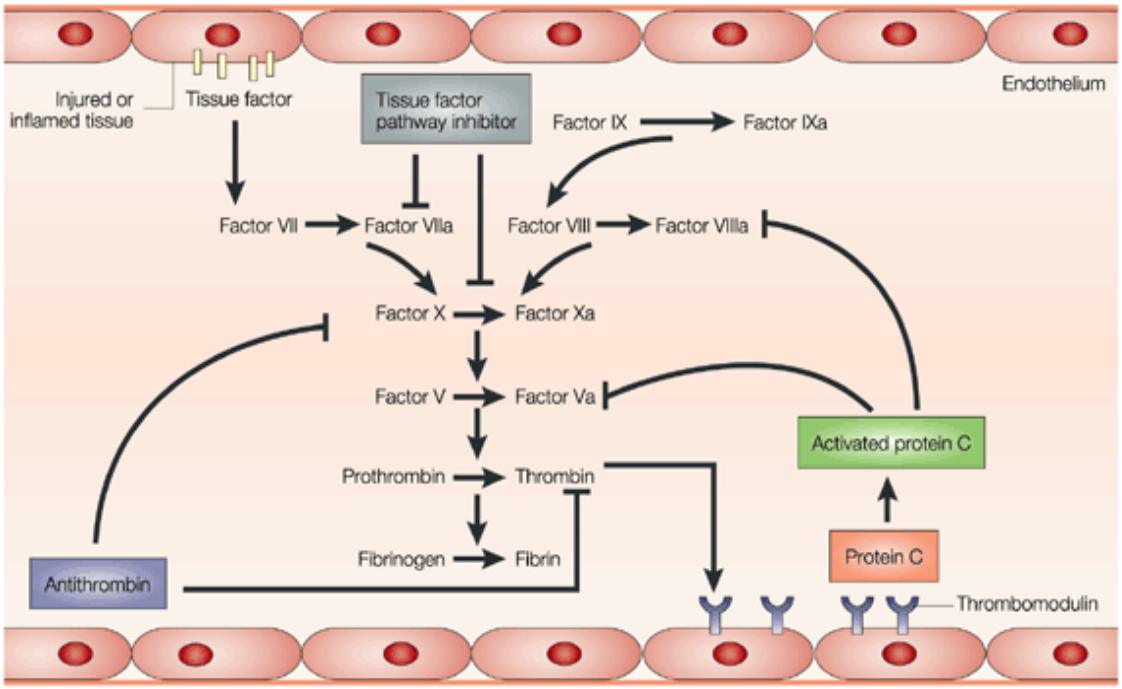

A. EC regulation of the coagulation cascade.

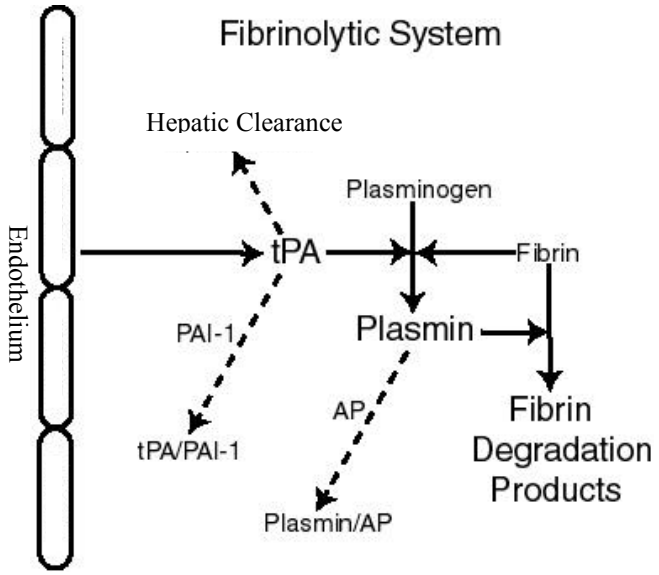

B. EC regulation of fibrin content within the blood

Figure 2.9 Endothelial cell regulation of coagulation. EC produce regulatory molecules that influence the coagulation cascade (A) or the concentration of fibrin (B) [162].

2.8.4 Blood Vessel Repair

Minor injuries of the EC layer heal by initial migration of ECs into the wound and proliferation to replace the damaged cells [163]. Major injuries require the additional proliferation and migration of medial SMCs and adventitial fibroblasts for remodeling. ECs produce many bioactive molecules that regulate this remodeling activity:

a. Basic fibroblast growth factor (bFGF) stimulates the proliferation and migration of ECs, SMCs and fibroblasts [164].

b. Platelet derived growth factor (PDGF) is mitogenic and chemotactic for SMCs, fibroblasts and microvascular ECs [165,166].

c. Transforming growth factor β (TGF-β) stimulates angiogenesis but

inhibits EC proliferation [167].

d. Heparin like inhibitor prevents SMC growth [168].

In areas of inflammation, macrophages and damaged/ diseased ECs produce cytokines (interleukin-1, interleukin -6, interleukin -8, tissue necrosis factor-α) that stimulate leukocyte chemotaxis toward the endothelium and vascular ECs to express binding sites for leukocytes, depicted in Figure 2.10. E-selectin and L-selectin attract leukocytes to the endothelium through weak binding, while endothelial leukocyte adhesion molecule-1 (ELAM-1), intracellular adhesion molecule-1 (ICAM-1) and vascular cell adhesion molecule-1 (VCAM-1) mediate the strong adhesion of monocytes and neutrophils [169-171].

Phospholipids on activated EC membrane bind factors IX, X and V to create serine protease complexes that facilitate thrombin synthesis [172]. Von Willebrand factor found in the basement membrane also binds to platelets promoting clot formation in the absence of ECs, as in vessel injury [173]. Tissue factor (TF) is expressed by sub-endothelial cells (i.e. SMCs) and upon injury is exposed to the blood where it acts as a necessary cofactor in the activation of Factor VII and fibrin formation (Figure 2.9) [174]. Additionally, perturbed ECs secrete plasminogen activator-inhibitor (PAI-1) that inhibits t-PA and thus promote clot formation, displayed in Figure 2.9 [175].

2.8.5 Vasodilatory Properties of Endothelial Cells

Vascular ECs modulate SMCs by producing vasodilators. Rapid blood flow

causes a shear stress on ECs because of viscous drag. This causes the ECs to contort in the direction of flow stimulating them to release NO, which stimulates the production of cGMP in SMCs resulting in SMC relaxation and vasodilatation [176]. PGI_2 also has vasodilatory functions [177]. Endothelin is a powerful vasoconstrictor produced when ECs are damaged by force or by toxins and prevents loss of blood from severe blood vessel damage [178].

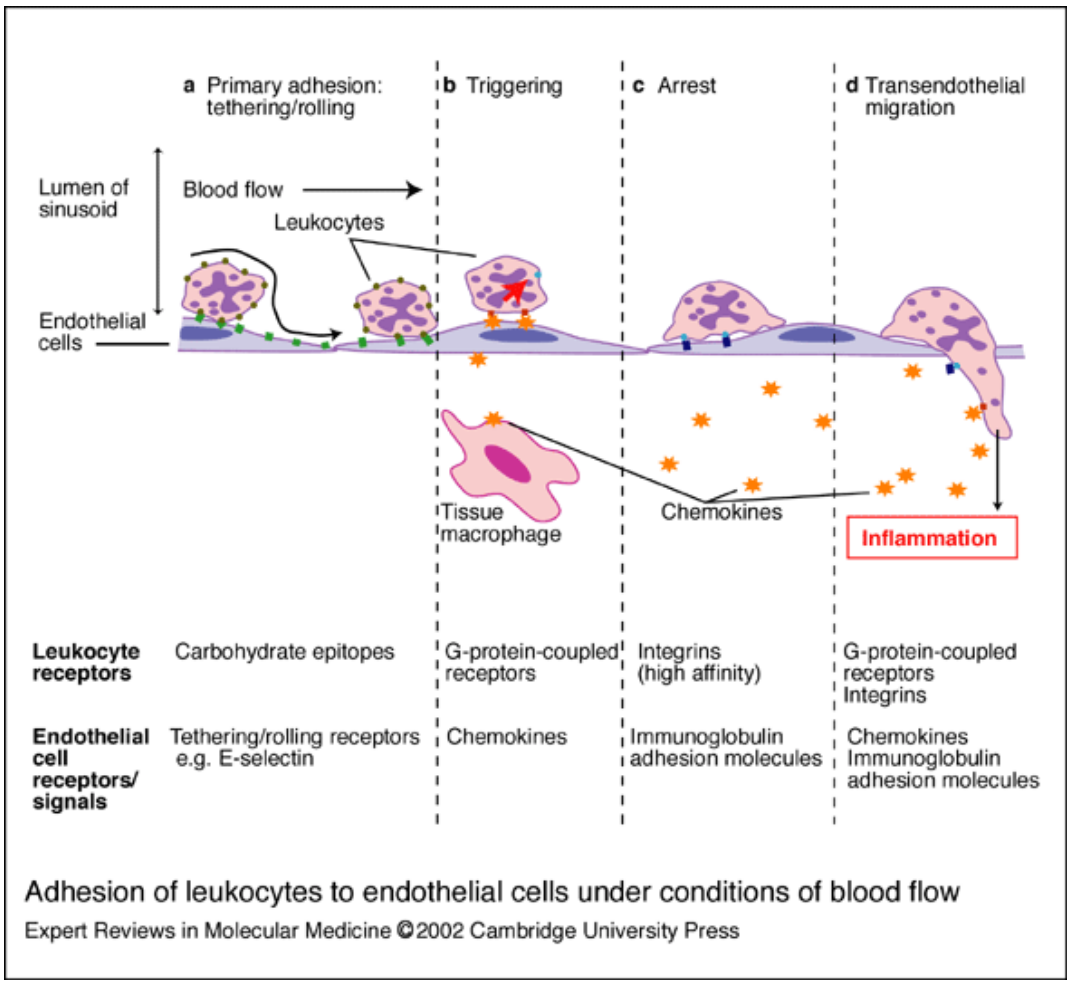

Figure 2.10 The endothelial cell inflammatory response.

2.9 Engineering Vascular Biomaterials to Promote Endothelialization

Most conventional vascular biomaterials (i.e. ePTFE, Dacron) are incapable of meeting the requirements for endothelialization. Therefore, surface modification of these biomaterials has been attempted to stimulate endothelial growth and maintain their normal functionality [84].

2.9.1 Plasma Treatment of Surfaces

One approach to altering the surface properties of biomaterials to improve their ability to recruit, adhere, and retain functional ECs, is by plasma treatment. In this process, a biomaterial is placed in a chamber under high vacuum. A gas is then introduced into the chamber and ionized by radio waves or microwaves to create plasma that reacts with the biomaterial creating surface functional groups that are dependant on the substrate and gas used. The most common surface functional groups created by this process are hydroxyl, carboxyl, carbonyl, ketone, carbonate and amine. Plasma treatment is used to create a chemically more reactive surface for secondary immobilization procedures, increase biocompatibility or enhance cell attachment, with the added benefit of material sterilization. A concern with this process is material degradation due to the generation of free radicals, though the treatment is fairly rapid (on the order of seconds) limiting the damage to only extremely susceptible materials. This procedure was successfully accomplished on the clinically available biomaterials (Dacron [179], ePTFE [179], stainless steel [180]) for vascular intervention to improve cell attachment. Plasma treatment was also used to functionalize ePTFE prior to chemically adhering biomolecules onto the

surface that promoted EC attachment [181].

2.9.2 Antibody Coating

Monoclonal antibodies directed against integrins of the endothelial cell membrane and ECM can also improve cellular attachment. Adsorbed monoclonal antibodies against EC membrane proteins, fibronectin or von Willebrand factor improved cell adhesion and proliferation [182]. A similar avdin-biotin system was also created to enhance EC attachment and spreading [183].

2.9.3 Protein Coating

Protein coatings on biomaterial surfaces can provide additional binding sites for cell adhesion receptors, and is frequently used to improve the attachment and spreading of ECs on vascular biomaterials. Many proteins have been deposited onto the surface of vascular biomaterials to enhance EC attachment (laminin, poly-l-lysine, gelatin, fibrin) but the most common protein coatings are collagen and fibronectin particularly due to their presence in the endothelial basement membrane. When these proteins adsorb onto a biomaterial surface, conformational changes may be induced depending on the characteristics of the protein and material surface [184]. In body fluids (i.e. plasma) proteins are made up of a hydrophobic core surrounded by a hydrophilic surface that permits solubilization in aqueous media. Upon interaction with hydrophobic materials, these proteins undergo conformational changes to expose their hydrophobic domains and strongly adsorb onto the material surface. Hydrophilic materials do not induce a

conformational change of adsorbed proteins, but bind more weakly with hydrophobic surface groups on the protein surface [185,186]. Structural changes to proteins can drastically influence the availability of protein binding sites for cells. In one study, the effectiveness of EC binding to fibronectin adsorbed onto hydrophilic glass and hydrophobic silanized glass was compared. It was found that the fibronectin coated onto the non-functionalized glass enhanced the spreading, adhesion and development of focal contact points of ECs [187]. It was also shown that the conformation of fibronectin is dependent on the surface to which it is absorbed [180].

Implantation studies were performed to test fibronectin functionalized vascular biomaterials seeded with ECs in the dynamic body environment. Fibronectin-coated ePTFE and PU of 4 mm in diameter were seeded with ECs and implanted in sheep carotid arteries. EC coverage was 80-90% at week 3 while the thrombus free surface area remained low until 3 – 6 weeks suggesting a lag phase in the recovery of EC function [188]. The increase in thrombus free surface area of endothelialized biomaterials was confirmed by another study using a 6 mm diameter Dacron conduits implanted in dogs [189]. Gelatin coated Dacron conduits with ECs seeded onto its lumen were implanted in dogs. Scanning electron microscopy revealed a confluent EC covering 5 mm from the edge of the implant and isolated EC in the center [190].

Vascular biomaterials endothelialized in the above manner have also been clinically investigated. ePTFE conduits pretreated with fibronectin were endothelialized *in vitro* with autologous cells and implanted into patients. After 7 years of implantation, the endothelialized fibronectin coated biomaterials performed significantly superior to

endothelialized ePTFE without the fibronectin coating and ePTFE without ECs or fibronectin treatment [191]. The same procedure was used in other experiments and the results provide strong evidence that an endothelial lining improves the patency and facilitates healing of the biomaterial [192].

2.9.4 Peptide Coating

A novel approach for enhancing EC attachment on vascular constructs is through immobilization of specific protein peptide sequences involved in cell attachment. The most common integrin binding site is the RGD (arginine, glycine, aspartic acid) sequence found on many proteins including fibronectin (RGDS), von Willebrand factor (RGDS), vitronectin (RGDV), collagen I (RGDT), collagen IV (RGDX, X is a variant), thrombospondin (RGDA) and laminin (RGDN). Other integrin binding sites include REDV and LDV on fibronectin [193] and YIGSR on laminin [194]. In one study, RGD and YIGSR peptides were covalently bound to Dacron and ePTFE and found to significantly enhance EC attachment and spreading [195]. Also, RGD containing peptides coated onto ePTFE improved the attachment and retention of EC after shear stress as compared to fibronectin coated ePTFE [196].

2.9.5 Coating composed of ECM Protein Mixtures

The ECM is composed of many biomolecules that surround and support cells. The four classes of EMC molecules are: structural proteins (i.e. collagen, elastin), specialized link-proteins (i.e. fibronectin, laminin), proteoglycans (i.e. versican, fibromodulin), and

glycosaminoglycans (i.e. hyaluronic acid, heparan sulfate). The combination of these components as in the basement membrane appears to support EC attachment in a more superior manner to single protein coatings. Completely de-endothelializing a human artery and re-seeding the cells under flow conditions resulted in 94% EC attachment [197]. Another group stimulated ECs to produce an ECM with β-FGF; then removed the cells and found the surface to enhance EC growth better than laminin, poly-L-lysine and fibronectin coated surfaces [198].

The ECM, predominantly composed of collagen, glycoproteins, proteoglycans and elastic fibers, is responsible for the passive biomechanical properties of blood vessels, providing mechanical strength, resilience, and compressibility. In addition to providing ECs with an adhesive surface (e.g. collagen I, IV, elastin), vascular ECM molecules are an integral part of maintaining vascular homeostasis and the structural integrity of blood vessels. Hence, alterations in composition or spatial arrangement of its elements affect vessel performance. Vascular SMCs routinely reproduce certain components of the ECM (i.e. collagen) throughout adulthood in response to its degradation but their capacity to synthesize elastin greatly decreases with age, compromising the integrity of blood vessels when they are degraded due to disease or injury. Therefore, as with the luminal EC monolayer, the regeneration of vascular elastin is vital to the viability of a vascular implant material for the treatment of vascular disease.

2.10 Vascular Elastin

Vascular SMCs are surrounded by an ECM that provides and modulates a variety

of biochemical and mechanical cues that guide cell function. Within blood vessels, elastic fibers constitute a major part of the ECM, especially within large elastic vessels (30-57% w/w in the aorta) [199]. Elastin is a structural protein that is predominantly distributed in the *tunica media* (Figure 2.2) layer of arteries where stretching and elasticity is required [200].

2.10.1 Vascular Extracellular Matrix

The ECM is a major component of the normal blood vessel wall, accounting for up to 60% of the intimal volume. The ECM is not only a scaffold for cells, but is also central to controlling vascular remodeling. It is a dynamic structure that can control cell behavior by storage of growth factors, and as a site for arterial lipoprotein binding [201]. Given this diversity, ECM can serve many functions, such as providing support and anchorage for cells, and regulating intercellular communication via specific cell surface cellular adhesion molecules (CAM), also known as integrins [200]. The ECM consists of elastic lamellae and three major protein components, including proteoglycans, collagen and multi adhesive matrix proteins. The highly viscous proteoglycans cushion cells are largely responsible for the volume of the ECM, insoluble collagen fibers provide strength and resilience, and soluble multi-adhesive matrix proteins bind components to receptors on the cell surface. SMCs are linked to the elastic lamellae by fibrillin-1 and type VI collagen-containing bundles of microfibrils [201]. Table 2.1 lists the major components of the vascular ECM.

The composition of the ECM largely determines the physical elastic properties of the vessel wall and is maintained and remodeled in the face of continual mechanical

stresses. SMCs have the capacity to produce most elements of the ECM as well as proteolytic enzymes (i.e. matrix metalloproteinase, MMP; serine proteases, SPs; cysteine proteases, CP) capable of degrading its components. Naturally occurring inhibitors of MMP activity in the vessel wall, known as tissue inhibitors of metalloproteinases (TIMPs), are also produced by SMCs preventing ECM degradation [202]. In this manner SMCs regulate the composition and structure of the ECM. However, certain components of the ECM, such as elastin, are irreplaceable under normal conditions due to a lost ability of SMCs to produce elastin during adulthood [203]. Elastin is an extremely important component of the blood vessel providing both biochemical signaling pathways and mechanical support, that if disrupted can initiate and progressively lead to the pathology of life threatening complications such as atherosclerosis, aneurysm and vasospasms [9,10].

Collagens		**Glycoproteins**		**Proteoglycans**	
Family	**Type**	**Family**	**Type**	**Family**	**Type**
Fibril-Forming	I, II III, V XI	**Connective Tissue**	Fibronectins Tenascins Fibrillins Elastin	**Small Leucine Rich**	Fibromodulin Lumican Epiphycan Fecorin Biglycan Decorin
Basement Membrane	IV	**Microfibril-Associated Proteins**	Matrilins Thrombospondins	**Modular**	Perlecan Agrin Testican Aggrican Versican
FACIT	IX, XII XIV, XVI XIX	**Basement Membrane**	Laminins Nidogen/ entacin Fibulin		
Multiplexins	XV, XVIII				
Orphans	VI, VII VIII, X XIII, XVII				

Table 2.1 Structural Components of the ECM [204].

2.10.2 Chemical composition of Elastin

Elastin contains a high concentration of non-polar amino acids (alanine, glycine, valine, praline), as shown in Table 2.2, resulting in a hydrophobic protein. The polypeptide chains in elastin are cross-linked by unique polyfunctional heterocyclic acids called desmosine and isodesmosine, as opposed to typical disulfide bridges. These distinctive internal linkages and inherent hydrophobicity make elastin a stable protein, resistant to the normal breakdown characteristic of most proteins [3].

Amino Acid	**Aorta**
Proline	11.27
Glycine	33.24
Alanine	22.39
Valine	13.13
Leucine	5.82
Phenylalanine	2.97
Isodesmosine[1]	0.55
Desmosine[1]	0.96

Table 2.2. Amino acid composition of elastin derived from bovine aorta. Values are expressed as a percentage of the total amino acid residues. [1]Expressed as lysine equivalents [200].

2.10.3 Elastin Fiber Assembly

Mature elastic fibers are composed of a central core of elastin surrounded by glycoprotein microfibrils (10-12 nm in diameter) [205]. During the early stages of elastogenesis, these microfibrils are formed first and play a major role in organizing

elastin into elastic fibers. The major microfibrillar components are fibrillin -1 and -2 that polymerize in a head-to-tail manner to yield the microfibrils. Calcium binding stabilizes the linear and rigid structure of fibrillin monomers, their interactions, the lateral packing of microfibrils, and thus the three-dimensional organization of their macroaggregates. Elastin is then deposited as small clumps of amorphous material within these bundles of fibrillin.

The soluble elastin precursor, tropoelastin, is secreted from cells and finds its way through the extracellular space where it interacts with the microfibrils and becomes oriented within a growing elastic fiber for eventual crosslinking [206]. This assembly process is mediated at the cell surface by an elastin-binding complex, which consists of three proteins. Two among these are integral membrane proteins (55 and 61 kDa) that form a transmembrane link between the extracellular compartment and the cytoskeleton. The third subunit is a 67 kDa bifunctional elastin binding protein (EBP) that also has galactolectin properties. It binds the hydrophobic VGVAPG sequence in elastin, the cell membrane, and galactosugars via three separate sites, as shown in Figure 2.11. The binding of galactosugars lowers its affinity for both tropoelastin and for the cell-binding site, resulting in the release of bound elastin and the dissociation of the 67-kDa subunit from the cell membrane. Galactosugar-containing microfibrillar glycoproteins may therefore be involved in the coordinated release of tropoelastin by the cell [207].

The tropoelastin deposited onto the microfibril matrix is then crosslinked into mature elastin. Crosslinking of elastin is initiated by the action of lysyl oxidase (LOX), a Cu^{2+} dependant endogenously produced enzyme that catalyses the oxidative deamination

of lysine residues into allysine [205]. This is the only enzymatic step involved in elastin crosslinking. Subsequent formation of crosslinks between tropoelastin molecules by desmosine and isodesmosine occurs as a series of spontaneous condensation reactions, resulting in the production of a complete elastic fiber. The relative proportion of microfibrils to elastin declines with increasing age of the animal, adult elastic fibers having only a very sparse peripheral mantle of microfibrillar material.

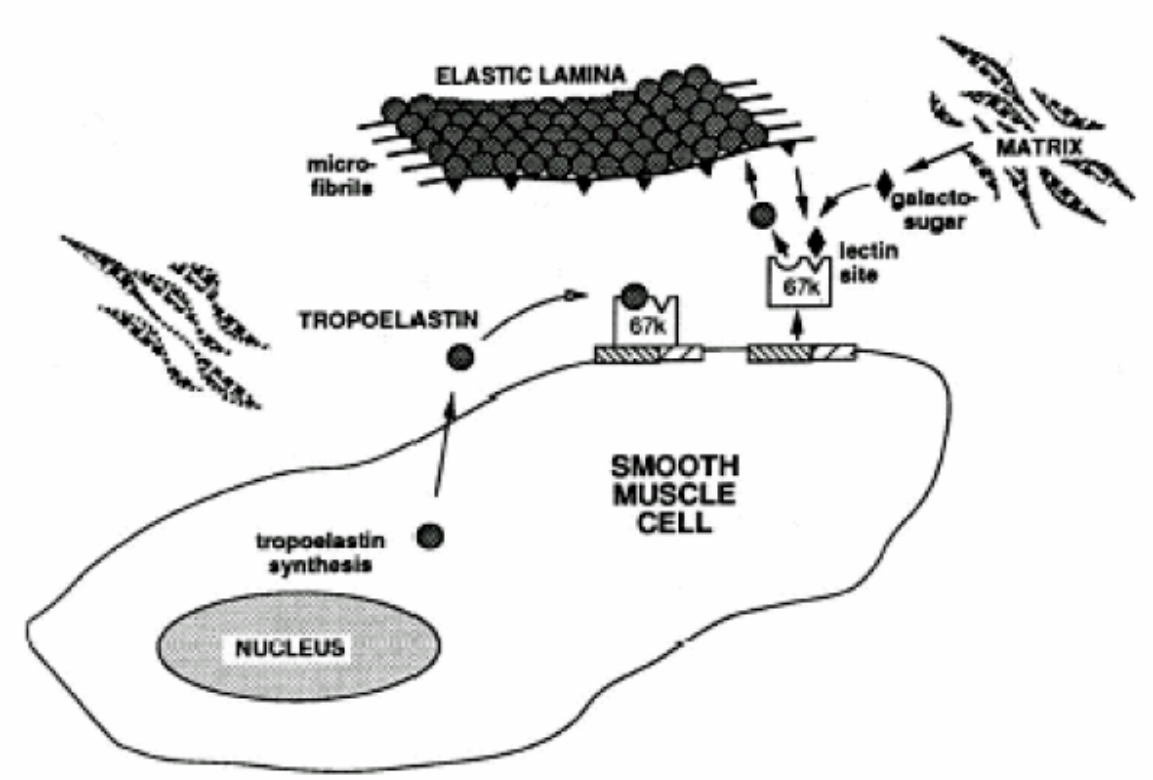

Figure 2.11. Schematic of possible mechanism of elastin fiber assembly [206].

Elastin fibers form random coiled structural networks that allow them to be stretched and then to recoil to their original state upon load-release (Figure 2.12). Elastic fibers formed by such aggregation vary in thickness, length and three-dimensional

architecture depending on the direction and magnitude of the forces exerted upon the tissue. This morphological diversification can be seen in different organ systems. In the aortic wall, elastic fibers form thick concentric lamellae in the tunica media with interlaminar connecting fibers scattered radially. Additionally, microfibrils are present as a complex meshwork throughout the aortic wall. It can be generalized that the elastic fibers are responsible for dilation and recoil, with the microfibrils acting as flexible links that make the aortic wall a working unit [205].

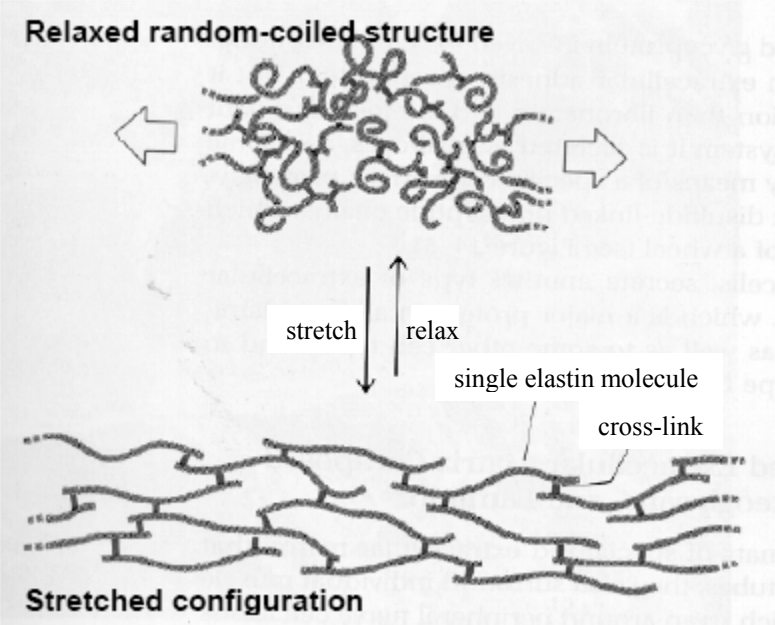

Figure 2.12. Elastin molecule in relaxed and stretched conformations [205].

2.10.4 Dynamics and mechanical properties of elastin

The mechanical properties of blood vessels influence a broad spectrum of physiologic phenomena, including blood pressure, flow rates, wall shear stress,

biomolecules, and mass cell transport that, in turn, critically impact cardiovascular homeostasis. As mentioned previously, the mechanical properties of blood vessels stem from microstructural wall components, such as collagen and elastin fibers, smooth muscle cells, and fibroblasts [205]. Since these individual components take up loads at different stress levels, their source and location-specific differences, content and distribution within blood vessels, and their alteration in diseased states can render the mechanical properties of blood vessels complex and difficult to predict. Collagen and elastin affect the mechanical behavior of vessels in different ways (Figure 2.13). Strain is initially accommodated by elastin allowing the vessel to expand with minimal resistance, and, eventually strain is strongly resisted by collagen preventing overexpansion. While collagen provides rigidity, elastin allows the connective tissues in blood vessels to stretch and then recoil to their original positions [3]. A study by Gundiah *et al.* [208] has shown that axial elastin fibers in intimal and adventitial layers, and circumferential medial fibers help distribute tensile stresses during vessel inflation and relaxation, conclusively providing evidence that emphasizes mechanical importance and indispensability of elastin fibers in the aortal anatomy.

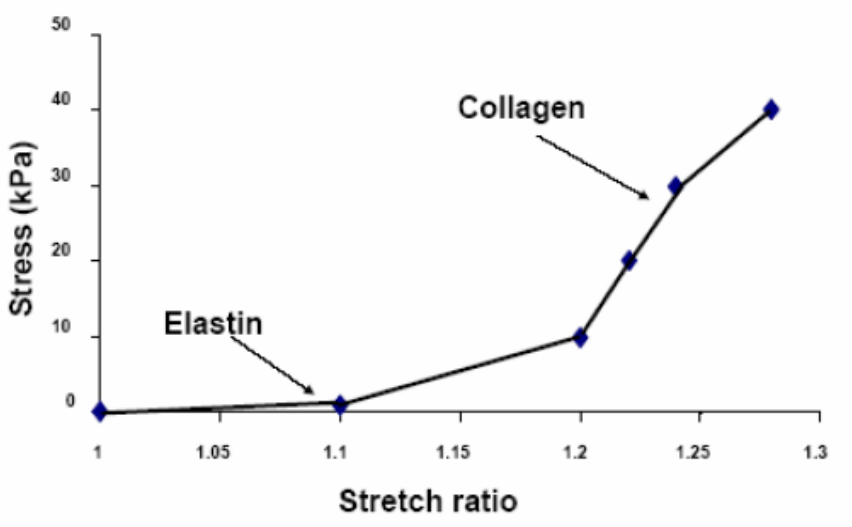

Figure 2.13. A typical stress-strain curve for a blood vessel. Shown are the respective regimes affected by physiologic state and organization of collagen and elastin. Reproduced with data from [209].

2.10.5 Elastin in Vascular Disease

A common pathologic feature of vascular disease is the disruption of elastic fibers and the accumulation of SMCs within the intima between the endothelium and medial layer of the vessel wall resulting in the progressive occlusion of blood flow. Under normal conditions, vascular SMCs in the *tunica media* of blood vessels are quiescent and embedded in a network of elastin-rich ECM that acts as a barrier to SMC migration and proliferation [205]. During atherosclerosis, different cell types, including ECs, platelets, and inflammatory cells release mediators, such as growth factors and cytokines that induce phenotype change of vascular SMC from the quiescent "contractile" phenotype state to the active "synthetic" state, causing them to release matrix proteases degrading the ECM (including elastin) allowing them to aggressively migrate into the subendothelial space and contribute to neointima formation, as depicted in Figure 2.14 [210]. The degradation of

vascular elastin exposes other medial components (i.e. collagen, SMCs) to very high tensile stresses [208]. The high plasticity of SMCs makes these cells susceptible to mechanically induced phenotypic changes that may result in continued aggravated protease secretion and ECM degradation.

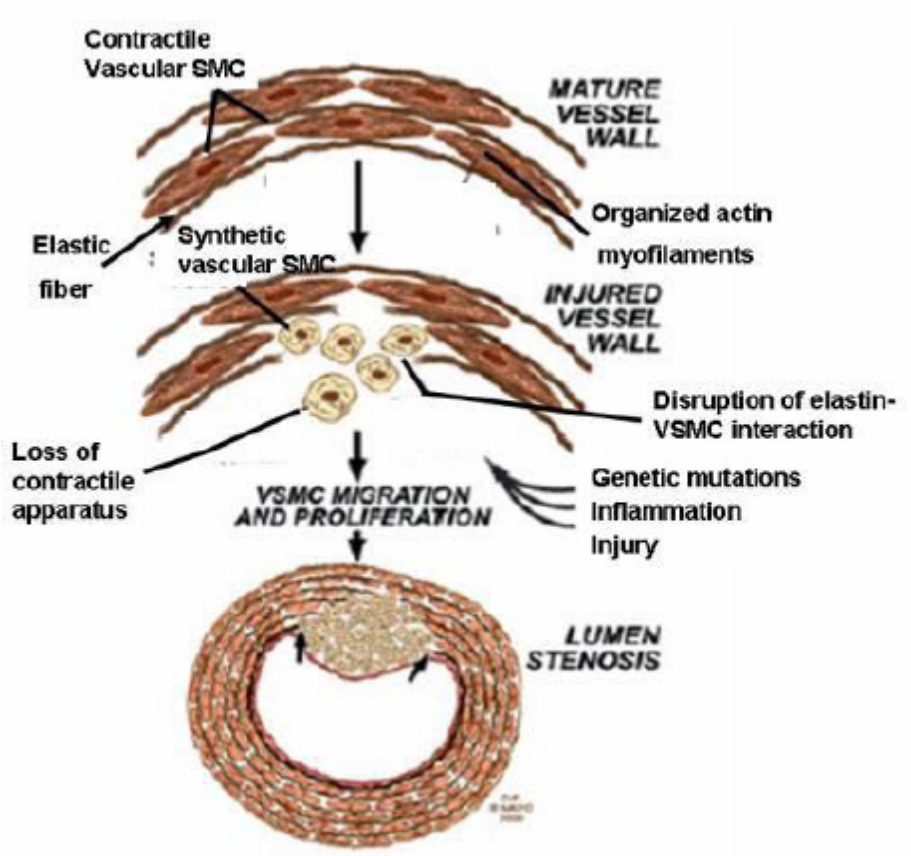

Figure 2.14. Model of elastin –SMC interactions in disease [211].

Since vascular SMCs modulate their phenotype readily, external factors in the arterial wall must instruct them to maintain a quiescent, contractile state if homeostasis is to be achieved. This regulation of vascular SMC activity occurs through defined receptor interactions and signaling pathways. In contrast to other matrix proteins, both *in vitro* and

in vivo studies implicate elastin matrix as a negative regulator of SMC activity within the arterial wall [211]. Thus elastin regulates vascular homeostasis by signaling SMCs through defined pathways to localize around the elastic fibers in organized lamellar units and remain in a quiescent, contractile state. The disruption of elastin by vascular disease, or direct mechanical injury can interrupt cell-matrix signaling and directly up-regulate SMC hyper-proliferation [205]. Thus, the disruption of elastin is not simply an end product of vascular disease, but an important contributor to the pathogenesis of occlusive vascular disease. Therefore, preventing elastin matrix degradation following vascular injury or restoring the lost/ degraded vascular elastin matrix is imperatative for vascular homeostasis restoration [211].

2.11 Engineering Vascular Biomaterials to Promote Elastin Regeneration

Elastin is crucial to maintaining the native structural configuration [128,212-214] and regulating the cell-signaling pathways [4-7] of blood vessels. Thus, the failure to reinstate a healthy elastin matrix, when damaged by disease (e.g., inflammation-mediated elastin degradation in atherosclerosis) can severely compromise vessel homeostasis [81,215]. Therefore, in addition to achieving functional and complete endothelialization, a major concern in the development of tissue-engineered vascular constructs is the ability of scaffolding materials to modulate SMC behavior and encourage the regeneration of elastin-rich matrix.

2.11.1 Synthetic Scaffolds

The most widely used synthetic scaffolds are poly-lactic (PLA), poly-glycolic acid (PGA), and poly-L-lactic acid (PLLA). Although these scaffolds are not ideal from the standpoint of eliciting poor cell attachment, PLLA has been shown to favor elastogenesis [216]. SMCs seeded onto polyhydroxyalkanoates synthesize uniformly alligned elastin and collagen fibers in the direction of blood flow. Previous attempts by Stock *et al.* [82] to regenerate elastin on laminin-coated PGA scaffolds *in-vitro*, did not replicate the amounts and ultrastructure of elastin, synthesized by the same scaffolds when implanted *in-vivo* [82]. This underlies the absence of cell signals controlling elastin mRNA expression *in vitro* and also leads to the conclusion that biosynthesis and crosslinking of elastin appears to be one of the most complex and tightly regulated processes during blood vessel maturation. Application of mechanical stimuli (e.g., dynamic stimulation), growth factors (e.g., TGF-β), and of stem cells (e.g., endothelial progenitor cells) can upregulate amounts of elastin biosynthesis within synthetic scaffolds but not to the extent of mimicking native arterial elastin [216]. Thus, biological scaffolds, and more importantly ECM scaffolds, which theoretically would be expected to elicit more closely native cell responses have gained much attention in the context of elastic tissue regeneration [216].

2.11.2 Biological Scaffolds

Biological scaffolds are normally fabricated from one or all the components such as elastin, collagen, glycosaminoglycans and more recently of fibrin, which has been

clinically approved for promotion of elastin biosynthesis when incorporated in a three dimensional (3D) arrangement within scaffolds. However, each of these components differs in the levels of elastin biosynthesis they elicit. Previously, Ramamurthi and Vesely showed enhanced elastin biosynthesis by rat neonatal SMCs cultured onto hyaluronic acid gel scaffolds as compared to controls (plastic) [216]. Collagen scaffolds fail to regenerate elastin *in vitro* even in presence of seeded vascular SMCs. Long and Tranquilo showed higher levels of elastin biosynthesis by neonatal vascular SMCs seeded onto fibrin scaffolds and within fibrin-collagen constructs [114]. Cells entrapped and cultured within 3D fibrin gels allowed formation of complex elastin geometries similar to that observed in native elastin. Although promising, above results were generated by neonatal SMCs and dermal fibroblasts; both cell types that retain high elastogenic potential, unlike adult SMCs [217]. Also, the organization of elastin fibers into structural networks, and their mechanical properties were not characterized. Yet, this study validates previous claims as to the overall superiority of 3D, ECM-based cell scaffolds over 3D synthetic scaffolds or two dimensional (2D) monolayer cell cultures to efforts to simulate the chemical and physical environment of tissues [64,114,218]. Cells with 3D scaffolds exist in a more natural environment in which they contact other cells and ECM in three dimensions and are therefore expected to more closely evoke native cell responses than 2D substrates. Lee *et al*. has demonstrated in a study involving SMCs seeded onto ECM scaffolds that the phenotype of SMCs in engineered tissues is strongly regulated by the chemistry of scaffold *in vitro*, as a result of which SMCs exhibited a differential cell growth and ECM production depending upon the scaffold to which they

adhered [219]. More specifically elastin production was stimulated on PGA scaffolds, used as controls in comparison to enhanced collagen production onto collagen I scaffolds [219]. So it was elucidated by this study that, 2D culture models still provide useful information since trends in scaffold chemistry- dependent variations of cell phenotype and matrix synthesis are maintained, but not necessarily to the same levels, when translated into a 3D culture system. The physical and mechanical characteristics of the scaffold are important only to exaggerate or dampen scaffold-chemistry-dependent cell responses or direct the structural organization of the synthesized matrix towards defined end goals [219]. Since gene expression of cells cultured within 3D scaffolds, as within native tissues, can be regulated by various scaffold-derived cues including cell adhesion molecules, growth factors, and mechanical stimuli, ECM-based scaffolds are more likely to evoke native integrin-ECM interactions and preserve the native cell phenotype; similar variations in the type and extent of cell receptor-ECM ligand interactions with different ECM molecules can profoundly influence cell phenotype and matrix (e.g., elastin) synthesis [64,114,218]. Accordingly, successful up-regulation of elastin synthesis and it's organization into mature elastic tissue is crucially contingent on the selection of an appropriate scaffold material from among a sub-set of ECM molecules shown to actively facilitate elastogenesis *in vivo*. One class of ECM molecules that may have great potential as elastogenic cell scaffolds are glycosaminoglycans (GAGs) [220].

2.12 Hyaluronic Acid and its use as Vascular Regenerative Biomaterial

Over the years, the components of the ECM have proven to dynamically

contribute to tissue homeostasis. Hyaluronic acid, a GAG, in particular, appears to have three major characteristics resulting in an array of dynamic functions: unique hydrodynamic properties, interactions with extracellular hyaladherins and cell signaling capability. These properties of hyaluronic acid seem to be molecular weight dependant. Therefore, we seek to manipulate these characteristics by combining different molecular weights of hyaluronic acid into a vascular biomaterial capable of stimulating endothelialization and elastogenesis.

2.12.1 Glycosaminoglycans

The ECM, once regarded simply as a structural scaffold, is now recognized as an important modulator of cell phenotype and function. From the tissue engineering perspective, it is increasingly apparent that ECM molecules elicit cell responses that are less exaggerated and more representative of cell behavior in native tissues. This is largely due to the biomechanical and biochemical signaling provided by such substrates to cultured cells.

A class of ECM molecules that are increasingly studied in the context of cell culture scaffolds are glycosaminoglycans (GAGs). These molecules are long unbranched polysaccharides that contain a repeating disaccharide unit. The disaccharide units are composed of at least one of two modified sugars (N-acetylgalactosamine, GalNAc; N-acetylglucosamine, GlcNAc) and a uronic acid such as glucuronate or iduronate. Although each of these GAGs has a predominant disaccharide component, heterogeneity does exist [199]. GAGs have a high negative charge and extended conformation that imparts

a high viscosity to the solution. Along with the high viscosity of GAGs comes low compressibility, which makes these molecules ideal for a lubricating fluid in the joints. At the same time, their rigidity provides structural integrity to cells and maintains passageways between cells, allowing cell migration. GAGs are also capable of interacting with cell through specific receptors and binding cell signaling molecules controlling cellular events. The specific GAGs of physiological significance are hyaluronic acid, dermatan sulfate, chondroitin sulfate, heparin, heparan sulfate, and keratan sulfate [199]. These GAGs are found in a multitude of tissues, as listed in Table 2.3.

2.12.2 Hyaluronic Acid Structure and Properties

Hyaluronic acid is a large, linear, negatively charged GAG. First discovered in the vitreous humor by Meyer and Palmer in 1934 [221], the GAG was named hyaluronic acid due to its naturally glassy state and its high uronic acid content. The term *hyaluronan* was later proposed by Endre Balazs in the 1980's, to encompass the different forms the molecule can take such as the acid form (hyaluronic acid) and the salts (i.e. sodium hyaluronate), which form at physiological pH [30].

Type of GAG	Localization	Characteristics
Hyaluronate	Synovial fluid, vitreous humor, ECM of loose connective tissue	Large polymers, shock absorbers
Chondroitin sulfate	Cartilage, bone, heart valves	Most abundant GAG
Heparan sulfate	Basement membranes, components of cell surfaces	Contains higher acetylated glucosamine than heparin
Heparin	Component of intracellular granules of mast cells lining the arteries of the lungs, liver and skin	More sulfated than Heparan sulfates
Dermatan sulfate	Skin, Blood vessels, heart valves	
Keratan sulfate	Cornea, bone, cartilage aggregated with Chondroitin sulfates	

Table 2.3 Characteristics of glycosaminoglycans [199].

2.12.3 Structure of Hyaluronic Acid

The hyaluronic acid (HA) molecule is a polymer chain consisting of repeating disaccharide units of N-acetyl-D-glucosamine (GlcNAc) and D-glucuronic acid (GlcUA) [17] linked together by alternating b1,3 and b1,4 glycosidic bonds, as shown in Figure 2.15. Each repeating disaccharide unit has one carboxylate group, four hydroxyl groups and an acetamido group. The negative charge of the molecule is due to ionization of the carboxyl groups of the glucuronic acid constituents at physiological pH.

HA is unique among the GAGs in terms of its structure and cellular synthesis. Unlike other GAGs, HA is not sulfated or found covalently attached to proteins as a proteoglycan but it is a component of the proteoglycan complexes with in the ECM. HA polymers are very large (200 – 10,000 kDa) with an extended length of 2-25 μm allowing it to displace a large volume of water. This property makes them excellent lubricators and shock absorbers. Other GAGs are relatively smaller, on the order of 15 – 20 kDa. HA is

also synthesized on the inner surface of the plasma membrane, while other GAGs are produced by enzymes within the golgi apparatus of cells [128,222].

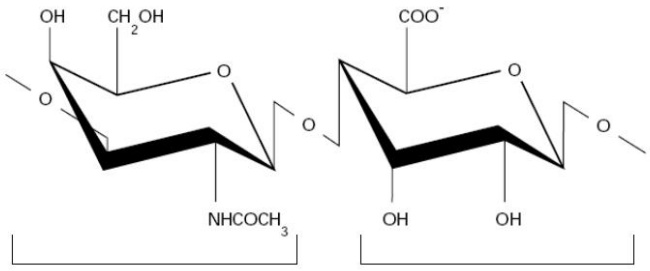

Figure 2.15. Structure of HA [63].

2.12.4 Synthesis of Hyaluronic Acid

Three transmembrane glycotransferase enzymes (HA synthases: HAS1, HAS2, HAS3) regulate the biosynthesis of HA. The amino acid sequences of these enzymes are similar but they are produced from genes located at three distinct locations of the chromosome. Each enzyme contains two components (or gylcosyltransferases), one adds GlcNAc and the other is responsible for GlcUA with each addition occurring at the reducing end of the growing chain. The HAS enzymes are trans-membrane proteins with an active site located on the inner surface of the plasma membrane where HA is polymerized from monomer units. As the HA chain is being synthesized, it is extruded through the plasma membrane via the HAS complex onto the cell surface or into the ECM. This unrestrained synthesis mechanism allows HA to amass into large chain lengths, exceeding four million daltons [223].

2.12.5 The Catabolism of Hyaluronic Acid

The turnover of HA within the body is relatively rapid compared to other ECM molecules. The half-life of HA in the blood is 5 minutes and in the skin epidermous is half a day, while collagens have half-lives of several weeks [30,224]. High molecular weight HA (HMWHA) is degraded extracellularly through enzymatic and non-enzymatic processes. Enzymatic degradation occurs by the action of hyaluronidases, chondroitinases and hexosaminidases. Non-enzymatic degradation of HA occurs during inflammation and tissue injury and involves reactive oxygen species, hydrogen peroxide and hydroxide radicals [225,226]. This partially fragmented HA is then engulfed and degraded in the lysosomes of tissue cells and macrophages or transferred to the lymph nodes where it is ingested and through an unknown mechanism. The highly degraded product is then transported by the blood to the liver where it is hydrolyzed to single sugars and metabolized [30].

2.12.6 The Biological Functions of Hyaluronic Acid

HA is present in almost every tissue of vertebrates but is most abundant in the ECM of soft connective tissue. Therefore, it is a very important physiologic molecule and has three known molecular functions: (1) It encompasses a large hydrodynamic domain by binding large quantities of salts, metal ions and water molecules; this allows HA to act as a physical barrier preventing disturbances to developing cells or create an uninhibited pathway for migrating cells. (2) HA interacts with HA binding proteins and proteoglycans to form composite ECM which is vitally important to the assembly and

structure of several tissues. (3) HA binds to cell surface receptors that mediate important signaling pathways. All of these molecular interactions with HA involve binding proteins, termed hyaladherins.

2.12.7 Hyaladherins

Hyaladherin is a term given to a diverse group of proteins capable of binding to HA. Many of the known hyaladherins bind to HA through a 100 amino acid sequence called a link module, which contains an immunoglobulin domain and two adjacent link modules. It is thought that the link modules mediate protein-HA binding and the immunoglobulin controls protein-proteoglycan interactions. Hyaladherins are classified as either extracellular or cellular [227-229].

2.12.8 Extracellular Hyaladherins

The interaction between hyaladherins and HA has been implicated in the development and stabilization of the ECM. Aggrecan, a major proteoglycan found within cartilage, strongly interacts with HA through the HA binding domain and stabilizes the ECM. Other major extracellular hyaladherins include vesrican, neurocan, and brevican. The interaction of these molecules with HA is responsible for retaining these proteoglycans within the ECM [228,230,231].

2.12.9 Cellular Hyaladherins

The most well known and characterized cellular hyaladherin is the CD44 receptor

[232]. CD44 is produced from a single gene but several exon splicing combinations result in different isoforms of the receptor. All isoforms are single-pass transmembrane glycoproteins consisting of four functional domains, though a link sequence within the distal extracellular domain is primarily responsible for HA binding. HA-CD44 binding is subject to numerous influences, including glycosylation, alternative splicing, dimerization, receptor clustering, and integrity of the cytoplasmic domain [233]. Depending on the cellular context, the binding of HA results in intracellular CD44 interactions with certain regulatory and adapter molecules including SRC kinases, RHO GTPases, VAV2, GAB1, ankyrin and ezrin [234-236]. Transcription of CD44 is also upregulated in response to proinflammatory cytokines (IL-1) and growth factors (EGF, TGF-b, BMP-7). IL-1 induced elevation of CD44 enhances the ability of SMCs to bind HA, which may be responsible for the increased levels of SMC CD44 expression and HA in atherosclerotic lesions [237,238]. Studies of embryonic development, regeneration and healing, cancer and vascular disease reported that the pericellular matrix surrounding proliferating and migrating cells is highly enriched with HA. This is accomplished by cell surface receptors and HA bound to HAS in addition to HA interactions with extracellular hyaladerins to create a complex, hydrated microenvironment that supports and promotes the behavior of mitotic cells [239,240]. HAS activity also fluctuates with the cell cycle and is maximum during mitosis [241]. Other cellular functions known to be influenced by the HA-CD44 interaction includes cell aggregation, cell-matrix signaling, and receptor-mediated HA internalization and degradation [3,239,242].

The receptor for HA mediated motility (RHAMM) is available in several isoforms

depending on the various splicing combinations and can be present on the cell surface, within the cell cytoplasm or in the nucleus. Surface RHAMM has been implicated in intracellular pathways that activate c-src, focal adhesion kinase and MAP kinases [122,243]. Intracellular RHAMM interacts with the actin cytoskeleton and microtubules. Both surface and intracellular RHAMM regulate Ras [227].

TSG-6 is a multifunctional protein and its actions include neutrophil migration and protease network modulation. It interacts with HA among other ligands, including heparin, chondroitin 4-sulfate, aggrecan, versican, IαI, pentraxin-3 and thrombospondin-1, and its interactions appear to be pH sensitive. Therefore, the function of TSG-6 is likely to be tissue specific with a dependence on pH and GAG content [244]. In addition, the TGS-6/ IαI complex may be able to stabilize the ECM by cross-linking the HA chains [244].

Other more recently discovered hyaladherins include the hepatic HA clearance receptor, LYVE-1 and layilin. The hepatic HA clearance receptor is present on the surface of endothelial cells and activated macrophages in the liver, spleen and lymph nodes. It is thought to remove HA from the blood during steady-state tissue remodeling [245]. LYVE-1 expression is limited to the lymph vessel endothelium and interacts with HA through a tightly regulated mechanism [246]. Layilin contains a membrane-binding site for talin, an ECM linker between the cytoskeleton and the cell membrane, and is thought to mediate cell migration and morphology [247].

2.12.10 Molecular Weight-Specific Biologic Effects of Hyaluronic Acid

HA is known to be involved in many fundamental physiological and pathological

processes such as cell development, migration, adhesion, proliferation and differentiation, immunogenicity, inflammation, wound healing, multi-drug resistance, angiogenesis, malignant transformation, and ECM stability and integrity. Some of the functions of HA appear to be molecular weight dependant. High molecular weight HA (HMWHA) binds cells and extracellular hyaladherins to maintain the structural stability and integrity of tissues with few stimulatory effects on cells. In contrast, low molecular weight HA (LMWHA) interacts with cellular receptors resulting in a multitude of cell signaling cascades. In addition, the large strands of HMWHA is capable of blocking biomolecules from stimulating the cell while LMWHA allows these biomolecules to influence cell behavior, as illustrated in Figure 2.16.

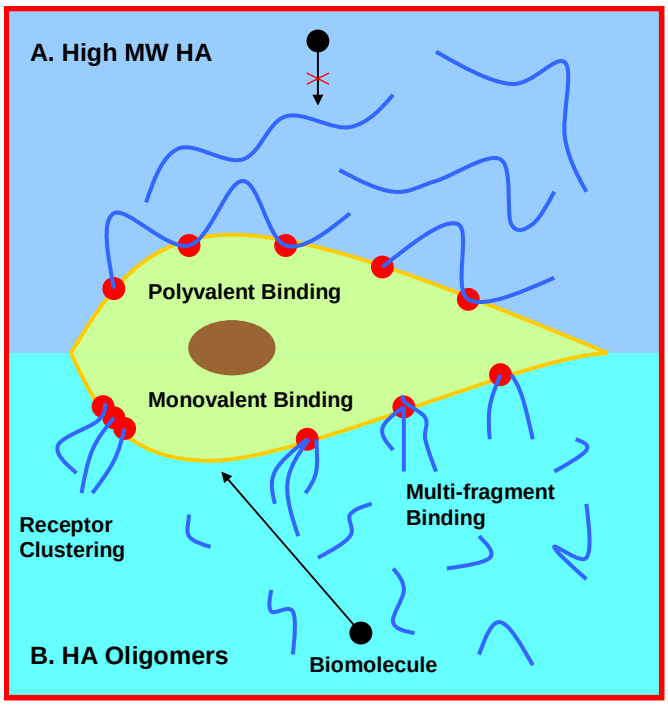

Figure 2.16. Molecular-weight dependent HA-cell interactions.

2.12.11 High Molecular Weight Hyaluronic Acid

HMWHA (> 1000 kDa) is considered to be a space-filling molecule primarily impacting cells through physical interactions. HMWHA binds to cells in a polyvalent manner and surrounds them creating a dynamic protective coating through additional interactions with extracellular hyaladherins (Figure 2.16). During embryonic development, HMWHA surrounds migrating and proliferating cells [229]. This coating isolates proliferating cells, allowing them to develop without being disturbed from the extracellular environment, and also provides hydrated migration pathways for cells. In the same manner, HMWHA surrounds proliferative tumor cells and acts as the interface at the site of tumor invasion into the host tissue [241]. Additionally, HMWHA is inherently anti-inflammatory and immunosuppressive by preventing free radicals and infectious organisms from migrating into the tissue [218]. Therefore, HMWHA allows tissues to heal by inhibiting the entry of damaging molecules and organisms, and thus reduces scar formation. This may be significant in the fetal circulation where HMWHA is found in high concentrations. HMWHA also appears during the early stages of wound healing by creating spaces through which leukocytes can infiltrate the wound area and binding fibrinogen to induce clot formation. However, HMWHA must be fragmented in order stimulate-receptor mediated cellular responses.

2.12.12 Hyaluronic Acid Oligomers

HA oligomers (0.75–10 kDa) are capable of binding to cell surface receptors in a monovalent manner resulting in the stimulation of specific cell signaling cascades,

possibly by allowing HA–bound receptors to cluster and/or multiple HA molecules to bind to a single receptor, as depicted in Figure 2.16. Therefore, this form of HA communicates directly with the cells influencing their metabolic functions.

Based on previous studies, HA oligomers, formed by enzymatic digestion of larger HMWHA, are thought to play a role in wound healing due to their ability to promote angiogenesis *in vivo* and the proliferation of vascular endothelial cells cultured *in vitro* [23,229]. The reason for this occurrence may involve specific receptors and signaling pathways of these endothelial cells. The stimulation of the CD44 receptors enhances EC production of vascular endothelial cell growth factor (VEGF) and therefore promotes endothelial cell proliferation [26]. In addition, it has been shown that HA oligomers stimulate endothelial cells to produce angiogenic proteins [248] and enhance the synthesis of collagen types I and VIII which are produced by ECs of the angiogenic phenotype. This angiogenic HA oligomers also stimulate EC proliferation, migration and adhesion by activating focal adhesion kinase and mitogen activated protein kinase pathways [249,250]. HA oligomers have been discovered within proliferating ECs and SMCs possibly interacting with intracellular receptors.

HA oligomers can, under specific circumstances, promote early inflammation, which is critical for initiating wound healing, but then can moderate later stages of the process, allowing matrix stabilization and reduction of long term inflammation [18]. Studies have shown that HA fragments induce the expression of cytokine gene expression in macrophages, which is crucial for initiating and maintaining the inflammatory response. HA oligomers are potent activators of dentric cells, an antigen presenting cell of the

immune system, and most pro-inflammatory HA fragments can signal dendric cells and ECs through TLR-4 [251,252].

The production of ECM, specifically elastin, is highly upregulated in SMCs cultured in the presence of HA oligomers [220]. Recent studies by our group found SMCs, in the presence of exogenously supplemented HA oligomers, increased production of tropoelastin, desmosine and crosslinked elastin [31,32]. In addition, the elastin fibers were laterally aggregated and thicker than those produced by SMCs cultured with HA of higher MW. These findings encourage further study into the utility of HA biomaterials as scaffolds for elastic tissue regeneration.

These studies provide a general idea of how HA can be used as a biomaterial. But in order to create a long-term HA implant, it must be converted into a stable, insoluble biomaterial. HA is amenable to chemical derivatization and cross-linking, and can yield a variety of biomaterials that exhibit a wide range of biologic, chemical, and mechanical characteristics [253-255].

2.12.13 Hyaluronic Acid Derivitization and Cross-linking Strategies

Chemical modification of HA has been well recognized as a means to enhance the biostability and mechanical properties of the material. Two possible methods to modify HA are through derivatization and cross-linking. Both derivitization and cross-linking can be achieved through reactions between the available functional groups of HA (COOH, OH). Derivitization of the hydroxyl groups include carbodiimide-mediated reactions, especially with adipic dihydrazides (ADA), and esterification [256,257]. ADA modified HA

can be loaded with drug molecules and highly esterified HA (HYAFF) is temporarily insoluble is water and can be fabricated into a degradable biomaterial. Carboxyl group derivitization strategies consist of sulfation, esterification, isourea coupling and periodate oxidation [258]. Sufation was used to increase the blood compatibility of HA, and esterification and isourea coupling processes were used to bind therapeutic agents to HA. Periodate oxidation may damage the HA molecule but is used to create reactive bisaldehyde on HA. Reductive amination of the reducing end of HA is used to fluorescently label HA molecules and quantify them through electrophoresis. Some of these derivitization techniques are also used as cross-linking strategies.

A number of cross-linking mechanisms involving carbodiimides [259], hydrazides [260], bisepoxides [259] and esters [261] have been documented, as seen in Figure 2.17. These cross-linking mechanisms do not involve the biologically active acetyl groups and hence retain the highly biocompatibility and non-antigenicity of the native HA molecule [262]. Carbodiimide cross-linking combines the carboxyl groups of HA generating two N-acylurea linkages in a by product free environment [259]. An interesting HA derivative involves cross-linking HA with small amounts of an aldehyde, such as formaldehyde to produce a unique soluble polymer fluid with very high viscoelasticity [200]. Similar materials can be obtained by cross-linking of HA with divinyl sulfone (DVS). Both of these cross-linkers preferentially react with the hydroxyl groups of the HA molecule. Balazs first coined the term *hylans* to describe these cross-linked HA gels. Limited testing has suggested the biocompatibility of hylans to be close to that of uncross-linked HA [262,263]. The nondestructive environment involved in photo-cross-linking has the

advantage of allowing cellular incorporation within the gel as it forms. In this process, the HA hydroxyl groups were derivatized with glycidyl methacrylate and in the presence of a photoinitiator were irradiated at 365 nm resulting in stable cross-links [264]. With the advent of such cross-linked HA gels and films, there are now a number of biomedical products on the market aimed towards the prevention of post-surgical tissue adhesions [263] (i.e. Seprafilm® and Sepracoat® from Genzyme, Lubricoat® from Lifecore Corporation. The biomedical applicability of these biomaterials is based on their non-interactivity with these cells rather than ability to evoke healthy cell responses [263].

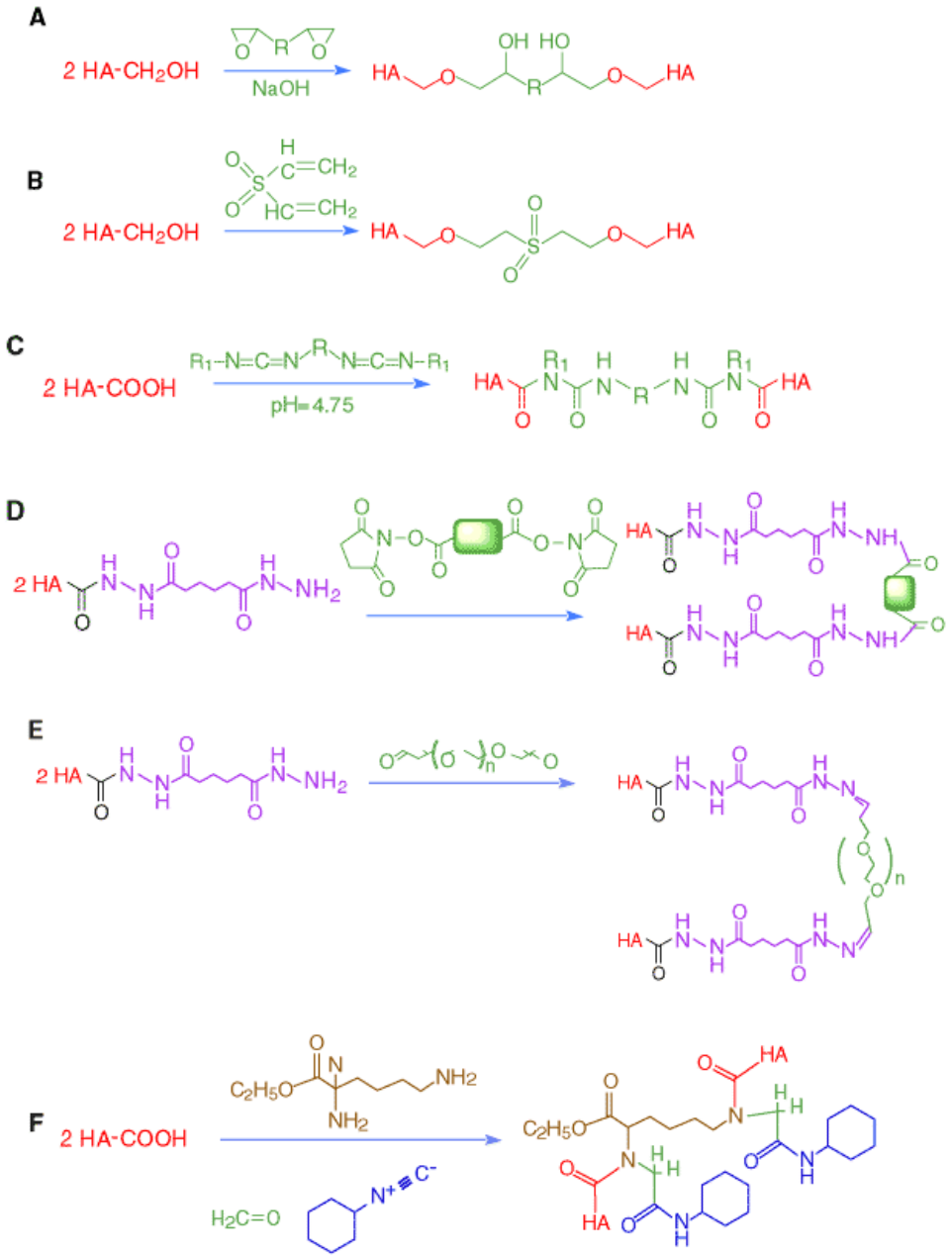

Figure 2.17 Chemical cross-linking strategies for HA. (A) bisepoxide cross-linking, (B) divinylsulfone cross-linking, (C) biscarbodiimide cross-linking, (D) ADH cross-linking with a homobifunctional linker, (E) ADH cross-linking with a macromolecular linker, (F) HA cross-linking using four-component condensation with formaldehyde, cyclohexyl isocyanide, and lysine ethyl ester [258].

2.12.14 Hyaluronic Acid Biomaterials

HA occurs naturally in connective tissues. Most cells have the ability to synthesize HA at some point during their cell cycle, implicating its function in several fundamental biological processes [18]. HA is also highly biocompatible and does not elicit a foreign-body response upon cross-transplantation due to the homology of the HA structure across species [18] and its dissolution into simple sugars. In addition, its physical properties (viscoelasticity, hydration) make it suitable for various medical applications. Commercially, HA is isolated from tissue sources including the umbilical cord, synovial fluid, skin and rooster comb, or produced through bacterial fermentation. Therefore, HA has been used as a biomaterial for various medical and pharmaceutical applications.

In recent years, HA has been recognized for its excellent potential as a biomaterial for effective tissue regeneration. Although the mechanism interaction between HA and the human body is still incompletely elucidated but its promising characteristics have assured its extensive use as a tissue engineering scaffold, most recently for cartilage [20] and skin repair [21]. It is also used as a viscoelastic, ophthalmic filler material to support the implantation of intraocular lenses in cataract patients [265]. HA and its derivative formulations have been developed as topical, injectable and implantable vehicles for the controlled and localized delivery of biologically active molecules for the treatment of bone and skin disease [266,267]. In recent years, HA has found applicability abroad as a joint lubricant in arthritic joints, owing to its favorable rheological properties [268]. Recently, Anika, Biomatrix, and Fidia obtained FDA approval for the use of HA as an injectable in the USA [269]. Since the molecule is highly anionic, hydrophilic and not conducive to

protein deposition, HA or its derivatives (i.e. sulfated HA) have been explored as hydrophilic coatings for catheters, guidewires, and sensors, to improve their biocompatibility [270]. In addition, HA has been used as an implant fluid /film to improve lubricity, and reduce fouling and tissue abrasion [218]. In these applications, the long-term success of the product is significantly facilitated by the inherently non-antigenic and non-immunogenic properties of HA, a result of their strong homology of structure across species [263].

2.13 Project Scope

Our objective is to investigate the potential use of HA as a regenerative vascular material. Specifically, we aim to examine the size-specific ability of HA to promote vascular endothelialization and elastogenesis, as an exogenous supplement, a surface coating and a chemically-crosslinked hydrogel. The results of this study will allow us to determine the optimal fragment size (i.e. HMWHA, HA fragments, HA oligomers) and presentation modality (i.e. exogenous, surface coating, hydrogel) of HA for the regeneration of the endothelium and production of an elastin rich matrix by SMCs.

CHAPTER 3

EXOGENOUS HYALURONIC ACID CUES TO PROMOTE FUNCTIONAL ENDOTHELIALIZATION OF VASCULAR CONSTRUCTS

3.1 Introduction

With the evolution of tissue engineering, the choice of scaffolding materials for vascular regeneration has shifted from purely synthetic biomaterials to biological polymers, such as extracellular matrix (ECM) proteins (i.e. collagen, fibrin), that could hypothetically more faithfully elicit native cell responses and likewise regenerate damaged tissue [208,271]. However, the necessity to chemically stabilize such biopolymers, and process them to remove immunogenic donor epitopes can compromise their native biological/ mechanical characteristics. Thus, recent studies have focused on other ECM molecules such as certain glycosaminoglycans (GAGs), which are non-immunogenic [272], and do not induce chronic inflammation [273] likely due to the preserved structural homology across species [18]. One such GAG is hyaluronan (HA), whose content and form in vessels varies with their state of development and health [274,275]. In vivo, HA vitally regulates embryonic development, tissue organization [276], wound healing, and angiogenesis [21]. In a biomaterials context, long-chain or high molecular weight HA (HMW >1000 kDa) is non-cytotoxic [264], non-thrombogenic [277], and can endure chemical stabilizion with little biologic alteration. Since various functional groups (hydroxyl, carboxyl) are present on the HA chains, HA can be variably derivatized and crosslinked to generate biomaterials with diverse physical and mechanical properties [278], and also bound to peptides, matrix proteins, and growth factors to help modulate cell responses.

However, due to the vast excess of HA over incorporated crosslinker amounts and the fact that biologically active functional groups (e.g., acetyl) are not involved in crosslinking, favorable biologic properties of the parent HA chains can be retained. These properties in addition to the presence of HA in the vascular intima and media, and its mechanical versatility render it an attractive biomaterial for effective cardiovascular tissue regeneration.

Prior studies have suggested that biologic effects of HA are highly specific to HA molecular weight (i.e. fragment size) and the cell type they interact with [18,19,23,26,229,234,241,249-252]. HMWHA typically stabilizes tissues and impacts cell behavior through physical, rather than via biologic interactions. It aids embryonic development by surrounding cells with a fluid environment that permits their migration, and under specific circumstances, creates pericellular sheaths that prevent cell-cell communication and cell response to extracellular cues [229]. Additionally, HMWHA is inherently anti-inflammatory and immunosuppressive by preventing free radical-generating microbes from migrating into tissues [18]. In contrast, oligomers of HA (0.75–10 kDa) interact dynamically and differently with cellular HA receptors (e.g., CD44, Receptor for HA-Mediated Motility or RHAMM, Toll-Like Receptors or TLRs) to induce a multitude of cell signaling cascades.

A key challenge to reinstating vascular homeostasis is the restoration of an intact, complete, normally functional, and non-activated EC lining along the luminal vessel/ graft surface [279], by EC recruitment from the surrounding tissue. Since synthetic materials poorly evoke such a response, other, more readily endothelializable materials must be

explored. In this context, HA oligomers cues have been shown to promote angiogenesis *in vivo* and proliferation of ECs derived from various tissue sources (e.g. vascular, pulmonary) when cultured *in vitro* [19,23] by stimulating EC receptors that trigger their migration [280,281] and enhance the production of vascular endothelial cell growth factor (VEGF), an angiogenic stimulator [26]. However, to date, there has been no systematic and comprehensive study that has simultaneously investigated the size-specific effects of HA on all aspects of EC behavior, including their proliferation, angiogenic potential, functionality, and activation.

Previous studies concentrate only on HMWHA and HA oligomers, therefore, in elucidating the effects of HA on EC behavior, we have presently chosen to initially investigate a wide range of HA molecular weights to determine the fragment size that most ardently stimulates HA proliferation. Continued study was then focused on HMWHA and the most proliferative fragment. Since pure HA oligomers (6mers, MW=1156 Da), which we previously showed to usefully promote EC proliferation, are prohibitively expensive to procure and can be arduous to prepare, we sought to determine if rough enzymatic digests of high MW HA would elicit identical EC responses, and thus be used instead.

3.2 Materials and Methods

3.2.1 Preparation of HA Oligomer Mixtures

Closely-defined mixtures of oligomers were generated by enzymatic digestion of *streptococcus equi* - produced HA sodium salt (5 mg/ml) of MW = 1500 kDa (HA 1500;

Sigma, St Louis, MO) in digest buffer (150 mM NaCl, 100 mM CH_3COONa, 1 mM Na_2-EDTA, pH 5.0). HA was digested with 0.45, 1.8, 4.5 and 9 mg/ ml of *testicular hyaluronidase* (Sigma, St Louis, MO; 439 U/mg) for 3 - 60 h at 37 °C. The enzyme was then precipitated and its activity terminated by boiling (2 min), and then cooled on ice. Following centrifugation (2800 rpm, 10 min), to separate the enzyme from the mixture, the supernatant was dialyzed in water (12 h) using Tube-O-Dialyzer™ tubes (Millipore, Billerica, MA) with a MW cut-off of 1 kDa, and then freeze-dried overnight to generate HA oligomers. Aliquots of the mixture were then analyzed by fluorophore assisted carbohydrate electrophoresis (FACE) for size-characterization of HA fragments.

3.2.2 Size - Characterization of HA Fragments in Oligomer Mixtures

For FACE analysis, a 50-µg sample of the digest was dissolved in 40 µl of a 0.0125 M solution of the fluorescent dye 2-aminoacridone (AMAC, Sigma) prepared in acetic acid/ DMSO (3:17 v/v), and incubated for 15 min in the dark. A 40-µl aliquot of an aqueous solution of 1.25 M sodium cyanoborohydride (Sigma) was then added to each sample and incubated (37 °C, 16 h, dark). Following this, 20 µl of glycerol was added to each sample. The standards (oligomer ladder, 2mer, 6mer; Associates of Cape Cod, East Falmouth, MA) were prepared in the same manner.

For electrophoresis, all 8 lanes of a polyacrylamide MONO® gel (Glyko, San Leandro, CA) were loaded simultaneously with 4 µl of sample/ standard and run with MONO® gel running buffer (Glyko) at < 10 °C, as described previously [282]. Samples were electrophoresed at a constant 500 V with a starting current of 25 mA/ gel and a final

current of 10 mA/ gel for 80 min. After electrophoresis, the gels were illuminated with UV-B light (λ = 365 nm) in a FluorChem 8900 (Alpha Innotech, San Leandro, CA) and band intensities quantified and compared to an HA oligomer ladder (10-20mer; 1915-3811 Da) and commercially procured HA 2mer (397 Da) and HA 6mer (1156 Da; Associates of Cape Cod, East Falmouth, MA) to determine the size range of HA fragments within the digest.

3.2.3 Model to Predict Oligomer Content within Enzymatic Digests of HMWHA

To limit the necessity for iterative changes in digestion parameters towards obtaining specific HA fragment-size distributions, a mathematical model was developed based on the observed digestion outcomes. The effects of hyaluronidase enzyme concentration and digestion time on the amount of HA oligomers (HA 6mer and HA 12mer) produced, was fit using a hierarchial regression analysis (HRA), wherein a new predictor was added to or dropped from that used in the previous analysis based on the statistical significance of a particular model [283]. The quadratic regression model used accommodated linear, curvature and interdependence of digestion time (x) and enzyme concentration (y) and was described as:

$$R = a + b*x + c*y + d*x*y + e*x^2 + f*y^2 \qquad \text{(Eq 3.1)}$$

where R is the dependent variable (amount of HA oligomer), a, b, c, d, e, and f are the estimated regression coefficients. After initialization with the full quadratic regression model given in Equation 1, the backward elimination procedure [284,285] was used to reduce

the number of terms in the model until all the remaining terms were statistically significant ($p < 0.05$). We chose to utilize two digest mixtures in further experiments: D1 (0.45 mg/ ml, 18 h) and D2 (4.5 mg/ ml, 48 h).

3.2.4 Cell Culture

To prepare the HA stock solutions used for exogenous supplementation of HA into the culture media, all forms of HA were dissolved in water (24 h, 4 °C). The HA solutions were then filter-sterilized by passage through a low-protein binding 0.22 μm syringe filter (Millipore). All HA boluses were prepared fresh prior to addition to cell cultures.

Low passage (6-8) adult rat aortic ECs (Cell Applications, San Diego, CA) were selected for this study to be consistent with our intention to conduct future *in vivo* studies in a rat model. Stock cells were trypsinized (0.25% trypsin/ 0.1% v/v EDTA; Invitrogen, Carlsbad CA), pelletted by centrifugation (500*g*, 7 min), resuspended in MCDB-131 supplemented with 10% v/v FBS (Invitrogen), 1% v/v penicillin–streptomycin (Invitrogen), 50 μg/ ml EC growth supplement (Becton Dickinson, Franklin Lakes, NJ), 4 mmol/L L-glutamine (Invitrogen), and 30 U/ml heparin (Sigma). Spent medium was replaced thrice weekly over the 14 days of culture.

3.2.5 DNA Assay for Cell Proliferation

The DNA content of EC monolayers was used to compare the number of cells present at days 1 and 14, and hence quantify the proliferation of ECs in culture. ECs were

seeded at 1×10^4 cells/ well in 6-well plates (A = 9.6 cm^2) with exogenous HA of 1500, 200, 20 kDa (HA 1500; HA 200, Genzyme, Cambridge MA; HA 20, Lifecore Biomedical, Chaska MN), HA 6mer and enzymatic digests of HA oligomers (D1, D2) at doses of 0 (negative control), 0.2, 2, and 20 μg/ ml to assess the size- and dose- specific affects of HA on EC proliferation. To measure their DNA content, briefly, cell layers were rinsed with 1% v/v PBS, free of Ca^{2+} and Mg^{2+}, incubated with 1 ml of 0.25% v/v trypsin/ 0.1% v/v EDTA per well (37 °C, 5 min). The adherent cells were scraped off the substrate, pelletted by centrifugation (500*g*, 7 min) and resuspended in 1 ml of NaCl/ Pi buffer (4 M NaCl, 50 mM Na_2HPO_4, 2 mM EDTA, 0.02% w/v Na Azide, pH 7.4). Aliquots (495 μl) of this cell suspension were sonicated over ice, and the DNA in the homogenate measured using the fluorometric method described by Labarca and Paigen [286] (n = 3). Actual cell counts were then calculated based on the average DNA content of a diploid cell in G1 phase (6 pg), assuming this amount remained unchanged through the period of culture [287]. Results are reported as the ratio of cells at day 14 to day 1 (proliferation ratio).

3.2.6 Tube Formation (Angiogenesis) Assay

The ability of ECs to form tubes (a measure of angiogenic potential) when cultured with exogenous HA, was measured. Matrigel™, a matrix that promotes EC tube formation *in vitro*, was cast in 24-well culture plates (Beckton-Dickson; 100 μl/ well), heat-treated for 30 min at 37 °C to stimulate crosslinking, seeded with ECs (7.5×10^4 cells/ well) and incubated with exogenous HA (HA 1500, D2, HA 6mer; 0 and 2 μg/ ml)

for 48 h at 37 °C. Suramine (40 μM, Calbiochem, San Diego, CA) was used as a negative control; TNF-α (10 ng/ ml) was added as an additional positive controls. After incubation, the media was aspirated and the cells were washed twice with Hank's Balanced Salt Solution (HBSS) and stained with Calcein AM (8 μg/ ml, Invitrogen) for 30 min at 37 °C. The cells were washed with HBSS to remove excess dye and imaged on an inverted florescent microscope (Eclipse TE2000-S, Nikon, Melville, NY) and the number and length of tubes formed quantified using Image Pro Plus software (n = 10 regions/ culture; n = 3 cultures/condition).

3.2.7 Flow Cytometry

Expression levels of functionality marker proteins and cell adhesion molecules (CAMs) by ECs, in presence or absence of added HA/ oligomer cues, were compared by flow cytometry. Monolayers of ECs (n = 3/ marker) were grown to semi-confluence (~80%) in 6-well plates (3 cultures/ maker; 2-3 × 10^6 cells/ culture) over 3 - 4 days, and were then supplemented with HA (HA 1500, D2, HA 6mer; 0 and 2 μg/ ml) for 48 h, rinsed with PBS containing 0.1% w/v sodium azide (PBS-azide) and finally incubated (10 min, 37 °C) with 1 ml of cell dissociation solution (Sigma) to gently release the cells into solution. The suspended cells were washed once with PBS-azide and then labeled for the expression of von Willebrand factor (vWF; for EC identity), low density lipoprotein receptor (LDLR; for EC identity), endothelial nitric oxide synthase (eNOS; for EC anti-platelet activity) and vascular endothelial cell receptor 2 (VEGFR2; for EC function). EC activation was gauged from the extent of expression of CAMs involved in attracting

leukocytes and platelets to the EC surface. These included platelet-endothelial cell adhesion molecule 1 (PECAM-1), intracellular adhesion molecule 1 (ICAM-1), and vascular cell adhesion molecule 1 (VCAM-1).

For direct immunolabeling, cell suspensions were incubated at 4 °C for 1 h with fluorescein isothiocyanate (FITC)-conjugated mouse anti-rat CD54 (ICAM-1; Abcam, Cambridge, MA) and Alexa 488-conjugated mouse anti-rat CD106 (VCAM-1; Biolegend, San Diego, CA) diluted 1:100 v/v in PBS-azide. For indirect immunolabeling, cell suspensions were incubated under the same conditions with the following anti-rat antibodies diluted 1:100 v/v in PBS-azide: rabbit anti- vWF, rabbit anti- eNOS, rabbit anti- LDLR, rabbit anti-VEGFR2 and mouse anti-CD31 (PECAM-1) (all from Abcam). The cells were subsequently washed once with PBS-azide and immunolabeled with a secondary antibody (1:1000 v/v in PBS-azide) of donkey anti-rabbit IgG coupled with phycoerythrin (PE) or donkey anti-mouse IgG coupled with PE (Abcam) for 1 h at 4 °C. For immunolabeling of vWF and eNOS, cells were permeablized with methanol for 1 min prior to incubation with the antibodies. ECs incubated with the secondary antibodies processed under PE conditions and untreated EC processed under FITC/ Alexa 488 conditions were used as additional negative controls to confirm indiscriminate binding/ fluorescence did not occur. The CAM samples were also compared to cultures supplemented with TNF-α (10 ng/ ml, positive control). The shifts of the peak intensities are reported normalized to the no HA condition.

3.2.8 Thrombomodulin Assay

Endothelial cell surface expression of thrombomodulin, a potent inhibitor of coagulation, was measured as described previously [288]. Briefly, ECs grown to semi-confluence in 24-well plates (A = 1 cm^2), were incubated with HA (HA 1500, D2, HA 6mer; 0 and 2 μg/ ml) for 48 h, washed twice with phenol red-free DMEM: F12 media (Invitrogen) and incubated (1 h) with 250 μl of medium containing human α-thrombin (0.1 NIH U/ ml; Haematologic Technologies, Essex Junction, VT) and human protein C (12 μg/ ml; Haematologic Technologies). The α-thrombin was subsequently inactivated with the addition of access hirudin (4 ATU/ ml; American Diagnostica, Stamford, CT). Aliquots (70 μl) of this solution was combined with 30 μl of S-2366 (450 mM; Chromogenix, Milano, Italy) and incubated at room temperature for 5 min before measuring the absorbance at λ = 410 nm using a spectrophotometer (Molecular Devices, Sunnyvale, CA) (n = 3). The samples were compared to cultures supplemented with TNF-α (10 ng/ ml), a second positive control.

3.2.9 Platelet Adhesion

The thrombo-protective properties of ECs cultured with exogenous HA/oligomers were quantitatively estimated by the lack of platelet attachment onto their surface. ECs were grown to confluence in 4-chamber polystyrene chamber slides, then cultured with exogenous HA (HA 1500, D2, HA 6mer; 0 and 2 μg/ ml) for 48 h. These samples were compared to cultures supplemented with TNF-α (10 ng/ ml, positive control). Following removal of the culture medium, and a gentle rinse with phosphate-buffered saline (PBS,

1X), aliquots (150 µl) of rat plasma (Innovative Research, Southfield, MI) were overlaid atop each of the the EC monolayers and incubated (15, 45 min) at 37 °C (n = 3 /substrate). Aliquots of this overlaid suspension were then recovered and counted for platelets in a coulter counter (Beckman-Coulter, Fullerton, CA) (n = 6). The stock plasma platelets were also counted. Platelet deposition on the EC monolayers was estimated by quantifying the number of platelets removed from the stock suspension.

3.2.10 Electron Microscopy of Adherent Platelets

SEM was used to confirm the degree of platelet adhesion onto EC layers, as quantitatively measured (see section 3.2.9) and their activation, when exposed to HA/oligomer. Activation of adhered platelets was assessed from EC-induction of platelet aggregation/focal clumping. In preparation for SEM, following a gentle rise with 1X PBS, the adhered platelets were fixed with 2% w/v glutaraldehyde in 0.1 M Na-cacodylate buffer with 0.1 M sucrose (1 h, room temperature), treated with filtered 1% tannic acid in sodium cacodylate buffer (1 h, room temperature), and incubated with 1% w/v osmium tetroxide in 0.1 M Na-cacodylate buffer (1 h, room temperature). The samples were then dehydrated in a graded series of ethanol (70-100% v/v), and dried by incubation with HMDS (hexamethyldisilazane, Electron Microscopy Sciences, Fort Washington, PA) for 3 min. The HDMS was aspirated and the samples were allowed to air-dry in a desiccator (25 min), sputter-coated with gold over 60 seconds in a sputter-coater (VG Microtech) and visualized by SEM.

3.2.11 Cytokine Array

The type and amount of cytokines produced by ECs in response to the presence or absence of exogenous HA/oligomers was determined using an ELISA-based cytokine array to deduce the inflammatory potential of ECs deduced in each case. ECs were cultured in 6-well plates to semi-confluence, and then subjected to exogenous HA (HA 1500, D2, HA 6mer; 0 and 2 μg/ ml) for 48 h. These samples were compared to cultures supplemented with TNF-α (10 ng/ ml, positive control). The release of 19 different cytokines, chemokines and growth factors from cultured ECs into the media were detected by a ChemiArray^{TM} rat cytokine array I (Millipore) consisting of the corresponding antibodies spotted in duplicate onto a membrane. The membranes were processed in accordance with the manufacturer's protocol and the imaged under chemiluminescence (20 min exposure time) in a FluorChem 8900 gel imaging station (Alpha Innotech), to quantify relative spot intensities. The intensities due to each cytokine were normalized according to the positive signal of each membrane, and the corresponding intensity under conditions of no HA. Results were averaged from outcomes of three replicate experiments.

3.2.12 Statistical Analysis

As appropriate, statistical significance between and within groups ($n \geq 3$/group) as determined using Microsoft Excel's statistical function for t-tests, assuming unequal variance and two-tailed distribution. Differences were considered statistically significant at $p < 0.05$. Quantitative results are reported as mean standard deviation.

3.3 Results

3.3.1 Composition of HA Oligomer Mixtures

The amounts of enzyme and the digestion periods were varied methodically until a minimal number of different sized HA fragments, lying within a narrow size range were produced (primarily HA 6mer and HA 12mer). Low enzyme concentrations (0.45 μg/ ml, 1.8 μg/ ml) produced broad ranges of oligomers even over long periods of digestion (60 h and 24 h, respectively). However, higher enzyme concentrations (4.5 μg/ ml, 9 μg/ ml) degraded HA 1500 to predominantly generate two fragment sizes HA 6mer and HA 12mer in 24 h and 6 h, respectively. From this matrix of digestions (Table 3.1, Figure 3.1) we chose two sets of conditions to incorporate into our further experiments. Previous work in our lab showed HA digests generated with 0.45 mg/ ml of enzyme for 18 h were bioactive and stimulated SMCs to produce an enhanced amount of matrix. Therefore, this formulation (D1) was used on ECs as well and FACE analysis found these digests to contain 13.9 ± 3.6% HA 6mers and 8.0 ± 1.6% HA 12mers. Previous studies suggest the most angiogenic HA oligomers are 6 – 12mers. As a result, a much more concentrated digest was also used in this study involving ECs. Digestion of HA 1500 with 4.5 mg/ ml of enzyme over 48 h generated an oligomer mixture (D2) that was shown to contain 33.3 ± 2.44% w/w of HA 6mers and 39.2 ± 2.68% w/w of HA 12mers by FACE, with other oligomers forming the balance.

		Hours of Digestion									
Enzyme (mg/ ml)	**%**	**3**	**6**	**9**	**12**	**15**	**18**	**21**	**36**	**48**	**60**
0.45	% 6mer	7.5	7.9	9.5	10.2	11.1	13.9	14.8	24.3	27.1	30.2
	% 12mer	4.9	5.4	6.2	6.7	6.9	8.0	8.9	15.3	16.3	16.7
1.8	% 6mer	10.1	12.9	16.6	18.8	22.1	24.1	27.4	-	-	-
	% 12mer	6.8	7.3	9.8	11.1	15.0	17.9	22.0	-	-	-
4.5	% 6mer	15.7	22.1	22.9	23.2	23.4	23.5	23.9	-	33.3	-
	% 12mer	10.5	12.4	16.7	18.1	21.3	23.4	31.4	-	39.2	-
9	% 6mer	24.7	27.2	23.6	22.6	21.0	19.9	17.3	-	-	-
	% 12mer	18.9	27.2	31.4	37.6	40.9	44.7	48.4	-	-	-

Table 3.1 Quantification of HA digestions based on the concentration of HA 6mer and HA 12mer. The concentration of HA 6mer and HA 12mer gradually increased over time for enzyme concentrations below 9 mg/ ml. The digest containing 9 mg/ ml dramatically increased HA 12mer concentration but slowly decreased the concentration of HA 6mer over time.

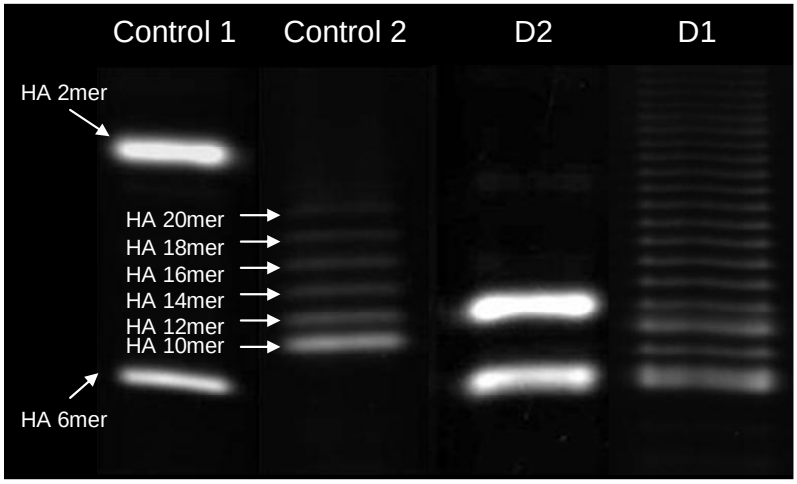

Figure 3.1 FACE analysis of the enzymatic digest of HA. The sample bands were obtained by digesting HA 1500 with0.45 mg/ ml enzyme for 8 h (D1) and 4.5 mg/ ml enzyme for 48 h (D2). The two primary bands correspond to HA 6mer and HA 12mer, the predominant fragment sizes in the digest.

3.3.2 Mathematical Model to Predict Digestion Outcomes

The mathematical model designed as a fit to digestion outcomes is a three-level full factorial with no repetitions of the digest preparations, which leaves 24 degrees of freedom for regression analysis in each case. In this fashion, we can report with good

certainty on linear and curvature trends of enzyme concentration and digest time, without repetitions. The parameters for the non-linear regression models and their significance values are given in Table 3.2. It is observed that in the case of HA 6mers, the experimental observations were handled in terms of only 1st-order (trend) terms significant at the 95% confidence level and an interdependence term ($x*y$), while a significant 2nd-order dependence on enzyme concentration was apparent for HA 12mer production. As shown in Figure 3.2, each of the non-linear regression models adequately fits the respective experimental data for 6-mer and 12-mers observed in this study. In both cases, residual analyses and ANOVA indicated that the residuals had a normal distribution, constant variance and average equal to zero, confirming that the proposed models (data not shown) represented good fits. According to Montgomery and Peck [285], all the above criteria should be fulfilled in order to conclude that a statistical model has been successfully adjusted to the experimental data.

HA oligomer (%)	***Non-linear regression model***	***Regression coefficients***	***Statistical significance of coefficients (p)***	***Statistical significance of the non-linear regression fit***
6-mer	$R = a + b*x + c*y + d*x*y$	*a = 4.8529*	*0.052*	*P = 0.001*
		b = 0.7426	0.0002	
		c = 2.6109	0.0001	
		d = -0.1199	0.0013	
12-mer	$R = a + b*x + d*x*y + f*y^2$	*a* = 4.2122	0.0008	*P = 0.001*
		b = 0.282	0.0061	
		d = 0.1399	0.0001	
		f = 0.153	0.0001	

Table 3.2 Model of HA digestions. Results obtained from non-linear regression analysis of the HA oligomer production by time-dependent enzymatic digests. In these models, R represents the amount of HA oligomer produced (%), while *x* and *y* represent the digest time and enzyme concentration, respectively.

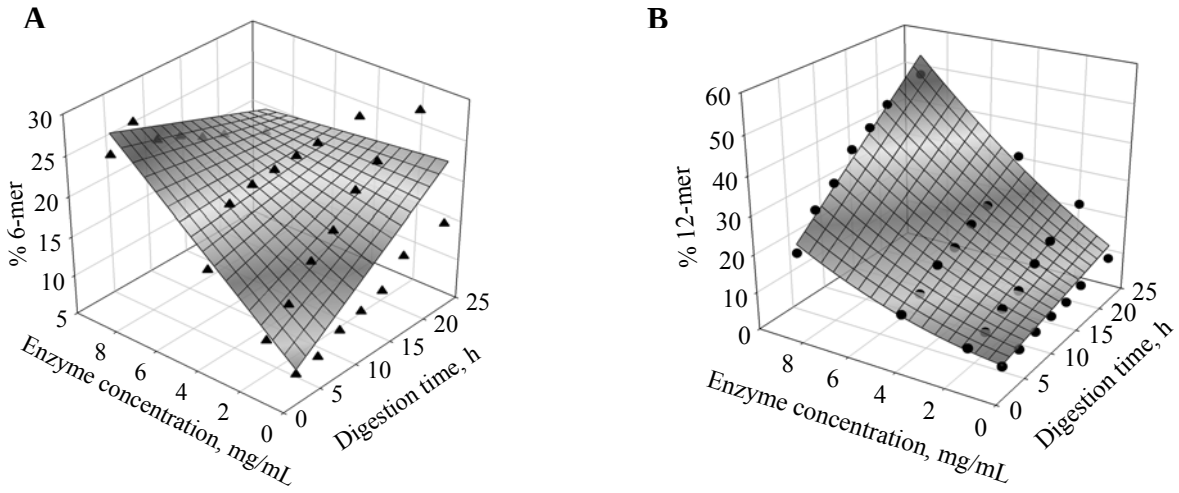

Figure 3.2 Plot predicting yield of HA 6mers and HA 12mers within t. hyaluronidase digests of long-chain HA, under different conditions of digestion. The concentration of HA 12mer (B) within all digests increased with time and the amount of enzyme utilized. The concentration of HA 6mer (A) followed a similar trend until higher enzyme concentrations and longer digestion periods were used, at which point it began to decrease.

3.3.3 Cell Proliferation

Towards compositional optimization of HA biomaterials capable of endothelialization, we sought to assess the size- and dose- specific effects of exogenous HA fragments on the proliferation of cultured adult rat aortic ECs. In general, ECs cultured with HA cues (HA 1500, HA 200, HA 20 D1, D2, HA 6 mer) proliferated much more rapidly than those cultured without. Cell proliferation ratios (i.e., ratio of cell numbers at day 14 to day 1) appeared dependent on provided dose of HA/oligomers; higher doses stimulated more rapid EC proliferation (Figure 3.3). Identical doses of D1, D2 and pure HA 6 mers induced similar levels of EC proliferation and greater levels of EC proliferation than did HA 1500. However, in all cases D1 and HA 6mer stimulated a

slightly greater amount of ECs proliferation than D2. Therefore, continued experimentation involved only HA 1500 and D2.

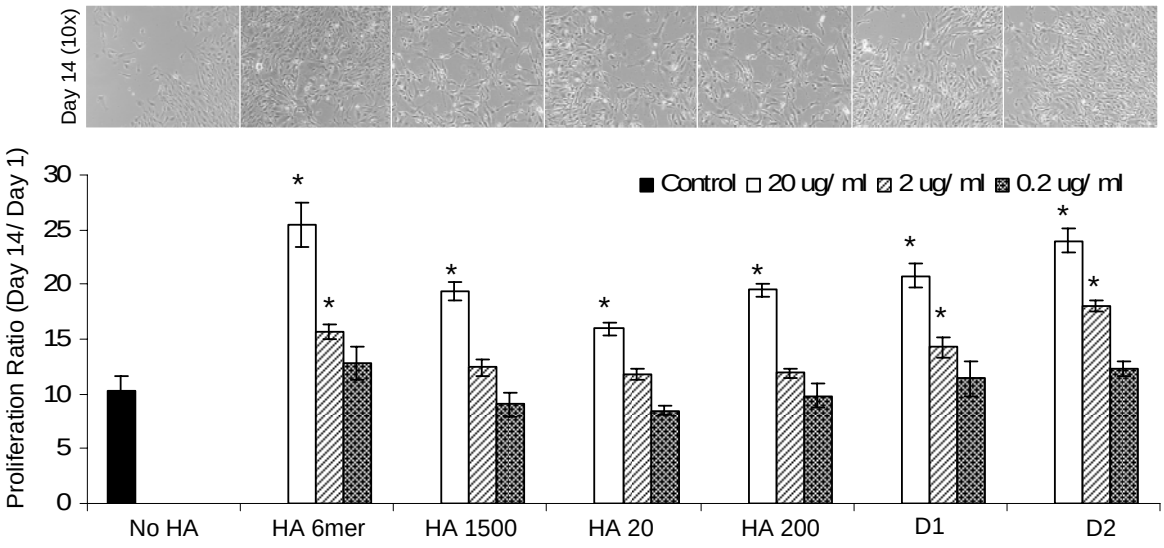

Figure 3.3 Proliferation of HA-supplemented EC cultures. The proliferation ratios of ECs increased with HA concentration, independent of fragment size. At all tested doses, ECs treated with HA 6mer and D2 proliferated to a greater degree than HA 1500.

3.3.4 Angiogenesis

ECs cultured on matrigel developed capillary projections that connected to form tubular networks (Figure 3.4). As expected, cultures that received suramin, an inhibitor of various growth factors (e.g., IGF, EGF, PDGF, TGF-β, VEGF, bFGF), and hence of EC proliferation and migration, did not exhibit any tube formation. HA 1500 induced formation of thicker, and longer individual tubes (Panel H), but showed few laterally branching tubes resulting in low tube numbers relative to that formed by control ECs (no HA addition; Panel F). Lengths of individual tubes (Figure 3.5A) in TNF-α– (E), HA 6mer- (G) and D2- (I) stimulated cultures were similar to that in the controls but the

numbers of tubes (Figure 3.5B) were significantly higher, resulting in a greater cumulative tube length (Figure 3.5C). These tube lengths were in the order TNF-a > HA-6mer > D2 > HA 1500. In all cultures, except those that received suramin and TNF-α, tubes appeared fairly regular, and extended between clusters of cells. In general, tubes formed by TNF-α-supplemented ECs appeared incompletely formed and also appeared much thinner than in other cases.

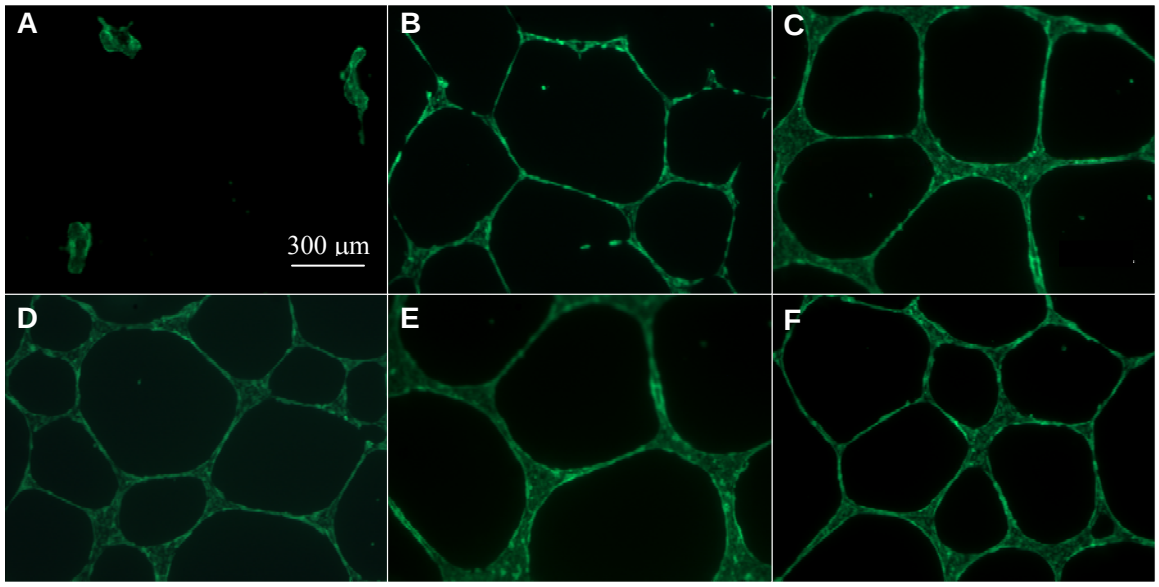

Figure 3.4 Fluorescence images of EC tubes formed on matrigel. Suramin (A) drastically inhibited tube formation and tubes in TNF-α-supplemented cultures (B) seemed to be incomplete, with gaps between junctions. The number of tubes formed was enhanced by HA 6mer (D) and D2 (F), and inhibited by HA 1500 (E), relative to HA-free controls (C). ECs were labeled with Calcein AM (green).

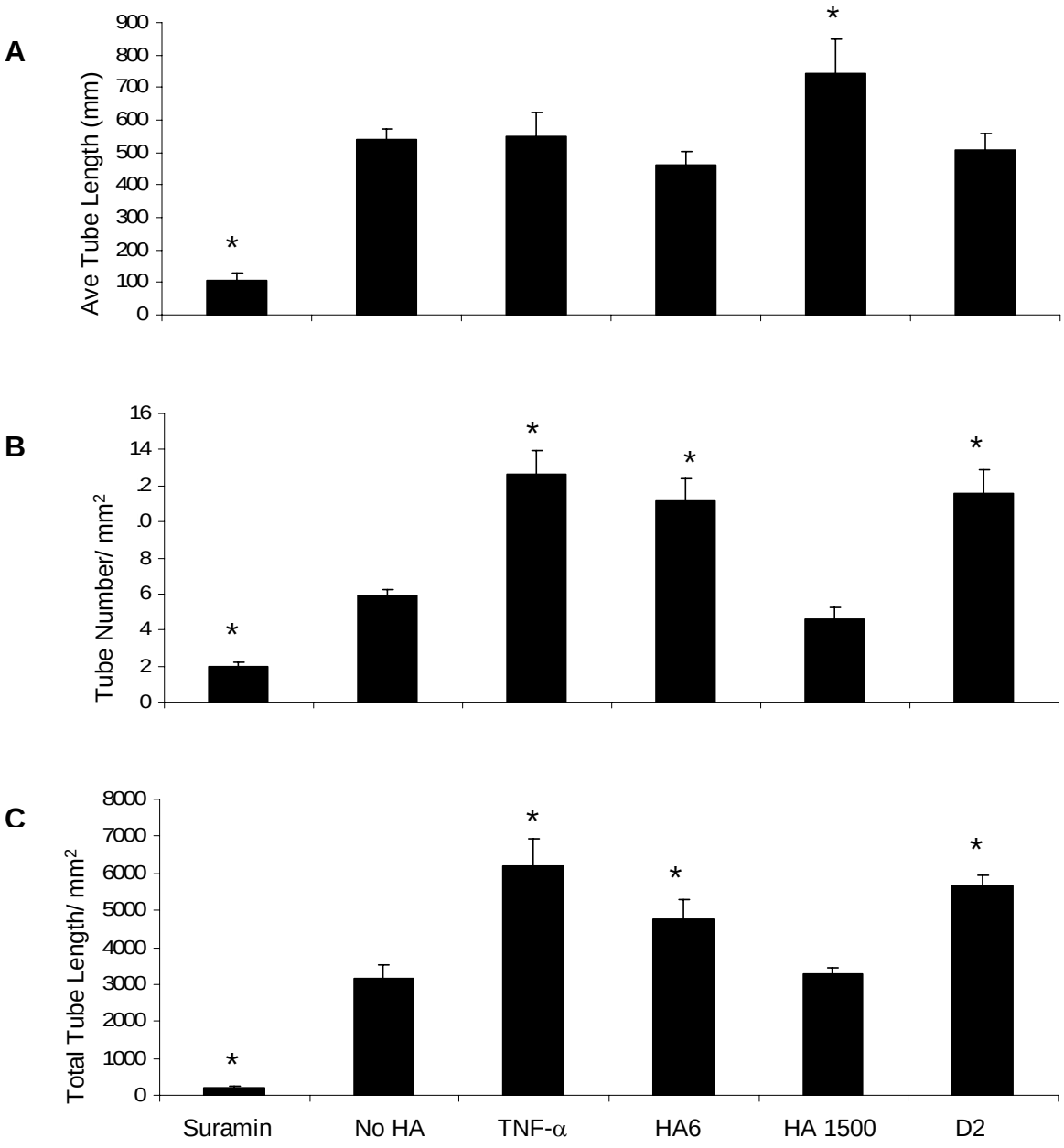

Figure 3.5 Impact of HA and HA oligomers on EC tube formation on matrigel. HA 1500 increased individual tube lengths (A) but decreased tube densities (B) resulting in a cumulative tube length (C) similar to the non-HA control. Lengths of individual tubes in TNF-α–, HA 6mer- and D2- stimulated cultures were similar to that in the controls but the number of tubes were significantly higher, resulting in a greater cumulative tube length. [* denotes a p-value < 0.05 in comparison to the no HA control].

3.3.5 Functionality Marker- and CAM- Expression

Irrespective of added HA fragment size, HA-supplemented EC cultures showed mild enhanced expression levels of LDLR, VEGFR2 markers and a moderate suppression of vWF and eNOS expression levels relative to HA-free control ECs, suggesting a possible alteration of the control phenotype (Figure 3.6A). D2 and HA 6mers similarly altered control expression levels of all tested EC functional markers. HA 1500 induced the same effects, although the magnitude of the increases or decreases in marker expression (relative to control) was less than that observed with the HA oligomers. HA 1500 elicited expression levels of EC activation markers that were mostly attenuated and identical to non-HA control cultures (Figure 3.6B). HA 6mers enhanced expression levels of ICAM-1 and VCAM-1, but not PECAM-1, however these increases were limited relative to the increases in EC CAM expression induced by TNF-α; D2 CAM expression levels were higher than HA 6 mers in all cases, but again, lower than that in TNF-α-supplemented cultures. This suggests the combination of HA 6mer and HA 12mer is a somewhat more potent stimulus of EC CAM expression.

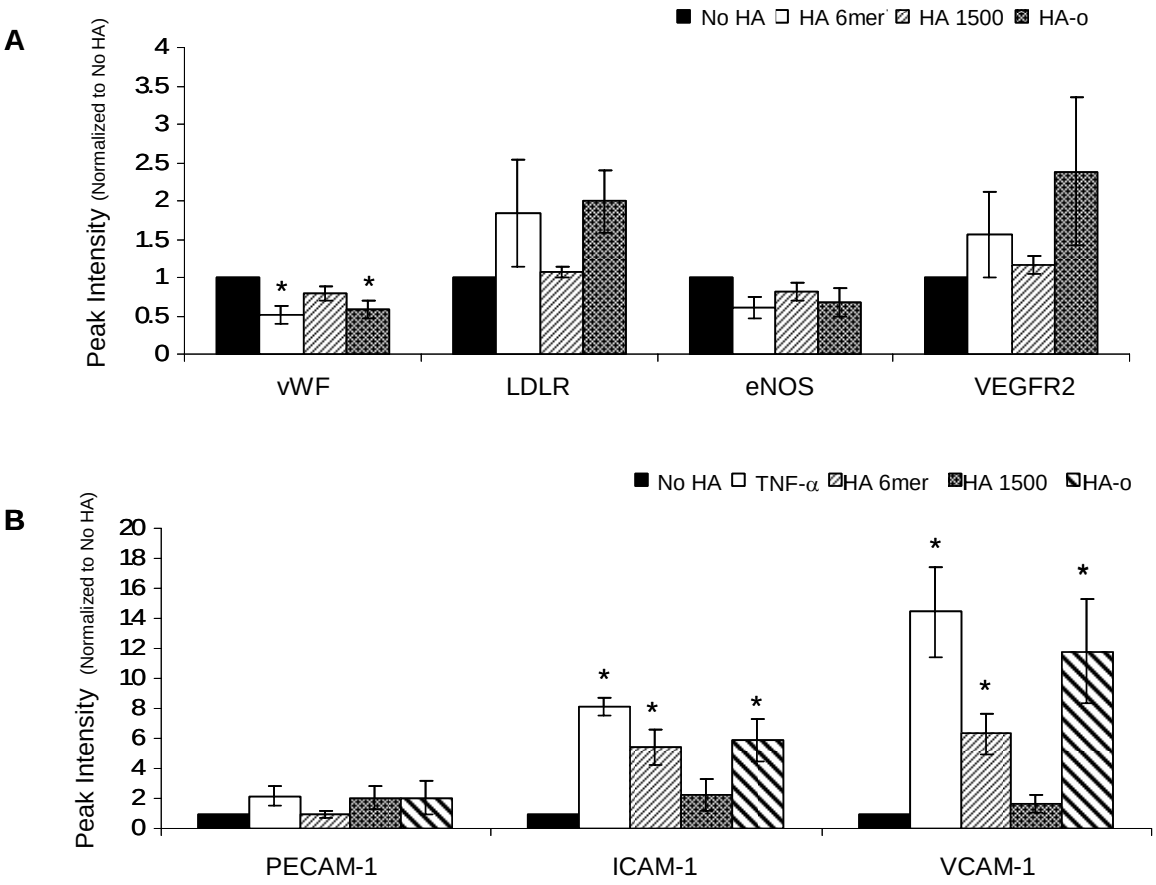

Figure 3.6 FACS analysis of EC protein expression. All fragment sizes of HA mildly enhanced expression levels of LDLR and VEGFR2, and suppressed expression levels of vWF and eNOS relative to non-HA control ECs (functionality markers; A). D2 elicited greater expression of EC cell adhesion molecules (PECAM-1, ICAM-1, VCAM-1; B) than did HA 1500 and in controls. HA 6mer CAM expression levels were lower than D2. [* denotes a p-value < 0.05 in comparison to the no HA control]

3.3.6 Coagulation and Thrombogenic Potential

ECs cultured with HA 6mer, D2, and HA 1500 exhibited thrombomodulin activity levels very similar to control ECs, and significantly greater than ECs stimulated with TNF-α, indicating the retention of a healthy phenotype capable of regulating blood coagulation (Figure 3.7). On the other hand, significant differences in platelet adhesion were observed (Figure 3.8); HA 1500 drastically inhibited platelet adherence to ECs,

while HA 6mer and D2 mildly enhanced platelet adhesion beyond that in non-additive control cells. This increase in platelet adhesion was, however, highly attenuated relative to that induced in EC cultures upon stimulation with TNF-α, or on cell-free glass substrates. The incubation time (15 min or 45 min) of the plasma with the cell layers/glass substrate did not impact platelet adhesion. There were no differences in platelet adhesion within cultures supplemented with D2 versus those that received HA 6mers.

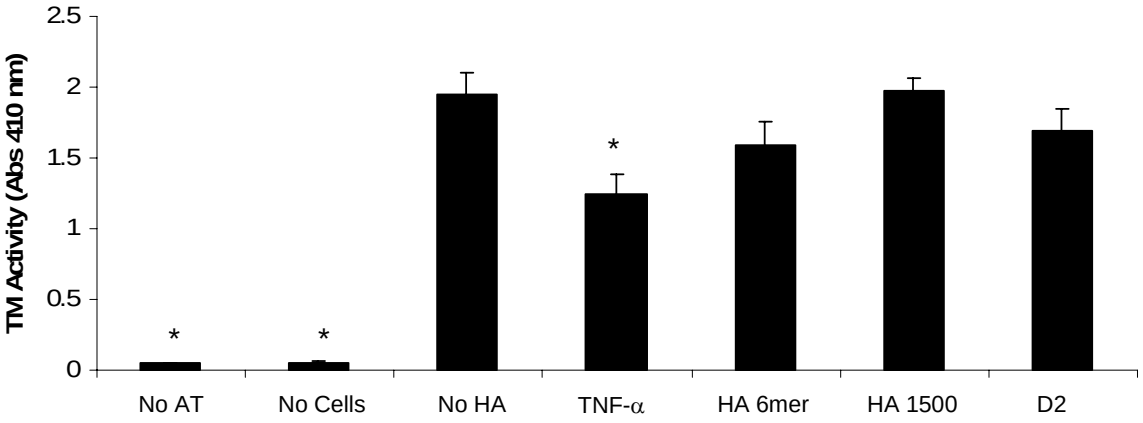

Figure 3.7 Thrombomodulin expression of ECs. ECs cultured with both D2 and HA 1500 exhibited thrombomodulin activity levels very similar to control ECs, and significantly greater than ECs stimulated with TNF-α. [* denotes a p-value < 0.05 in comparison to the no HA control]

SEM micrographs of EC cultures are shown in Figure 3.8. ECs that had been cultured on tissue culture plastic (plasma-treated polypropylene) without any additives (HA-free control; Panel B), and those stimulated with HA 1500, both elicited sparse attachment of discrete and rounded platelets when contacted with human plasma (Panels B, F respectively). However, the surface of the ECs in the latter cultures appeared

textured, likely due to deposition of the long-chain HA. D2- and HA 6mer-stimulated ECs induced mildly greater platelet adherence (Panels D, E). Though most of these platelets were discrete and rounded a few platelet aggregates were also seen; some ECs were completely void of platelets. TNF-α–stimulated ECs induced severe platelet deposition and aggregation, with the aggregates covering the ECs completely (Panel C).

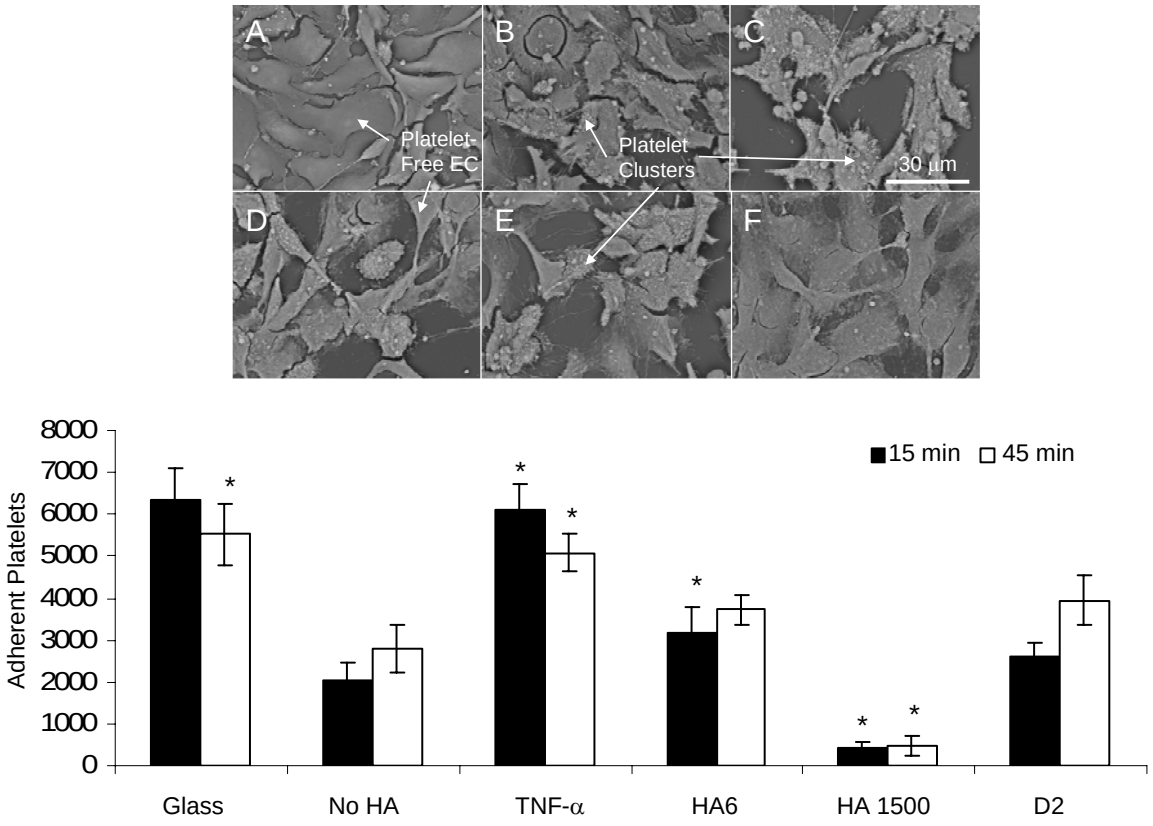

Figure 3.8 Impact of HA and HA oligomers on platelet adhesion to cultured ECs. HA 1500 drastically inhibited platelet adherence to ECs, while HA 6mer and D2 mildly enhanced platelet adhesion beyond that in non-additive control cells, but to a far lesser extent than when TNF-α was added. The incubation time (15 min or 45 min) of the platelet solution did not alter their attachment levels or clumping. [* denotes a p-value < 0.05 in comparison to the no HA control]. Scanning electron micrographs of platelets adhered on EC layers are also shown: (A) no platelets, (B) no HA, (C) TNF-α, (D) HA 6mer, (E) D2, (F) HA 1500.

3.3.7 Cytokine, Chemokine and Growth Factor Release

Cytokine arrays detected the presence of all 19 cytokines under each culture condition with their relative amounts shown in Figure 3.9. Here we focus on the 9 cytokines, chemokines and growth factors that showed altered EC expression levels in response to HA/oligomers. Both HA 1500 and D2 up-regulated the EC expression of interferon γ (IFN-γ), tissue inhibitor of metalloprotease 1 (TIMP-1), and granulocyte macrophage colony stimulating factor (GM-CSF), and suppressed Fraktalkine (FKN) production, beyond that of no HA controls and tumor necrosis factor α (TNF-α) - added cultures. ECs cultured in presence of D2 showed a greater expression of vascular endothelial cell growth factor (VEGF) and TNF-α, relative to no HA controls. The EC production of macrophage inflammatory protein 3α (MIP-3α), monocyte chemotactic protein 1 (MCP-1), and leptin were modestly enhanced by both HA 1500 and D2; TNF-a supplemented cultures on the other hand dramatically increased MCP-1 expression, but did not alter control levels of MIP-3α expression.

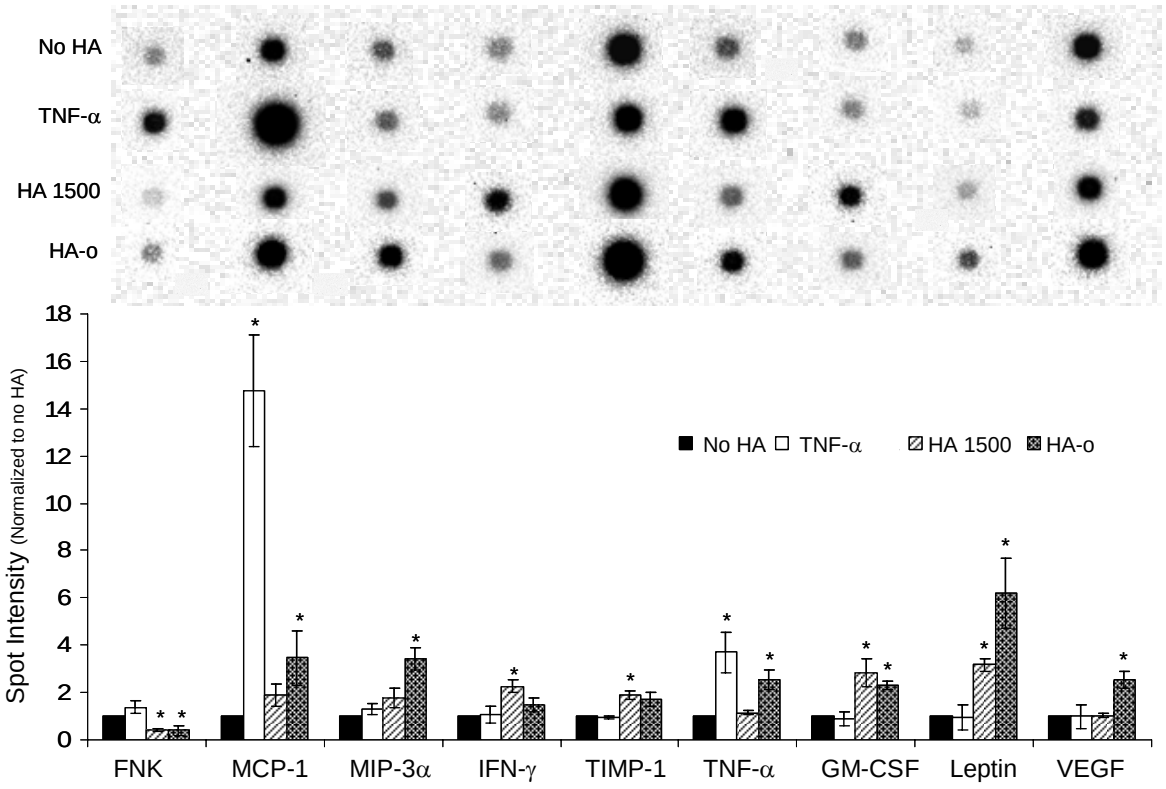

Figure 3.9 Cytokine production by ECs. Of the 19 cytokines tested in each cytokine array, we reported 9 that were significantly altered by HA fragment size and their corresponding spot intensities. In general, D2 upregulated the production of angiogenic growth factors and hormones, but in addition mildly enhanced chronic inflammatory cytokines. HA 1500, in general, had a more mild effect on ECs. [* denotes a p-value < 0.05 in comparison to the no HA control]

3.4 Discussion

On of the long-term goals of our research is to develop vascular biomaterials that recruit and sustain a complete normal functional luminal endothelium. A healthy and confluent EC lining is crucial to reinstate anti-thrombotic and anti-hyperplasic endothelial signaling pathways that are disrupted by vascular injury or disease.

The choice of hyaluronan (HA) as the basis for these vascular implant materials stems from it's biocompatibility and non-immunogenicity, outcomes of it's highly conserved structure across species [18], and its potential, as a ECM component, to evoke

non-exaggerated, healthy responses from cultured vascular cells. HA has also been shown to elicit angiogenic responses, although these effects, as with other phenomena observed with other cell types, appear to be highly specific to HA of certain fragment sizes [19]. In a previous study, we showed that cells, including ECs, respond to HA oligomers (< 10 kDa) more exuberantly than they do to larger-sized HA fragments and long-chain HA (> 1000 kDa) [289]. Other studies collectively indicate that different aspects of cell behavior have unique dependencies on HA fragment size. However, it has also been shown that HA fragments and HA oligomers can induce inflammatory responses under specific conditions [18]. Thus, the distribution of bioactive HA fragments and oligomers within mechanically stable implant materials based on biocompatible, long-chain HA must be defined and optimized to elicit desired outcomes (i.e., functional endothelialization) and prevent unwanted ones (i.e., inflammation). Currently, we thus seek to investigate the effects of HA/oligomers on EC function and eventually use this information to tailor the oligomer content within these HA biomaterials so as to promote vascular endothelialization, while preventing untoward effects.

In order to limit potentially adverse inflammatory responses, we exposed ECs to a low concentration of HA digest (HA-o; 2 μg/ ml). This dose lies within a range of doses (0.2 – 200 μg/ ml) that we have shown to significantly impact SMC behavior [31,32]. Also, we have shown that HA-o stimulates ECs to proliferate faster than when other, or no cues are provided. To account for this, expression levels of markers have been normalized to the number of cells present at the time of analysis, and are thus effectively reported on a per cell basis.

HA oligomer mixtures (D2) were obtained by digesting HMWHA (HA 1500) with *testicular hyaluronidase*. Previous studies partially digested HA using relatively small quantities of this enzyme (~40 U enzyme/ mg HA) to generate a ladder of different sized HA fragments including small amounts of HA fragments of interest, which were then purified and supplemented to cells [23,171,290]. Our approach bypasses the laborious and inefficient oligomer purification process, and highlights our eventual need to mass produce HA oligomers of sizes deemed useful, with consistency and good predictability for incorporation into vascular scaffold constructs.

The digestion time and enzyme concentrations were optimized to obtain the highest yield of HA 6mer and HA 12mer within the digest. As expected, a greater amount of enzyme and longer digestion periods resulted in narrower fragment size distributions of the oligomers. However, 9 mg/ ml of enzyme consistently reduced the amount of HA 6mer over time with a concurrent increase in intensity of the HA 12mer band. These outcomes suggest that *testicular hyaluronidase* favors production of the HA 12mer; generation of the HA 6mer product is also favored but to a lesser extent. Other hyaluronidases have shown such specificity in HA oligomer production such as hyaluronidase *Streptomyces hyalurolyticus*, which gives mixtures of HA 6mer and HA 4mer as final degradation products of HA [291]. Also, it has been reported that *testicular hyaluronidase* is only active for 5 h in solution at 37 °C [292]. Here we show that this enzyme retains its activity over periods longer than 5 h, though, this may decrease with time. The degradation products of HA 6mer and HA 12mer were modeled as a function of enzyme concentration and digestion time. These models can be used to generate HA

oligomers with a specific concentration of HA 6mer and HA 12mer without optimizing the digest conditions. As our results in section 3.3 confirm that both D2 (containing HA 6 mers and 12 mers) and pure HA 6mers elicit almost identical EC responses, which justifies the use of these composition-defined mixtures in future applications.

The ability of D2 to promote EC proliferation (an important aspect of endothelialization and angiogenesis) was tested through exogenous supplementation. Previous studies on the influence of HA oligomers on EC proliferation were limited to a few hours and resulted in modest yet significant changes [23,290]. Our prolonged culture study over 2 weeks showed similar results, and confirmed that HA (both HA 1500 and D2) is conducive to EC proliferation, in a dose dependant manner, and useful to achieve rapid endothelialization of vascular grafts. The angiogenic nature of D2 was confirmed by a tube formation (angiogenesis) assay. The large HA 1500 polymer strands reduced the cumulative capillary production but increased the length of each individual tube, likely due to physically limiting the EC migration pathways and inhibiting capillary branching. The small fragments of D2 did not influence EC migration physically but stimulated a greater extent of capillary production possibly through interactions with EC receptors.

CD44 is a trans-membrane receptor found in several cell types, including ECs, and is one of the most well characterized cell membrane receptors for HA, the others being Receptor for HA Mediated Motility (RHAMM), and Toll-Like Receptor 4 (TLR4) [232]. Studies have shown that HA oligomers can incite very different cell responses when bound to CD44 receptors, than when HMWHA interacts with them, because HA

oligomers can cause clustering of multiple receptors and thus alter intracellular responses [293]. Under inflamed conditions, ECs have been shown to enhance their expression of CD44 and TLRs [294]. The stimulation of CD44 receptors by HA oligomers has been suggested to enhance the production of vascular EC growth factor (VEGF) and therefore promote EC proliferation [26]. Our results show that VEGFR2 is also mildly up-regulated by D2. Additionally, cytokine-arrays showed D2 stimulate ECs to produce certain angiogenic factors (Leptin, VEGF, TNF-α) that could potentially further enhance their proliferation and angiogenic potential through autocrine effects [295,296]. HA 1500 and D2 also very marginally enhanced EC production of TIMP-1, an inhibitor of matrix metalloproteases (MMPs) which can in turn temper the ability of MMPs to degrade the ECM and thus facilitate endothelial migration and new blood vessel sprouting [297]. Collectively, these results indicate that HA 6mer and HA 12mer mostly up-regulate angiogenesis, while HA 1500 provides some degree of protection against excessive MMP-mediated ECM degradation. Thus a key strategy to formulate HA gels capable of endothelialization, and yet prevent excessive vascularization is to combine both HMWHA and HA oligomers into a single material, and optimize the concentration of each.

Lower flow shear rates in small diameter vessels favor platelet deposition and thrombus formation, which can severely compromise the long-term patency of vascular implants [72]. Under healthy conditions ECs in intact vessels express thrombomodulin and release nitric oxide (NO), which serves to regulate coagulation and attenuate thrombosis, respectively; thrombomodulin, an integral surface membrane protein of ECs, binds

thrombin and activates protein C in the plasma. Protein C in conjunction with protein S, produced by ECs, inhibits the activation of factor V and VIII preventing thrombin formation and hence clot formation [158,159]. On the other hand, NO released by ECs is taken up by platelets where it binds to and activates guanylyl cyclase. This enzyme catalyzes the dephosphorylation of GTP to cGMP, which serves as a second messenger for many important cellular functions, particularly preventing platelets from adhering to the EC surface and aggregating with one another [298]. The results show that HA 1500 and D2 do not alternated thrombomodulin expression, though D2 did mildly decrease eNOS expression, relative to controls, possibly marginally enhancing platelet deposition and aggregation on ECs.

The adhesion of platelets to injured endothelial layers is a coordinated multi-step process that involves platelet activation, subsequent firm adhesion to the vascular wall, and further strong activation and degranulation of platelets to cause their aggregation to form thrombi. The initial initial activation of platelets is mediated by cell adhesion molecules (CAMs) expressed on the surface of activated ECs in response to inflammatory stimuli, or injury [299]. Our results show that EC expression of ICAM-1 and VCAM-1 is enhanced in the presence of D2, possibly contributing to the greater level of platelet deposition and aggregation relative to non-HA controls, and HA 1500-supplemented cultures. However, as seen in the SEM micrographs, clearly, platelet adhesion and aggregation as induced by D2 is far less than that induced by inflammatory factors such as TNF-α.

Another very important determinent of vascular graft patency is the interaction

between ECs and leukocytes. Upon initial activation, due to injury or stimulation by inflammatory agents, ECs release CXC chemokines (interleukin 8, IL-8) and acute inflammatory cytokines (TNF-α; interleukin 1, IL-1) into the circulation to attract polymorphomuclear neutrophils (PMNs) and T-cells to the site of EC activation (acute inflammation) [300]. If continuously agitated, they also summon monocytes/macrophages, activated T cells, B cells, eosinophils, basophils, and dendritic cells by releasing CC chemokines (MCP-1, MIP-3α) [301] to stimulate chronic inflammation and possible graft failure. In addition, the cytokine GM-CSF is known to prolong the circulating half-life of PMNs and induce a delay in PMN apoptosis and thus prolong inflammatory responses [302]. HA fragments in the oligomeric size range are known to be produced in areas of inflammation by enzymatic degradation of long-chain HA, to trigger a healing response. However, continued degradation of HA has also been noted to induce prolonged inflammatory responses including the activation of leukocytes [303]. Therefore, it is not surprising that D2 stimulated TNF-α production caused a modest increase in MCP-1, MIP-3α and GM-CSF release. On the other hand, HA 1500 had no effect on TNF-α production and only very marginally enhanced MCP-1, MIP3α and GM-CSF. The EC expression of acute inflammatory chemokines/ cytokines, other than TNF-α was not affected by HA 1500 or D2 (data not shown). Other cytokines released in response to HA/oligomers were IFN-γ and FKN (mild increase relative to controls). IFN-γ appears to cause early suppression of IL-8 to inhibit PMN-EC interactions, but stimulates IL-1β and TNF-α production by neutrophils during a later inflammatory stage to promote these very interactions [304]. FKN exists in two forms, one that is secreted as a potent chemoattractant,

and one that is membrane bound and supports adhesion of monocytes and T cells [305]. These results suggest that D2 and HA 1500 have both leukocyte- agonist and antagonist capabilities. In general, it is important to note, any increase in release of pro-inflammatory cytokines by D2, can be muted when presented to ECs in a biomaterial together with an abundance of HA 1500.

3.5 Conclusions

In summary, our results show that both D2 and HA 1500 interact with ECs in a positive manner; D2 enhanced EC proliferation, and angiogenesis, while HA 1500 significantly alternated platelet attachment to ECs and their aggregation and activation. In addition, D2 stimulated modest inflammatory cytokine production and CAM expression, while HA 1500, in general, had a more limited effect. Therefore, in the near future we seek to develop vascular scaffold materials composed of optimized ratios of D2 and HA 1500 capable of stimulating ECs to grow on its surface regenerating a normally functional endothelium.

CHAPTER 4

A SURFACE-TETHERED MODEL TO ASSESS THE SIZE-SPECIFIC EFFECTS OF HYALURONIC ACID ON VASCULAR ENDOTHELIAL CELL FUNCTION AND ELASTOGENESIS OF SMOOTH MUSCLE CELLS

4.1 Introduction

The extracellular matrix (ECM), once regarded simply as a structural scaffold, is now recognized as an important modulator of cell phenotype and function. From a tissue engineering perspective, it is increasingly apparent that ECM structures/ substrates provide the necessary biomechanical and biochemical stimulatory cues to cultured cells to create micro-environments similar to native tissues. A class of ECM molecules that are increasingly studied in the context of cell culture scaffolds are glycosaminoglycans (GAGs). One such GAG, hyaluronic acid (HA), occurs naturally in connective tissues (e.g. skin) as a simple linear molecule consisting of repeating dissacharide units of N-acetyl-D-glucosamine and D-glucuronic acid [17]. Most cells have the ability to synthesize HA at some point during their cell cycle, implicating its function in several fundamental biological processes [18].

In recent years, HA has been recognized as a biomaterial for potentially effective tissue regeneration. It is now known that HA, when degraded into smaller-sized fragments, facilitate wound healing by promoting angiogenesis [19]. HA fragments can, under specific circumstances, also promote early inflammation, which is critical to initiate wound healing, but can also modulate later stages of the process, allowing for matrix stabilization and reduction of long term inflammation [18]. HA is also highly

biocompatible and does not elicit a foreign-body response upon cross-transplantation due to the high degree of structural homology of HA across species [18]. Although mechanisms of interaction between HA and the human body are still incompletely elucidated, its promising characteristics have assured its extensive use as a tissue engineering scaffold, most recently for cartilage [20] and skin repair [21].

Our lab is focuses on investigating the potential use of HA biomaterials for small vessel grafting or regeneration. It is generally understood that complete endothelialization of the graft lumen is essential to ensure long-term patency of vascular grafts and thus key to the long-term success of intravascular implants. In the previous section (chapter 3) we reported on the size-specific effects of exogenous HA/ fragments on ECs. Briefly, we found exogenous supplementation of a mixture (D2) of HA oligomers containing predominantly 6mers and 12mers, to stimulate EC proliferation, angiogenesis and the secretion of angiogenic growth factors reinforcing our conviction that HA fragments may be suitable as vascular biomaterials. In addition to achieving complete lumenal coverage with functional ECs, enabling regeneration of medial elastin is another crucial requirement critical to maintaining vascular homeostasis in part by native biomechanical-transductive cues to cells. Vascular SMCs typically synthesize elastin as soluble tropoelastin, which is then post-translationally crosslinked by lysyl oxidase into a structural matrix. In a previous study, we showed the elastogenic effects of exogenous HA fragments on SMCs to also be size-specific [31,32]. However, only exogenous supplements of broad HA oligomer mixtures (D1), containing a lower concentration of 6mers and 12mers, up-regulated elastin synthesis by adult SMCs, and enhanced the

formation of an elastin fiber-rich matrix. It was clear from our previous studies [31,306] that while exogenous supplementation models broadly predict cell responses to substrate/ scaffold components, presentation of these very components to cells, immobilized on a 2-D substrate, may more closely simulate cell responses within 3-D scaffolds.

Studies such as that of Deed et al. [171], have suggested that since exogenous HA/fragments likely only transiently interact with cells, they may inadequately simulate cell response to HA substrates; thus, the true effects of HA size on cell response as a scaffolding material may more accurately be predicted by long-term cell contact with surface-immobilized HA/HA fragments. Therefore, investigation of the differential effects, if any, of exogenous vs. surface-tethered HA/fragments is important to determine the validity of use of an exogenous supplementation model in ascertaining the fragment-size specific effects of HA on endothelialization and SMC elastognesis. The current study will also elucidate how chemical immobilization of HA on the surface of scaffolds will influence their ability to interact with cells, in the absence of other possible influencing parameters such as crosslinks, present within a 3-D scaffolding microenvironment [307]. This study thus describes our attempts to immobilize native HA, in a wide range of fragment sizes, on 2-D glass surfaces and test EC angiogenic responses and SMC upregulation of elastin synthesis.

4.2. Materials and Methods

4.2.1 Preparation of HA Oligomer Mixtures

As mentioned in section 3.2.1, HA 1500 was enzymatically digested to produce

two mixtures of HA oligomers: D1 and D2. Briefly, HA 1500 (5 mg/ ml) was digested with bovine *testicular hyaluronidase*, (439 U/mg) in a solution of digest buffer (37 °C). The different oligomer mixtures were produced by altering the enzyme concentration (D1: 0.45 mg/ ml; D2: 4.5 mg/ ml) and time of digestion (D1: 18 h; D2: 48 h). The enzyme was then precipitated, its activity terminated by boiling (2 min), and cooled on ice. Following centrifugation (2800 rpm, 10 min), to separate the enzyme from the mixture, the supernatant was dialyzed in water (12 h) and then freeze-dried overnight to generate lyophilized HA oligomers. Previously, these mixtures were analyzed by FACE and found to contain a broad (D1: 13.9 ± 3.6% HA 6mers and 8.0 ± 1.6% HA 12mers) and narrow (D2: 33.3 ± 2.44% w/w of HA 6mers and 39.2 ± 2.68% w/w of HA 12mers) range of oligomers.

4.2.2 Immobilization of HA, HA Fragments, and Oligomers

HMW HA, large HA fragments, and HA oligomers were tethered onto glass surfaces using a carbodiimide linking chemistry [308]. HA 1500, HA 200, HA 20, and in-house prepared oligomer mixtures (D1) were immobilized onto 4-well glass chamber slides (Nalge Nunc International, Napersville, IL). The chamber slides were incubated in 1 M NaOH for 1 hour to de-protonate the exposed hydroxyl groups and render the glass surface uniformly reactive. The glass surface was rinsed with DI water and 95% v/v ethanol (Sigma, St Louis, MO), and then activated by incorporation of aminosilanes. A 3% v/v solution of 3-aminopropyl-trimethoxysilane (APTMS; Fluka Chemical Corp., Milwaukee, WI) in 95% v/v ethanol was prepared and the silane was allowed to convert

into silanol over 5 minutes. A 1-ml aliquot of the solution was then reacted with the glass slide (30 min, 23 ºC) with shaking. The slides were then briefly rinsed in 100% v/v ethanol (Sigma), dried under a steady stream of argon gas, and finally heated in an oven (1 hr, 115 °C), rinsed three times with 95% v/v ethanol, and dried again under argon gas.

Immobilized amines were covalently reacted with the carboxyl groups present on HA, using a carbodiimide reaction (Figure 4.1). Briefly, an aqueous HA solution (3 mg/ml) was prepared with 200 mM 1-Ethyl-3-[3-dimethylaminopropyl]carbodiimide hydrochloride (EDC; Pierce Biotechnology Inc., Rockford, IL) and 100 mM *N*-hydroxysuccinimide (NHS; Pierce Biotechnology Inc.). A 1-ml aliquot of this solution was applied to each well and allowed to react for 16 hours with continuous agitation on a shaker. The slides were then soaked in DI water for 2 hours to leachout unbound HA, and finally air-dried under inert argon gas.

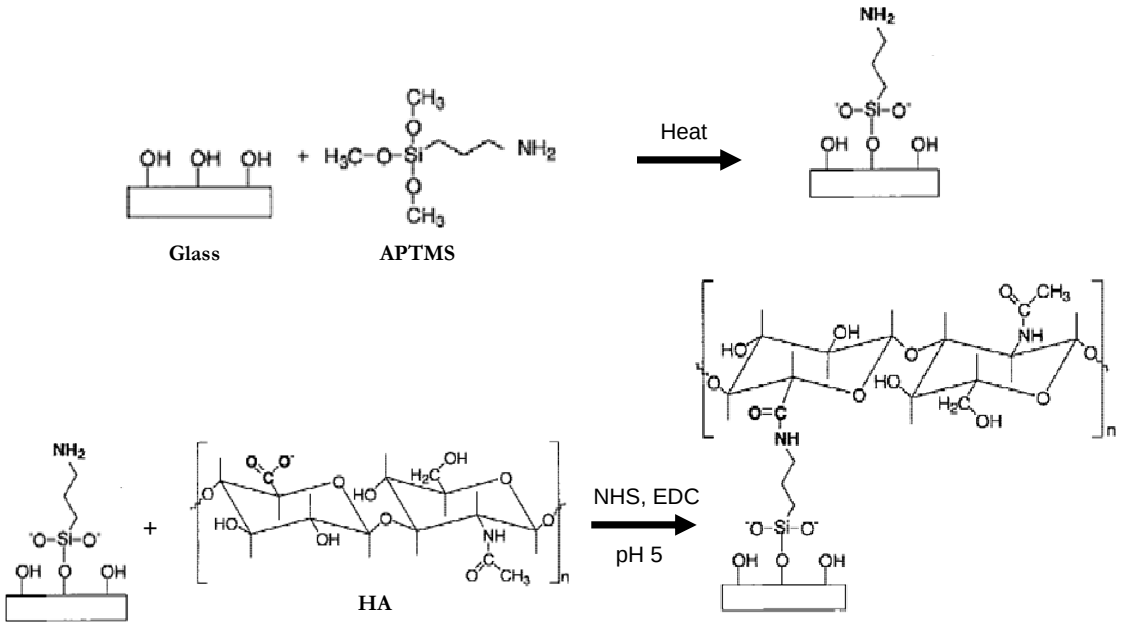

Figure 4.1 Schematic of the chemistry involved in the immobilization of HA.

4.2.3 s-SDTB Assay for Quantification of Tethered Amine Groups

Aminosilanated surfaces were rinsed with 50 mM $NaHCO_3$ buffer, pH 8.5. A 1-ml aliquot of this buffer containing 2% v/v dimethyl formamine (DMF) and 0.1 mM sulfo-succinimidyl-4-O-(4,4'-dimethoxytrityl)-butyrate (s-SDTB) was incubated (30 min, 23 ºC) with each well of the aminosilanated chamber slides to allow s-SDTB to bind to the exposed amine groups. The slides were then gently rinsed with methanol to remove unreacted s-SDTB, and then treated with a 50% v/v solution of 60% v/v perchloric acid in methanol (10 min, 23 ºC) to elute the 4, 4'-dimethoxytrityl cation from the bound s-SDTB. The amount of cation was measured using a spectrophotometer (Molecular Devices, Sunnyvale, CA) at λ = 498 nm. The concentration of the cation, and hence surface amines, was determined by comparison of the unknowns with a calibration curve generated with known amounts of 4, 4'-dimethoxytrityl chloride prepared in perchloric acid/ methanol solution.

4.2.4 Fluorescence Microscopy for Detection of Surface-Immobilized Molecules

Successful surface-immobilization of amine groups was confirmed by fluorescence labeling with an Alexa-488-conjugated amine-reactive dye (Molecular Probes, Temecula, CA; 1:1000 v/v in $NaHCO_3$ buffer, pH 8.5). The dye solution was allowed to react with the aminosilane surfaces (1 hour, dark), then removed and the surface was washed with $NaHCO_3$ buffer and DI water. The slides were mounted with Vectashield (Vector Labs, Burlingame, CA). Negative controls were not treated with the amine reactive dye. The slides were visualized using a Ziess Axiovision-200

epifluorescence microscope fitted with a FITC filter.

Surface-bound HA/ HA fragments were detected by immunofluorescence, either using a biotinylated HA binding protein (HABP) and rhodamine-conjugated streptavidin, or with FITC-pre-conjugated HA. A solution of biotinylated-HABP (b-HABP; 0.5 mg/ml, diluted 1:100 in PBS; Associates of Cape Cod, E. Falmouth, MA) was added to the slide chambers and allowed to react with the HA-tethered surfaces (1 hour). Excess biotinylated-HABP was removed by rinsing with PBS. A solution of bovine serum albumin (BSA; 5% v/v in PBS) was added to the slides as a blocking agent (20 minutes). The slides were then again washed with PBS to remove the blocker. Texas Red-conjugated neutravidin (Molecular Probes; 1:500 v/v in PBS) was allowed to react with the b-HABP on HA (1 hour, dark). The solution was then aspirated, the surfaces washed with PBS and DI water, and the slides mounted with Vectashield. The negative control was not treated with HABP. The slides were imaged using a confocal microscope (Leica TCS SP2 AOBS, Allendale, NJ).

4.2.5 Scanning Electron Microscopy

Glass, aminosilanated glass, and HA-tethered glass surfaces were visualized using scanning electron microscopy (SEM) to assess the homogeneity of the coated layers. Argon-dried surfaces were coated with gold (60 s) in a sputter coater (VG-Microtech, Uckfield, UK) and visualized using a SEM 3500 (Hitachi Ltd, Tokyo, Japan) at 150× to 1500× magnification.

4.2.6 Atomic Force Microscopy

Atomic force microscopy (AFM) was performed on glass, aminosilane and HA-tethered substrates to determine the surface roughness and gauge the uniformity of the coatings at the cellular (micron) scale. Argon-dried surfaces were analyzed using a Digital Instruments CP-II (Veeco, Woodbury, NY) AFM equipped with an Utralever contact mode tip (Veeco, Woodbury, NY) and titanium cantilever. Three areas per sample were imaged under contact mode and analyzed with Proscan 1.9 and Image Analysis 2.1 to obtain a linescan section profile used to measure the peak heights.

4.2.7 X-ray Photoelectron Spectroscopy

X-ray photoelectron spectroscopy (XPS) was used to compare the elemental composition and chemical structure characteristics of the glass, aminosilane and HA-coated surfaces. Dried slides were stored in a desiccator prior to analysis using an Axis 165 XPS system (Kratos, Chestnut Ridge, NY) with a monochromatic aluminum target x-ray source (15 kV and 10 mA). Samples were analyzed at a pressure of 10^{-9} torr and temperature of 23 ºC with a takeoff angle close to 0º. Scans between 1200 eV and 0 eV were performed and the resulting spectra were referenced to the substrate C 1s peak. Higher resolution spectra were also generated to monitor the formation of functional groups upon HA immobilization.

4.2.8 Assays for Quantification of HA Loss from the Surface

Loss of surface-bound HA over 3 weeks of incubation was assessed in serum-free

culture medium using (a) colorometric toluidine blue assay and (b) *F*luorophore *A*ssisted *C*arbohydrate *E*lectrophoresis (*FACE*). For both assays, HA-tethered surfaces were incubated in culture medium (MCDB-131, Invitrogen, Carlsbad, CA; 37 ºC) for 0, 1, 4, 7, 14, and 21 days. On these respective days, the supernatant medium was aspirated and a 500-µl aliquots of aqueous toludine blue solution (0.075 mg/ml) added to the HA surfaces, and agitated by shaking for 10 minutes. The absorbance of this solution, following removal toluidine blue by binding to surface-tethered HA, was measured spectrophorometrically at λ = 630 nm, and compared to it's absorbance prior to incubation with the surfaces. The decrease in absorbance indicated the presence of HA.

FACE analysis was used to quantify the amount of HA/ HA fragments remaining on the slide surface after 1, 14 and 21 days of incubation with culture medium. In preparation for *FACE*, 20 mU of *hyaluronidase SD* (Associates of Cape Cod, East Falmouth, MA) solubilized in 0.1 M ammonium acetate, pH 7.0, was added to each well of the chamber slide and incubated (37 ºC, 6 hrs) to digest HA off the surfaces. The resulting solution, containing HA disaccharides (ΔDiHA), was freeze-dried and then re-suspended in 40 µl of 0.0125 M solution of the fluorescent dye 2-aminoacridone (AMAC, Sigma) prepared in acetic acid/ DMSO (3:17 v/v) and incubated (23 ºC, 15 min, dark). A 40 µl aliquot of an aqueous solution of 1.25 M sodium cyanoborohydride (Sigma) was then added to each sample and incubated (37 ºC, 16 hrs, dark). Following this, 20 µl of glycerol was added to each sample. Standards were also prepared using known amounts of commercially available HA disaccharides (V-Labs, Covington, LA). If necessary, samples were stored at -20 ºC, prior to use.

For electrophoresis, all 8 lanes of a polyacrylamide MONO® gel (Glyko, San Leandro, CA) were loaded simultaneously with 4 μl of sample/standard using an 8-channel glass syringe (Hamilton, Reno, NV) and run with MONO® gel running buffer (Glyko), as adopted from a previously published method [282]. Briefly, the electrophoresis apparatus (Glyko) was placed in a trough of ice to maintain the buffer temperature below 10 ºC throughout the electrophoresis process. Samples were electrophoresed at a constant 500 V with a starting current of 25 mA/gel and a final current of 10 mA/gel for 80 minutes. After electrophoresis, the gels were illuminated with UV-B light (λ = 365 nm) in a FluorChem 8900 (Alpha Innotech, San Leandro, CA) and the band intensities were quantified and compared to the standard to quantify the amount of ΔDiHA present.

4.2.9 Endothelial Cell Culture

As stated in section 3.2.4, rat aortic ECs (passage 6-8) were cultured in MCDB-131 supplemented with FBS, pen/strep, ECGS, and L-glutamine. Spent medium was replaced thrice weekly.

4.2.10 DNA Assay for Cell Proliferation

The DNA content of EC cultured on surface-tethered HA 1500, HA 200, HA 20, D1, and D2 was used to compare the number of cells present at days 1 and 14, and hence quantify the proliferation of ECs in culture. The protocol for this assay is outlined in section 3.2.5.

4.2.11 Calcein AM Labeling

Calcein acetoxymethyl ester (Calcein AM; VWR) was used to fluorescently detect live cells and assess their morphology when cultured on HA surfaces. Metabolically active (alive) cells take up non-fluorescent calcein AM where intracellular esterases cleave the AM moiety producing highly fluorescent calcein within the cell outlining its morphology. ECs were seeded onto the HA surfaces at a concentration of 2×10^4 cells/ well of a 4-well culture slide and cultured for 1 week. Cells were then incubated with calcein AM (8 mg/ ml) in Hank's Buffered Salt Solution (HBSS; VWR; 45 min) and fixed in 4% w/v paraformaldehyde (Sigma). Surface adherent ECs were imaged on a TCS SP2 AOBS confocal microscope (Leica, Allendale, NJ).

4.2.12 Immunolabeling for CAM Expression

Expression levels of cell adhesion molecules (CAMs) by ECs cultured on D2-immobilized and fibronectin-coated (control; VWR) 4-well chamber slides, and with exogenously supplemented TNF-α (control; VWR) were compared by immunofluorescence and quantified by calculating the mean fluorescence intensity (MFI) on a per cell basis. EC activation was gauged from the extent of expression of intracellular adhesion molecule 1 (ICAM-1) and vascular cell adhesion molecule 1 (VCAM-1), previously shown to be elevated when EC cultured were exogenously supplemented with D2. ECs were seeded onto the HA surfaces at a concentration of 2×10^4 cells/ well of a 4-well and cultured for 1 week. The cells were then fixed with 4% w/v paraformaldehyde and incubated at 4 °C for 1 h with fluorescein isothiocyanate (FITC)-

conjugated mouse anti-rat CD54 (ICAM-1; Abcam, Cambridge, MA) and Alexa 488-conjugated mouse anti-rat CD106 (VCAM-1; Biolegend, San Diego, CA) diluted 1:100 v/v in PBS-azide. The slides were mounted with Vectashield containing 4,6-diamidino-2-phenylindole (DAPI, Vector Labs, Burlingame, CA) to stain the nuclei and cells were imaged using a Ziess Axiovision-200 epifluorescence microscope fitted with a FITC filter. To quantify the CAM expression, the MFI and cell number (based on number of nuclei) was calculated with Image J (n = 9/ condition), and the quotient was computed to determine the MFI/ cell. All images of CAM expression were taken with an exposure time of 100 ms.

4.2.13 SMC Cell Culture

Adult rat aortic smooth muscle cells were isolated by a method based on that described by Oakes *et. al.*[127]. Adult male Sprague-Dawley rats, each weighing 250-300 grams, were sacrificed previously by CO_2 asphyxiation as per protocols approved by the Animal Research Committee at the Medical University of South Carolina and at Clemson University. Aortal segments were removed from euthanized rats, from arch to the celiac axis, under sterile conditions, and spliced lengthwise in petri dishes containing cold phosphate-buffered saline (PBS) containing 2 mM Ca^{2+}. These spliced sections were then transferred to a dish containing 1-2 ml of collagenase (2 mg/ml; Worthington, Lakewood, NJ) and incubated for 10 minutes at 37 °C. DMEM:F12 media was then added to these collagenase treated samples and mixed well with gentle pippetting. Isolated aortal segments were further chopped crosswise into 0.5-m long pieces and

transferred using fine needles onto sterile petri dishes, pre-scratched to facilitate cell attachment. The explants were incubated in limited volumes of the above medium at 37 °C for a week, to establish primary culture. Cells were periodically observed microscopically in order to monitor attachment and proliferation. At the end of one week, the explants were removed carefully and sufficient DMEM:F12 added to the dish to promote cell proliferation.

Low passage rat aortic smooth muscle cells (SMCs; P4-8) were obtained by passaging primary cells isolated from adult rat aortal explants. Stock cells were trypsinized (0.25% trypsin/ 0.1% v/v EDTA; Invitrogen), pelletted by centrifugation (500*g*, 7 min), re-suspended in DMEM: F12 containing 10% v/v FBS and 1% v/v penicillin-streptomycin and seeded onto D1-coated 1-well glass chamber slides (Nalge NUNC International, Naperville, IL; culture area = 8 cm^2) at a density of 10^4 cells/ cm^2. The SMCs were also cultured on unfunctionalized 1-well glass chamber slides with and without exogenously supplemented D2 at a concentration equivalent to the average surface-tethered density (4 μg/ well). In all cases, cells were harvested at 21 days of culture (n = 9 wells/case). Spent medium was replaced twice weekly during the duration of culture, and pooled at the end of the 21-day culture period, along with the harvested cell layers.

4.2.14 Fastin Assay for Elastin

A Fastin assay was used to quantify the total amount of elastin matrix within cell layers (matrix elastin), and that released into the culture medium as a soluble precursor

(tropoelastin). Matrix elastin derived from the 21-day-old cell layers was digested with 0.1 N NaOH (98 °C, 1 h), and centrifuged (10,000g, 10 min) to yield an insufficiently crosslinked, alkali soluble fraction (S1), and a mature, mostly highly crosslinked, insoluble pellet (P2). Since the Fastin assay (Accurate Scientific and Chemical Corporation, Westbury, NY), quantifies only soluble α-elastin, the insoluble elastin was first reduced to a soluble form before subjecting to the assay. To do this, the elastin pellet (P2) was dried to a constant weight, solubilized with three cycles of treatment with 0.25 N oxalic acid (1 h/cycle, 95 ºC), and the pooled digests then filtered in microcentrifuge tubes fitted with low molecular weight (10,000 Da) cut-off membranes (Amicon, Houston, TX). The insufficiently crosslinked, soluble elastin fraction retained in the oxalic acid-free fraction (S3) and in the water-reconstituted hydrolysate (S2) were also quantified using the Fastin assay. The weight of insoluble elastin using the Fastin assay was compared to that determined by weighing the dry elastin pellet (P2), to affirm low/ no loss of elastin material during matrix processing. In each case, the ratio of matrix elastin to total (tropo+ matrix) elastin was compared to gauge efficiency of crosslinking into a structural elastin matrix.

4.2.15 Desmosine Assay

Desmosine content was assayed using an ELISA [221] to confirm the extent of crosslinking within the matrix elastin. Briefly, cell layers were scraped off, re-suspended in 1 ml of 5%v/v trichloroacetic acid, and centrifuged (3000g, 10 min, 4 °C). The pellet was digested with collagenase type VII (Sigma-Aldrich; 12 h, 37 °C) and re-centrifuged

(3000g, 10 min, 4 °C) to obtain a supernatant (D1) and a pellet. The pellet was digested with pancreatic porcine elastase type III (Sigma Aldrich; 12 h, 37 °C) to obtain soluble peptide fractions (D2). Fractions D1 and D2 were pooled together, hydrolyzed with 6 N HCl at 110 °C and dried to powder under inert nitrogen over 18–24 h. The dried samples were reconstituted in double deionized water and diluted for assay. The wells in micro-titer plates to be used for assay were pre-blocked using desmosine-albumin conjugate (EPC, Owensville, MO) in 0.05M sodium carbonate buffer (pH 9.6, 4 °C), then washed with 0.05% v/v Tween-20 and phosphate-buffered saline (PBS) solution (1 h, 25 °C). Desmosine standards/samples were incubated (12 h, 25 °C) with rabbit antiserum to desmosine–hemocyanin conjugate (Elastin Products Company, Owensville, MO). After removal of primary antibody solution, the wells were successively incubated with peroxidase-conjugated anti-rabbit IgG 0.05% v/v Tween 20-PBS solution (2 h, 25 °C). Finally, 0.08mg of the colorimetric compound 2,2 (E-Azinobis (3-ethylbenzothiazoline-6-sulfonic acid)) (Sigma), dissolved in 0.1M citrate phosphate buffer containing 0.003% v/v hydrogen peroxide (pH 4), was added to the wells and incubated (1 h, 25 °C). Absorbances were read in a UV spectrophotometer at $\lambda = 405$ nm.

4.2.16 Analysis of Matrix Ultrastructure

TEM was used to selectively compare the distribution and ultra-structure of matrix elastin between cell layers cultured with exogenous or surface-tethered HA oligomers, or in their absence (control). For TEM, the adhered cell layers (n = 3/ case) were fixed in 2.5% w/v glutaraldehyde, post-fixed in 1% w/v OsO_4, dehydrated with

ethanol, then embedded in resin, cut into 70 nm thick sections and finally stained with uranyl acetate and lead citrate.

4.2.17 Statistical Analysis

All experiments were performed in triplicate, unless otherwise mentioned. Statistical significance between and within groups was determined using Microsoft Excel's statistical function for t-tests, assuming unequal variance and two-tailed distribution. Differences were considered statistically significant at $p < 0.05$. Quantitative results are reported as mean ± standard deviation.

4.3 Results

Surface Characterization

4.3.1 Characterization of the Aminosilane Surface

An amine reactive dye was initially used to determine the presence of primary amines on the glass surface after treatment with the aminosilane (Figure 4.2). The silanated surface fluoresced brightly and uniformly indicating homogeneous tethering of amines. SEM and AFM micrographs (Figures 4.4B, 4.5B) and XPS spectra (Figure 4.6, Table 4.1) confirmed the presence of homogenous silane coatings, distinctly different from glass surfaces (Figures 4.4A, 4.5A). The s-SDTB amine assay indicated a surface amine density of 9 ± 3 amine groups/ nm^2.

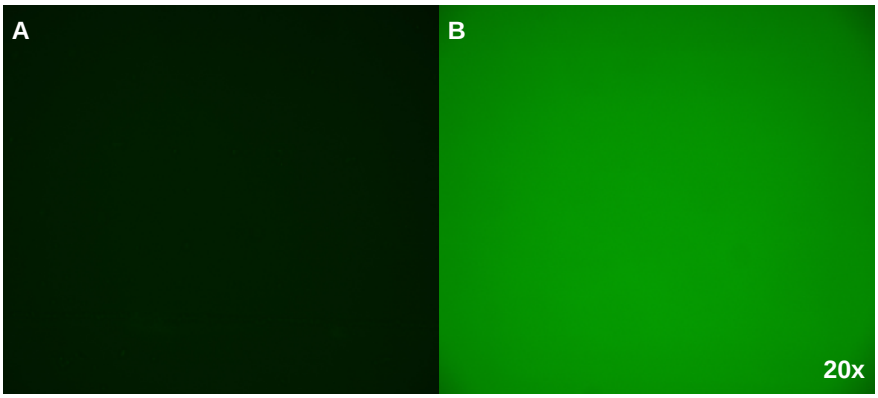

Figure 4.2 Amine reactive dye detection of APTMS. On non-functionalized glass (A) and absence of amines, the dye remained non-fluorescnece. However, upon interaction with amine groups on APTMS functionalized surfaces (B) the dye fluoresced green.

4.3.2 Microscopic Visualization of HA-Coated Surfaces

The presence of HA (HA 1500), or its fragments (HA 200, HA 20) chemically bound to the surface-tethered amine groups was confirmed by red fluorescence (Figure 4.3A-C). HA 1500 surfaces appeared somewhat less homogeneous with some gaps between areas of intense fluorescence while the HA 200 and HA 20 surfaces fluoresced more uniformly. Fluorescently-tagged HA 90 immobilized onto the chamber slides also appeared coated on the glass substrates (Figure 4.3D) similar to HA 20. Controls, HA surfaces not treated with biotinylated HABP (Figure 4.3E) or FITC-imaged aminosilanated glass (Figure 4.3F), did not fluoresce.

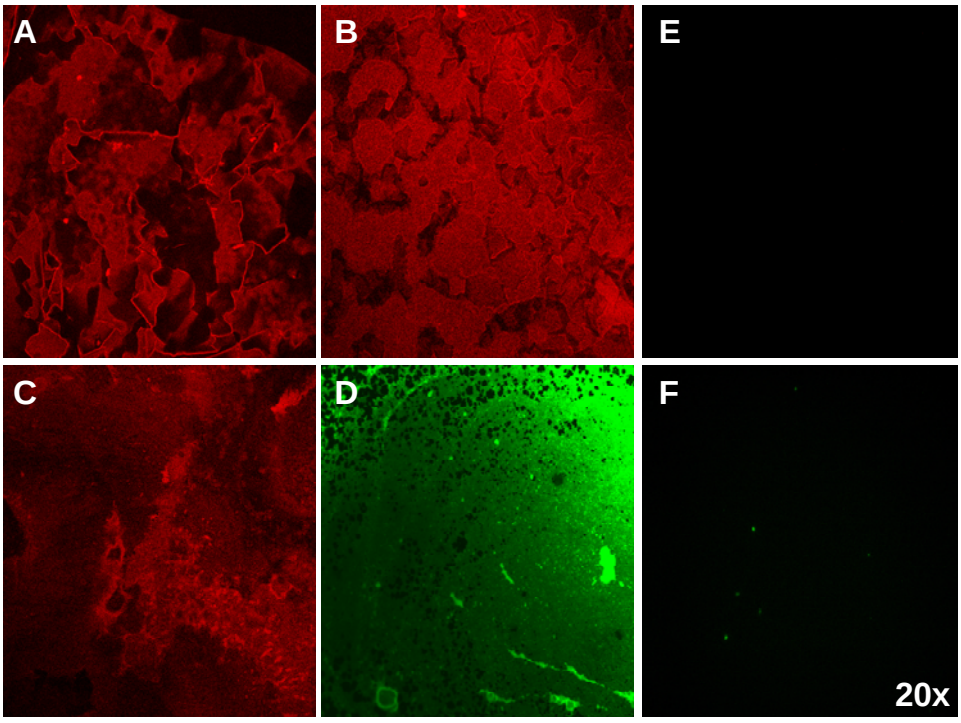

Figure 4.3 Immunofluorescence detection of surface-immoilized HA. HA 1500, HA 200, and HA 20 were tagged with b-HABP and a rhodamine-conjugated streptavidin and appear homogeneously coated (red) on the surface (A, B, C). FITC-conjugated HA (MW 90 kDa) was also uniformly bound (D; green). Controls, HA surfaces not treated with biotinylated HABP (E) or FITC-imaged aminosilanated glass (F), did not fluoresce. Magnification: 20×.

Scanning electron micrographs of the glass surfaces showed random circular patches, a likely attribute of commercial plasma treatment (Figure 4.4A). On silane-treated surfaces, these speckled patches were not seen although other structures, assumably aminosilane molecules, were seen across all replicate samples indicating a successful silane coating (Figure 4.4B). HA-coated surfaces (Figures 4.4C-F) were void of these structures, but instead showed smooth (HA 1500) or more fenestrated (HA 200, HA 20, D1) sheets, not seen on untreated glass and aminosilanated glass.

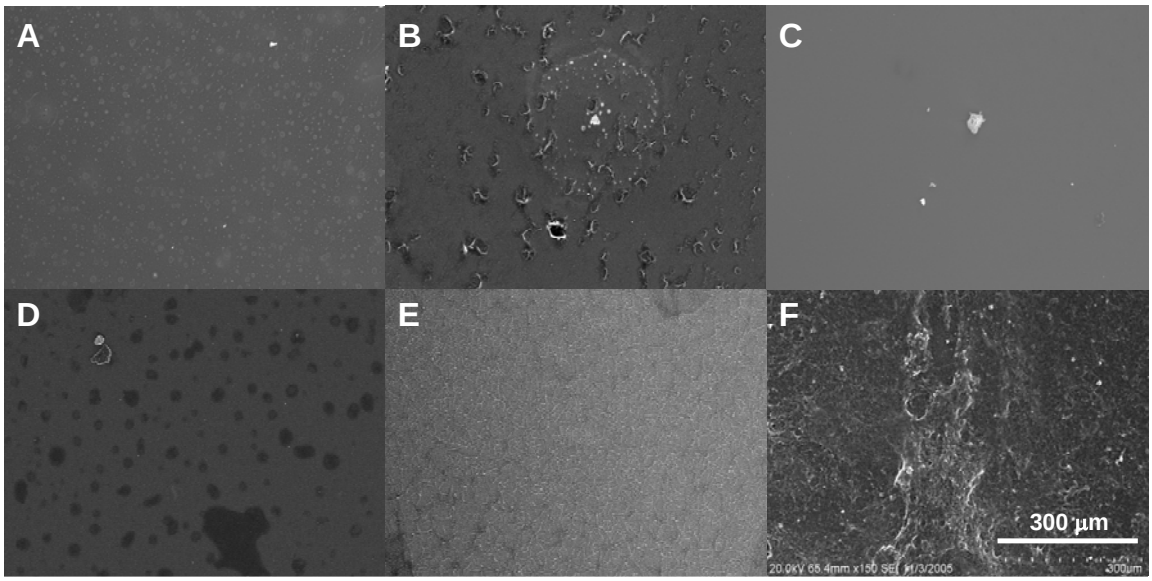

Figure 4.4 Scanning electron micrographs of glass, APTMS, and HA-tethered surfaces. Glass surfaces appear smooth with spotted disfigurements attributed to the commercial plasma coating (A). Aminosilane-treated glass shows the presence of APTMS molecules (B). HA 200, HA 20 and D1 appear as fibrous sheet-like networks (D, E, F) with some gaps within, while HA 1500 coated the surfaces as a smooth sheet without any detected morphology (C). Magnification: 150×.

AFM also conclusively demonstrated the presence of tethered aminosilane groups, HA and HA fragments and, for the most part, their formation of homogeneous layers. The increase in average peak height (roughness) of the aminosilane treated surfaces (0.1305 ± 0.0695 μm) in comparison to untreated glass (0.004 ± 0.001 μm), as indicated by AFM, confirmed the successful immobilization of the aminosilane. The roughness of the HA surfaces showed an inverse correlation to molecular weight of HA fragments (Figure 4.5). The average peak height atop surfaces coated with HA 1500, HA 200, HA 20 and D1 were 0.09142 ± .06699 μm, 0.0.4934 ± 0.2002 μm, 0.8345 ± 0.3771 μm and 0.8871 ± 0.3734 μm, respectively (n = 3/ surface).

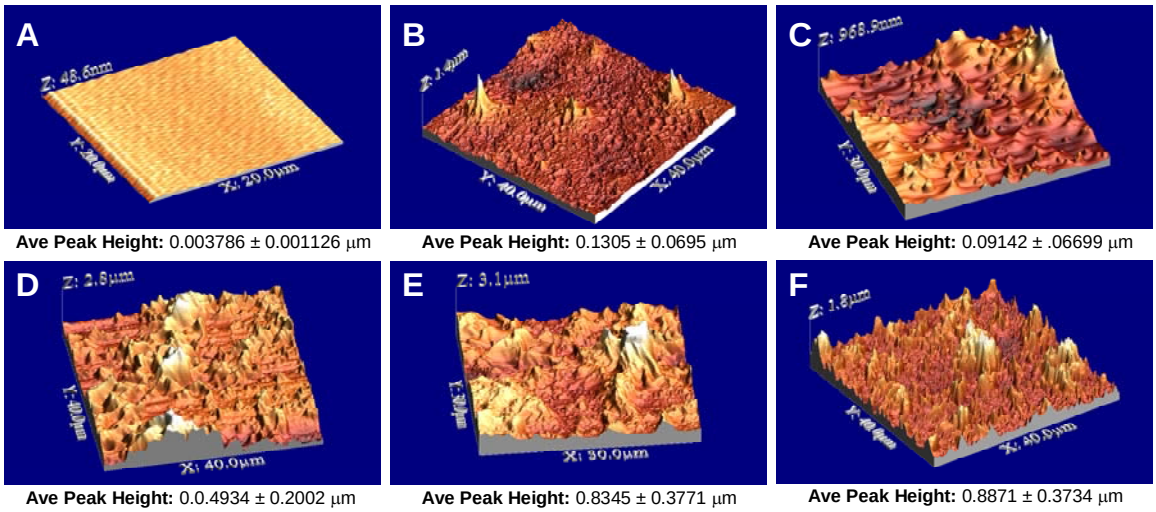

Ave Peak Height: 0.003786 ± 0.001126 µm | **Ave Peak Height:** 0.1305 ± 0.0695 µm | **Ave Peak Height:** 0.09142 ± .06699 µm

Ave Peak Height: 0.0.4934 ± 0.2002 µm | **Ave Peak Height:** 0.8345 ± 0.3771 µm | **Ave Peak Height:** 0.8871 ± 0.3734 µm

Figure 4.5 Atomic force micrographs and the corresponding peak heights of glass, APTMS and HA-tethered surfaces. Glass surfaces appear very smooth with a consistent atomic topography (A). The addition of aminosilane to the glass surface resulted in a much rougher surface (B). The peak heights indicate that the HA surface roughness are inversely proportional to MW of tethered HA chains. In accordance, HA 1500 (C) and HA 200 (D) appear more smooth than HA 20 and D1.

4.3.3 Elemental and Chemical Structure Analysis of Coated Surfaces

The results of elemental and chemical structure analysis of treated substrates, as determined by XPS, are shown in Table 4.1, Table 4.2 and Figure 4.6. XPS spectra generated on glass surfaces exhibited strong peaks for elemental silicon and oxygen, with carbon, calcium and sodium as minor contaminants. Tethering aminosilanes onto the surface reduced detection of silicon and oxygen while the elemental content of carbon and nitrogen was enhanced. The XPS elemental scan and high resolution spectra generated by the HA-coated surfaces varied as a function of their molecular weight, as will be discussed later. The high resolution spectra for HA 1500 and HA 200 were quantitatively similar, as were those for HA 20 and D1. Therefore, only one spectrum from each group was included.

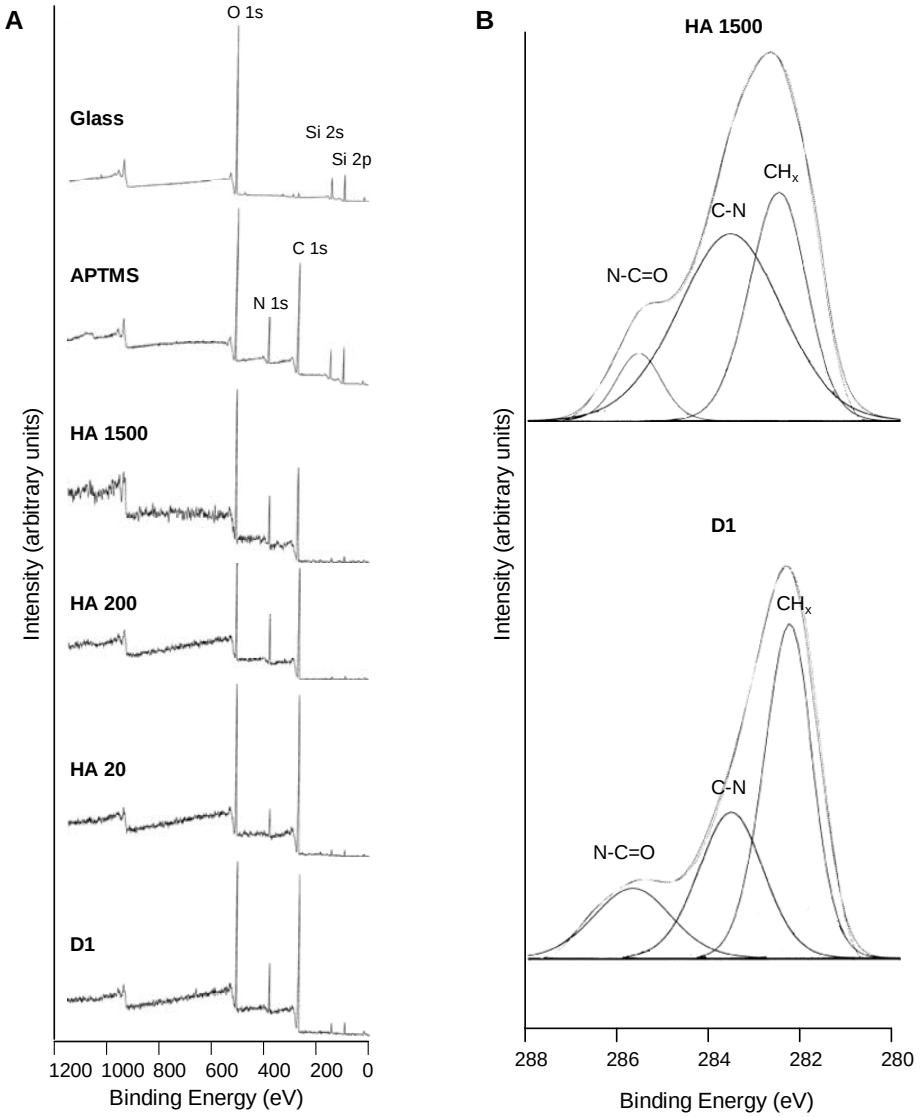

Figure 4.6 XPS elemental scan and C1s high resolution spectra of glass, APTMS and HA/ fragments/ oligomer-tethered surfaces. The prominent peaks observed corresponded to oxygen, silicon, nitrogen, and carbon (A). High resolution spectra of the HA C1s peaks indicated that the relative amount of N-C=O functional groups was inversely proportional to MW of tethered HA chains (B). Presumably, this is due to the inefficient binding of HMW HA to the aminosilanes.

	XPS Atomic Composition (%)			
Surface	Si	O	C	N
Glass	26.3 ± 0.2	66.5 ± 0.4	5.9 ± 0.4	—
APTMS	11.0 ± 0.2	23.8 ± 1.4	53.0 ± 1.0	12.1 ± 0.4
HA 1500	1.5 ± 1.7	29.7 ± 2.5	57.6 ± 1.7	11.2 ± 2.1
HA 200	0.6 ± 0.4	28.8 ± 2.6	59.9 ± 1.0	10.7 ± 2.0
HA 20	2.0 ± 0.7	24.4 ± 0.8	68.6 ± 1.8	5.0 ± 1.9
D1	2.9 ± 0.3	23.0 ± 1.2	65.4 ± 0.6	8.3 ± 0.9

Substance	XPS Atomic Composition (%)			
Quartz	66.6	33.3	-	-
APTMS	9.1	27.3	54.5	9.1
HA	-	42.3	53.8	3.8

Table 4.1 XPS analysis of glass, amine-bound and HA-bound surfaces and the corresponding theoretically predicted elemental profiles. Glass is composed primarily of oxygen and silicon. An increase in carbon and decrease in silicon is observed with the introduction of APTMS, a carbon based structure. Likely, the large chains of HA 1500 and HA 200 significantly block the detection silicon while a substantial spectral peak corresponding elemental nitrogen was still observed. The smaller chains of HA 20 and D1 allowed enhanced detection of elemental silicon but reduced the nitrogen peak. Results represent mean ± SD of readings obtained from n = 2 regions/ sample with a total of n = 4 samples/ substrate.

	XPS C1s Composition (%)		
Surface	CH	C-N/ C-O	O-C-O/ N-C=O
HA 1500	39.0	53.0	8.0
HA 200	13.7	76.4	9.9
HA 20	60.6	28.4	11.0
D1	57.3	27.6	15.1

Table 4.2 High resolution C1s composition of the HA surfaces. A greater amount of C-N and lower quantity of N-C=O was detected on surfaces with larger HA fragments (HA 1500, HA 200) indicating a higher binding efficiency of the smaller HA fragments (HA 20, D1) with the silane amines.

Quantification of HA Loss from the Surface

4.3.4 Toluidine Blue Assay

The amount of HA bound to the aminated glass surfaces was estimated from the decrease in absorbance due to loss of toluidine blue from a contacting solution, by reaction with surface-tethered HA (Figure 4.7). Absorbances of toluidine blue solution contacted with HA/ fragment-tethered surfaces were consistently much lower than glass and amine-tethered surfaces, indicating successful immobilization of HA. A high absorbance was generated on glass (3.07 ± 0.03) and APTMS-treated surfaces (2.89 ± 0.05), similar to fresh toluidine blue solution (3.07 ± 0.19). Toluidine blue incubated with the HA 1500 surface exhibited absorbances (0.85 ± 0.20) much lower than that for both HA 200- and HA 20-tethered surfaces (1.60 ± 0.38, 1.76 ± 0.39) and remained unchanged over 21 days of incubation of the substrate with culture medium. Retention of D1 on surfaces was tested with toluidine blue only on 0 and 21 days of incubation with medium, and generated the highest absorbances of the HA surfaces (2.45 ± 0.12).

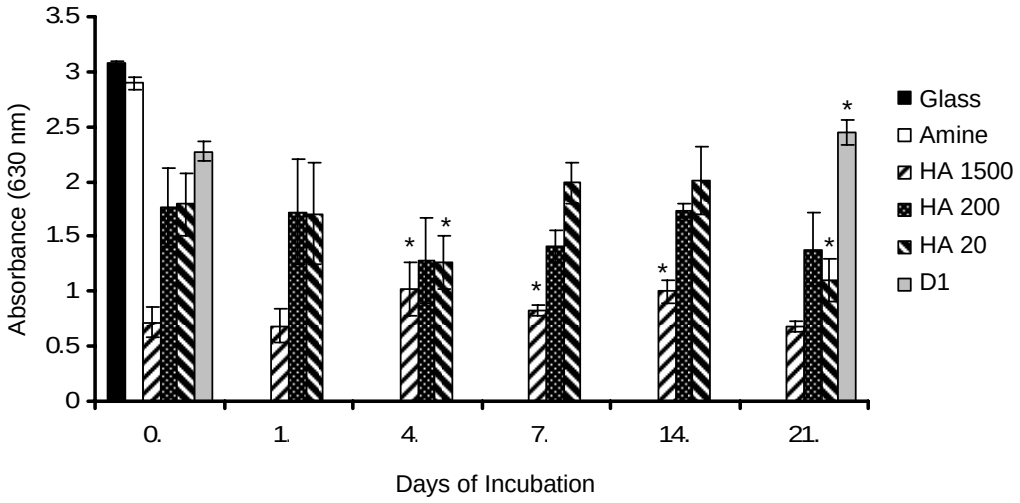

Figure 4.7 Toluidine blue assay of glass, APTMS and HA-tethered surfaces. Irrespective of fragment size, tethered HA appears to be stably retained over 21 days of incubation with serum-free medium as evidenced by a lack of absorbance change (i.e. increase) of the toluidine blue solution. Higher molecular weights of HA were able to bind more toluidine blue molecules from the solution due to a greater number and availability of unreacted carboxyl groups. [* denotes a p-value < 0.05 in comparison to day 0]

4.3.5 FACE Analysis

FACE analysis was used to quantify the amount of HA present on the surfaces. At day 0, HA 1500-tethered surfaces contained approximately 9 times the amount of HA dissacharide units (9.36 ± 1.68 μg) than the other fragment sizes (Figure 4.8). At day 0, HA 200, HA 20 and D1 surfaces contained approximately the same amount of HA dissaccharides (1.00 ± 0.48 μg, 1.31 ± 1.15 μg, 0.92 ± 0.56 μg, respectively). These coated amounts remained unchanged after 21 days of incubation with medium suggesting negligible loss from the surface irrespective of tested HA fragment size.

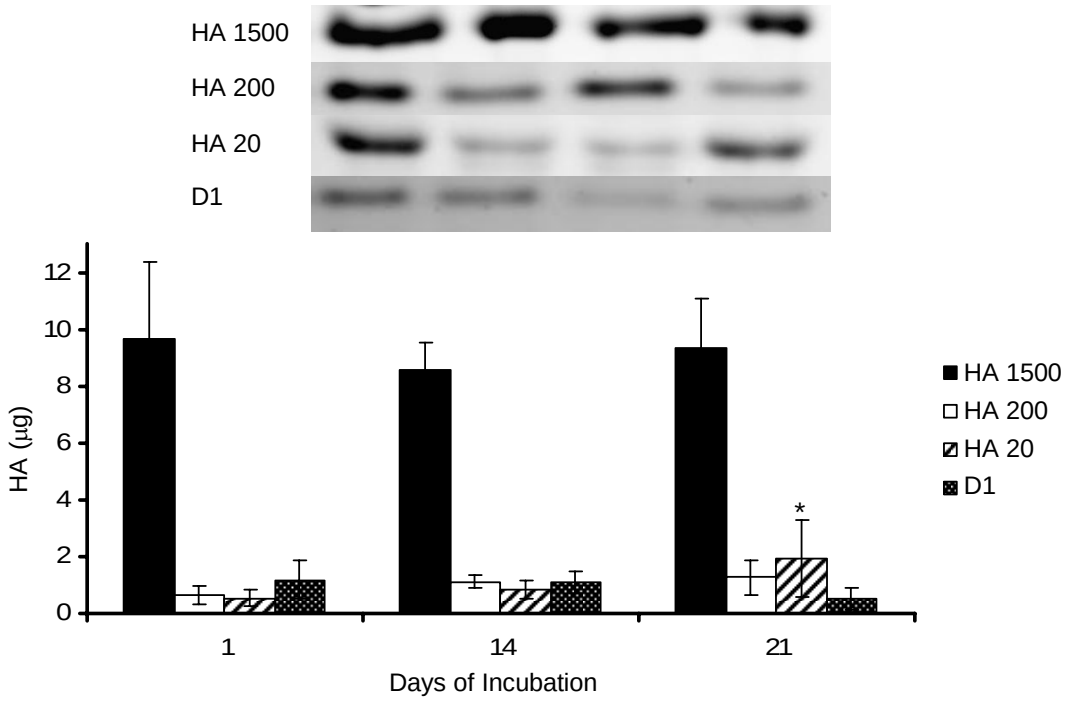

Figure 4.8 FACE analysis of HA surfaces. More HA 1500 was present on the surface than the other molecular weights. The amount of HA 200, HA 20 and D1 was similar. In all cases, the amount of HA was stable on the surfaces throughout the 21 days. [* denotes a p-value < 0.05 in comparison to day 1]

Endothelial Cell Culture

4.3.6 Endothelial Cell Proliferation

HA 1500, HA 200, HA 20 and D1-tethered surfaces did not incite significant proliferation of rat aortic ECs over 14 days of culture; the proliferation ratios were comparable to that obtained on the APTMS surfaces (negative controls; Figure 4.9). However, D2 provided the necessary stimulus for vascular EC proliferation; proliferation ratios were similar to that of the positive control cultures, i.e. cells cultured on glass and fibronectin.

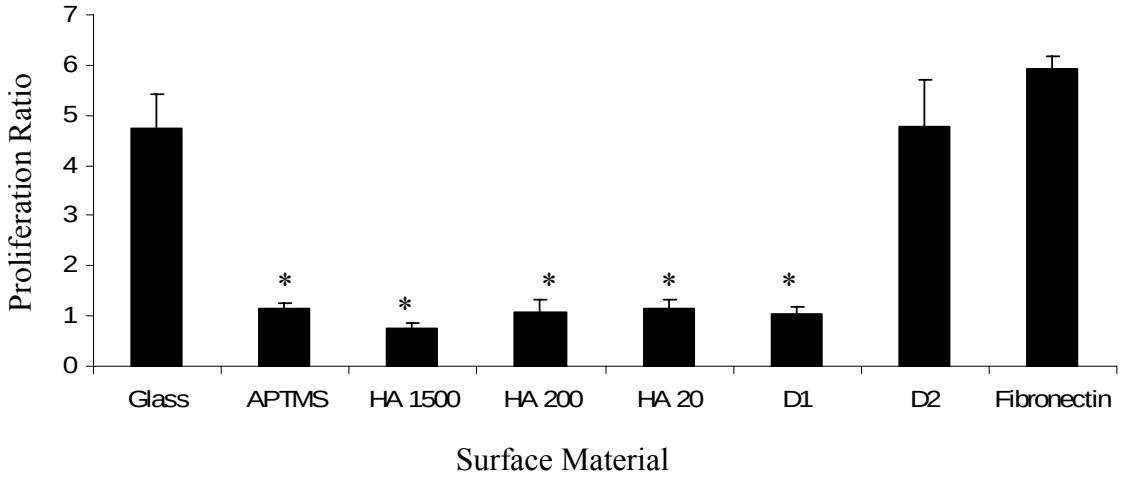

Figure 4.9 Proliferation of rat aortic smooth muscle cells on glass, APTMS, HA/ fragment/ oligomers, and fibronectin surfaces. Most HA surfaces (HA 1500, HA 200, HA 20, D1) did not support cell proliferation and induced similar proliferation ratios as the APTMS substrate. However, D2 surfaces stimulated EC proliferation to levels similar to glass and fibronectin. [* denotes a p-value < 0.05 in comparison to the glass control]

4.3.7 Endothelial Cell Morphology

HA 1500 (C) and large HA fragments (HA 200, D; HA 20, E) were unable to support EC adhesion, as seen in Figure 4.10. ECs attached to both D1 (F) and APTMS (negative control, B) but appeared rounded on D1 (F) surfaces and exhibited an abnormal morphology on APTMS surfaces. D2 (G) surfaces allowed ECs to attach and spread similarly to glass (A) and fibronectin (H) surfaces (positive controls).

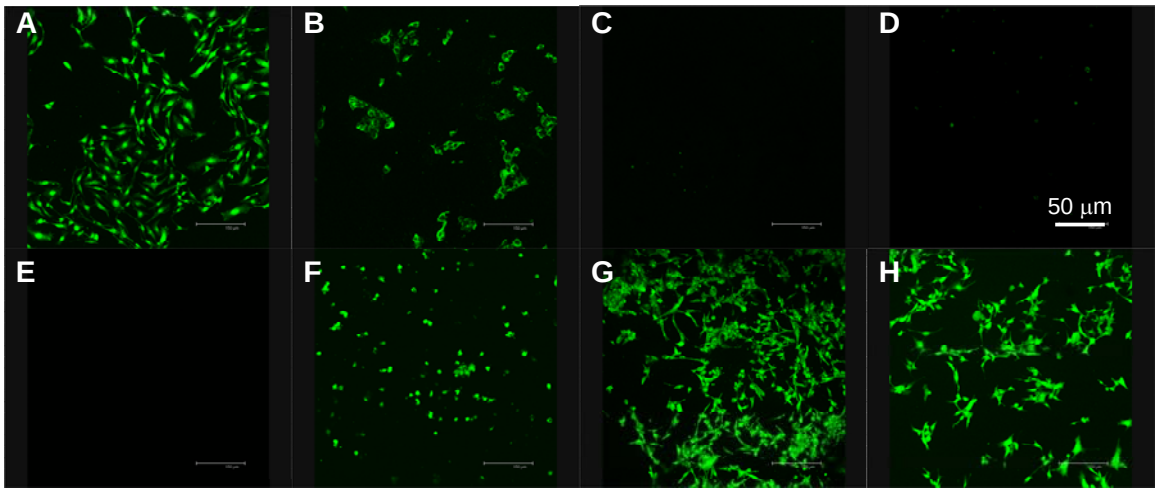

Figure 4.10 Cell morphology of ECs cultured on HA surfaces. Most HA surfaces (HA 1500, HA 200, HA 20) did not support EC attachment (C, D, E). ECs were able to attach to APTMS (B) and D1 (F) surfaces but retained a strange phenotype or remained rounded. D2 surfaces (G) supported EC attachment and spreading similar to glass (A) and fibronectin (H) surfaces.

4.3.8 Expression of Cell Adhesion Molecules

D2 surfaces elicited expression levels of EC activation markers that were greater than fibronectin surfaces but more attenuated than TNF-α-stimulated ECs. D2-tethered surfaces enhanced cellular expression levels of ICAM-1 (Figure 4.11) and VCAM-1(Figure 4.12) beyond that of fibronectin-coated surfaces (negative control), although these increases were significantly less relative to the increases in EC CAM expression induced by TNF-α (positive control). In addition, VCAM-1 expression levels were higher than ICAM-1 in all cases.

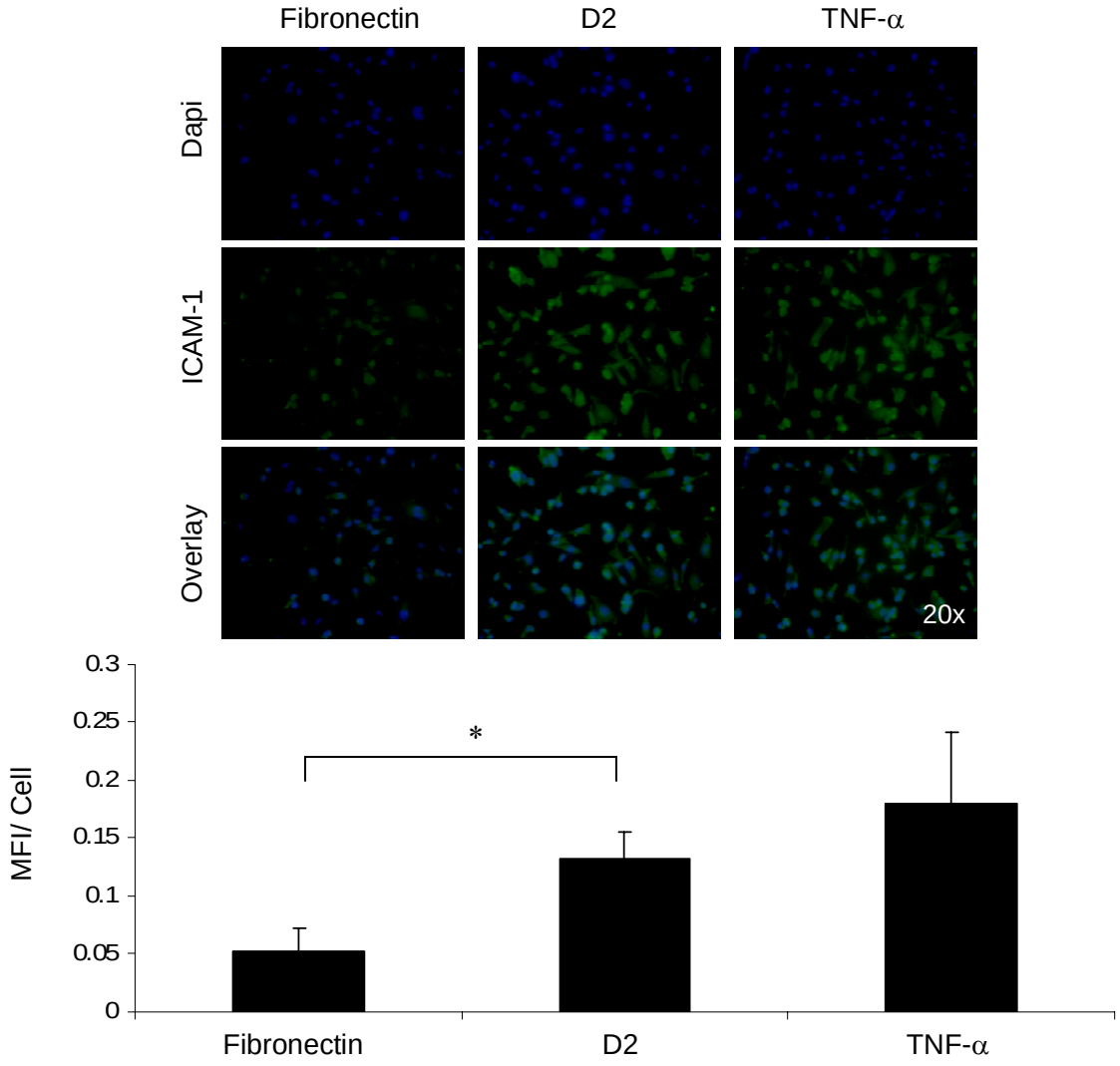

Figure 4.11 ICAM-1 expression of ECs cultured on fibronectin and D2 surfaces, and with TNF-α. D2 stimulated an increased amount of ICAM expression relative to fibronectin surfaces, however, this expression level was attenuated compared to TNF-α stimulated ECs. [* denotes a p-value < 0.05]

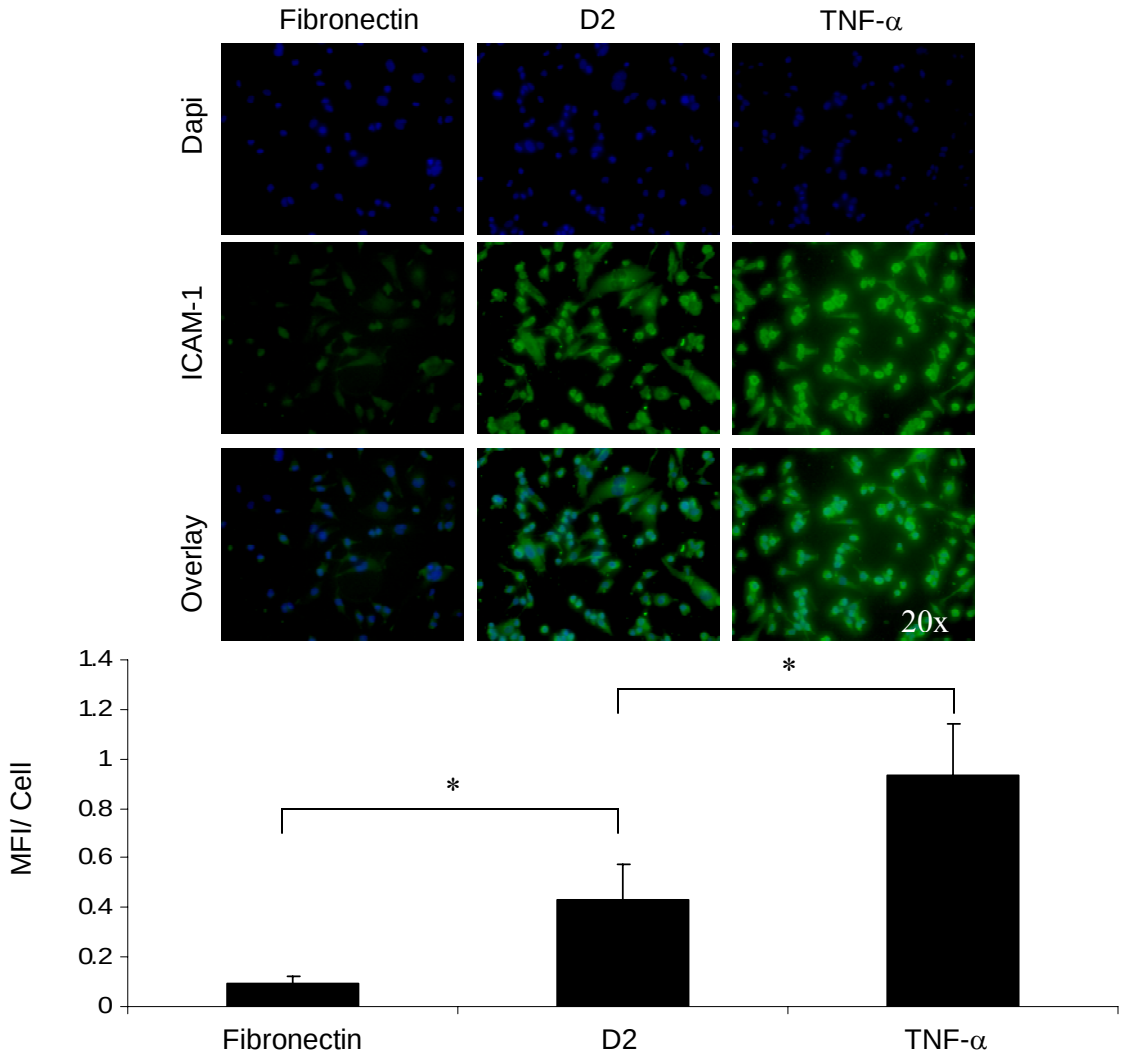

Figure 4.12 VCAM-1 expression of ECs cultured on fibronectin and D2 surfaces, and with TNF-α. D2 surfaces stimulated ECs to express a greater amount of VCAM then fibronectin surfaces, but these expression levels did not reach those of ECs cultured with TNF-□. [* denotes a p-value < 0.05]

Smooth Muscle Cell Culture

4.3.9 Tropoelastin Synthesis

Measured tropoelastin amounts (ng) were normalized to the average DNA content (ng). SMCs cultured on surface-presented and exogenous supplemented D1 showed 1.75 ± 0.001 and 1.74 ± 0.001 times the tropoelastin output, respectively, relative to the non-HA control cultures (156,509 ± 151 ng/ ng, 155,590 ± 116 ng/ ng respectively). There were no statistical differences in tropoelastin synthesis between cultures supplemented and surface-tethered with D1 (Figure 4.13).

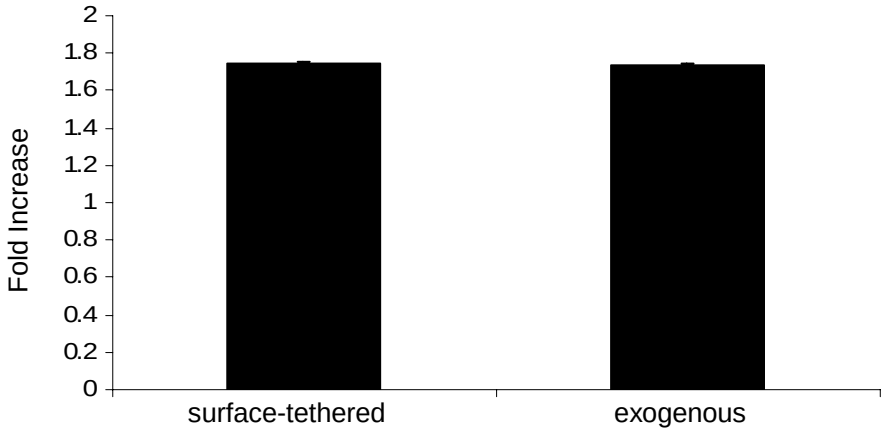

Figure 4.13 Effects of surface-tethered D1 oligomer mixtures on tropoelastin synthesis by adult RASMCs. Shown are the mean ± SD of average tropoelastin/ DNA (ng/ng) ratios normalized to corresponding measurements in control cell layers (no HAoligomers) plotted for surface-tethered and exogenous HA oligomers. The culture period was 21 days. Note that error bars are too small to be seen.

4.3.10 Crosslinked Matrix Elastin Synthesis

Elastin incorporated into the extracellular matrix was measured as a sum of two fractions, namely, a highly crosslinked, alkali-insoluble elastin pellet, and a more weakly crosslinked, alkali-soluble fraction. In general, the total DNA-normalized output of

matrix elastin for HA-oligomer supplemented cell cultures was significantly higher than that of control (non HA) cultures. In the presence of surface-tethered D1, DNA normalized matrix elastin output was 2.6 ± 0.04 times that produced by controls (931 ± 26 ng/ng). Similarly the DNA normalized matrix elastin output by cells cultured with the exogenous HA oligomer mixture was 2.7 ± 0.02 times that produced in controls (Figure 4.14). Differences between the test cultures were deemed statistically insignificant.

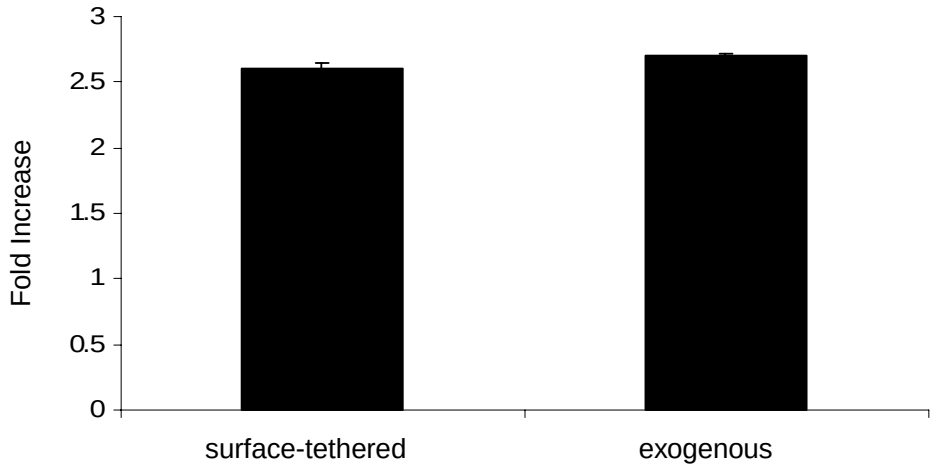

Figure 4.14 Effects of surface-tethered D1 on crosslinked elastin matrix synthesis by SMCs. Shown are the mean ± SD of average matrix elastin/ DNA (ng/ng) ratios normalized to corresponding measurements in control cell layers (no HA-oligos) plotted as functions of HA-oligos (surface-tethered and exogenously supplemented). The elastin matrix amounts respresent the sum of alkali-soluble and alkali-insoluble fractions.

4.3.11 Alkali-Insoluble Matrix Elastin Synthesis

In general, the total DNA-normalized output of alkali-insoluble matrix elastin for HA-oligomer supplemented/ tethered cell cultures was significantly higher than that of control (non HA) cultures cultured on glass substrates (Figure 4.15). In the presence of surface-tethered HA oligomers, DNA normalized matrix elastin output was 9.6 ± 0.6 times that produced by controls (682 ± 41ng/ng). Similarly, the DNA-normalized matrix

elastin output by cells cultured with the HA oligo mixture exogenously supplemented was 10.9 ± 0.2 times that produced in their controls (777 ± 12 ng/ ng; Figure 4.15). However, differences in between the test cultures (surface-tethered and exogenous HA oligomer mixtures) were deemed statistically insignificant.

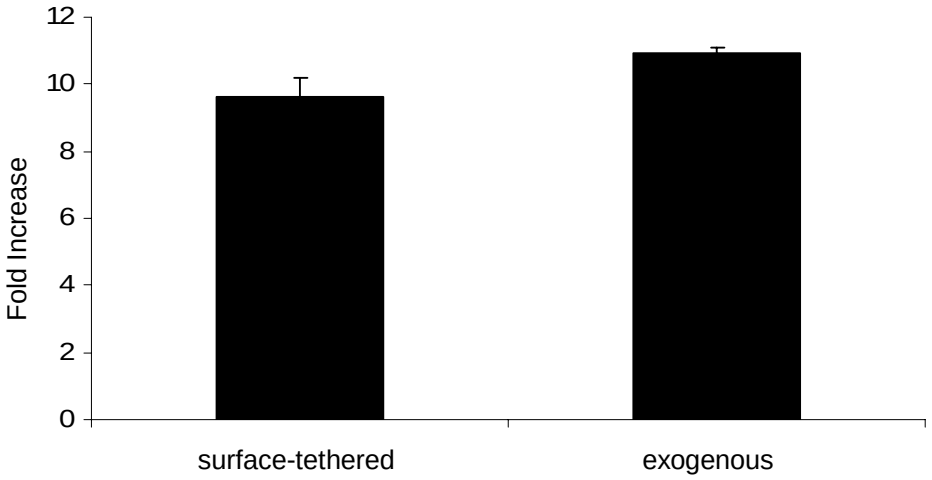

Figure 4.15 Comparison of amounts of alkali-insoluble pellet elastin synthesized by HA-oligomers (surface-tethered and exogenously supplemented) in comparison to their controls. Shown are mean ± SD of the measured amounts of pellet elastin/ DNA (ng/ ng) normalized to corresponding measurements in control cell layers (no HA), plotted as functions of HA oligomer mixtures either surface-tethered or exogenously supplemented.

4.3.12 Desmosine Assay for Matrix Elastin

Cells cultured with D1 showed greater amounts of desmosine synthesis respective controls. In addition, SMCs cultured on surface-tethered D1 further enhanced desmosine production beyond exogenous D1 indicating a benefit of surface immobilization (Figure 4.16).

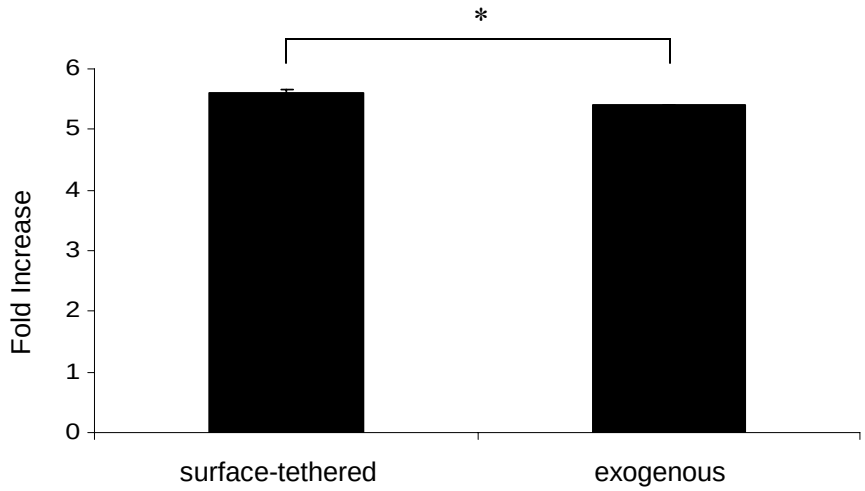

Figure 4.16 Comparison of desmosine synthesis by cells cultured with HA-oligomers (surface-tethered and exogenously supplemented) versus their controls. Shown are mean ± SD of the measured amounts of desmosine/ DNA (ng/ ng) and matrix elastin/ DNA (ng/ ng) normalized to corresponding measurements in control cell layers (no HA), plotted as functions of HA oligomer mixtures either surface-tethered or exogenously supplemented. [* denotes a p-value < 0.05]

4.3.13 Ultrastructural Analysis of Elastin Matrix

TEM micrographs of cell layers cultured with exogenous and surface-tethered HA oligomer mixtures for 21 days contained multiple layers of elongated, aggregating elastin fibrils and clumps uniformly sandwiched between alternating cell layers (Figure 4.17A, B). These deeply staining microtubules surrounded the periphery of aggregating elastin fibrils (Figure 4.17D). TEM of HA oligomer surface-tethered cell cultures showed a denser elastin-fiber network than exogenous oligomer supplemented cultures. Control cell layers at 21 days could be distinguished from sample cell layers due to the presence of far fewer elastin fibrils and amorphous clumps (Figure 4.17C). Elastin fibrils appeared to laterally aggregate; symbolizing formation of thicker elastin fibers in both surface-tethered and exogenous HA oligomer supplemented cultures (Figure 4.17A, B).

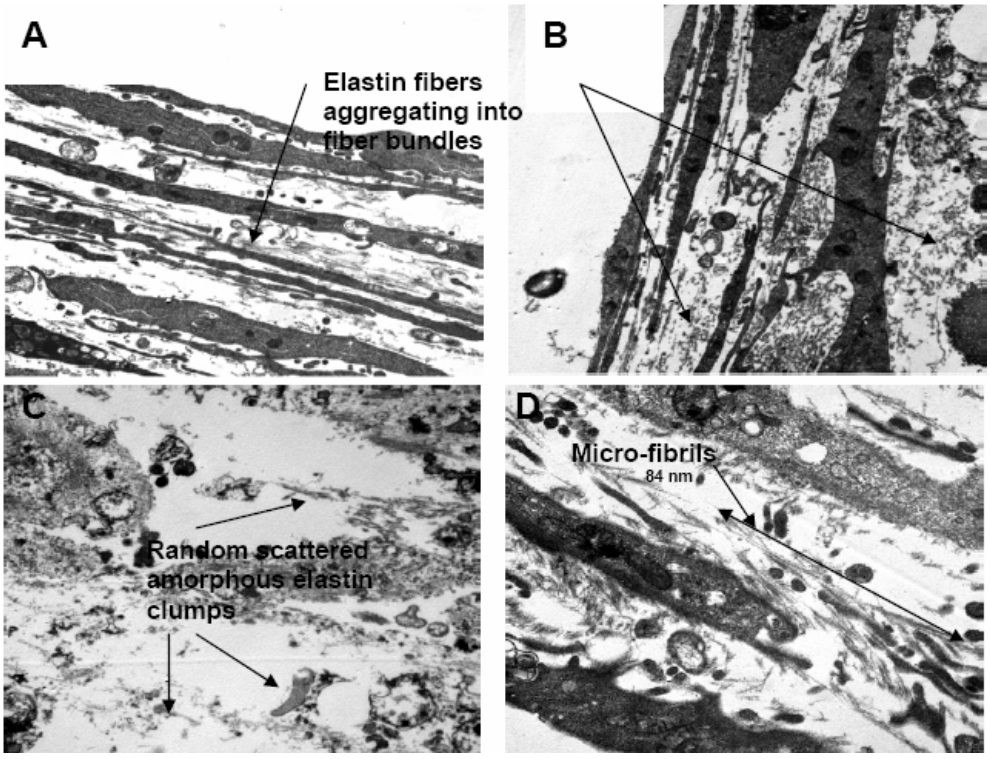

Figure 4.17 Matrix ultrastructure and fibrillin-mediated elastin deposition. Shown are representative transmission electron micrographs of 21 day-old cell layers cultured in the presence of HA oligomers, either exogenously supplemented (4 µg/ 5 ml; panel A), or surface-tethered (4 µg/ 5 ml; panel B) or in it's absence (C). In each case, representative images were selected from nearly 20 captured micrographs. A qualitative comparison of the matrix within test (A, B) and control (C) cell layers reveals differences in the amount and nature of elastin deposited. Both HA oligomer-supplemented (A, B) and control cell layers (C) preserved normal fibrillin microtubule-mediated elastin deposition. These deeply staining microtubules surrounded the periphery of aggregating elastin fibrils (D). Magnification: A-C is 15,000×, D is 25,000×.

4.4 Discussion

The long-term goal of our research is to develop HA-based scaffolds for vascular regeneration that will be conductive to the development of a normally functional luminal endothelium and stimulate SMCs to synthesize elastin. A healthy, confluent EC lining is crucial to maintaining the anti-thrombotic and anti-hyperplasic endothelial signaling pathways and the presence of elastin preserves homeostasis and provides the necessary

mechanical properties to blood vessels to accommodate blood flow. Both luminal ECs and elastin within the vessel wall are disrupted by injury or disease, therefore, the regeneration of these vascular elements are vital to the reinstatement of vascular homeostasis during treatment of vascular disease.

The choice of HA as a vascular implant material stems from it's biocompatibility and non-immunogenicity, an outcome of the high degree of homology in its structure across species [18], and its potential, as a ECM component, to evoke native, non-exaggerated responses from cultured vascular cells. HA has also been shown to exhibit angiogenic tendencies, although these effects, as with other phenomena observed with other cell types, appear to be highly specific to HA fragment size [19]. In our previous work, we have also seen that cells respond to HA oligomers more exuberantly than to larger sized HA, and show significant size-specificity in their responses, even within the oligomer size range. However, other studies have also shown HA fragments and HA oligomers to be capable of inducing inflammatory responses [18]. Thus, the distribution of bioactive HA fragments and oligomers within an HA-based scaffold must be defined and optimized to elicit desired outcomes (i.e. functional endothelialization, SMC elastogenesis) and prevent unwanted ones (i.e. inflammation). We thus seek to comprehensively determine the specific fragment-size effects of HA on EC function and SMC elastin synthesis.

Prior studies [31] determined that a model of exogenous supplementation of scaffolding materials inadequately predicted cell responses to the same materials when presented as a substratum, likely due to the absence of continuous cell-material contact.

In addition, fragmented HA/ oligomers cannot by themselves be crosslinked into stable solid scaffolds to test their stand-alone impact. Therefore, we have developed a surface-tethered model of HA to compare to the exogenous supplementation model.

Silane coupling agents are often used to durably link organic, and inorganic groups such as those present on glass. We chose to use a aminotrialkoxysilane due to its presentation of an exposed -NH_2 group and its hydolytic stability [309]. Trialkoxysilanes form 3D silane networks of bonded multilayers on the glass surface that restrict the infiltration of hydrolytic substances from solution. If necessary, however, silanes incorporating even more hydrolysis-resistant aromatic groups may be used in the future.

Among the chemically reactive groups on HA (-OH, -COOH) [200], we targeted the carboxyl groups specifically due to their ability to react with primary amines. To do this, the carboxyl groups of the component HA disaccharide monomers were activated with EDC into the chemically reactive and unstable O-acylisourea. This complex can either react with a primary amine to form stable amide bonds or undergo hydrolysis in the presence of water to reform the carboxyl. To prevent the hydrolysis of O-acylisourea, NHS is added to the solution. NHS combines with O-acylisourea to form a semi-stable and amine reactive NHS-ester to increase the efficiency of EDC-mediated coupling reactions [310]. In the past, some studies have used charged sulfo-NHS instead of NHS because of its increased solubility. No experiments were conducted to compare the solubility and relative reactivity of these molecules but NHS was found to readily and completely solubilize in aqueous solutions and therefore was used in these experiments. Although no concrete proof is available, one previous study expressed doubts in a similar

method of HA immobilization based on XPS results that deviated from the expected theoretical values. Therefore, we have presently characterized the created aminosilane and HA-tethered surfaces using various analytical techniques.

Analysis of the HA surfaces by fluorescence, SEM and AFM indicate that at the cellular scale (~10-20 μm), the HA coatings are highly homogeneous and continuous. Results of XPS analysis correctly reflected the changes in surface-elemental composition that might be expected to occur upon aminosilane treatment and HA immobilization. However, the relative content of these elements showed slight differences from that might be theoretically expected based on the stochiometry of HA, likely due to steric hindrance. Upon aminosilane treatment, an expected increase in nitrogen and carbon content was observed. The elemental profiles were similar to that theoretically expected APTMS. Assuming complete reaction of all tethered amine groups on the surface to the carboxyl groups on HA, the % elemental composition of HA-tethered substrates should be independent of their molecular weight. Yet, the XPS results show differences in elemental composition between HA 1500, HA 200, HA 20 and D1 surfaces. Specifically, as seen in Table 4.1, the % composition of nitrogen atoms on HA 1500- and HA 200-tethered surfaces was somewhat higher than that of HA 20 and D1 (11.2%, 10.7% vs. 5.0%, 8.3%). We believe that these differences stem from the greater gaps within the higher MW HA coatings and the less efficient binding to available tethered amine groups. High resolution XPS analysis confirms this since a higher % content of C-N and lower N-C=O bonding functionalities were detected for HA 1500 and HA 200 relative to the other sized HA fragments.

When a single disaccharide unit of polymeric HMW HA binds to an APTMS amine, the remaining strand may effectively prevent other such strands from binding to the APTMS molecules in the local vicinity by directly binding to them or sterically inhibiting their interaction with other strands. As a result, binding of HMW HA to surface amines is less efficient. It is also possible that the large size of the HMW HA strands also causes substantial strand entanglement to produce a compact zone of HA close to the aminated surface, yet creating sporadic gaps devoid of HA. This theory was supported by our low magnification immunofluorescence micrographs which indicated areas of intense fluorescence, likely due to large HA strands stacked on top of one another, adjoining darker ones (gaps/ pores) less densely covered with HA. Such a distribution of HA could more easily permit the detection of un-reacted, exposed nitrogen containing amine groups, to thus increase the elemental concentration of nitrogen above that expected theoretically. With regard to shorter HA fragments, such entanglement and steric hindrance were apparently far less of an issue as evidenced by fluorescence detection of uniform intensity, and much lower levels of detection of APTMS amines and a higher degree of C-N=O structures by XPS, which suggest more efficient reaction between APTMS amines and HA. Also, when imaged under high magnification (SEM), a fibrous surface was revealed, with clustered short HA fibers. Likely, these fibers were concentrated around the APTMS amine functional groups preventing their detection. In support of these observations, AFM data indicate higher peaks on surfaces tethered with HA 20 and D1 than that tethered with HA 1500 and HA 200. This suggests the shorter HA fragments were not entangled with one another to create a compact zone, but rather individually attached to

the amines.

The FACE outcomes support our hypothesis that HA 1500 forms entangled networks on the surface, unlike shorter HA fragments and oligomers; indeed, the amount of HA 1500 immobilized on glass was far greater than that of HA 200, 20 or D1. Shorter HA fragments likely do not stably entangle with one another due to their smaller size. Thus excess fragments were released from the surface when rinsed immediately after preparation but just prior to incubation with medium.

FACE and the toluidine blue assay both confirmed the long-term (21 days) retention of the immobilized HA/ fragments/ oligomers but each used a different process. FACE directly measures the amount of enzyme-digested tethered HA, while the toluidine blue assay utilizes an indirect approach. Toluidine blue binds to carboxyl groups present on HA dissacharides [311]. Since the number of disaccharides in each case is dependant on HA chain length, tethered amount between different HA size groups. However, for each HA size we can reliably monitor the retention of HA/ fragments / oligomers on the surface over time.

Since cells cultured on an HA scaffold would encounter HA as a substratum and not freely diffusing HA molecules, we sought to create HA-substrates that would somewhat replicate this environment. Yet, the results indicate that almost all forms of HA, bound utilizing the available carboxyl functional groups, do not allow EC attachment. This may be due to the high charge densities and smooth surface topographies of larger HA fragments; both of which are known to inhibit cell adhesion [312,313]. The only fragment size that provided a surface that allowed EC attachment was the highly

concentrated oligomer digest (D2). This may result in altered physical attributes, increased surface roughness that provides greater opportunities for cell anchorage and lower anionic charge densities that render cell-surface interactions thermodynamically favorable, or receptor-ligand interactions. In addition, the D2-tethered surface supplied ECs with a substrate conducive to proliferation, similar to fibronectin, with the potential to support a confluent EC layer. However, the D2-tethered surface also incited an increase in inflammatory marker expression (ICAM-1, VCAM-1). These results are similar to what we observed in the exogenous study (chapter 3), indicating the exogenous model closely mimics EC responses to different fragments of HA when presented in scaffold form. It can be inferred from these results that derivatized HA oligomers immobilized on a surface and exogenous HA oliogmers interact with EC receptors in a similar manner.

Although the reasons for the unique interactions of different-sized HA fragments with ECs is unclear, it is believed to be due to their differential interactions with cell surface receptors specific for HA. CD44 is a trans-membrane adhesion receptor found in several cell types, including ECs, and is the most studied among three cell membrane receptors for HA currently identified, the others being Receptor for HA-Mediated Motility (RHAMM), and Toll-Like Receptor 4 (TLR4) [232]. Studies have shown that HA oligomers can incite very different cell responses when bound to CD44 receptors, than when HMW HA interacts with them, because HA oligomers can cause clustering of multiple CD44 receptors and thus alter intracellular responses [293]. The stimulation of CD44 receptors by HA oligomers has also been suggested to enhance the production of

vascular EC growth factor (VEGF) and therefore promote EC proliferation [26]. The CD44 receptor is also known to mediate cellular adhesion [314]. This study shows that the interactions of HA oligomers and CD44 receptors are not altered by chemical derivatization and immobilization chemistries. In addition to their importance to EC function, CD44 receptor has also been shown to modulate vascular SMC behavior.

Another concern of this study was the potential alteration of HA oligomers to stimulate an elastogenic response by SMCs when immobilized onto a surface. Previous studies have shown SMCs stimulated with exogenously supplemented D1 produce increased amounts of tropoelastin and crosslinked matrix elastin, and in this study we investigated whether this phenomenon was maintained when the oligomers were presented to SMCs in a modulated scaffold environment. FACE analysis found the D1 digest of HA to contain 13.9 ± 3.6% HA 6mers and 8.0 ± 1.6% HA 12mers (chapter 3), while Matrix Assisted Laser Desorption/Ionization-Time of flight (MALDI-TOF) mass spectrometry suggests a 75.0 ± 0.4% HA 4mer content [31]. The elastogenic responses of vascular SMCs to exogenous and surface-tethered D1 were directly compared. In specific, we sought to compare the quality, quantity and desmosine concentration of cultured elastin, generated by SMCs in presence of both exogenous and tethered D1. We selected the dose of exogenous D1 (4 μg) to be equivalent to the amount of surface-tethered D1 (based on the FACE analysis) calculated as an average value (0.5 μg/ cm^2; 8 cm^2 total area) of the amount initially tethered onto the 1-chamber glass slide and the ultimate amount surviving hydrolysis over 21 days of culture.

Comparing quantitative matrix synthesis outcomes of SMCs presently cultured

atop HA-oligomer-tethered surfaces or with exogenous HA oligomers, it is clear that silane coupling of HA oligomers preserves innate cellular responses to these fragments. The amounts of tropoelastin, total matrix elastin and alkali-insoluble matrix elastin in test cultures were dramatically up-regulated relative to non-HA control cell layers. In addition, the quantity of tropoelastin, total matrix elastin and alkali-insoluble matrix elastin was not particularly influenced by mode of presentation of HA oligomers to the cells. We can infer from this finding that D1 enhances SMC production of elastin precursor and final crosslinking into matrix elastin, irrespective of the method by which they are presented to SMC cultures. This strongly supports a hypothesis that HA oligomers enhance recruitment of soluble tropoelastin and facilitates it's crosslinking into an insoluble matrix form. While this may be purely a charge effect wherein tropoelastin coacervates in presence of HA oligomers and is preferentially crosslinked, an alternate explanation might be that HA oligomers receptor interactions may have downstream effects such as increased activity and expression of lysyl oxidase (LOX), an important initiator of desmosine crosslinking. Yet another possibility is the absence of any effort to block endogenous elastase activity, wherein HA oligomer-cell interactions might instead interfere and affect elastase activity thus leading to enhanced elastin turnover, resulting in accumulation of matrix elastin.

An important difference between cell layers cultured with exogenous and surface-presented HA oligomers, was with respect to their desmosine content. The amounts of desmosine synthesized by both groups, was higher than that in control cultures, and statistically different among themselves; surface-tethered D1 increased desmosine

synthesis relative to exogenously supplemented D1. This in turn suggests that intimate cellular contact with D1 may be responsible for enhanced desmosine crosslinking. This phenomenon may also be attributable to previous suggestions that surface-tethered D1 attracts, coacervates and cross-links elastin deposited on its surface, thereby facilitating its crosslinking by lysyl oxidase into a more stable elastin matrix [315]. This finding is also supported by observation from our previous studies [220] that cells atop HA crosslinked gel scaffolds cause enhanced crosslinking of elastin matrix due to a possible effect of highly anionic HA which possibly attract, and coacervate elastin on their surfaces.

TEM analysis provided conclusive evidence that tethered D1 prompted cells to lay down a matrix characterized by the presence of amorphous elastin clumps and numerous aggregating elastin fibers, the latter barely seen in control (non-HA) cultures. Although biochemical analysis indicated insignificant differences in elastin amounts within cell cultures incorporating exogenous and surface-tethered D1, there were some visual differences in the organization of elastin. In the surface-tethered cultures, fewer amorphous elastin clumps and more fibers were observed indicating a more stable form of elastin.

Thus, the results of this study strongly suggest that presentation of HA oligomers, either as an exogenous supplement or tethered onto a surface, does not alter its influence on EC functionality or SMC elastin synthesis, as would be deduced from EC proliferation and CAM expression, and quantitative analysis of SMC elastin production. However, the presentation of D1 immobilized on a cell substrate appears to somehow benefit the crosslinking of soluble elastin and facilitate its organization into elastin fibers.

The results of our exogenous (chapter 3) and this surface-immobilized studies indicate that HA oligomers may stimulate modest inflammatory CAM expression, while HA 1500, in general, had a more limited effect. In order to limit the inflammatory response of ECs to HA oligomers we aim to incorporate moderate concentrations these HA oligomers into a more bioinert HA 1500 scaffold formed by crosslinking HA into a hydrogel. We believe these scaffolding materials composed of optimized ratios of HA oligomer and HA 1500 will diminish the inflammatory response of ECs to HA oligomers but maintain the ability of HA oligomers to stimulate ECs to growth, regenerating a normally functional endothelium on the hydrogel surface.

4.5 Conclusions

Two of the main obstacles in vascular graft development are the regeneration of a confluent EC layer on the luminal surface and restoration of a mature elastin matrix within the vessel wall. HA has been shown to be beneficial in this regard as an exogenous supplement but the utility of HA fragments/ oligomers as a scaffolding material is unclear. Therefore, we sought to immobilize HA fragments/ oligomers onto a surface to investigate if this effected their stimulation of EC function and SMC elastogenesis. In this study, we successfully chemically bound a wide range of HA fragment sizes onto glass chamber slides creating culture surfaces useful towards determining the size-specific cellular responses of surface-tethered HA. EC culture on these surfaces indicated that these cells only attached to HA surfaces composed of a highly concentrated digest of HA oligomers (D2), while larger sized fragments of HA deter cell adherence. The D2

surfaces also stimulated EC proliferation and CAM expression similarly to our observations with exogenous D2, in section 3. SMCs cultured on a less concentrated mixture of HA oligomers (D1) increased tropoelastin and crosslinked matrix elastin production similarly to exogenously supplemented D1. However, surface-tethered D1 exhanced desmosine crosslinking and elastin fiber organization relative to exogenously supplemented D1. These results support the beneficial use of HA oligomers within HA-based vascular scaffolding materials due to the maintenance of their function when immobilized onto a substrate. However, the enhanced CAM expression elicited by both exogenous and immobilized HA oligomers is a concern. Therefore, the next step in this project is to incorporate moderate concentrations of these HA oligomers into scaffolds composed of HA 1500 to reduce EC CAM expression, maintain their proliferative characteristics, and yet create a biomaterial with good handling properties.

CHAPTER 5

THE IMPACT OF HA OLIGOMER CONTENT ON PHYSICAL, MECHANICAL, AND BIOLOGIC PROPERTIES OF DIVINYL SULFONE-CROSSLINKED HA HYDROGELS

5.1 Introduction

To overcome the poor or, alternatively, exaggerated vascular cell responses to synthetic materials, there has been a recent shift toward the development and use of "natural or tissue-based" biomaterial scaffolds that could potentially evoke more appropriate, and accelerated regenerative/ healing responses by vascular cells. The extracellular matrix (ECM), once regarded simply as a structural scaffold, is now recognized as an important modulator of cell phenotype and function [263]. From a tissue engineering perspective, it is thus increasingly apparent that the presence of ECM molecules is vital to developing a biomechanical and biochemical environment that mimics the cellular surroundings within native tissues. One class of ECM molecules that is increasingly studied in the context of designing regenerative materials are glycosaminoglycans (GAGs). One such GAG, hyaluronic acid (HA), occurs naturally in connective tissues (e.g. skin) as a simple, linear molecule consisting of repeating dissacharide units of N-acetyl-D-glucosamine and D-glucuronic acid [17]. Most cells have the ability to synthesize HA at some point during their cell cycle, signifying that the molecule has vital function in several fundamental biological processes [18].

From a biomaterials standpoint, HA has been increasingly recognized as an appropriate biomolecule to modulate tissue regeneration, since it can be chemically

derivatized into biomaterials with little change to it's inherent biologic properties. It is now known that HA, when physiologically degraded into smaller-sized fragments, facilitates wound healing by promoting angiogenesis [19]. HA fragments can, under specific circumstances, also incite early inflammation, which is critical to initiate wound healing, and then modulate later stages of the process to stabilize the matrix and reduce of long-term inflammation [18]. In an uncrosslinked state, HA is also highly biocompatible and has been shown to poorly elicit a foreign-body response upon cross-transplantation due to the high degree of structural homology that HA exhibits across species and tissue types [18]. In addition, HA is amenable to binding peptides, matrix proteins, and growth factors capable of further modulating cell responses [220,316]. Although the modes of interaction between HA and the human body are still incompletely understood, the favorable characteristics outlined above have assured its extensive use as a scaffolding biomaterial for tissue engineering applications, most recently for cartilage [20] and dermal [21] repair and regeneration. Our lab is currently investigating the potential use of HA as a vascular regenerative implant material. Since HA forms a significant (4-7% w/w) component of vascular ECM [22], we hypothesize that HA modified biomaterials will provide biomechanical and biochemical signals to vascular cells to ensure a healthy physiologic-like phenotype.

In previous sections (chapters 3, 4) we reported on the size-specific effects of HA on vascular ECs. Briefly, we found exogenous supplementation of a mixture of HA oligomers (D2), containing predominantly 6mers and 12mers, to stimulate EC proliferation, secretion of pro-angiogenic growth factors, and formation of a micro-

vascular network. The chemical immobilization of these HA oligomer mixtures onto 2-D cellular substrates (glass) did not alter their impact on EC behavior differentially from when the same mixtures were exogenously delivered to ECs (see chapter 4). This reinforced our hypothesis that chemical derivatization of HA oligomers does not necessarily alter their cellular interaction and hence, could likely be incorporated into cell-contacting biomaterials, with little or no detriment. However, under both presentation modes, this pro-endothelial HA oligomer mixture somewhat elevated EC expression of inflammatory CAMs. In addition, when HA oligomers are crosslinked, the resulting biomaterials are fluid-like and exhibit very poor handling properties. One way to address these problems, is to incorporate the bioactive HA oligomers within mechanically robust constructs containing chemically-crosslinked, highly biocompatible and rather bioinert, high molecular weight (HMW) HA (MW > 1×10^6 Da).

Previous studies with divinyl sulfone (DVS)-crosslinked HA hydrogels, composed of HMW HA alone, showed them to be bioinert and non-conducive to cell spreading and proliferation [306]. However, it was shown that such gels could be bio-activated by controlled surface-irradiation with UV light (λ = 254 nm), a process that randomly splices HMW HA to generate HA fragments of a range of sizes, including HA oligomers [306]. It was observed that vascular cells readily attached, spread, proliferated and generally exhibited a healthy phenotype, and normal functionality when cultured atop these bio-activated gels. Since the effects of UV light can be difficult to control, and can potentially cause random ionizations that are structurally disruptive, a better approach is to create 'bioactivated' gels containing bio-inert long-chain HA, necessary to maintain

mechanical integrity and potentially provide a high degree of biocompatibility, and smaller, more cell-interactive HA fragments/ oligomers. In pursuing this approach, it is however important to incorporate optimally-sized HA fragments, and modulate their content within the HA biomaterial such as to evoke desired cell responses, and yet prevent exaggerated responses (e.g. inflammation) that can be potentially elicited by HA oligomers. At the time this study was conducted, the use of HA oligomers as biomaterials for enabling functional vascular endothelialization and tissue regeneration had not been thoroughly investigated. Particularly, the effects of crosslinking HMW HA/ HA oligomers to obtain HA scaffolds with good handling properties, and the densities at which bioactive HA oligomers need to be presented on these biomaterials to achieve the desired EC responses were unknown. In the current study we therefore specifically investigate the impact of crosslinking HMW HA and HA oligomer mixtures with divinyl sulfone (DVS) on the physical, mechanical and biological properties of the resulting material.

5.2 Materials and Methods

5.2.1 Preparation of HA Oligomer Mixtures

As mentioned in section 3.2.1, HA 1500 (MW 1.5 – 1.8 × 10^6) was enzymatically digested to produce a mixture of HA oligomers (D2). Briefly, HA 1500 (5 mg/ ml) was digested with bovine *testicular hyaluronidase*, (4.5 mg/ ml; 439 U/mg) in a solution of digest buffer (37 °C) for 48 h. The enzyme was then precipitated, its activity terminated by boiling (2 min), and cooled on ice. Following centrifugation (2800 rpm, 10 min), to

separate the enzyme from the mixture, the supernatant was dialyzed in water (12 h) and then freeze-dried overnight to generate lyophilized HA oligomers. The mixture was analyzed by FACE and found to contain 33.3 ± 2.4% w/w of HA 6mers and 39.2 ± 2.7% w/w of HA 12mers, with oligomers of closely-related sizes forming the balance (see chapter 3).

5.2.2 Hydrogel Formulation

HA hydrogels crosslinked with DVS (DVS-HA) were formulated using methods loosely based on a previously described protocol [317]. Briefly, HA 1500 with added D2 (0, 5, 10, 20% w/w) was completely dissolved at a concentration of 45 mg/ ml in a 1:4 v/v solution of 1M sodium hydroxide (NaOH; to maintain a high pH): 1M sodium chloride (NaCl; to increase the dissolution rate of HA), pH 13.0. Thorough mixing of the resulting viscous solution was achieved by repeated transfer of the mixture between two sterile syringes (Beckton Dickenson, Franklin Lakes, NJ) through a 3-way stopcock (Kimble Kontes, Vineland, NJ). The mixture was then centrifuged for 5 min at 1000 *g* to remove air bubbles and aliquoted into cylindrical molds (for rheology, compression: 2 cm^2, 0.5 ml; for all other analytical techniques: 0.79 cm^2, 0.2 ml). The aliquoted mixtures were homogenously crosslinked by adding DVS (Sigma; Density = 1.177 g/ ml) directly into the aliquoted HA solutions at two concentrations (1:1 or 1:2 w/w DVS:HA), which translated to added volumes of 7.6 μl and 3.8 μl for the 0.79 cm^2 mold. A spatula was used to mix DVS into the solution and the hydrogel was allowed to form (2 hr) through radical addition reaction between the vinyl groups of DVS and hydroxyl groups of HA

(Figure 5.1). The crosslinked gels were thoroughly washed in DI water (3 cycles; 2 hr/ cycle) to leach out unreacted DVS, and then finally equilibrated in sterile PBS. There were therefore a total of 8 formulations (4 oligomer concentrations × 2 crosslinker densities). The dimensions (height and diameter) of the swollen cylindrical hydrogels crosslinked in the 0.79 cm^2 mold were measured with a digital caliper (Fisher, Pittsburgh, PA).

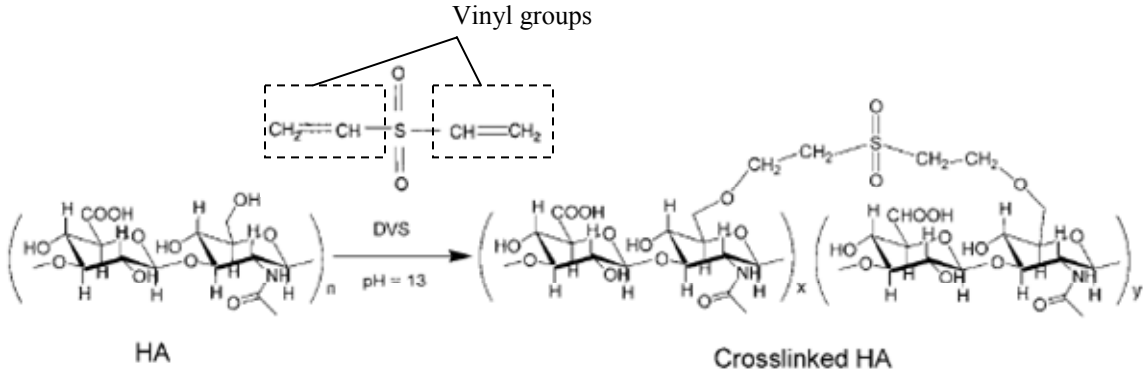

Figure 5.1 Chemical schematic of DVS-HA hydrogel formation. The vinyl groups of DVS combine with the hydroxyl groups of HA through radical addition.

5.2.3 Fourier Transform Infrared Spectroscopy

Fourier transform infrared – attenuated total reflectance (FTIR-ATR) was performed to determine the chemical alternations induced by incorporation of DVS into the HA hydrogel. Crosslinked DVS-HA was freeze-dried and analyzed on a Varian 660-IR FTIR spectrometer (Varian, Palo Alto, CA) and compared to uncrosslinked HA (n = 3). The spectra were recorded in a frequency range between 400 cm^{-1} and 4000 cm^{-1} with a spectral resolution of 4 cm^{-1}. A spectral library (Mentor Pro, Biorad, Hercules, CA) was used to identify the peaks and the corresponding bond vibrations.

5.2.4 Fluorescent Method to Detect Incorporation of HA Oligomers within Gels

HA oligomers (D2) were fluorescently labeled prior to incorporation within the hydrogel to evaluate their retention within the respective gels. D2 was dissolved (1.25 mg/ ml) in a 0.0125 M solution of the fluorescent dye 2-aminoacridone (AMAC, Sigma) prepared in acetic acid/ DMSO (3:17 v/v), and incubated for 15 min in the dark. An equivalent amount of 1.25 M sodium cyanoborohydride (Sigma) was then added and incubated (37 °C, 16 h, dark). The fluorescently labeled-D2 was then recovered and purified by precipitation in acetone and re-dissolution in DI water (3 cycles), and finally precipitated in acetone and freeze-dried in the dark. Fluorescent D2 was then incorporated into DVS crosslinked hydrogels, as described in section 5.2.2, and the fluorescence intensities (λ = 365 nm) of the gels (n = 4), was monitored at regular intervals over 21 days of incubation in PBS (37°C) using a FluorChem 8900 (Alpha Innotech, San Leandro, CA). Gels were imaged with a constant exposure time of 200 msec.

5.2.5 Apparent Crosslinking Density

The structural integrity of DVS-HA is primarily maintained by DVS crosslinks, bonding the HA strands to one another and limiting their freedom of motion. The incorporation of HA oligomers may reduce the effectiveness of these crosslinks, diminishing the overall mechanical properties of the gel. In addition, the crosslinking efficiency of DVS may not be 100%. Accordingly, we deemed it necessary to define the apparent crosslinking parameter, which in essence represents the effective crosslinking

within each gel formulation. Uniaxial compression testing was performed to calculate the apparent crosslinking density within the gels. Cylindrical gel samples (8 mm diameter) were punched out of a larger gel using a 8-mm-diameter corneal trephine (BRI, Malden, MA) and were compressed without constraining the edges (unconfined compression testing) on a DMA Q800 (TA Instruments, New Castle, DE). The gels were subject to an initial force of 0.05 N and were then compressed at a rate of 20% strain/ min (n = 8). All tests were performed in air, though the gels were kept hydrated in PBS while being compressed. Stress/ strain curves were developed according to the following formula developed by Flory [318].

$$\sigma = RT\left(\frac{\upsilon_e}{V_o}\right)\phi_{2,x}^{2/3}\phi_{2,s}^{1/3}\left(\alpha - \frac{1}{\alpha^2}\right) \qquad \text{(Eq 5.1)}$$

where σ – uniaxial compressive stress (Pa), P – universal gas constant (J/ mol K), T – temperature (K), $\phi_{2,x}$ – polymer volume fraction post-crosslinking, $\phi_{2,s}$ – polymer volume fraction swollen, ν_e/V_o – apparent crosslinking density (mol/ cm^3), and α – compressed fraction. This formula was developed for fully hydrated samples and water within DVS-HA was forced out of the gel during compression. Therefore, the initial slope of the curve (0 – 30% strain) was used to estimate the apparent crosslinking density of the gel.

5.2.6 Rheology

To further characterize the impact of crosslinking and oligomer incorporation on

hydrogel mechanics, rheological oscillatory shear stress experiments were performed. The strength or stiffness was experimentally determined by measuring the storage (G') and loss (G") moduli. An AR G2 rheometer (TA Instruments, New Castle, DE) was used in the parallel plate geometry, with a 25-mm plate and constant normal force of 0.2 N. A deformation angle of 1 mrad was maintained throughout each frequency sweep of 0.01–10 Hz (n = 4).

5.2.7 Swelling Ratio

Swelling tests were performed to study the effects of HA oligomer content and DVS concentration on the bulk hydrodynamic properties of the gels. Fully hydrated gels were blotted to remove excess PBS and the weight of the swollen samples were recorded using a sensitive balance (OH AUS, Pine Brook, NJ). The gels were then freeze-dried and weighed again. The swelling ratio was calculated by the following formula (n = 4).

$$SwellingRatio = \frac{W_s}{W_d} \qquad \text{(Eq 5.2)}$$

where W_s is the swollen mass of the gel (mg), and W_d is the dry mass of the gel (mg).

5.2.8 Scanning Electron Microscopy

SEM was performed to determine whether D2/ DVS concentration alters the surface morphology of the gel. In preparation for SEM, swollen gels were dehydrated

with acetone and the dried gel samples were coated with gold for 4 min using a SPI-Module Sputter Coater (Structure Probe, Inc., West Chester, PA) and imaged on an SEM (Jeol 100-JSM 5410 LV, Pleasanton, CA) at 150× magnification (n = 3).

5.2.9 In Vitro Degradation

In vitro enzymatic degradation of the hydrogels was measured as a function of time by incubating the gels in *testicular hyaluronidase* and monitoring the remaining dry mass of the hydrogel. The gels were initially soaked in digest buffer (150 mM NaCl, 100 mM CH_3COONa, 1 mM Na_2-EDTA, pH 5.0) overnight to reach swelling equilibrium. Bovine *testicular hyaluronidase* (Sigma-Aldrich) in digest buffer (2 mL of 50 U/ ml) was then added to each gel and incubated for 8 h at 37°C with mild mixing on a platform shaker. The dry masses of the gels were determined at 0, 2, 4, 6, and 8 h, and the enzyme solution replaced at each analysis time point (n = 3). This degradation profile was fitted according to first-order degradation kinetics using non-linear regression to estimate gel degradation rates.

$$C(t) = C_o e^{-kt} \qquad \text{(Eq 5.3)}$$

where, C(t) is the dry mass of the gel at time t (mg), C_o is the initial dry mass of the gel (mg), k is the degradation rate (h^{-1}), t is time (h).

5.2.10 In Vivo Biocompatibility

The biocompatibility of the hydrogels was determined by subcutaneous implantation in rats. Prior to implantation, hydrogels were sterilized in 95% v/v ethanol (Sigma) for 2 h and then re-hydrated in sterile 1× PBS overnight. Sprague-Dawley rats (~250 g) were anesthetized (0.01 ml/ g intramuscular injection of 4% chloral hydrate), shaved, and a 5-cm incision made in the skin along the spine. Blunt dissection was used to form a pocket between the skin and muscle, and muscle surface was cleared of fascia. Hydrogels and matrigel (Sigma) were placed directly into these pockets (8 implants/ animal; n = 7), as shown in Figure 5.2. After implantation, the surgical incision was closed with 4-0 silk suture with a FS-2 cutting needle (Ethicon, Piscataway, NJ).

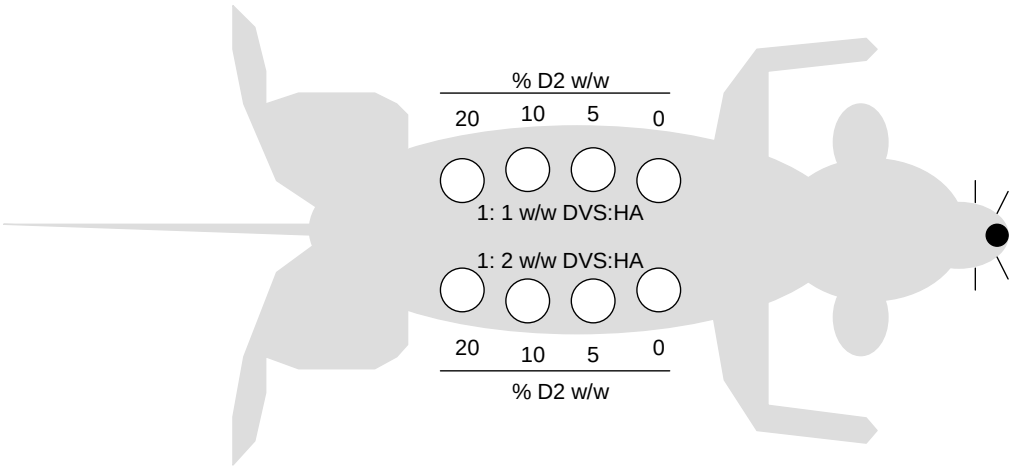

Figure 5.2 Illustration of subcutaneous implantation scheme of DVS-HA in the back of rats. All DVS-HA formulations were implanted into the same rat. Due to the lack of space, matrigel controls were implanted in separate rats.

At 3 weeks, the hydrogels and the adherent tissue capsules were explanted from the subcutaneous pockets, fixed in 4% v/v paraformaldehyde and soaked for 1 h intervals in 30% w/v sucrose, 1:1 30% sucrose: optimal cutting temperature (OCT; Sakura, Torrance, CA) compound and finally pure OCT. The explants were then embedded within OCT , frozen on dry ice and stored at -80°C. Prior to sectioning, frozen blocks were acclimated to -20°C (overnight) and cryosectioned perpendicular to the skin and muscle surfaces. The 8-μm thick sections were transferred onto HistoBond® glass slides (VWR) and stained with Haematoxylin and Eosin to detect inflammatory cell infiltration towards or within the implant. The tissue sections were imaged on a Leica DM IRB microscope equipped with a JVC TK-C1380 color camera. In addition, immunofluorescence methods were used to detect the collagen, and hence presence of a fibrous capsule within the tissue mass surrounding the implant. Sections, 15 μm thick, were initially quenched with 1% v/v phosphomolybdic acid to eliminate autofluorescence from collagen and then incubated with a primary antibody for collagen I for 1 h (rbt vs. rat col I; 1:100 in PBS; Chemicon, Temecula, CA). A solution of donkey serum (5% v/v in PBS) was added to the sections as a blocking agent (20 minutes) to prevent nonspecific binding of the secondary antibody. The sections were then treated with a FITC-conjugated secondary antibody (dky vs. rbt IgG; 1:500 in PBS; Chemicon) for 1 h. Draq 5 (1:2000 in PBS, 10 min; Biostatus, Leicestershire, UK) was used to fluorescently label the cell nuclei and visualize the cell density in the region surrounding the implant. Fluorescently labeled sections were imaged on a TCS SP2 AOBS confocal microscope (Leica, Allendale, NJ) using the z-axis function to image 5 μm sections, which were then

compressed into a single image.

5.2.11 Cell Culture

Hydrogels were initially sterilized in 95% v/v ethanol (2 h) and re-equilibrated in sterile PBS prior to EC seeding onto the gel surfaces. As stated in section 3.2.4, rat aortic ECs (passage 6-8) were cultured in MCDB-131 medium supplemented with 10% v/v FBS (Invitrogen), 1% v/v penicillin-streptomycin (Invitrogen), 50 μg/ ml EC growth supplement (BD), 4 mM L-glutamine (Invitrogen), and 30 U/ ml heparin (Sigma). Spent medium was replaced thrice weekly. Due to the high water content and anionic charge of these gels, adherent ECs may be unable to fully spread and remain rounded on the gel surface failing to achieve a natural morphology. We sought to address this by adsorbing a mixture of adhesive proteins (matrigel: laminin, collagen IV), similar to the composition of the vascular basement membrane, onto the hydrogel surfaces by incubating each gel in 3 ml of a sterile matrigel/PBS solution (10 μg/ ml; 4 h) prior to EC seeding. ECs were cultured for 2 wks on both matrigel-free and matrigel-adsorbed gels, and imaged on a phase contrast microscope to monitor their morphology. The gel condition (matrigel-free or matrigel-adsorbed) that was determined to support ECs exhibiting a spread cobblestone morphology was used in further culture experiments.

5.2.12 Protein Adsorption Assay

The protein content in the bulk solution of matrigel incubated with each HA hydrogel was quantified by a D_C protein assay (Bio-Rad, Hercules, CA). Via this method,

we estimated the amount of protein lost by adsorption onto the HA hydrogels. Briefly, 100 μl of bulk solution was combined with 500 μl of reagent A and 4 ml of reagent B of the assay kit, and incubated for 15 min. A 200-μl aliquot of the reacted sample solutions was pipetted into micro-well plates and their absorbances were measured at λ = 750 nm. Background absorbance from control wells containing PBS without matrigel was subtracted from the sample absorbance measurements. The detected absorbances (n = 4) were compared to standards prepared with bovine plasma gamma globulin (Bio-Rad) to determine the depletion of proteins from the matrigel stock solution, and thus calculate the total amount of protein deposited onto the DVS-HA hydrogels.

5.2.13 Fluorescent Detection of Cell Viability

As stated in section 4.2.11, calcein AM was used to fluorescently detect live cells and determine their morphology when cultured on HA hydrogels. ECs were seeded onto the HA gel surfaces at a concentration of 2×10^4 cells/ gel and cultured for 1 week prior to calcein AM detection. Surface adherent ECs were imaged on a TCS SP2 AOBS confocal microscope (Leica) using the z-axis function to image 5 μm sections on the concave surface of the gels (n = 4). These sections were then compressed into a single image.

5.2.14 MTT Assay for EC Proliferation

EC proliferation on gels was quantified using a colorimetric MTT assay, described previously by Denizot and Lang [319]. The MTT reagent is reduced by the

mitochondria of live attached cells to yield a blue formazan product, which can be extracted, and quantified by absorbance spectroscopy. ECs were seeded onto the gels at a density of 1×10^4 and cultured for 2 wks. The number of live, attached cells on each set of samples was quantified at 1 and 14 days, respectively, after seeding. At the end of the culture period, medium was aspirated from the wells, and the gels with adherent cells were transferred to fresh wells. Gels were briefly rinsed with 1× PBS to remove unattached cells. A 2-ml aliquot of 2-(4,5-dimethylthiazol-2-yl)-2,5-diphenyl tetrazolium bromide (MTT) reagent (1 mg/mL in phenol red-free DMEMF12) was added to each gel and incubated for 3 h at 37°C. Each sample was then overlaid with 2 ml of *n*-propanol and mixed for 15 min on a rotary shaker. The formazan product produced by cells was extracted by the propanol, 200 μl of the extract was pipetted into micro-well plates, and the absorbance was measured at λ = 550 nm (n = 4). Background absorbance from control wells containing no cells was subtracted from the sample absorbance measurements. For use as standards, between 5×10^3 and 3×10^5 ECs were seeded in 6-well polystyrene culture plates and allowed to attach overnight before they were quantified.

5.2.15 Immunolabeling for EC CAM Expression

Expression levels of CAM (ICAM-1, VCAM-1) by ECs cultured on HA hydrogels were compared by immunofluorescence and quantified by calculating the mean fluorescence intensity (MFI) on a per cell basis. ECs were seeded onto the gels at 2×10^4 and cultured for 1 wk prior to analysis. The cells were then fluorescently labeled for

CAM expression, as described in section 4.2.12, and imaged on a TCS SP2 AOBS confocal microscope (Leica) using the z-axis function to image 5 μm sections on the concave surface of the gels (n = 9) at a constant gain and offset (FITC - 650, 0.8). Draq 5 (1:2000 in PBS, 10 min; Biostatus) was also used to fluorescently label the cell nuclei. These sections were then compressed into a single image prior to MFI per cell calculations using Image J.

5.2.16 Statistical Analysis

All experiments were performed in triplicate with triplicate samples/ cultures per formulation, unless otherwise mentioned. Statistical significance between and within groups was determined using Microsoft Excel's statistical function for t-tests, assuming unequal variance and two-tailed distribution. Differences were considered statistically significant at $p < 0.05$. Quantitative results are reported as mean ± standard deviation.

5.3 Results

5.3.1 Crosslinked HA Hydrogels

HMW HA and HA oligomers (D2) were combined into hydrogels by crosslinking with DVS, resulting in 8 total gel formulations: 2 crosslinking concentrations (1:1, 1:2 w/w DVS:HA) × 4 oligomer concentrations (0, 5, 10, 20% w/w D2/HA). Figure 5.3 shows the swollen hydrogels crosslinked in 0.79 cm^2 molds and their measured dimensions. The HA oligomer (D2) content appeared to minimally affect hydrogel size with limited increases in height (h) and diameter (d). On the other hand, increasing the

DVS content drastically reduced the size of the gels resulting in more compact strands of HA and an opaque coloration.

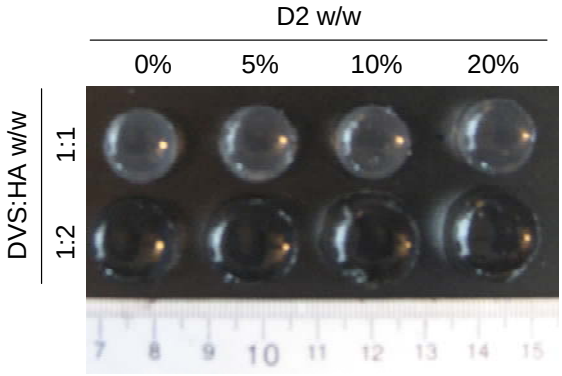

	D2 w/w 0%	5%	10%	20%
h (cm)	0.350	0.358	0.368	0.372
d (cm)	1.386	1.418	1.458	1.474
h (cm)	0.433	0.451	0.463	0.474
d (cm)	1.716	1.787	1.835	1.876

Figure 5.3 Size of swollen DVS-HA hydrogels. Increasing the amount of DVS within the gels resulted in reduced gel sizes and an opaque coloration. Measuring the dimensions of the DVS-HA hydrogels showed that both height (h) and diameter (d) of the cylindrical gels also slightly increased with HA oligomer content. The ruler marks cm increments.

5.3.2 FTIR Spectroscopy

FTIR-ATR spectra of dried DVS-HA and the corresponding starting material of uncrosslinked HA were measured. Spectra were taken of HA, and DVS-HA with all concentrations of D2 (0, 5, 10, 20% w/w) and DVS (1:1, 1:2 w/w), but, due to their similarity, Figure 5.4 shows only a spectrum representative of all DVS-HA formulations in comparison to uncrosslinked HA. The spectrum of HA agrees well with that provided by the American Society for Testing of Materials (ASTM). The most significant difference between DVS-HA and HA is the higher intensity of the absorption band at 1284.14 cm^{-1} in the DVS-HA spectrum, which corresponds to the presence of sulfonyl groups [320].

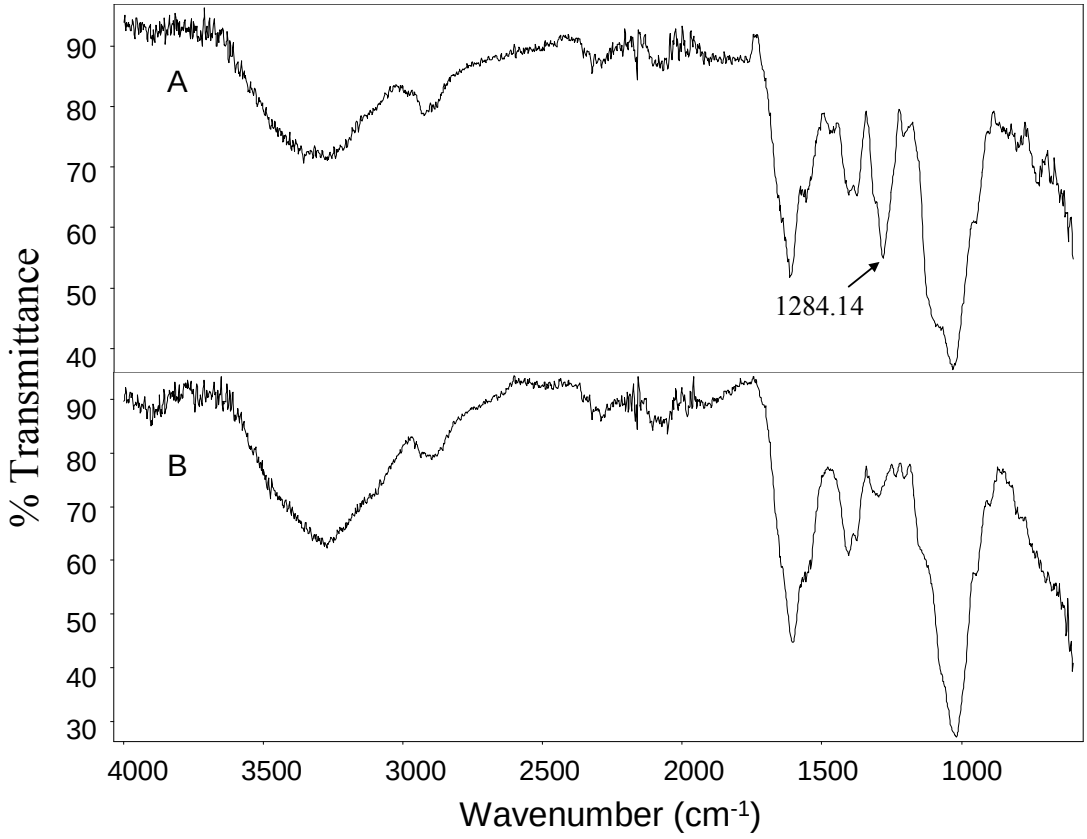

Figure 5.4 FTIR-ATR spectra of DVS-HA (A) and uncrosslinked HA (B). The most significant difference between HA and DVS-HA is the higher intensity absorption band at 1284.14 cm^{-1} in the DVS-HA spectra indicating the presence of sulfonyl groups, specific to DVS.

5.3.3 Hydrogel Oligomer Content

D2 oligomers were tagged with AMAC prior to crosslinking within DVS-HA in order to verify that the relative differences in HA oligomer content within DVS-HA were maintained upon crosslinking. By this method, we sought to monitor the retention of these oligomers within the hydrogels in their swollen state, and upon their further, long-term incubation in PBS. Higher D2 content within the DVS-HA gels corresponded with increased fluorescence intensity, in gels of both crosslinker concentrations (Figure 5.5). However, 1:1 w/w DVS-HA gels fluoresced to a greater degree than 1:2 w/w DVS-HA

gels and their fluorescence intensity was relatively stable over 21 days of incubation in PBS. Gels containing 1:2 w/w ratios of HA to DVS showed a sharp increase in fluorescence intensity between day 0 and 1, and a mild decrease in fluorescence intensity was observed between day 1 and 14 but remained constant thereafter.

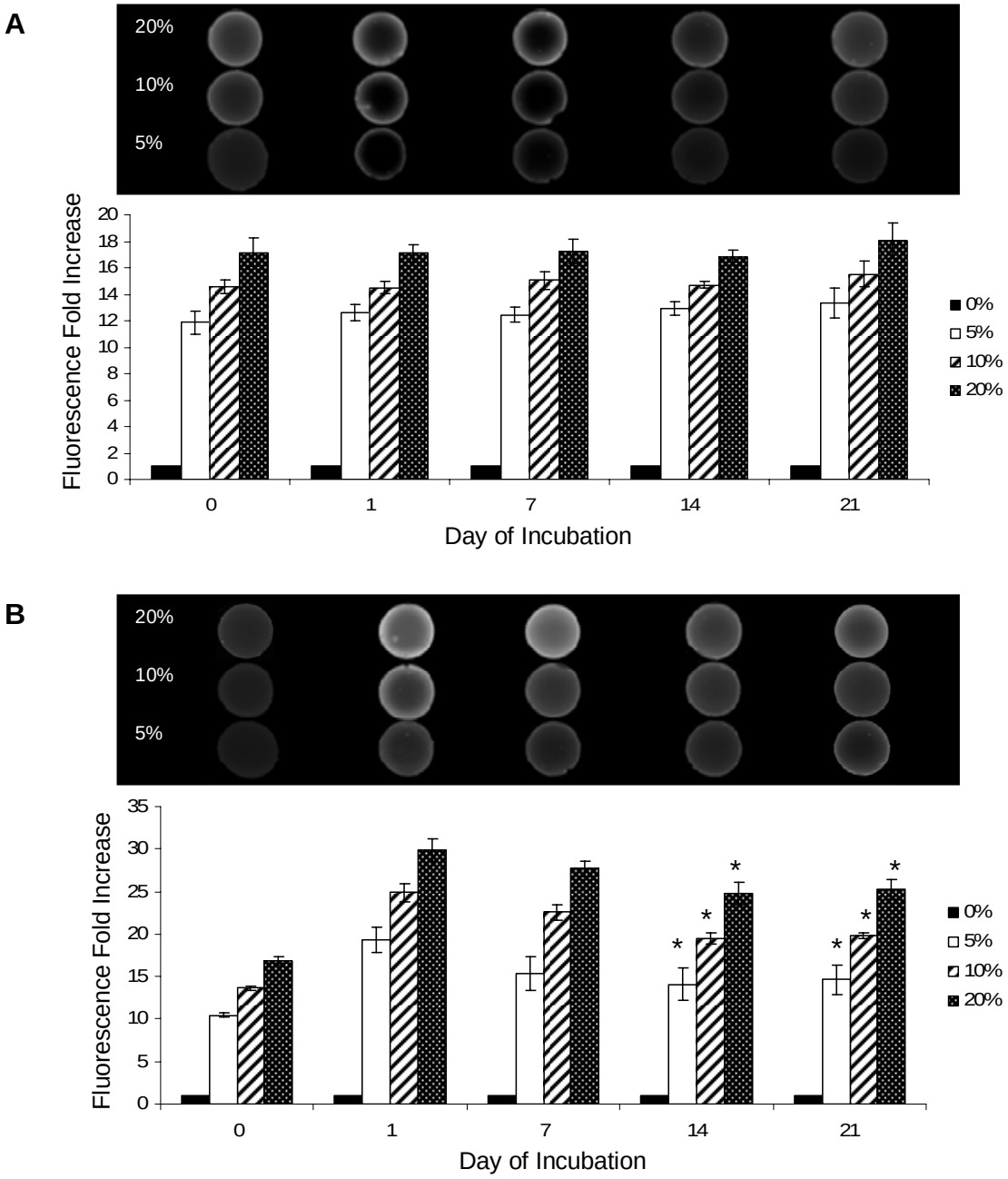

Figure 5.5 Fluorescence intensities of HA oligomers (D2) embedded within DVS-HA. The number of oligomers within 1:1 w/w DVS-HA (A) appeared to remain constant, whereas the oligomer content of 1:2 w/w DVS-HA (B) decreased slightly before reaching a plateau. However, within both DVS concentration groups, the differences in oligomer content were maintained. [* denotes a p-value < 0.05 in comparison to day 1]

5.3.4 Hydrogel Crosslinking

The apparent crosslinking density and swelling ratio of DVS-HA were used to estimate the degree of crosslinking within the hydrogels. The results show apparent crosslinking density (Table 5.1) and swelling ratio (Figure 5.6) were dependant on both concentrations of DVS and presence of D2. For a given crosslinker to HA ratio, the addition of D2 into the hydrogel construct increased the swelling capacity of the gels over gels composed only of HA 1500 though the extent of swelling did not appear to depend on the D2 concentrations. On the other hand, the apparent crosslinking density decreased in direct correlation with increases in concentration of D2, when other formulation parameters were unchanged. For each D2 concentration, increasing the incorporated amounts DVS within the gels reduced their ability to swell and increased their apparent crosslinking density. The differences in apparent crosslinking density, for each D2 concentration, was maintained at approximately a factor of 3. However, the measured crosslinking density was much lower than the calculated theoretical value, assuming 100% DVS reaction, resulting in an overall crosslinking efficiency of 10 – 15% for 1:1 w/w DVS-HA and 15 – 20% for 1:2 w/w DVS-HA.

	A		B	
D2 Conc. w/w	**Theoretical** ν_e (mol/ cm^3 x 10^6)	**Measured** ν_e (mol/ cm^3 x 10^6)	**Theoretical** ν_e (mol/ cm^3 x 10^6)	**Measured** ν_e (mol/ cm^3 x 10^6)
0%	143.37	21.35 ± 0.85	37.87	7.17 ± 1.71
5%	133.91	18.77 ± 1.11	33.53	6.59 ± 0.76
10%	123.16	16.77 ± 0.71	30.95	6.35 ± 0.78
20%	119.24	12.19 ± 0.76	28.96	4.72 ± 0.36

Table 5.1 Apparent crosslinking density of DVS-HA determined from the uniaxial compression data and Eq 5.1. Overall, 1:1 DVS-HA (A) exhibited a higher apparent crosslinking density than 1:2 DVS-HA (B). The addition of D2 into the hydrogels reduced the apparent crosslinking density and these values were approximately 10 – 20% of the estimated theoretical values assuming 100% DVS bonding.

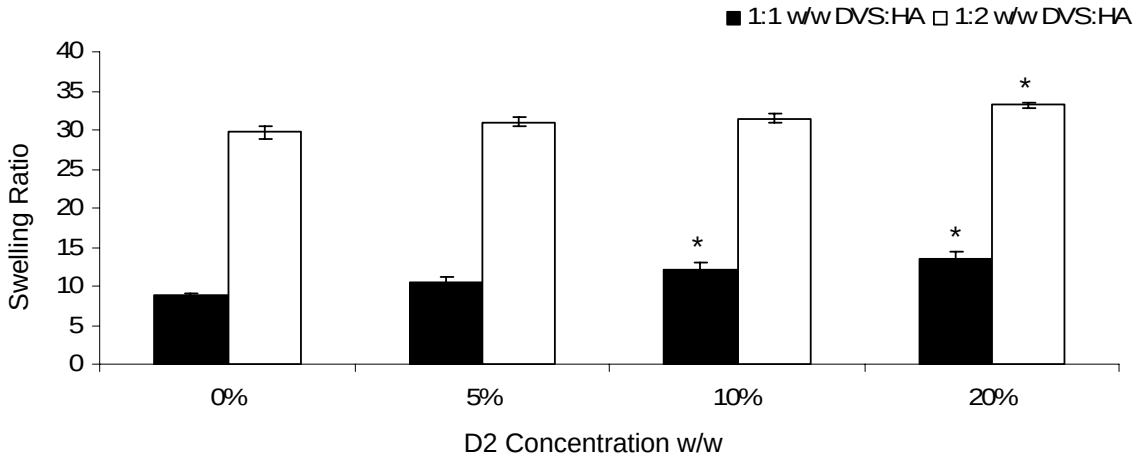

Figure 5.6 Swelling ratios of DVS-HA. The incorporation of D2 within the DVS-HA hydrogel mildly increased their swelling capacity irrespective of the crosslinking density. The swelling ratio was dramatically increased by a greater concentration of DVS within the gel. [* denotes a p-value < 0.05 in comparison to 0%]

5.3.5 Hydrogel Stiffness and Resistance to Degradation

Rheological analysis provided the quantitative evaluation of the viscous and elastic responses of DVS-HA with varying concentrations of D2 and DVS providing information on their stiffness. In general, both the storage moduli (G') and loss moduli

(G") for all cases were independent of frequency and G' values were always higher than G", as seen in Figure 5.7. As expected, a greater crosslinking density increased the hydrogel stiffness (G'), however, the addition of D2 within the hydrogel decreased its stiffness.

To determine the biodegradability of the DVS-HA hydrogels, we tested the sensitivity of the gels to a super-physiologic concentration of bovine *testicular hyaluronidase*. The degradation profiles of the stronger (less stiff) 1:1 w/w DVS-HA (Figure 5.8A, Table 5.2A) resulted in lower degradation rates than 1:2 w/w DVS-HA (Figure 5.8B, Table 5.2B), indicating a greater resistance to enzymatic digestion. Greater concentrations of D2 also increased the degradation rates of the hydrogels.

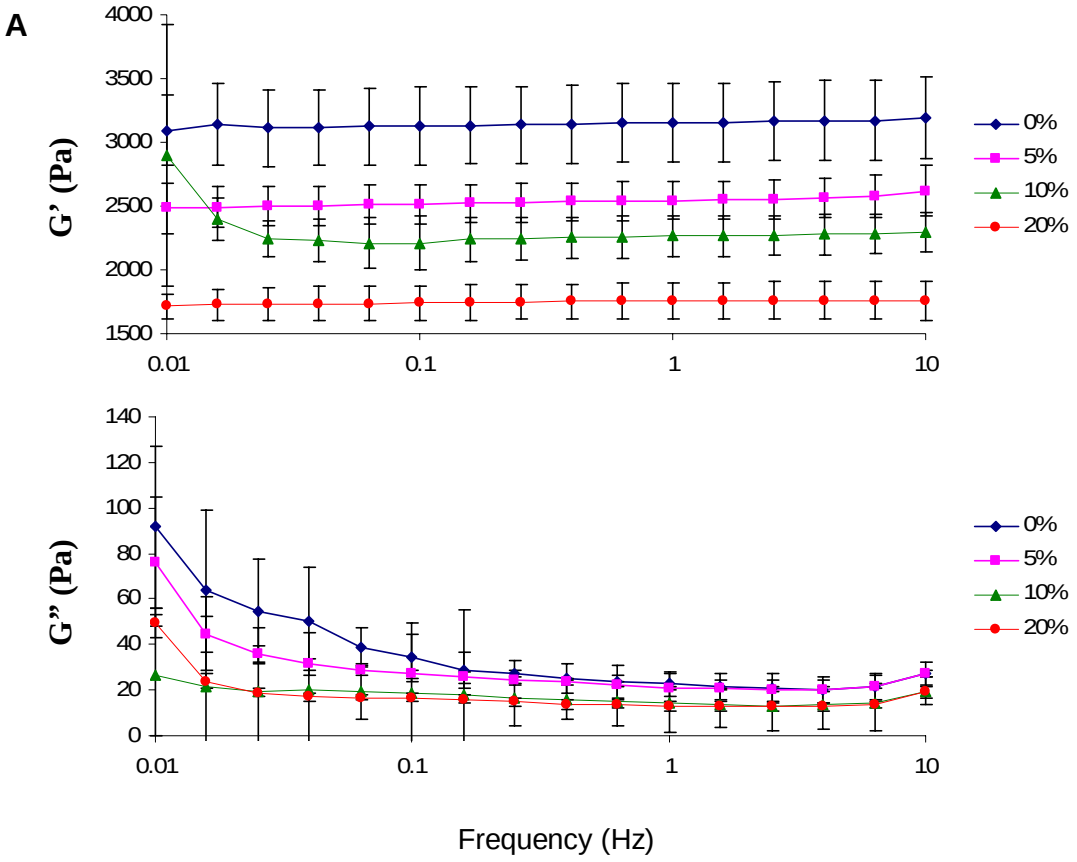

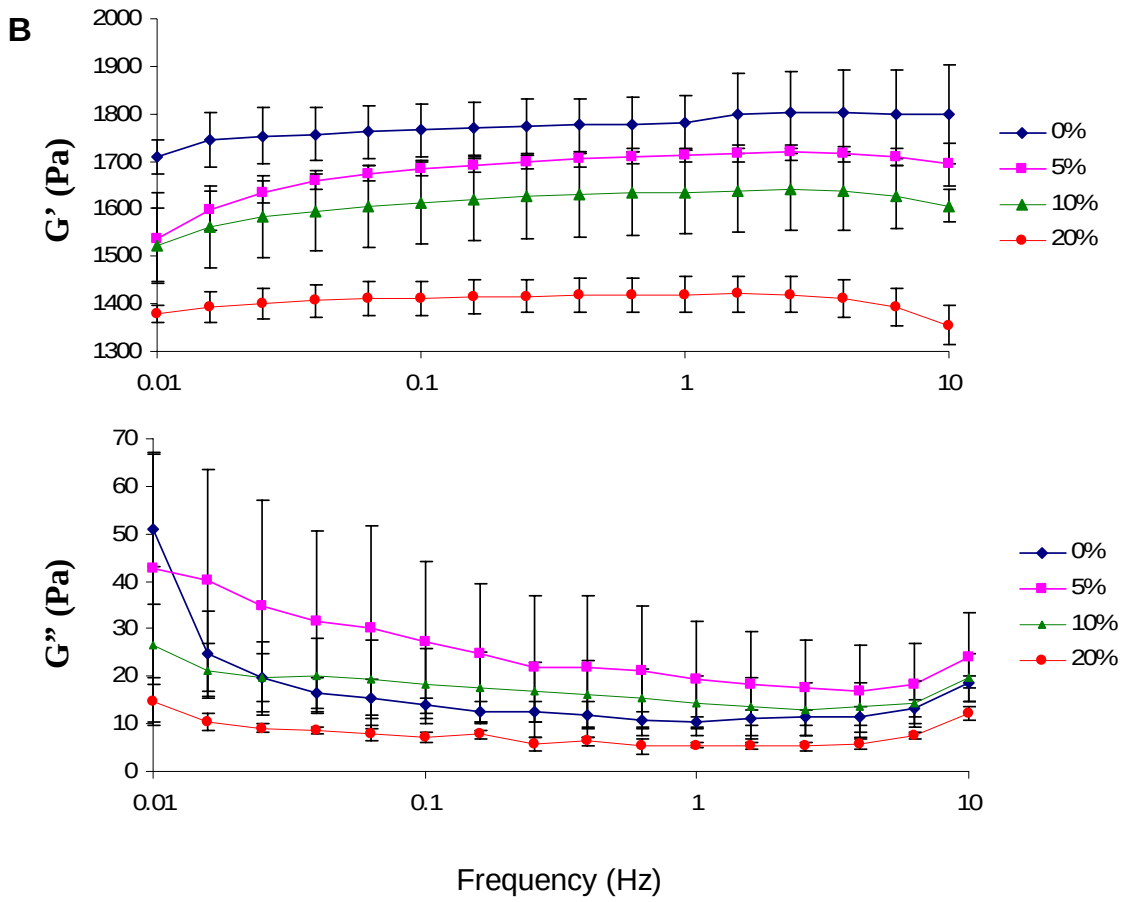

Figure 5.7 Viscoelastic properties of DVS-HA. The storage moduli (G') in all cases are greater than the loss moduli (G"). Increasing the concentration of DVS within the hydrogel, 1:1 w/w (A) vs. 1:2 w/w (B) DVS-HA, resulted in a greater G' and overall stiffness of the gels. The addition of D2, however, reduced the storage moduli indicating lowered stiffness of the hydrogels.

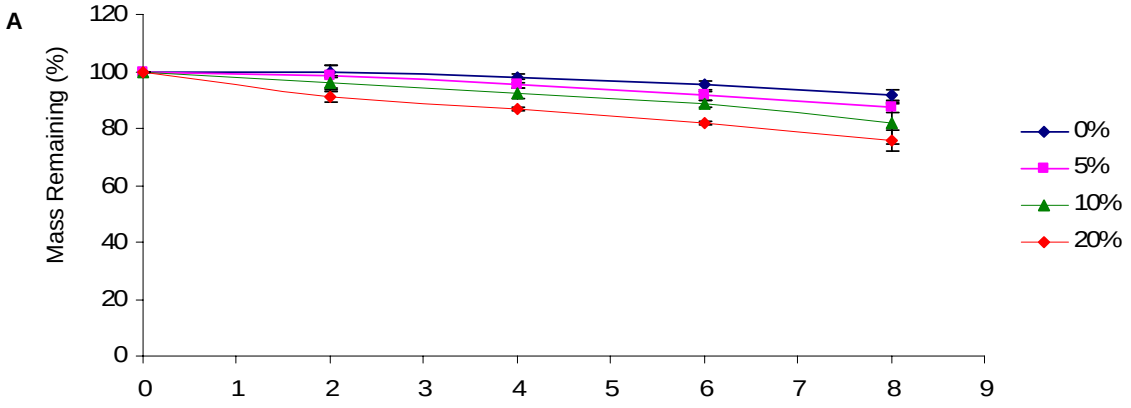

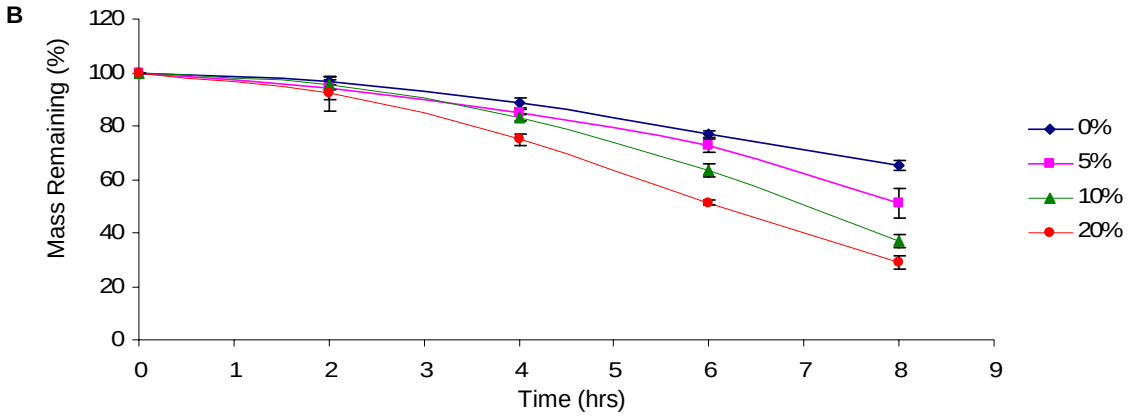

Figure 5.8 Degradation of DVS-HA *in vitro*. Hydrogels with a greater concentration of DVS, i.e., 1:1 w/w (A), vs. 1:2 w/w (B) DVS-HA, exhibited greater stability against degradation by *testicular hyaluronidase*. However, increasing the concentration of D2 within each of these gel formulations enhances the degradation rate.

	A		B	
HA-o Conc.	k (h^{-1})	pvalue	k (h^{-1})	pvalue
0%	0.0103	<0.00001	0.068	0.0045
5%	0.014	<0.00001	0.0708	0.016
10%	0.0136	0.0042	0.0969	0.02
20%	0.0221	0.0016	0.1227	0.018

Table 5.2 Degradation rate of DVS-HA *in vitro*. A greater DVS concentration, i.e. 1:1 w/w of DVS to HA (A) vs. a 1:2 w/w ratio (B) within DVS-HA gels, and increasing the D2 content, resulted in a higher rate of degradation when incubated with *testicular hyaluronidase* enzyme.

5.3.6 Hydrogel Surface Morphology

SEM shows the change in surface morphology of hydrogels that were dehydrated. The dehydration process resulted in ripple formation on the surface of the gels (Figure 5.9). However, increases in DVS and/or HA oligomer (D2) content appeared to reduce the formation of these ripples. Also, hydrogels with a higher concentration of D2 possessed a surface topography that appeared more granular, potentially forming a

surface with a greater roughness.

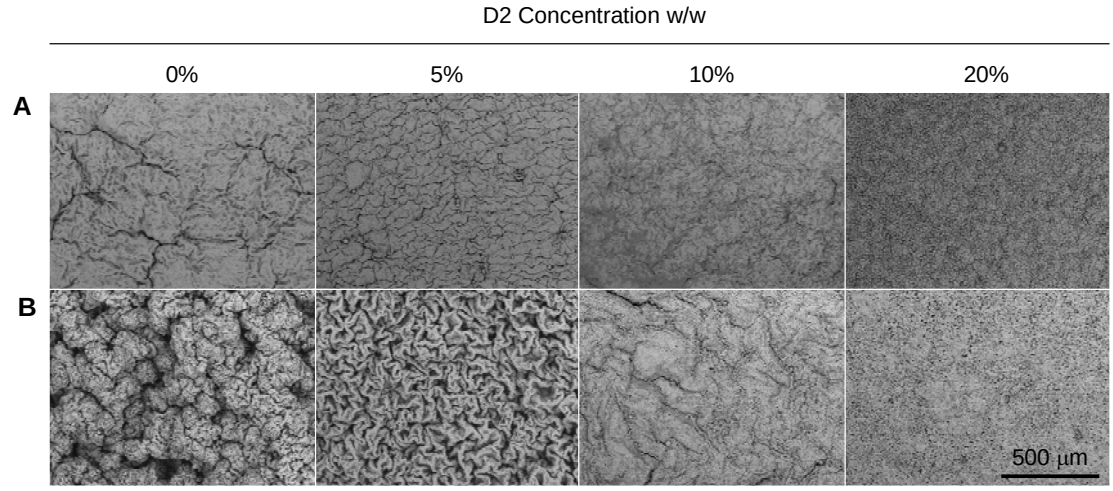

Figure 5.9 Surface morphology of DVS-HA. The dehydration process resulted in the development of ripples on the surfaces of the hydrogels, with bulkier ripples visible on 1:2 w/w DVS-HA gels (B) than on 1:1 w/w DVS-HA gels (A). The addition of D2 reduced ripple formation and rendered the surface more granular.

5.3.7 Hydrogel Biocompatibility

In all cases, H&E staining revealed a distinct ring of cellularized tissue around the defect created by the implant. The thickness of this highly cellularized region appeared to increase with increases in DVS concentration and with HA oligomer content (Figure 5.10). Since the cells were not flattened, and did not show alignment with collagen fibers, typical of fibroblasts, it is highly likely that these were inflammatory cells. Additionally, the fact that these cells were present around all implants and indeed were far more numerous around select gels, with a reduced presence of collagen (Figure 5.11), strengthens our hypothesis that these cells are inflammatory and not fibroblasts. As can be seen in Figures 5.10, the gels containing the greater concentration of DVS crosslinker (panels A in both figures) stimulated much greater inflammatory cell recruitment (see

darkened region near defect) than the less robustly crosslinked gels (panels B). The cells distributed farther from the implants appeared more flattened, and aligned with matrix fibers, and are thus likely to be fibroblasts. Immunofluorescence studies (Figure 5.11) confirmed these results in that greater cellularity (blue) was noted in the region immediately surrounding all the implants, than further afield, and that the thickness of this layer was greater around gels that contained (a) greater DVS content and (b) higher oligomer content. These studies also confirmed a depletion in collagen (green) immediately surrounding the defect region. Very little tissue infiltration was observed within DVS-HA, as compared to the matrigel control (Figure 5.12). The defect containing 1:1 w/w DVS-HA gel implant was consistently void of any inward tissue projections. However, some tissue projections were observed for 1:2 w/w DVS-HA gels.

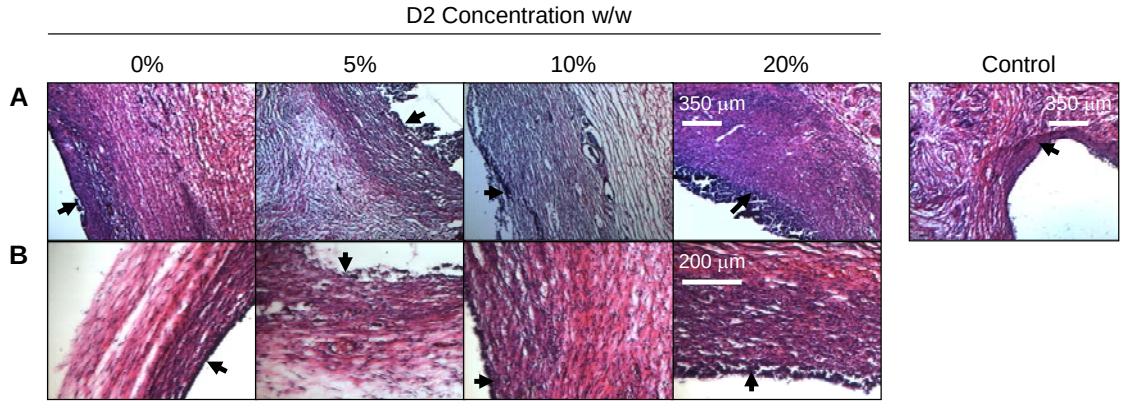

Figure 5.10 Biocompatibility of DVS-HA. In all cases, a distinct, darkened ring of inflammatory cells (see arrows) surrounded the implant and the thickness of this highly cellular region appeared to be increase with DVS concentration. Hydrogels with a greater DVS concentration, 1:1 w/w (A) vs. 1:2 w/w (B), stimulated an enhanced inflammatory response from the surrounding tissue that was greater than the matrigel control. Likewise, gels containing greater HA oligomer (D2) content, appeared to incite a greater inflammatory response, though these effects were muted compared to the impact of DVS crosslinking.

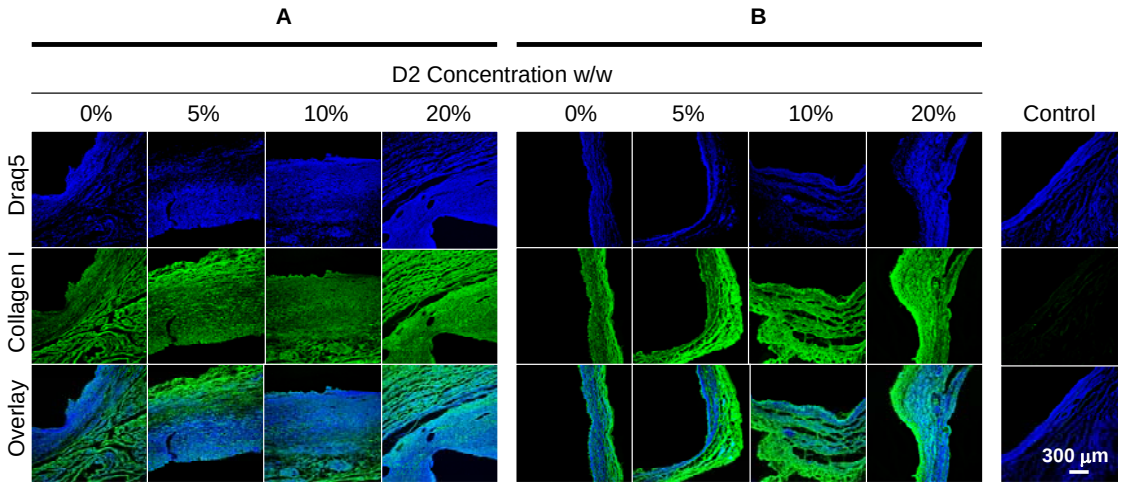

Figure 5.11 Immunofluorescence analysis collagen I surrounding implant. Gels containing greater crosslinker (DVS) content (A) prompted greater cellularity in the region surrounding the gels than the gels in panel B, or controls. However, the collagen I (green) content appeared depleted immediately surrounding the implant. The recruitment of the inflammatory cells (blue) appeared to be enhanced by increasing HA oligomer (D2) content.

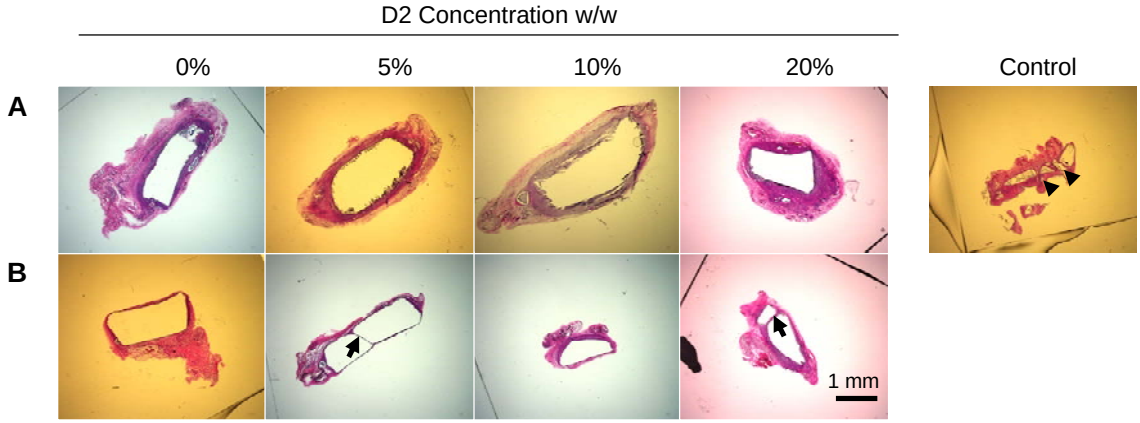

Figure 5.12 Tissue infiltration into DVS-HA. Very little tissue infiltration was observed within DVS-HA, as compared to the matrigel control. The implant region of DVS-HA 1:1 w/w (A) remained consistently void of inward tissue projections. However, some tissue projections (see arrows) were observed in DVS-HA 1:2 w/w (B).

5.3.8 EC Morphology and Protein Adsorption

Upon seeding ECs on uncoated DVS-HA hydrogels, we found that ECs attached readily and the incorporation of D2 within the gels appeared to enhance the extent of attachment. However, these ECs exhibited a rounded morphology even 2 weeks after seeding, different from those ECs cultured on polystyrene (PS), which exhibited a more typical cobblestone shape (Figure 5.13). Therefore, the cell-adhesive proteins of matrigel were adsorbed onto the surfaces of the DVS-HA gels. The total protein content within the bulk matrigel-coating suspention decreased following incubation with DVS-HA gels indicating successful adsorption of protein onto the hydrogel surfaces (Figure 5.14). The total amount of protein adsorbed onto 1:2 w/w DVS-HA gels was greater than the 1:1 w/w DVS-HA gels but when adjusted for increased swelling, and therefore increased surface area (SA), of 1:2 w/w DVS-HA (SA = 3.8 ± 0.3 cm^2 for 1:2 w/w DVS-HA gels vs. 2.4 ± 0.1 cm^2 for 1:1 w/w DVS-HA gels) we found the adsorbed protein density was the same on gels containing both crosslinker densities. Likewise, regardless of crosslinker amounts, matrigel adsorption on the gels was independent of the content of incorporated HA oligomers (D2), see Figure 5.14. ECs cultured atop these matrigel-adsorbed DVS-HA gels appeared more spread, and exhibited a natural cobblestone morphology (Figure 5.15). Therefore, all further culture studies were performed only with matrigel-adsorbed DVS-HA hydrogels. This spread cobblestone morphology of ECs cultured atop matrigel-adsorbed gels was more readily apparent when visualized after calcein AM staining (Figure 5.16). ECs appeared as isolated clusters on 1:2 w/w DVS-HA gels (B), while on 1:1 w/w DVS-HA gels (A) ECs were more homogeneously

distributed.

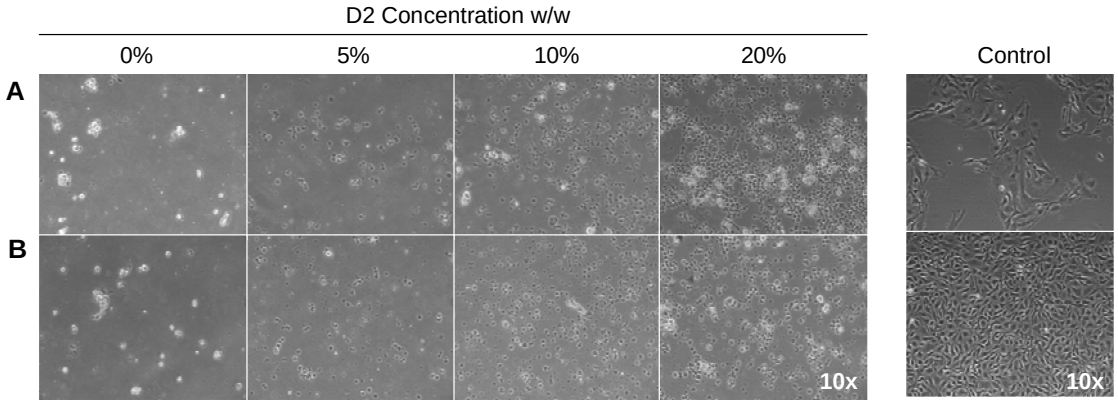

Figure 5.13 Attachment and morphology of ECs cultured on DVS-HA gels. Very little difference in the attachment and morphology of ECs was observed between 1:1 w/w (A) and 1:2 w/w DVS-HA. The addition of D2 clearly increased the number of adherent ECs; however, the cells remained rounded exhibiting an abnormal rounded morphology.

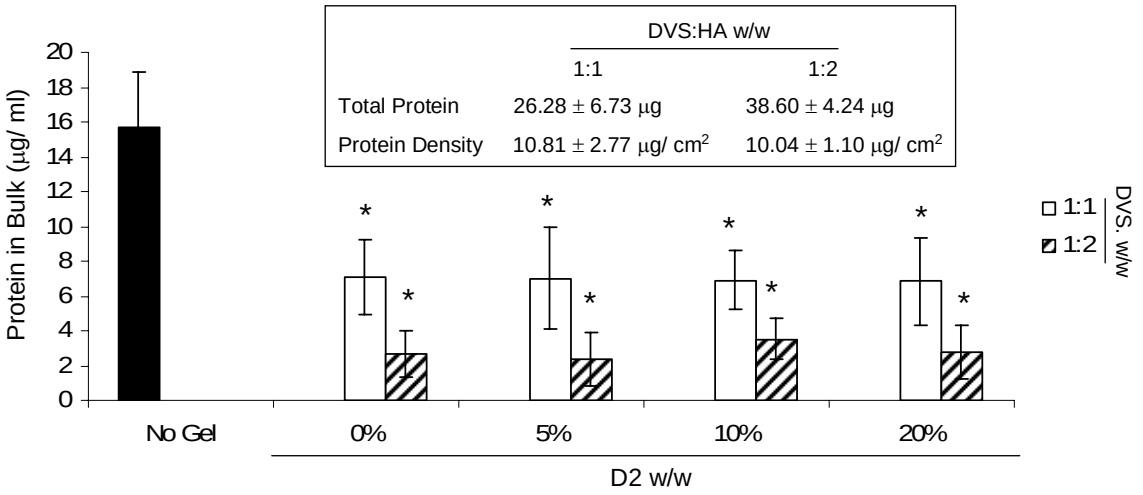

Figure 5.14 Matrigel adsorption onto DVS-HA gel. A drop in protein content within the bulk coating suspension was observed indicating protein adsorption onto the gel surfaces. Calculations revealed that protein was the same on all DVS-HA gels, regardless of crosslinker density. [* denotes a p-value < 0.05 in comparison to no gel]

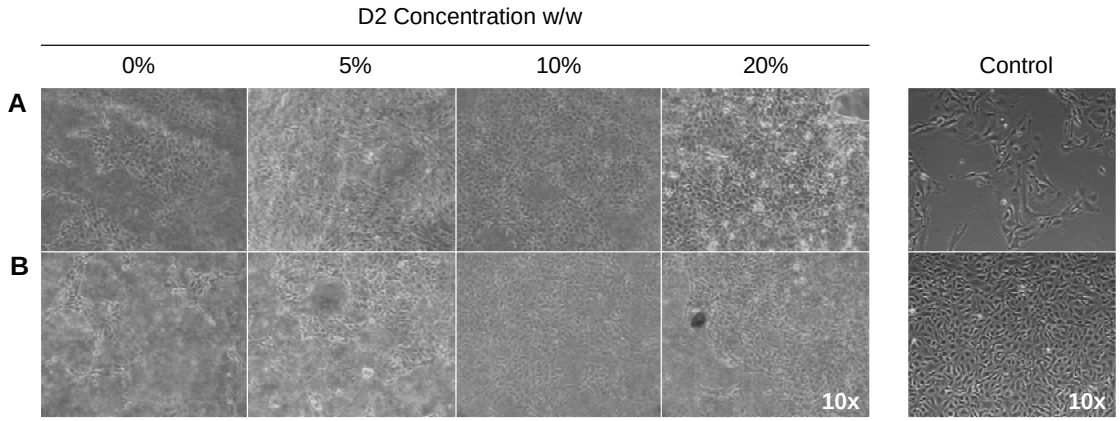

Figure 5.15 EC morphology atop DVS-HA gels with surface-adsorbed matrigel. The addition of matrigel allowed the ECs to spread and assume a more native-like cobblestone morphology and enhanced attachment to some extent as well. No difference in cell morphology was observed between 1:1 w/w (A) and 1:2 w/w (B) DVS-HA gels.

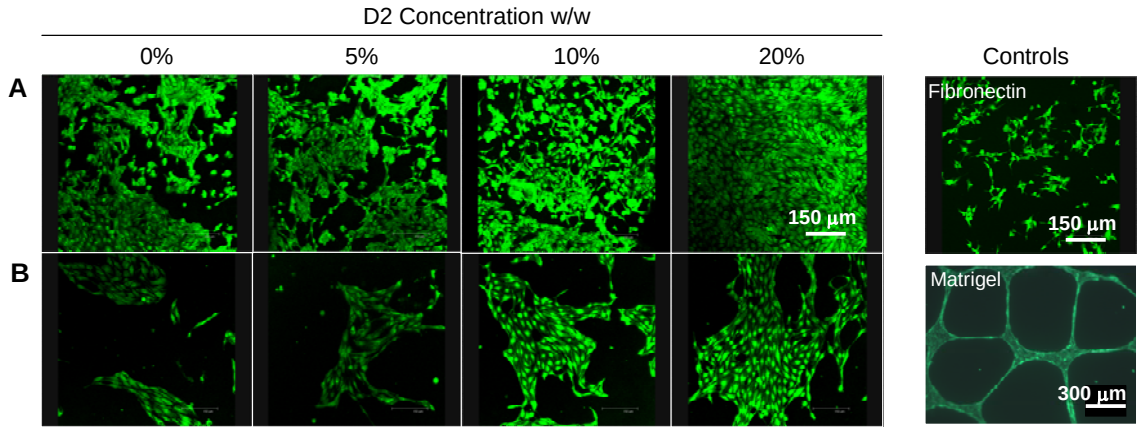

Figure 5.16 Morphology of ECs cultured on matrigel-adsorbed DVS-HA gels. The incorporation of D2 enhanced EC adherence on the gels. The ECs appeared to spread and exhibited a natural cobblestone morphology similar to cells cultured on fibronectin. ECs appeared as isolated clusters on 1:2 w/w DVS-HA (B), while on 1:1 w/w DVS-HA (A) ECs were more uniformly distributed.

5.3.9 EC Proliferation

All gel formulations, irrespective of DVS and D2 content adsorbed identical amount of matrigel on a per unit area basis, therefore, any proliferation differences were

purely an affect of oligomer content and/or DVS concentration. In absence of any oligomers, EC proliferation on 1:1 DVS-HA hydrogels was greater than the less crosslinked 1:2 w/w DVS-HA gels (Figure 5.17). This difference was maintained even when the HA oligomers were incorporated into the gels. Within each crosslinking group, EC proliferation increased in direct correlation with incorporated D2 amounts. However, even on the gels incorporating the highest amounts of D2 (i.e. 20%), EC proliferation over 14 days of culture was much lower relative to those ECs cultured on matrigel and fibronectin substrates.

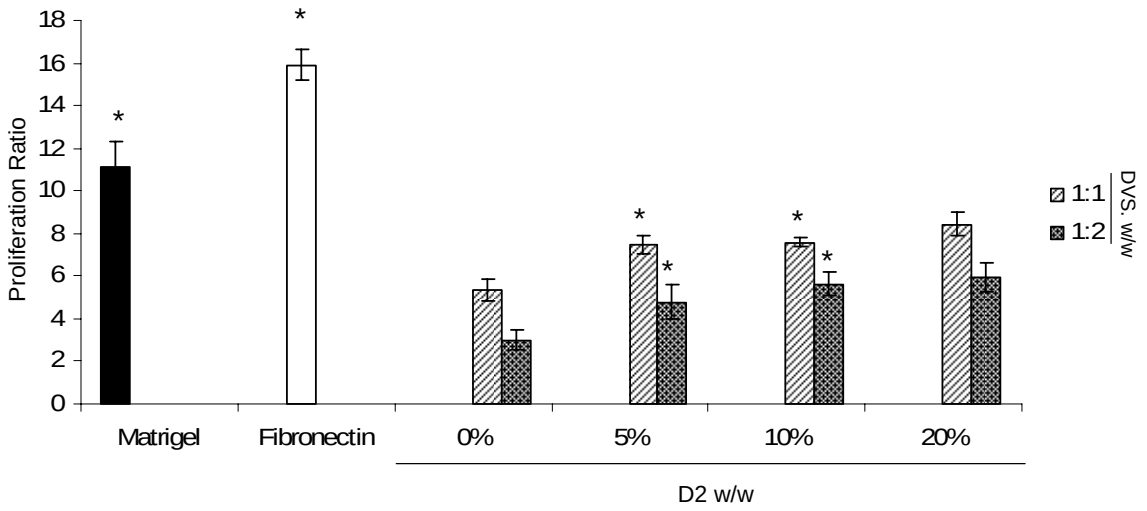

Figure 5.17 Proliferation of ECs cultured on DVS-HA. 1:1 w/w DVS-HA stimulated greater EC proliferation than 1:2 DVS-HA, as did increased D2 concentration within either gel type. In all cases, the ECs were able to interact with the embedded oligomers enhancing proliferation. However, EC proliferation levels on these gels were lower than that attained by ECs cultured on matrigel and fibronectin substrates. [* denotes a p-value < 0.05 in comparison to 0%]

5.3.10 EC CAM Expression

It is apparent from the fluorescent images that the ICAM expression levels (Figure 5.18) of ECs cultured on matrigel-coated DVS-HA are similar to ECs grown on fibronectin substrates and matrigel surfaces, and much lower than TNF-α-stimulated ECs. Quantification of these expression levels confirmed this observation and additionally showed ICAM expression to remain unchanged upon incorporation of D2 into DVS-HA (Figure 5.20). VCAM-1 expression levels (Figures 5.19, 5.20) were also unaffected by D2 content within DVS-HA gels and remained much more attenuated in comparison to TNF-α stimulated ECs. However, VCAM-1 expression of ECs was slightly elevated beyond ECs cultured on pure matrigel and fibronectin substrates.

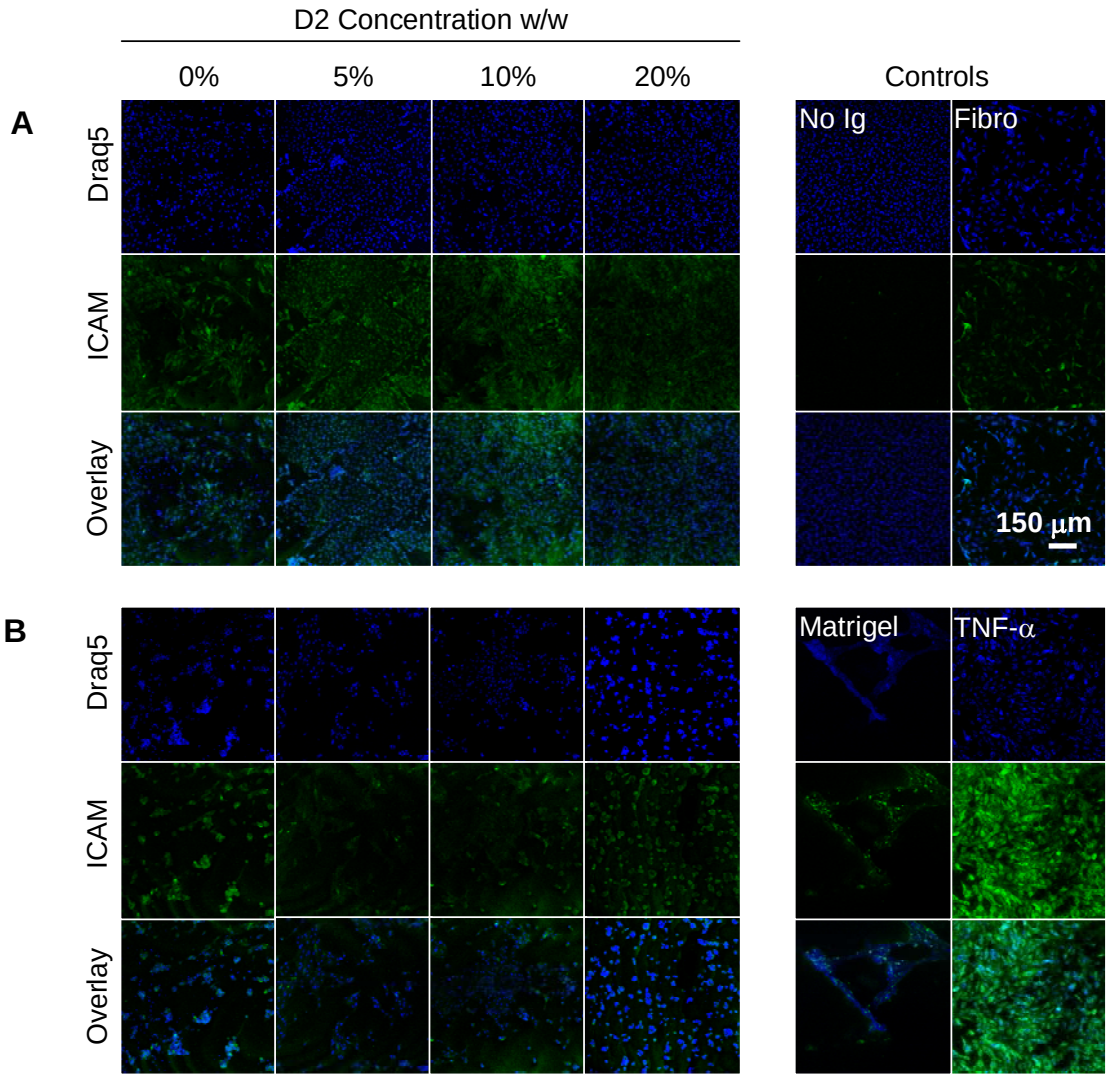

Figure 5.18 ICAM-1 expression of ECs cultured on DVS-HA. Similar ICAM-1 expression was detected on all DVS-HA formulations and the degree of expression appeared similar to the fibronectin and matrigel controls, and much lower than TNF-α stimulated ECs.

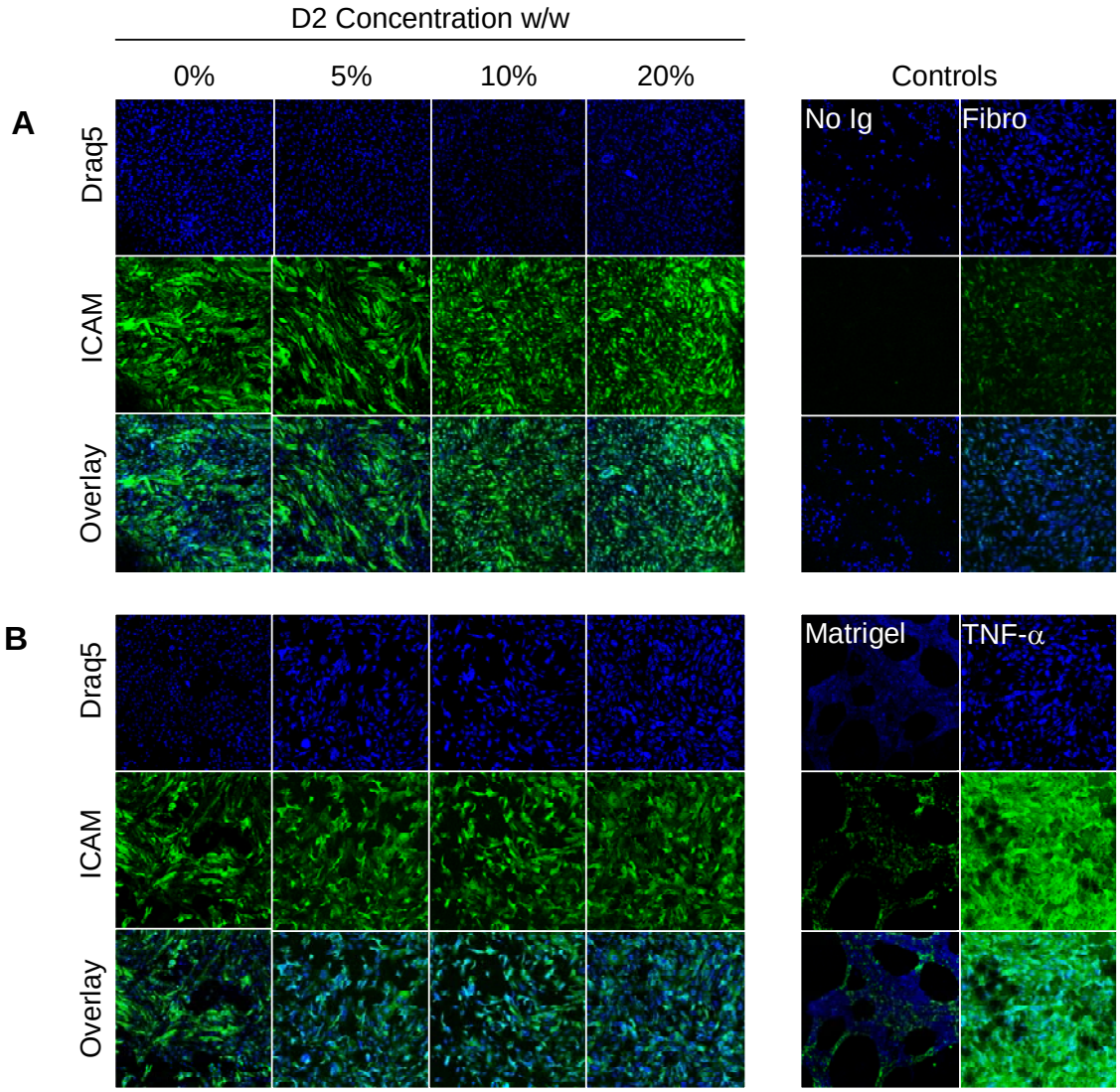

Figure 5.19 VCAM-1 expression of ECs cultured on DVS-HA. Similar VCAM-1 expression was detected on all DVS-HA formulations and remained below TNF-α stimulated ECs, however, the expression level appeared elevated beyond that of the fibronectin and matrigel controls.

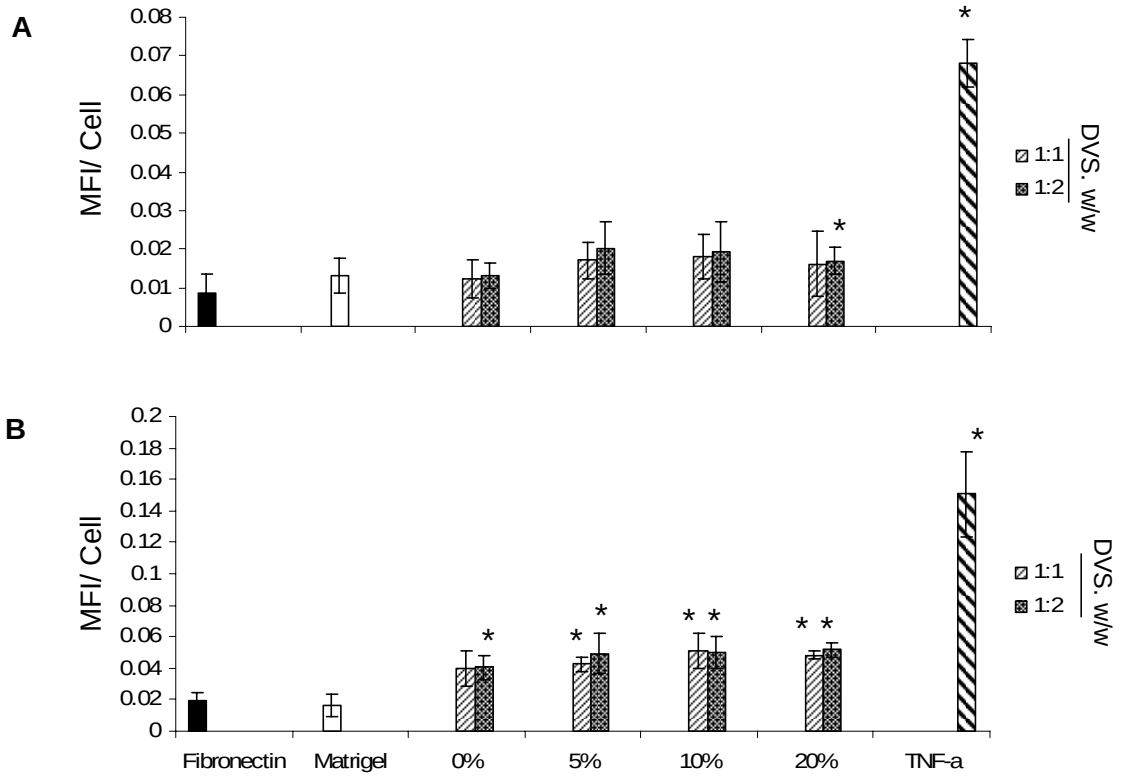

Figure 5.20 Quantification of ICAM-1 and VCAM-1 expression of ECs cultured on DVS-HA. This confirms the fluorescence intensity of each EC CAM remained the same on all DVS-HA formations. While the fluorescence intensity of ICAM-1 (A) was suppressed to similar levels as fibronectin and matrigel, VCAM-1 (B) expression was slightly elevated compared to the controls. Both ICAM-1 and VCAM-1 expression levels did not reach that of TNF-α stimulated cells. [* denotes a p-value < 0.05 in comparison to fibronectin]

5.4 Discussion

In order to create a long-term HA implant, it must be converted into a stable, biocompatible, insoluble biomaterial with good handling properties and mechanics appropriate to the site of implantation. Chemical modification has been well recognized as a means to enhance the biostability and mechanical properties of native HA. Two possible methods to modify HA are through derivatization and cross-linking, both of which can be achieved through reactions between the available functional groups of HA

(-COOH, -OH). In the current study, we chose to use DVS to crosslink the hydroxyl (-OH) groups on the HA chains under alkaline conditions to yield stable hydrogels containing sulfonyl-bis-ethyl linkages, as has been shown in Figure 5.1. Such crosslinking produces a network of HA chains that is no longer water-soluble. Limited studies have suggested that crosslinked HA gels containing a low concentration of DVS-HA retain the biologic characteristics of un-crosslinked HA, especially their high biocompatibility [321]. DVS-HA exhibit significant flexibility in their mechanical properties and rheology, ideal for a wide variety of medical applications. For this reason, a number of clinical products approved by the Food and Drug Administration based on this formulation have been generated for use as post-surgical anti-adhesive films, ocular fillings, and joint lubricants, among others [322,323]. However, it is to be noted that all these applications do not involve substantial cell interactions with the biomaterial, and instead capitalize on the poor cell binding properties of DVS-HA. In other words, the applications have capitalized on the physical and mechanical properties of these gels rather than their biologic interaction with host cell types.

Previous studies have suggested that DVS-HA gels containing long-chain HA (MW>1×10^6 Da) interact poorly with cells and exhibit poor mechanics, both of which are detrimental to our intended use of them as cellular scaffolds for tissue regeneration [306,324]. This has been attributed variously to their physical properties (porosity, pore size, extreme hydrophilicity), chemical characteristics (anionicity, degree of hydration, crosslinker), and biologic composition (long-chain vs. fragmented HA). Of these parameters, the size of component HA chains seem to most critically influence cell

response. Native long-chain HA has been implicated in cell excluding mechanisms, whereas HA fragments, especially HA oligomers, elicit enhanced cell responses, although these may be exaggerated and undesirable [325]. The use of HA gels as tissue-engineering scaffolds may thus necessitate a need to optimize gel composition, derivatization and crosslinking chemistries, and post-formulation tailoring strategies to more closely modulate the physical and biologic characteristics to elicit ideal cell responses specific to target cell type on one hand and maintain material biocompatibility on the other. To enhance cell attachment, we have previously developed two techniques to micro-texture the gel surface by controlled exposure to UV light and γ-irradiation [220,317]. We demonstrated that both UV treatment and γ-irradiation alter the surface topography to create a less-uniform and ridged surface, more conducive to cell adherence and spreading. However, the greater impetus to ready cell adherence and proliferation on these irradiated gels was found to be due to shorter sized HA fragments generated on the gel surfaces by splicing of long-chain HA by random ionization caused by irradiation. Since the effects of UV and γ-irradiation are highly variable, such methods are neither closely replicatable nor easily controlled, so that gels with predictable and bioactivity and other biologic and physical properties are difficult to create. Accordingly, we decided to explore the possibility of directly incorporating HA oligomers into DVS-HA scaffolds thereby influencing cell behavior in a predictable and controlled manner.

In this study we explore the concept of incorporating bioactive HA oligomers into DVS-crosslinked mixtures of long-chain HA, to create standalone biomaterials for use as vascular scaffolds capable of functional and complete endothelialization. As mentioned

above, studies have shown that DVS-crosslinked HA containing only HMW HA do not support cell attachment due to the extremely hydrophilic nature and anionicity of HMW HA which renders the surface thermodynamically unfavorable for cell adherence and spreading. In an attempt to reduce the anionicity of these gels, we sought to incorporate HA oligomers to potentially enhance cellular attachment to the gel surface. As described in chapter 3, we demonstrated exogenous supplements of a mixture of HA oligomers (D2), containing predominantly 6mers and 12mers, stimulated proliferation, angiogenesis and the secretion of angiogenic growth factors by cultured ECs *in vitro*. Further, immobilization of derivatized D2 mixtures onto 2-D cellular substrates did not alter their modulation of EC behavior, reinforcing our hypothesis that HA oligomers may be chemically derivatized, as often required for formulating biomaterials, and yet retain their innate biologic properties. However, under both presentation modalities (exogenous vs. surface-immobilized), this HA oligomer mixture somewhat elevated EC expression of inflammatory CAMs. To circumvent these problems, we reason in the current study that incorporation of these oligomers within crosslinked constructs containing bioinert, HMW HA would temper the inflammatory effects of HA oligomers, while stimulating the adhesion and proliferation of ECs. In addition, the presence of HMW HA in crosslinked form would allow us to create solid biomaterials that may be handled easily, unlike the fluid mixtures that result when HA oligomers alone are crosslinked.

FTIR analysis found the stretching bands of carboxyl (-COOH) and acetamido groups (CH_3COONH) in DVS-HA were identical to those in HA, indicating that the carboxyl group is not involved in the crosslinking reaction. The retention of the carboxyl

groups is considered essential to maintaining the polyanionic character of HA, and therefore it is important to preserving its natural physicochemical and biological properties. Aside from the sulfonyl group absorption band, the infrared spectrographs of DVS-HA were indistinguishable from HA implying the basic structure of HA and hence its function was maintained as DVS-HA. However, the ability of DVS to stably crosslink HA oligomers (D2) into the bulk material of the hydrogel was still unknown and of concern.

In order to determine the initial incorporation and long-term retention of D2 within DVS-HA, the intensity of fluorescently-labeled D2 was monitored. Greater D2 concentrations within the gels resulted in higher fluorescence intensities at all analysis time points indicating that a difference in D2 content was maintained between the difference formulations. A difference in fluorescence intensity between 1:1 w/w and 1:2 w/w DVS-HA gels was noted, which is likely due to a difference in UV penetration through gel during imaging. 1:2 w/w DVS-HA swelled to greater degree than 1:1 w/w DVS-HA resulting in gels with a higher water content and, therefore, lower polymer density. During the 200 ms exposure time that was adopted for all gels, the transluminating UV light was able to penetrate farther through these low density gels stimulating more oligomers to fluoresce. This idea is reinforced by the fluorescence data of 1:2 w/w DVS-HA between day 0 and 1. Directly after crosslinking (day 0), the fluorescence levels of 1:2 w/w DVS-HA are similar to 1:1 w/w DVS-HA. However, upon incubation in PBS, 1:2 w/w DVS-HA swelled allowing more UV penetration and increased fluorescence. In case of 1:1 w/w DVS-HA gels, the fluorescence intensity was

maintained constant through the entire period of incubation in PBS, suggesting significant retention of the incorporated HA oligomers. On the other hand, an overall loss in fluorescence was observed from the 1:2 w/w DVS-HA gels over time. We believe that the lower DVS concentration within these gels may be insufficient to chemically crosslink all of the added D2 and that the un-reacted D2 was merely physically entrapped within DVS-HA during the crosslinking process. Upon incubation within PBS, un-reacted D2 began to elute out of the hydrogel leaving only chemically-crosslinked D2 within the hydrogel after 14 days.

Materials fabricated from naturally occurring molecules are more susceptible to degradation within the body due to presence of enzymes that specifically target these molecules. The turnover of HA within the body is relatively rapid compared to other ECM molecules (33% weight loss per day). The half-life of HA circulating in the blood is 5 minutes and that in the skin epidermis is half a day, while collagens have half-lives of several weeks [30,224]. High molecular weight HA (HMWHA) is degraded extracellularly through both enzymatic and non-enzymatic processes. Enzymatic degradation occurs physiologically through the action of hyaluronidases, chondroitinases and hexosaminidases. Non-enzymatic degradation of HA, on the other hand, occurs almost solely following tissue injury and during inflammation, and involves mediation of reactive oxygen species (ROS), hydrogen peroxide (H_2O_2) and hydroxyl radicals (OH^-) [225,226]. In this study we hoped that DVS crosslinking of HA would decelerate and possibly inhibit its natural breakdown. However, we found DVS-HA to still be susceptible to degradation. Therefore, we investigated the impact of incorporated oligomer content and

extent of crosslinking on the rate of degradation of DVS-HA gels when exposed to a super-physiologic concentration of *testicular hyaluronidase in vitro*. The degradation rates of these gels were influenced by the hydrogel swelling capacity (and thereby enzyme concentration within the gels) and apparent crosslinking density (or HA bonding with the gels). DVS-HA containing higher concentrations of DVS (1:1 w/w DVS-HA) and a lower D2 content exhibited reduced capacity for hydration, and thus, lower swelling ratios, which restricted the entry of enzymes from the bulk solution into the gel interior. The greater amount of bonding within these hydrogels (measured by the apparent crosslinking density) also required the enzymes to work longer to breakdown these gels, as is clear from the data presented in Figure 5.8.

Rheological analysis provided a quantitative evaluation of the viscous and elastic responses of DVS-HA. Both the storage moduli (G') and loss moduli (G") are independent of frequency and G' values are always higher than G", which is typical of a "strong hydrogel", whose answer to oscillating frequency is more similar to a solid than a liquid. By increasing the concentration of DVS within these gels we were able to obtain G' (1400 – 3000 Pa) and G" (10 – 40 Pa) that were much higher than commercially available DVS-HA products for soft tissue augmentation; the G' and G" of Hylaform (a dermal filler) are 185 Pa and 21 Pa, respectively, at 3.0 Hz [321]. However, vascular regenerative applications demand far more resilient biomaterials then does skin due to the dynamic and strenuous environment of blood vessels. A completely sulfated form of hyaluronic acid (Hyaff), which has shown potential as a regenerative vascular grafting material (but yet not particularly conducive to endothelialization), possesses G' and G"

values on the order of 420 kPa and 17 kPa, respectively, at 1 Hz [256,326]. The high strength of this and other successful vascular grafting materials indicates that our DVS-HA hydrogels would not by themselves be suitable for use as a vascular scaffolding materials, but rather must be composited with other existing natural or synthetic graft materials, at least from the standpoint of surviving the forces experienced in a vascular environment.

SEM was used to evaluate the changes in surface morphology of dehydrated hydrogels as a function of D2 and crosslinker content. Dehydration itself caused the gels to shrink, drawing the HMW HA strand toward one-another and the appearance of ripples on the gel surface. Higher concentrations of DVS (i.e., 1:1 w/w DVS-HA) restricted the movement of the HA 1500 strands to a greater degree, preventing ripple formation. The addition of D2 enhanced the ability of the hydrogel structure to compact, avoiding the need to create folds on the surface. Also, hydrogels with a higher concentration of D2 possessed a surface topography that appeared more granular, potentially forming a surface with a greater roughness and more conducive to cell attachment. Previous studies [327] showed that surface roughness, both at the level of cell adhesion (1 μm) and the level of protein adsorption (50 nm), can stimulate cell attachment. Likely, in our case, these physical changes to the gel surface must contribute in some manner to enhanced cell adherence to gels with incorporated D2 oligomers, although the predominant effect may be due to cell signaling.

In all cases, a distinct ring of inflammatory cells surrounded the implant and the thickness of this highly cellular region appeared to be dependant on DVS concentration. Hydrogels containing greater DVS-crosslinker densities stimulated an enhanced

inflammatory response from the surrounding tissue. Free-form DVS is known to be toxic, though, it has been shown to be biocompatible when used as a crosslinker for HA at low concentrations [328]. Here we show that the higher DVS concentrations, required from the standpoint of imparting good biomaterial handling properties and improved mechanics, results in an exaggerated inflammatory tissue response. The region around the implants also contained less collagen I than further afield, strongly suggesting that the dense population of cells in this region are inflammatory, and not collagen-producing fibroblasts. The primary cell types that respond to subcutaneous implants are typically fibroblasts and inflammatory cells. Fibroblast attempt to isolate the implant by surrounding it with a collagen I-rich fibrous capsule, while inflammatory cells degrade/ digest the implant. The lack of collagen I adjacent to the implant indicates an absence of fibroblastic activity. In addition, very little tissue infiltration was observed within DVS-HA, as compared to the matrigel control. The defect containing 1:1 w/w DVS-HA gel implant remained consistently void of inward tissue projections, though, some tissue projections were observed in 1:2 w/w DVS-HA gels, possibly due to the lower crosslinking density (lowered stiffness), which enables cells to readily infiltrate.

The goal of this work was to incorporate HA oligomers into a DVS-crosslinked gel containing HMW HA in order to promote EC attachment/proliferation on the hydrogel surface, while tempering the inflammatory cell response to HA oligomers by the presence of HMW HA. We found that ECs, cultured *in vitro*, attached onto gels with incorporated D2, and the D2 content appeared to enhance this attachment. However, the EC maintained a rounded morphology throughout the culture period. Two factors

influence cell morphology are surface charge and substrate hydrophilicity. Negatively-charged cells adhere far less strongly to substrates containing acidic or neutral groups than to those with basic (positively charged) groups [329]. In addition, the DVS-HA gels are very hydrophilic in nature and therefore contain a high water content. Previous studies have shown that extremely hydrophilic surfaces are thermodynamically unfavorable for cell attachment [330]. As a cell-binding ligand and via its ability to enhance surface roughness, D2 was able to promote EC adherence but the extreme anionicity of HMW HA and exuberant water content of DVS-HA gels dissuaded the ECs from spreading. Matrigel is a mixture of predominantly laminin and collagen IV, a substrate similar to the natural basement membrane of blood vessels. In order to promote EC spreading, a low concentration of matrigel was adsorbed onto the hydrogel surfaces, which allowed the ECs to exhibit their natural morphology while interacting with the HMW HA and HA oligomers also present on the hydrogel surface. Matrigel was successfully adsorbed onto the hydrogel surfaces and the D_c protein assay showed the concentration remained constant (~12 μg/ cm^2) on all hydrogel formulations. The natural cobblestone morphology of ECs on matrigel adsorbed DVS-HA indicate the adsorption process did not alter the conformation of laminin and collagen IV, a common problem with synthetic materials (i.e. polymethylmethacrylate). However, ECs remained fairly clustered in isolated locations on 1:2 w/w DVS-HA. This is likely due to the higher water content and anionicity of 1:2 w/w DVS-HA isolating cell attachment to specific regions of the hydogel surface. It is interesting to note that compared to ECs cultured on pure matrigel, those cultured on matrigel-coated HA gels, free of HA oligomers, exhibited much lower

levels of proliferation. This suggests that matrigel surface coatings of low density on the HA gels primarily influenced cell adherence and morphology, not proliferation. However, EC adherences and proliferation enhanced as a direct function of D2 content. This suggests that the ECs were able to interact with the embedded oligomers and as a result, up-regulate proliferation. Therefore, we can conclude that the incorporation of HA oligomers into vascular scaffolding constructs is beneficial to endothelialization by the promotion of EC proliferation. We believe the level of proliferation did not attain that of fibronectin and matrigel due to the vast excess of HMW HA on the hydrogel surface, which suppresses the effects of the HA oligomers. The level of ICAM-1 expression by the ECs was also suppressed by HMW HA. HA oligomers elevated both ICAM-1 and VCAM-1 expression of ECs when presented as an exogenous supplement or immobilized surface but when these oligomers were embedded within HMW HA, EC ICAM-1 expression remained similar to DVS-HA without HA oligomers and the fibronectin control. VCAM-1 expression, on the other hand, was elevated on all DVS-HA hydrogels irrespective of HA oligomer concentration. Possibly, this may be due to the high concentration of DVS within these hydrogels, which was also found to stimulate an exaggerated inflammatory response in the subcutaneous *in vivo* model.

5.5 Conclusions

In this study, we successfully developed hydrogels composed of high molecular weight HA and its oligomers, as potential biomaterials for the regeneration of luminal ECs of blood vessels. We showed the mechanical (degradation, viscoelasticity) and

physical (crosslinking density, surface structure, swelling) properties of these hydrogel can be adjusted by varying the crosslinker and oligomer densities within them. However, the overall strength of these hydrogels is too low for vascular applications as a stand-alone material and therefore, may only be used as a composite material. The presence of oligomers within DVS-HA seemed to enhance EC attachment and proliferation, supporting the notion that HA oligomers are more conducive to EC growth than other forms of HA. However, the high concentration of DVS, required to impart good handling properties of these gels, appeared to be somewhat toxic resulting in enhanced subcutaneous inflammatory response and VCAM-1 expression by ECs. Therefore, another crosslinker may be more appropriate to use, which could result in better mechanics and improved biocompatibility. In the case of such a formulation too, the HA oligomers would provide the stimulus for functional endothelialization. If no such crosslinker exists, a better approach might be to abandon the idea of a standalone HA vascular graft materials, and, as discussed in chapter 4, chemically derivatize and immobilize both HA oligomers and HMW HA in a controlled manner onto the lumenal surface of synthetic or tissue engineered grafts already in use, so that improved, predictable, and functional endothelialization may be achieved, while eliminating the need to address the biomechanics of the graft material at large. This method would also eliminate the need for crosslinking HA, which would likely circumvent the problems associated with crosslinker-mediated toxicity or inflammation.

CHAPTER 6

THE IMPACT OF HA OLIGOMER CONTENT ON PHYSICAL, MECHANICAL, AND BIOLOGIC PROPERTIES OF GLYCIDYL METHACRYLATE - CROSSLINKED HA HYDROGELS

6.1 Introduction

As mentioned in chapter 2, tissue engineering is an emerging interdisciplinary field of bioengineering that aims to regenerate diseased or injured tissues using the building blocks of cells, growth factors and scaffolding cues. The field has gradually transitioned from one of synthetic scaffolds to the use of extracellular matrix (ECM), a naturally occurring cell scaffolds. These natural materials provide cells inherent biological instructive cues to guide their proliferation and differentiation. In addition, they have some remarkable advantages over synthetic materials including selective cell adhesion, mechanical properties similar to that exhibited by native tissues, and biodegradability, which allows complete re-sorption of the matrix after tissue regeneration is complete. A class of ECM molecules that are increasingly studied in the context of regenerative materials are glycosaminoglycans (GAGs). One such GAG, hyaluronic acid (HA), occurs naturally in connective tissues (e.g. skin) as a simple linear molecule consisting of repeating dissacharide units of N-acetyl-D-glucosamine and D-glucuronic acid [17]. Most cells have the ability to synthesize HA at some point during their cell cycle, signifying that the molecule has vital function in several fundamental biological processes [18].

In recent years, HA has been recognized as a potential biomaterial for effective

tissue regeneration. Biologically, HA has three known molecular functions: (1) It encompasses a large hydrodynamic domain, permitting it to form a physical barrier around cells shielding them from disturbances, or alternatively, creating an uninhibited pathway for migrating cells. (2) It interacts with HA-binding proteins, proteoglycans, and other structural molecules to form composite ECM structures that act as macromolecular cues for cellular synthesis and organization of tissues. (3) It binds to cell surface receptors (CD44, RHAMM) to help mediate important intracellular signaling pathways. As a result, HA is a critical regulator in many biological phenomina including embryonic development, tissue organization, wound healing, and angiogenesis. HA is also highly biocompatible and does not elicit a foreign-body response upon cross-transplantation due to the preserved structural homology of HA across species [18]. For the same reason, HA meant for clinical use can be derived from many sources including bacterial fermentation and synthesized in large quantities [331]. Though HA is enzymatically degraded in vivo by hyaluronidases [332], and completely resorbed via several metabolic pathways, it can be chemically derivatized and/or crosslinked into stable hydrogels or solid biomaterials [253,256]. Although the modes of interaction between HA and the human body are still incompletely understood, the favorable characteristics outlined above have recently prompted an investigation into its utility as a scaffolding biomaterial for tissue-engineering applications, such as cartilage [20] and dermal [21] repair and regeneration. In this line of thinking, our lab is currently investigating the potential use of HA as an implant material for vascular regeneration. Since HA forms a significant (4-7% w/w) component of vascular ECM [22], we hypothesize that HA-derived biomaterials will mimic

the *in vivo* environment and provide healthy biomechanical and biochemical signals to cultured vascular cells.

Elastin is a critical structural protein in the medial layer of blood vessels, which facilitates their elastic recoil and provides the resilience necessary for cyclic distension and contraction [333,334]. It is secreted as a soluble protein precursor (tropoelastin) by SMCs, recruited onto a microfibrillar template (fibrillin), and crosslinked by desmosine mediated by lysyl oxidase (LOX) [335]. In addition to providing tissue elasticity, elastin also mechano-transduces SMC behaviour (e.g. proliferation) through binding to cell surface elastin–laminin receptors [6] to regulate SMC activity [42], particularly during vascular morphogenesis [336]. Thus, disruption of elastin due to inflammatory diseases [42,337], direct mechanical injury [211] or its malformation in congenital and inherited conditions can encourage SMC hyperproliferation and medial thickening, leading to reduced arterial compliance and hypertension [338]. In such cases, vascular elastin must be restored or regenerated as a priority.

Studies conducted by our group [31,32] have shown that HA oligomer mixtures (D1, see chapter 3) dramatically enhance elastin matrix deposition by adult SMCs; the extremely anionic high molecular weight (HMW) HA ($> 1 \times 10^6$ Da) did not cause such up-regulation but appeared to benefit matrix deposition and fiber formation, possibly by causing physical coacervation of elastin precursors to facilitate their crosslinking. We also showed immobilization of the oligomers onto 2-D cellular substrates (i.e. glass) did not alter its stimulation of SMC elastin production (chapter 4), reinforcing our hypothesis that HA oligomers, when chemically derivatized, retain their innate biologic signaling

characteristics, and are thus amenable to formation of biomaterials. In addition, we reported successful synthesis and recruitment of elastin by SMCs seeded atop bioactivated HA hydrogels whose surface contained a mixture of bioinert HMW HA and shorter, more bioactive HA fragments and oligomers [220] generated in situ by prolonged UV irradiation of the gels. However, since the effects of UV light can be difficult to control and replicate, and potentially cause random ionizations that can be structurally disruptive, a better approach is to create 'bioactivated' gels containing bio-inert long-chain HA, necessary to maintain mechanical integrity and potentially provide a high degree of biocompatibility, and smaller, more cell-interactive HA oligomers. In addition, it has been hypothesized that cells embedded within 3D scaffolds interact with each other and the surrounding scaffold in a more natural tissue environment than 2D culture and thus expected to more closely evoke native cell responses [339]. To examine the efficacy of stimulating elastin regeneration by cells encapsulated in a 3D space, we propose to generate photo-crosslinked HA [264] hydrogels containing HA oligomers, encapsulate SMCs within them, and investigate their ability to regenerate elastin matrix.

To date, the use of HA oligomers as biomaterials for enabling SMC mediated vascular elastin regeneration/ remodeling have not been thoroughly investigated. Also, the densities at which bioactive HA oligomers should be presented within such scaffolds to elicit the desired matrix regenerative responses, and yet not adversely impact gel handling, mechanics, and biocompatibility, are unknown. Therefore, in this chapter, we investigate the mechanical properties, biocompatibility, and elastin production of SMC elastogenesis encapsulated within oligomer-embedded HMW HA hydrogels crosslinked

with GM.

6.2 Materials and Methods

6.2.1 Preparation of HA Oligomer Mixtures

As mentioned in section 3.2.1, HA 1500 (MW = 1.5×10^6 Da) was enzymatically digested to produce a mixture of HA oligomers (D1). Briefly, HA 1500 (5 mg/ ml) was digested with bovine *testicular hyaluronidase*, (0.45 mg/ ml; 439 U/mg) in a solution of digest buffer (37 °C) for 18 h. The enzyme was then precipitated, its activity terminated by boiling (2 min), and cooled on ice. Following centrifugation (2800 rpm, 10 min), to separate the enzyme from the mixture, the supernatant was dialyzed in water (12 h) and then freeze-dried overnight to generate lyophilized HA oligomers. The mixture was analyzed by FACE and found to contain a broad range of oligomers (D1), specifically 13.9 ± 3.6% w/w of HA 6mers and 8.0 ± 1.6% w/w of HA 12mers.

6.2.2 Hydrogel Fabrication

HA hydrogels were crosslinked with glycidyl methacrylate (GM-HA) using a method based on one previously described (Figure 6.1) [264]. Briefly, HA 1500 with added D1 (0, 5, 10, 20% w/w) was dissolved (10 mg/ ml) in DI water, then mixed with triethylamine (3.6% v/v; Sigma; a chemical catalyst), glycidyl methacrylate (GM, 3.6% v/v; Sigma; a crosslinker), and tetrabutyl ammonium bromide (3.6% w/v; Sigma; a phase transfer catalyst). The batch reaction was allowed to continue overnight (18h, 23°C) and finally completed by incubation of the mixture for 1 h at 60 °C. The aqueous product

(GM-HA) was recovered/ purified by precipitation in acetone, re-dissolved in DI water (3 cycles), and finally precipitated in acetone (Sigma). The GM-HA precipitate was finally freeze-dried, and stored at -20 °C. To create hydrogels, GM-HA was dissolved in PBS (45 mg/ ml), and mixed with Irgacure 2959 (0.01% w/v; Ciba, Basel, Switzerland; a photo-initiator). Thorough mixing of the viscous solution that resulted was achieved by repeated transfer of the mixture between two sterile syringes (Beckton Dickenson, Franklin Lakes, NJ) through a 3-way stopcock (Kimble Kontes, Vineland, NJ). The mixture was then centrifuged for 5 min at 1000 *g* to remove air bubbles and aliquoted into cylindrical molds (for rheology, compression: 2 cm^2, 0.5 ml; for all other mechanical analytical techniques: 0.79 cm^2, 0.2 ml; for cell culture: 0.32 cm^2, 0.1 ml). The aliquoted solution was then exposed to UV light (λ = 365 nm, ~22 mW/ cm^2) for 1.11 min/ mg HA (2 cm^2 mold: 25 min; 0.79 cm^2 mold: 10 min; 0.32 cm^2 mold: 5 min). The dimensions (height and diameter) of the swollen cylindrical hydrogels, which were crosslinked in the 0.32 cm^2 mold, were measured with a digital caliper (Fisher, Pittsburgh, PA).

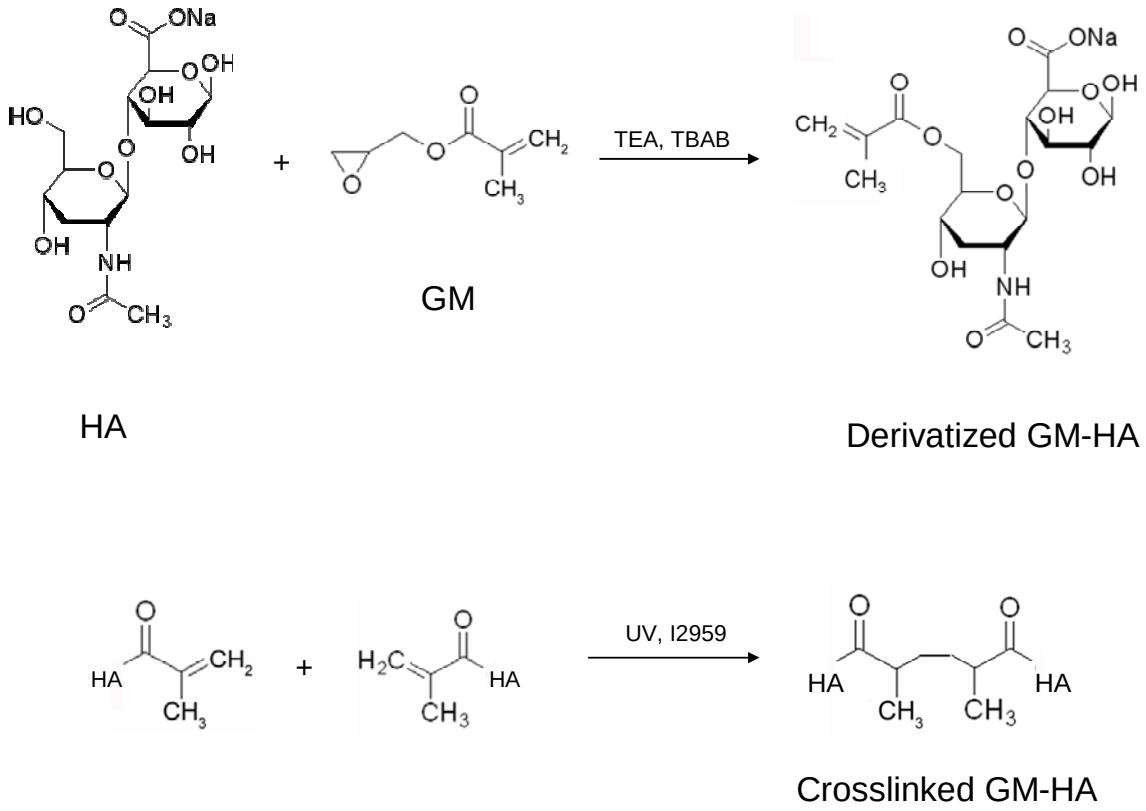

Figure 6.1. Crosslinking chemistry of GM HA. GM-HA hydrogels were prepared by a two step process. HA was initially incubated with GM, a chemical catalyst (TEA) and phase transfer catalyst (TBAB) in a batch reaction combining the glycidyl units of GM and hydroxyl units of HA to create the uncrosslinked GM-HA product. A GM-HA solution was then combined with a photoinitiator (I2959) and treated with UV to stimulate the radical reaction of the methacrylate units of GM-HA.

6.2.3 Fourier Transform Infrared Spectroscopy

Fourier Transform Infrared – Attenuated Total Reflectance (FTIR-ATR) was performed to determine the chemical alterations induced by the initial incorporation of GM onto the HA backbone and its UV-induced transition into a crosslinked GM-HA hydrogel. Freeze-dried samples of crosslinked GM-HA were analyzed on a Varian 660-IR FTIR spectrometer (Varian, Palo Alto, CA) and compared to uncrosslinked GM-HA and the HA starting material (n = 3). The spectra were recorded in a frequency range between 400 cm^{-1} and 4000 cm^{-1} with a spectral resolution of 4 cm^{-1}. A spectral library

(Mentor Pro, Biorad, Hercules, CA) was used to identify the peaks and the corresponding bond vibrations.

6.2.4 Apparent Crosslinking Density

The structural integrity of GM-HA is primarily maintained by GM crosslinks, which link the HA strands to one another and limit their freedom of motion. The incorporation of HA oligomers may reduce the effectiveness of these crosslinks, diminishing the overall mechanical properties of the gel. In addition, the efficiency of GM-HA derivatization and UV-induced crosslinking of GM may not be 100%. Accordingly, we deemed it necessary to define an apparent crosslinking parameter, which in essence represents the effective crosslinking within each gel formulation. Uniaxial compression testing was performed to calculate the apparent crosslinking density within the gels. Cylindrical gel samples (8-mm diameter) were punched out of a larger gel using a 8-mm-diameter corneal trephine (BRI, Malden, MA) and were compressed without constraining the edges (unconfined compression testing) on a DMA Q800 (TA Instruments, New Castle, DE). The gels were subject to an initial force of 0.05 N and were then compressed at a rate of 20% strain/ min (n = 8). All tests were performed in air, though the gels were kept hydrated in PBS while being compressed. Stress/ strain curves were developed according to Equation 6.1 developed by Flory [318] and the initial slope of the curve (0 – 30% strain) was used to estimate the apparent crosslinking density of the gel.

$$\sigma = RT\left(\frac{\upsilon_e}{V_o}\right)\phi_{2,x}^{2/3}\phi_{2,s}^{1/3}\left(\alpha - \frac{1}{\alpha^2}\right) \quad \text{(Eq 6.1)}$$

where σ – uniaxial compressive stress (Pa), P – universal gas constant (J/ mol K), T – temperature (K), $\phi_{2,x}$ – polymer volume fraction post-crosslinking, $\phi_{2,s}$ – polymer volume fraction swollen, ν_e/V_o – apparent crosslinking density (mol/ cm^3), and α – compressed fraction.

6.2.5 Rheology

To further characterize the impact of crosslinking and oligomer incorporation on hydrogel mechanics, rheological oscillatory shear stress experiments were performed. The gel stiffness was experimentally determined by measuring the storage (G') and loss (G") moduli. An AR G2 rheometer (TA Instruments, New Castle, DE) was used in the parallel plate geometry, with a 25-mm plate and constant normal force of 0.2 N. A deformation angle of 1 mrad was maintained throughout each frequency sweep of 0.08–10 Hz (n = 4).

6.2.6 Swelling Ratio

Swelling tests were performed to study the effects of HA oligomer content on the bulk hydrodynamic properties of the GM-HA gels. Fully hydrated gels were blotted to remove surface liquid. The weight of the swollen gel samples were recorded using a sensitive balance (OH AUS, Pine Brook, NJ). The gels were then freeze-dried and

weighed again. The swelling ratio was calculated by the following formula (n = 4).

$$SwellingRatio = \frac{W_s}{W_d} \quad \text{(Eq 6.2)}$$

where W_s is the swollen mass of the gel (mg), and W_d is the dry mass of the gel (mg).

6.2.7 Scanning Electron Microscopy

SEM was performed to determine how incorporating HA oligomers (D1), and their concentrations alter the interior pore structure of the gels. In preparation for SEM, swollen gels were dehydrated with acetone, snap-fractured and the interior surface coated with gold for 4 min using a SPI-Module Sputter Coater (Structure Probe, Inc., West Chester, PA) and imaged on an SEM (Jeol 100-JSM 5410 LV, Pleasanton, CA) at 150× magnification (n = 3).

6.2.8 In Vitro Degradation

In vitro enzymatic degradation of the hydrogels was measured as a function of time by incubating the GM-HA gels in a solution of *testicular hyaluronidase*, and then monitoring the dry mass of the samples that remained un-degraded at various time points. The gels were initially soaked in digest buffer (150 mM NaCl, 100 mM CH_3COONa, 1 mM Na_2-EDTA, pH 5.0) overnight to reach swelling equilibrium. Gels were then incubated in a solution of bovine *testicular hyaluronidase* (Sigma-Aldrich), prepared in

digest buffer (2 mL of 50 U/ ml), for 6 h at 37°C with mild mixing on a platform shaker. At 0, 2, 4, and 6 h of digestion, the surviving dry masses of the gels were measured (n = 3). The enzyme solution was replaced after each analysis time point. The HA mass degradation profile was fitted according to first-order degradation kinetics using non-linear regression to estimate gel degradation rate constant (k).

$$C(t) = C_o e^{-kt} \qquad \text{(Eq 6.3)}$$

where, C(t) is the dry mass of the gel at time t (mg), C_o is the initial dry mass of the gel (mg), k is the degradation rate (h^{-1}), t is time (h).

6.2.9 In Vivo Biocompatibility

The biocompatibility of the hydrogels was determined by their subcutaneous implantation in rats. Prior to implantation, the hydrogels were sterilized in 95% v/v ethanol (Sigma) for 2 h and then re-hydrated in sterile 1× PBS overnight. Sprague-Dawley rats (~250 g) were anesthetized (0.01 ml/ g intramuscular injection of 4% chloral hydrate), shaved, and a 5-cm incision made in the skin along the spine. Blunt dissection was used to form a pocket between the skin and muscle. The muscle surface was then cleared of fascia. GM-HA hydrogels of different formulations and matrigel (Sigma) were placed directly into these pockets (5 implants/ animal; n = 7), as shown in Figure 6.2. After implantation, the surgical incision was closed with 4-0 silk suture with a FS-2 cutting needle (Ethicon, Piscataway, NJ).

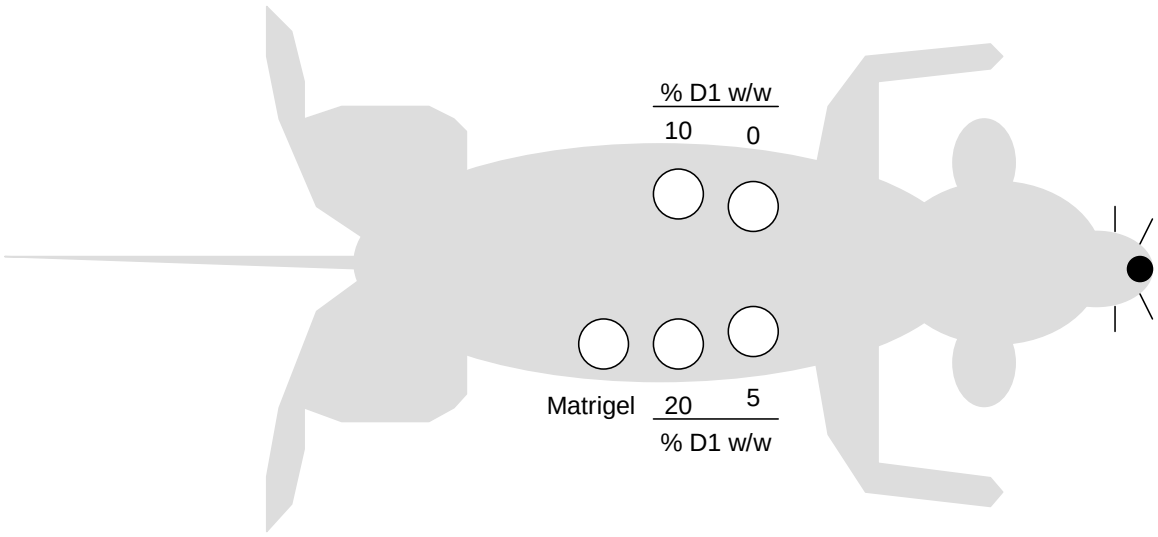

Figure 6.2 Illustration of subcutaneous implantation scheme of GM-HA in the back of rats. All GM-HA formulations and matrigel controls were implanted into the same rat.

At 3 weeks, the hydrogels and the adherent tissue capsules were explanted from the subcutaneous pockets, fixed in 4% v/v paraformaldehyde and soaked for 1 h intervals in 30% w/v sucrose, 1:1 30% sucrose: optimal cutting temperature (OCT; Sakura, Torrance, CA) compound, and finally in pure OCT. The explants were then embedded within OCT, frozen on dry ice, and stored at -80°C. Prior to sectioning, the frozen blocks were acclimated to -20°C (overnight) and cryosectioned perpendicular to the skin and muscle surfaces. The 8-μm thick sections were transferred onto HistoBond® glass slides (VWR) and stained with Haematoxylin and Eosin to detect inflammatory cell infiltration towards or within the implant. The tissue sections were imaged on a Leica DM IRB microscope equipped with a JVC TK-C1380 color camera. In addition, immunofluorescence methods were used to detect the collagen, and hence presence of a

fibrous capsule within the tissue mass surrounding the implant. The 15 μm thick tissue sections were initially quenched with 1% v/v phosphomolybdic acid to supress autofluorescence due to collagen, and then incubated with a primary antibody for collagen I for 1 h (rbt vs. rat col I; 1:100 in PBS; Chemicon, Temecula, CA). A solution of donkey serum (5% v/v in PBS) was added to the sections as a blocking agent (20 minutes) to prevent nonspecific binding of the secondary antibody. The sections were then treated with a FITC-conjugated secondary antibody (dky vs. rbt IgG; 1:500 in PBS; Chemicon) for 1 h. Draq 5 (1:2000 in PBS, 10 min; Biostatus, Leicestershire, UK) was used to fluorescently label the cell nuclei and visualize the cell density in the region surrounding the implant. Fluorescently labeled sections were imaged on a TCS SP2 AOBS confocal microscope (Leica, Allendale, NJ) using the z-axis function to image 5 μm sections, which were then compressed into a single image

6.2.10 Cell Culture

Neonatal rat aortic smooth muscle cells (NRASMCs) were harvested from the aortae of 3-day-old rat pups using methods previously described by Oakes et al. [340]. Aortae from Sprague–Dawley rat pups were excised and split longitudinally in sterile PBS (with 2mM Ca^{2+}, 4°C). The collagen-rich matrix was digested with collagenase (type II, 2 mg/ ml in serum-free medium; Worthington Chemical Corporation, Lakewood, NJ) for 10 min at 37°C. DMEM: F12 culture medium, containing 10% v/v FBS and 1% v/v penicillin-streptomycin, was added to the digested segments. After scraping off the endothelium, the aortal segments were minced into 0.5-mm-long pieces and explanted

within culture plates pre-wetted with DMEM:F12 culture medium. The explants were removed after 1 week of culture and the primary cells were cultured to confluence and passaged to expand the culture. Only low passage (P6-8) cells were used in this study.

The pre-gelation solution of uncrosslinked GM-HA was initially sterilized by syringe filtration, added to the wells of a sterile mold (0.32 cm^2 ,0.1 ml) and combined the rat aortic SMCs (3×10^6 cells/ ml) isolated from neonatal rats. GM-HA was then crosslinked by UV exposure (5 min) and the resulting hydrogels with encapsulated SMCs were cultured in DMEM: F12 containing 10% v/v FBS and 1% v/v penicillin-streptomycin. Spent medium was replaced thrice weekly during the duration of culture.

6.2.11 Fluorescent Detection of Cell Viability

As stated in section 4.2.11, calcein AM was used to fluorescently detect live SMCs within GM-HA and determine their ability to endure the extent UV treatment necessary for crosslinking GM-HA. SMCs were encapsulated in GM-HA with 0% w/w HA oligomer content using UV exposure times of 3, 5, 7 and 10 min, and cultured for 4 h prior to calcein AM detection. Draq 5 (1:2000 in PBS, 10 min; Biostatus) was also used to fluorescently label the cell nuclei. Encapsulated SMCs were imaged on a TCS SP2 AOBS confocal microscope (Leica) using the z-axis function to image 80 μm within each gel in 8 μm sections (n = 4). These sections were then compressed into a single image.

6.2.12 Immunolabeling of Elastin

The elastin produced by SMCs cultured within the GM-HA hydrogels were

compared by immunofluorescence and quantified by calculating the volumetric mean fluorescence intensity (MFI) on a per cell basis. Encapsulated SMCs were cultured for 3 wks prior to preparation for cryosectioning. The cryo-frozen samples were sectioned with a 15-μm thickness, in a direction perpendicular to the radial axis of the cylindrical GM-HA gels. The sections were transferred onto HistoBond® glass slides (VWR) and fluorescently labeled for elastin. To do this, briefly, the sections were quenched with 1% v/v phosphomolybdic acid to supress autofluorescence due to collagen and then incubated with a primary antibody for elastin for 1 h (rbt vs. rat elastin; 1:100 in PBS; Chemicon, Temecula, CA). A solution of donkey serum (5% v/v in PBS) was added to the sections as a blocking agent (20 minutes) to prevent nonspecific binding of the secondary antibody. The sections were then treated with a FITC-conjugated secondary antibody (dky vs. rbt IgG; 1:500 in PBS; Chemicon) for 1 h. Draq 5 (1:2000 in PBS, 10 min; Biostatus) was used to fluorescently label the cell nuclei. Fluorescently labeled sections were imaged on a TCS SP2 AOBS confocal microscope (Leica) using the z-axis function to image 5 μm sections at a constant gain and offset (FITC – 600, 0.9). These sections were then compressed into a single image (n = 9) prior to MFI per cell calculations using Image J.

6.3 Results

6.3.1 Crosslinked HA Hydrogels

HMW HA and HA oligomers (D1) were combined into hydrogels by crosslinking with GM, resulting in a total of 4 gel formulations. Briefly, these formulations contained

oligomer concentrations of 0, 5, 10, 20% w/w D1/HA. Figure 6.3 shows the hydrated hydrogels following crosslinking within the 0.32 cm^2 mold, and their measured dimensions. The HA oligomer (D1) content minimally affected the size of the fully-hydrated hydrogels with limited increases observed in their height (h) and diameter (d). Irrespective of their composition, and the gels remained fairly transparent.

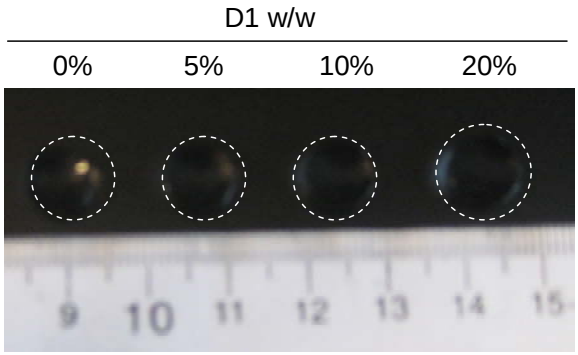

	D1 w/w 0%	5%	10%	20%
h (cm)	0.945	0.957	0.998	1.039
d (cm)	0.965	0.978	1.019	1.061

Figure 6.3 Size of hydrated GM-HA hydrogels. The height (h) and diameter (d) of the cylindrical GM-HA hydrogels slightly increased with increases in HA oligomer content. The transparency of the gels was maintained. The ruler marks indicated 1-cm increments.

6.3.2 FTIR Spectroscopy

FTIR-ATR spectra of lyophilized crosslinked GM-HA containing various concentrations of D1 (0, 5, 10, 20% w/w), uncrosslinked HA and uncrosslinked GM-HA (both HA 1500 and D1) were measured. Due to the similarity within each tested group of samples, Figure 6.4 shows only a representative spectrum of formulations in each stage in the formation process of GM-HA. The spectrum of uncrosslinked HA (A) agreed well with that provided by the American Society for Testing of Materials (ASTM). Upon adding GM to the HA backbone, the emergence of absorption bands at 936.12 and

1492.06 cm^{-1} (B) indicated the presence of the methacrylate carbon-to-carbon double bonds [320] and the successful derivatization of HA and HA oligomers (D1) with GM. UV exposure resulted in bonding between methacrylate groups, the radical breakdown of their carbon-to-carbon double bonds and the disappearance of the absorption bands at 936.12 and 1492.06 cm^{-1} within crosslinked GM-HA (C).

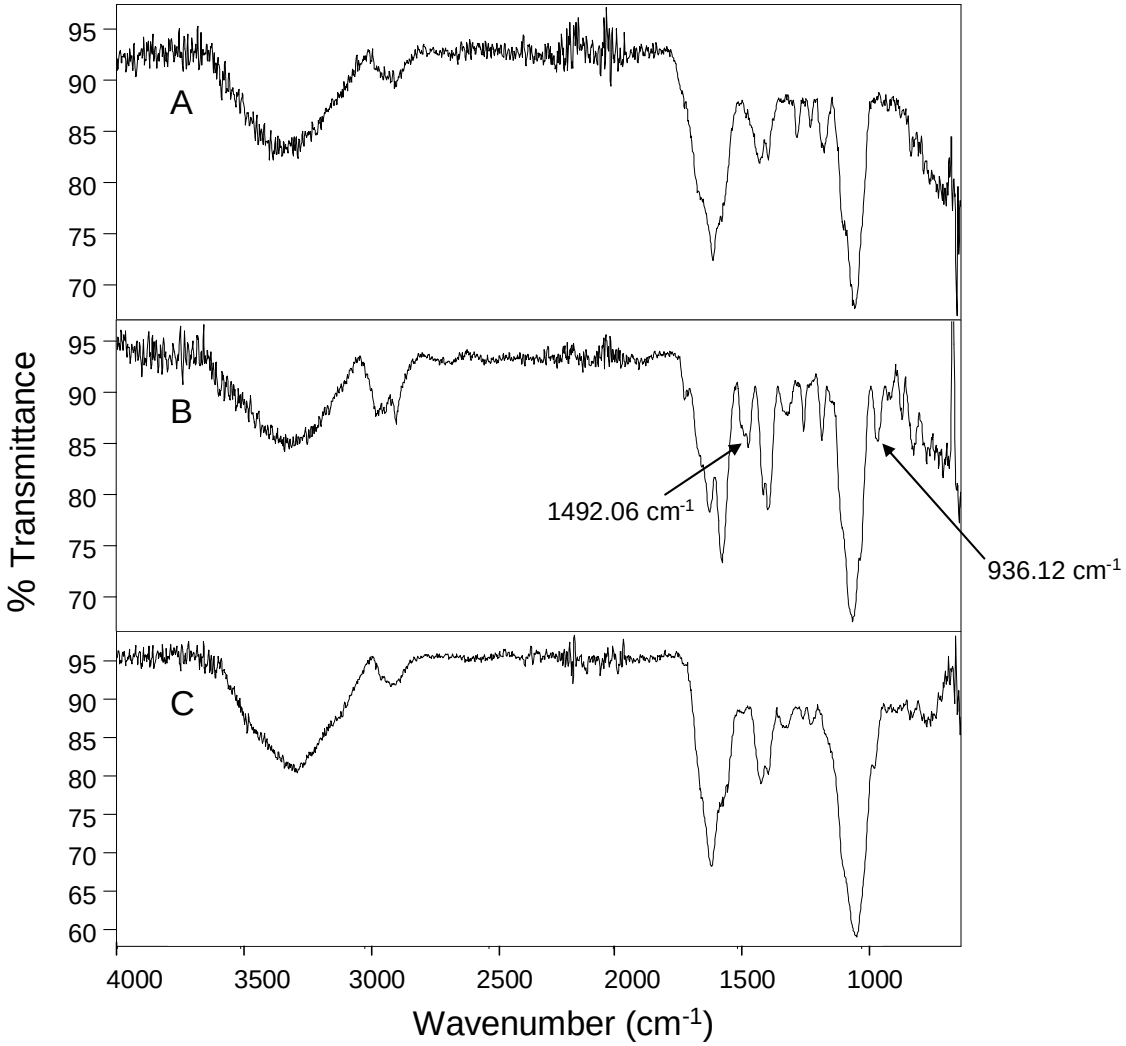

Figure 6.4 FTIR-ATR spectra of HA (A), uncrosslinked GM-HA (B), and crosslinked GM-HA (C). The initial addition of GM to HA resulted in an absorption band at 936.12 cm^{-1} identifying the carbon-to-carbon double bond of GM methacrylate. This absorption band disappeared upon UV exposure signifying the successful crosslinking between the methacrylate groups.

6.3.3 Hydrogel Crosslinking

The apparent crosslinking density and swelling ratio of GM-HA hydrogels were used to estimate the degree of crosslinking within them. Table 6.1 and Figure 6.5 show the apparent crosslinking density and swelling ratio, respectively, were dependant on the presence of D1. The addition of D1 into the hydrogels constructs increased the swelling capacity of the gels over gels composed only of HA 1500, though the extent of swelling did not appear to depend on the D1 content. On the other hand, apparent crosslinking density showed an inverse correlation to D1 content. The measured crosslinking density was much lower than the calculated theoretical value. Assuming 100% GM derivatization of HA (uncrosslinked GM-HA) and 100% UV crosslinking of derivatized GM-HA (crosslinked GM-HA), the apparent crosslinking density was calculated to be roughly of 1 – 2% of that theoretically calculated.

D1 Conc.	**Theoretical** ν_e (mol/ cm^3 x 10^6)	**Measured** ν_e (mol/ cm^3 x 10^6)
0%	1378.52	2.66 ± 0.24
5%	1325.72	2.14 ± 0.15
10%	1171.18	1.31 ± 0.81
20%	1035.80	0.88 ± 0.05

Table 6.1 Apparent crosslinking density of GM-HA determined from the uniaxial compression data and Eq 5.1. The addition of D1 into the hydrogels reduced the apparent crosslinking density. These values were approximately 1 – 2% of the estimated theoretical values.

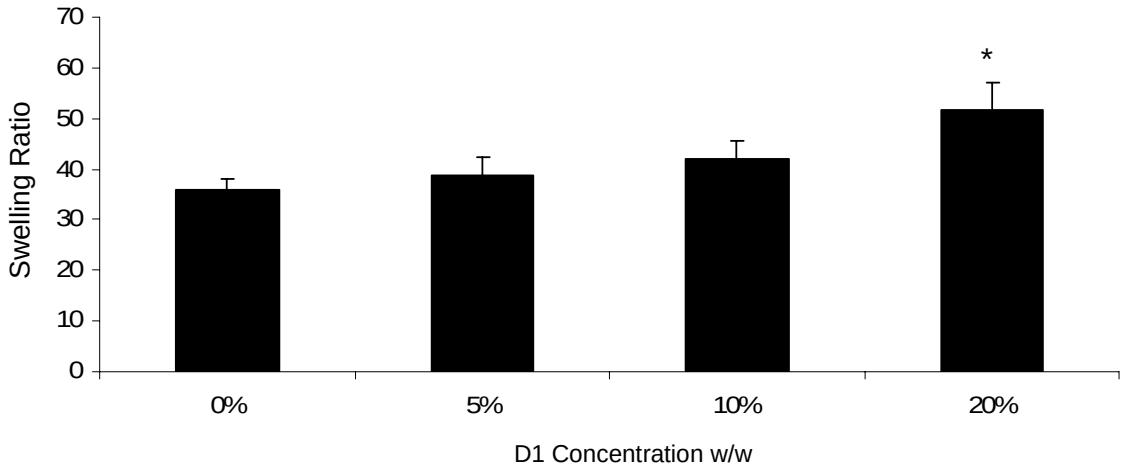

Figure 6.5 Swelling ratios of GM-HA gels. The incorporation of D1 within the GM-HA hydrogel mildly increased their swelling capacity. These increases were, however, not statistically significant except at high D1 content. [* denotes a p-value < 0.05 in comparison to 0%]

6.3.4 Hydrogel Strength and Resistance to Degradation

Rheological analysis quantified the viscous and elastic responses of GM-HA with varying concentrations of D1, thus providing information on their stiffness. In general, irrespective of their formulation, both the storage moduli (G') and loss moduli (G") of the gels were independent of frequency, with the G' values constantly higher than G" (Figure 6.6). The addition of D1 within the GM-HA gels decreased both G' and G", indicating reduced hydrogel stiffness. To investigate the biodegradability of the GM-HA hydrogels, we tested the sensitivity of the gels to a super-physiologic concentration of bovine *testicular hyaluronidase*. The weaker (less stiff) GM-HA gels containing greater concentrations of D1 also exhibited steeper degradation profiles (Figure 6.7) corresponding to increased gel degradation rates (Table 6.2).

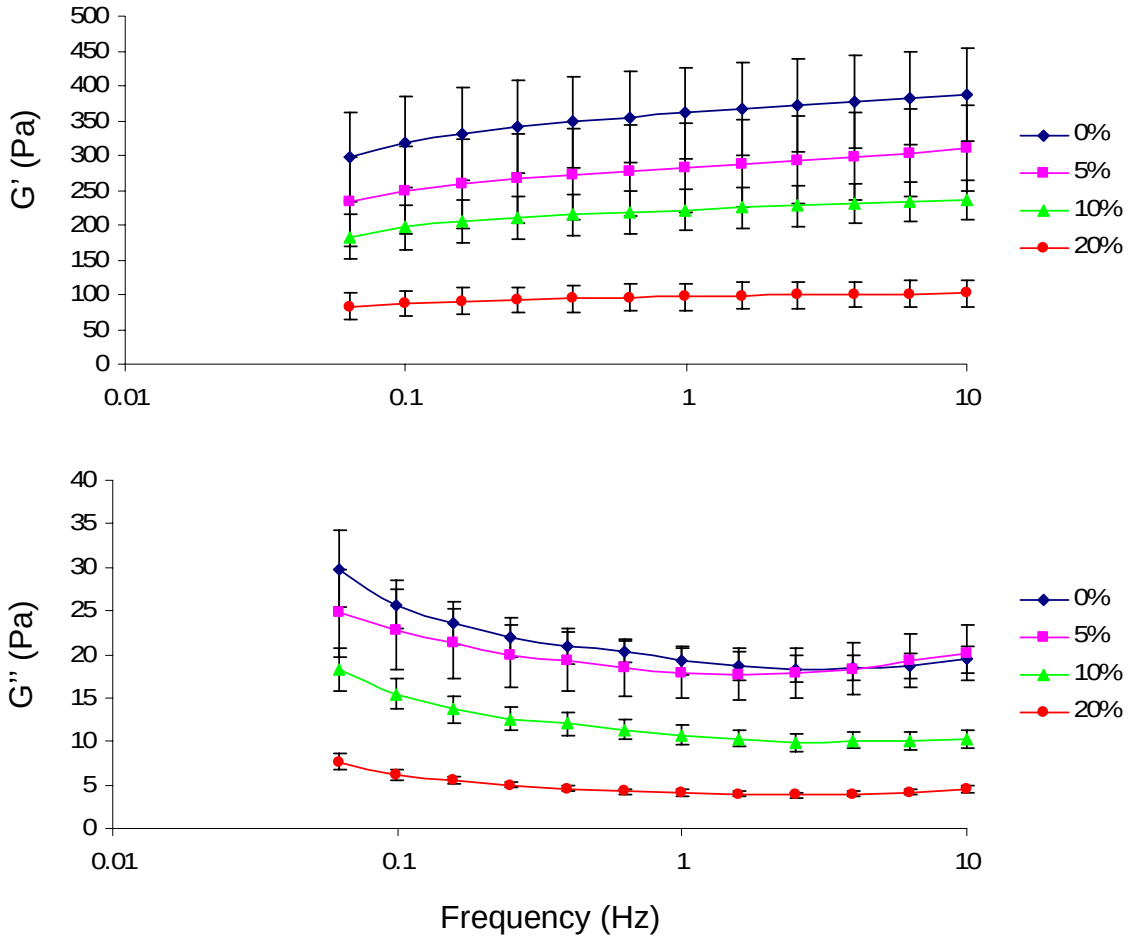

Figure 6.6 Viscoelastic properties of GM-HA. The storage moduli (G') in all cases was greater than the loss moduli (G"). The addition of D1 reduced the storage moduli, suggesting lowered gel stiffness of the hydrogels.

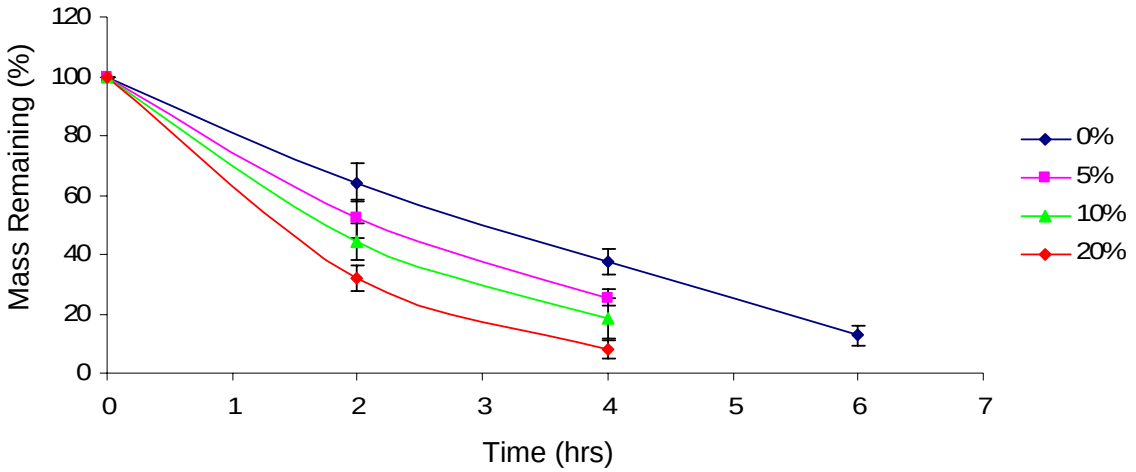

Figure 6.7 Degradation of GM-HA *in vitro*. Increasing the concentration of D1 within the gels reduced their resistance to degradation by *testicular hyaluronidase* and enhanced the degradation rate. GM-HA hydrogels containing oligomers were completely degraded after 6 h exposure to the super-physiologic concentration of the enzyme.

HA-o Conc.	k (h^{-1})	pvalue
0%	0.2696	0.017
5%	0.3358	0.018
10%	0.4161	0.012
20%	0.5842	0.026

Table 6.2 Degradation rate of GM-HA *in vitro*. Increasing the D1 content, resulted in a higher rate of degradation of GM-HA gels when incubated with a super-physiologic concentration of *testicular hyaluronidase* enzyme.

6.3.5 Hydrogel Interior Morphology

SEM, in Figure 6.8, shows the change in interior morphology of dehydrated GM-HA hydrogels. In the absence of incorporated oligomers, the process of dehydration resulted in a collapse of the HA strands within the GM-HA gels, to create a solid and

minimally porous mass. However, upon incorporation of D1 oligomers, the interior structure of GM-HA was rendered increasingly porous.

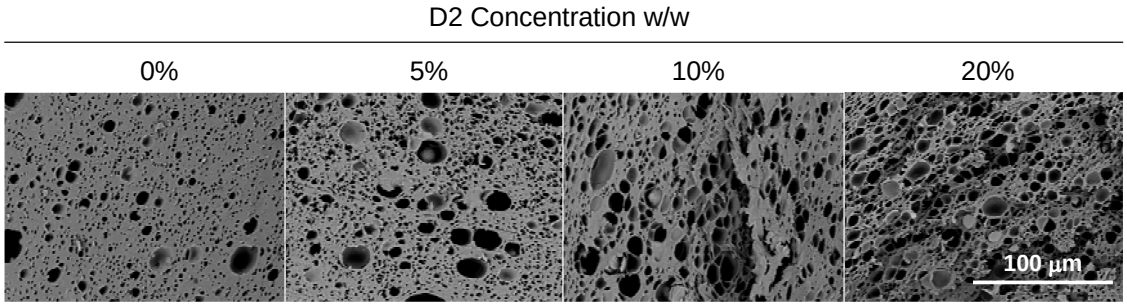

Figure 6.8 Interior morphology of GM-HA. The addition of HA oligomers into GM-HA gels resulted in enhanced porosity of the gels.

6.3.6 Biocompatibility of GM-HA Hydrogels

In all cases, H&E staining revealed limited cellularity immediately around the defect created by the GM-HA implants, as compared to that around the DVS-HA (see chapter 5); the cellularity of the tissue, however, appeared to increase slightly with increases in HA oligomer content (Figure 6.9). Most of the cells in the tissue surrounding the implants were flattened and aligned with the collagen fibers, suggestive of fibroblasts. However, the cluster of cells immediately around the gels were nonaligned, and in greater number around GM-HA gels containing higher concentrations of HA oligomers; likely these cells are inflammatory in nature. Thus, GM-HA gels containing a greater content of D1, elicited enhanced inflammatory responses relative to gels that contained a lower content of D1. However, even in gels containing 20% w/w of D1, the

inflammatory cell recruitment was very limited compared to DVS-HA (see Figure 5.9). A significant amount of tissue infiltration (see arrows in Figure 6.10), similar to that observed within matrigel controls, was observed within GM-HA gels. However, HA oligomer content did not appear to affect tissue infiltration into the gels. Immunofluorescence studies (Figure 6.11) confirmed the increases in cellularity (blue) in the tissue immediately surrounding implants that corresponded with a greater HA oligomer content in the implanted gels. These studies also indicated the distribution of collagen (green) surrounding the defect region was fairly homogeneous.

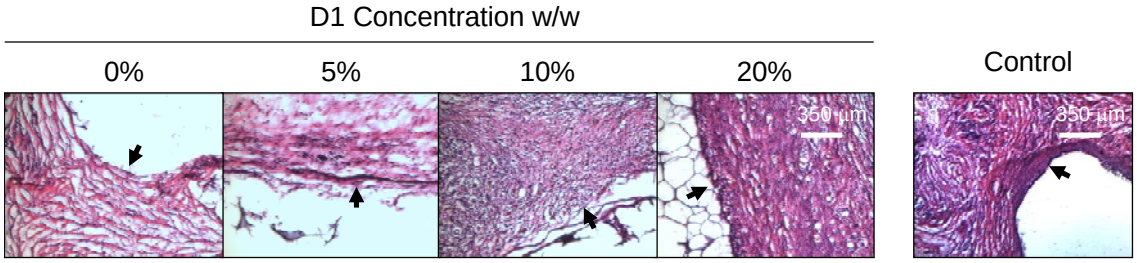

Figure 6.9 Biocompatibility of GM-HA. Very few inflammatory cells (see arrows) surrounded the implant but their density appeared to increase slightly with HA oligomer concentration.

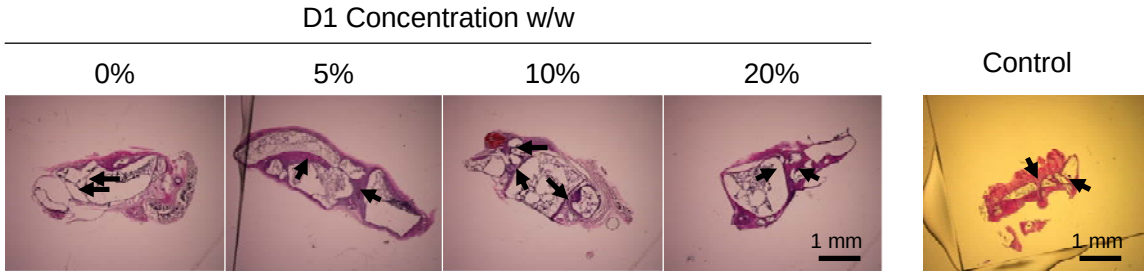

Figure 6.10 Tissue infiltration into GM-HA. A significant amount of tissue infiltration (see arrows) was observed within GM-HA similar to that of the matrigel control, and did not appear to be affected by HA oligomer content.

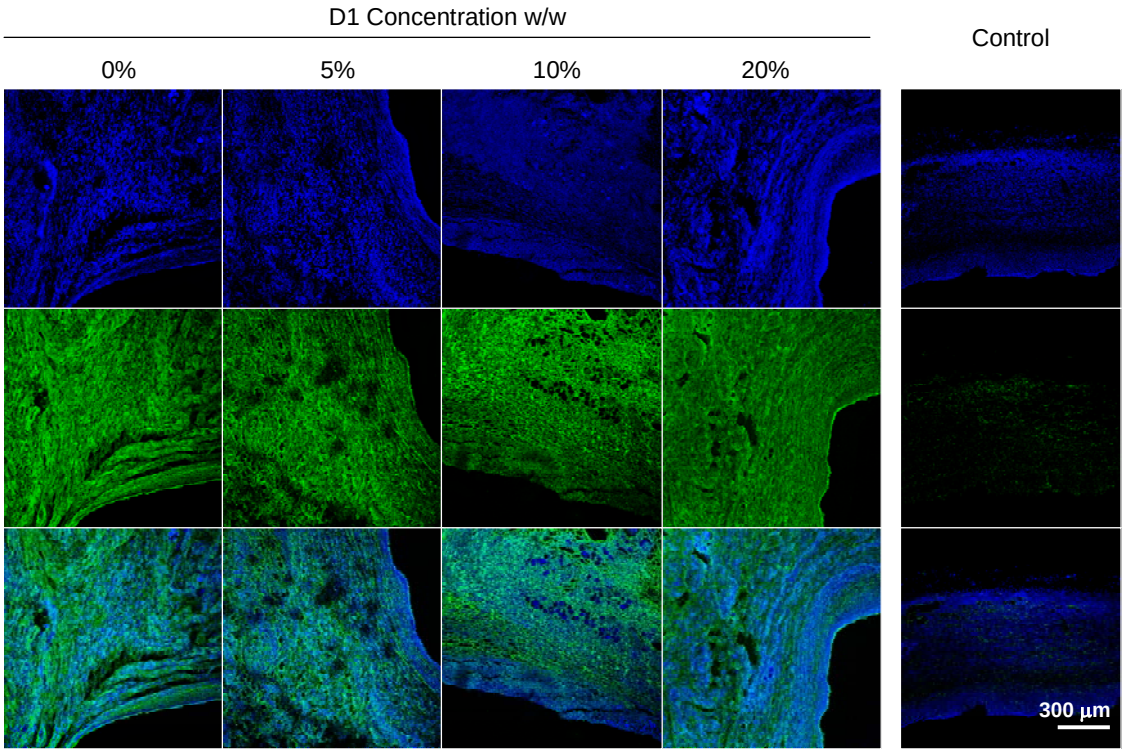

Figure 6.11 Immunofluorescence analysis collagen I surrounding implant. The cellularity (blue) in the region immediately surrounding implants increased slightly with a greater HA oligomer content and the distribution of collagen I (green) surrounding the defect region was fairly homogeneous.

6.3.7 SMC Survival

Fluorescence detection of calcein AM-labeled SMCs encapsulated within GM-HA gels showed that a majority of the cells survived UV-induced crosslinking for UV-exposure times of 0.67 – 2.22 min/ mg HA (Figure 6.12), which corresponds to 3 – 10 min for hydrogels crosslinked in 0.32 cm^2 molds. At this time (4 h of culture), the SMCs continued to retain a rounded phenotype.

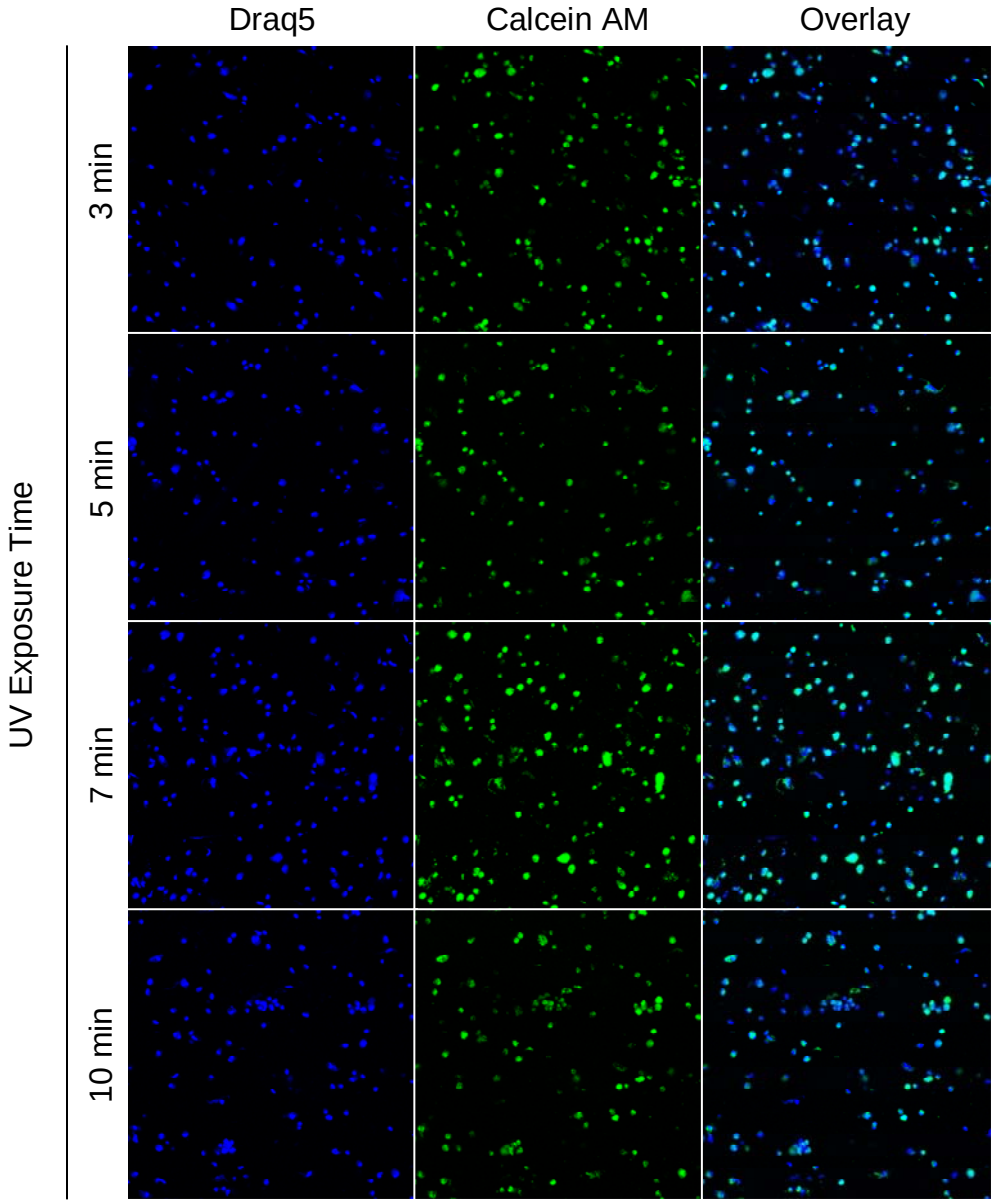

Figure 6.12 SMCs survival of UV crosslinking. Most of the embedded cells survived all exposure times of UV radiation, indicated by the overlaying of nuclei (blue) and live cell (green).

6.3.8 Elastin Production by Encapsulated SMCs

It is apparent from the fluorescent images in Figure 6.13, that the elastin content

(green) within GM-HA containing HA oligomers was visibly higher than the hydrogels that did not incorporate HA oligomers (Figure 6.13). Quantification of the volumetric fluorescence intensities of elastin and comparison between the gel formulations, confirmed this observation and additionally showed that increases in HA oligomer content do not enhance elastin production (Figure 6.14). Furthermore, the elongated appearance of cell nuclei in all cases suggests that the SMCs acquired a spread morphology quite different from the rounded nuclei observed at early culture time points (e.g. 4 h; see Figure 6.12).

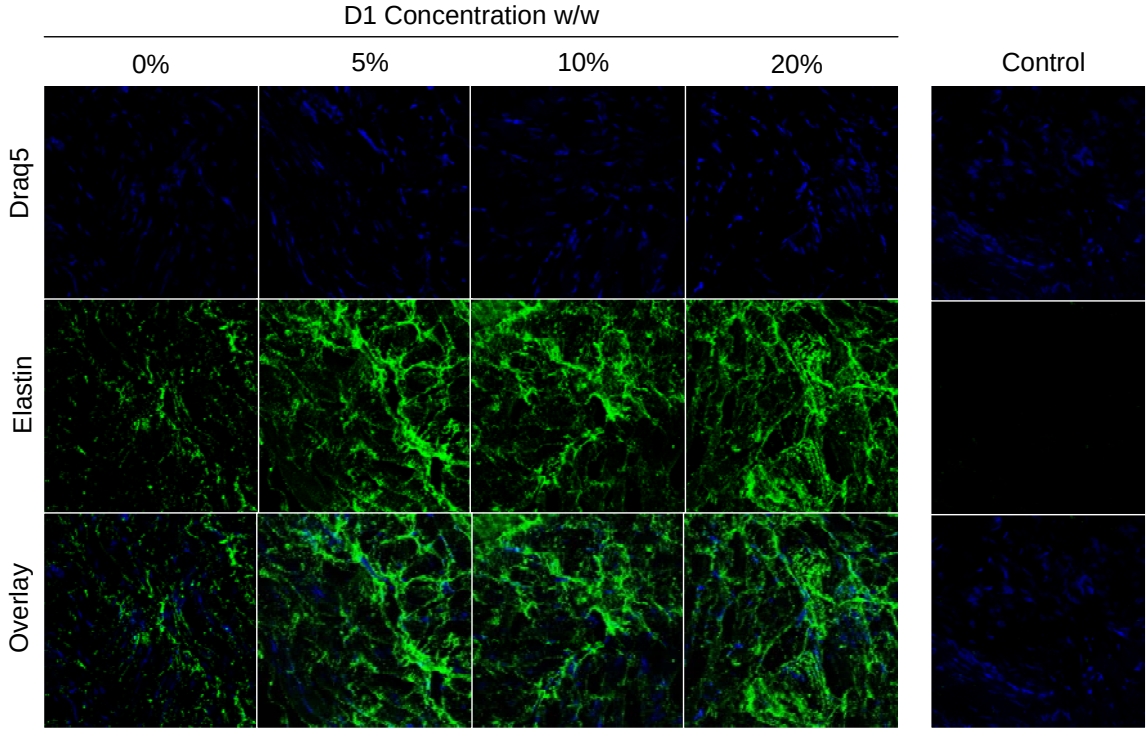

Figure 6.13 SMC elastin production within GM-HA. The elastin content (green) within GM-HA gels containing HA oligomers was higher than the hydrogels without HA oligomers. The nuclei of the embedded SMCs appeared elongated and, therefore, may have attained a natural spread morphology.

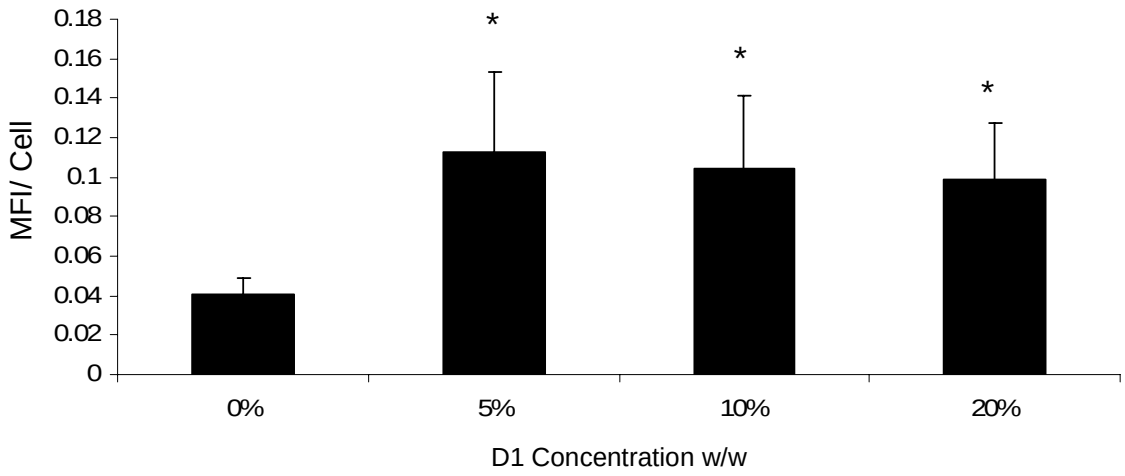

Figure 6.14 Quantification of volumetric fluorescence intensities due to elastin synthesized by SMCs cultured within GM-HA. The fluorescence intensity due to elastin was enhanced by the addition of HA oligomers into the GM-HA gel. The amount of elastin synthesized, however, was independent of the concentration of HA oligomers within the GM-HA gels. [* denotes a p-value < 0.05 in comparison to 0%]

6.4 Discussion

In the past, the relative bioinertness of natural polysaccharides such as HA, has prompted their extensive study as biocompatible biomaterials and bio-interfaces for clinical use [257,341]. As a vital component of tissue ECM, which contributes to sequestration [342] and prolonged release of cytokines and other growth factors, useful to direct cell behavior, HA with its multiple functional groups available for chemical derivatization, is also useful as a drug delivery vehicle/ carrier [267]. HA, particularly its fragmented forms (e.g., oligomers) also play prominent regulatory roles in wound healing in vivo, and thus would be potentially useful as raw materials for fabricating cellular scaffolding biomaterials for enabling tissue regeneration in vitro or in vivo. Many unique properties of HA, including its viscoelasticity and lack of immunogenicity, have made it an appealing cell scaffold platform for tissue engineering applications [343-345].

In order to create HA scaffolds capable of surviving prolonged periods of implantation, it must be converted into a stable, biocompatible, insoluble biomaterial with good handling properties and mechanics appropriate to the site of implantation. Chemical modification has been well recognized as a means to enhance the biostability and mechanical properties of native HA. Two possible methods to modify HA are through derivatization and crosslinking, both of which can be achieved through reactions between the available functional groups of HA (-COOH, -OH, -CH_3COONH). The crosslinking scheme described in the present study involves incorporation of photo-polymerizable methacrylate groups on the HA chain. This strategy presents several advantages over other crosslinking methods. Specifically, photo-polymerization avoids the disadvantages stemming from reactions that occur immediately upon solution mixing (non-uniform gelation) and those that depend on pH, ionic strength, or temperature (non-physiologic, detrimental to cells). With photo-polymerization, the solutions can be completely mixed prior to exposure to the appropriate wavelength of light required to trigger crosslinking, so that rapid, controllable, and minimally invasive crosslinking occurs [346,347]. Furthermore, since photo-polymerization can be performed under physiological conditions, it permits the co-polymerization of biomolecules that would retain their native activity thereafter, and incorporation of cells that would remain viable. *In vivo*, cells are exposed to a 3-D architectural microenvironment wherein the behavior is regulated by their interactions with other cells, ECM, and growth factors. HA hydrogels resemble the physical characteristics of the ECM [122] and can thus be used to encapsulate cells to provide a more *in vivo*-like microenvironment to cultured cells.

Previous studies have suggested that HA hydrogels containing long-chain HA (MW>1 × 10^6 Da) interact poorly with cells, which is detrimental to our intended use of these gels as cellular scaffolds for vascular tissue regeneration [306,324]. This has been attributed variously to their physical properties (small and random pore size, extreme hydrophilicity, smooth surface topography), chemical characteristics (anionicity, need for chemical derivatization/ crosslinking), and biologic composition (HA chain length). Of these parameters, the size of component HA chains appears to most critically influence cell response. Native long-chain HA has been implicated in cell-excluding mechanisms, whereas HA fragments, especially HA oligomers (< 20mers), are recognized to be more bioactive [325]. Investigation of size-specific effects of HA on matrix regeneration outcomes, particularly of hard-to-regenerate elastic fibers by adult SMCs, has been a major focus of research in out lab. We previously showed that elastogenesis and elastin matrix synthesis by SMCs was up-regulated by exogenous supplements of an HA digest containing a broad range of HA oligomers. FACE analysis found this digest (D1) to contain 13.9 ± 3.6% HA 6mers and 8.0 ± 1.6% HA 12mers (chapter 3), while Matrix Assisted Laser Desorption/Ionization-Time of flight (MALDI-TOF) mass spectrometry suggests a 75.0 ± 0.4% HA 4mer content [31]. Previous studies have shown SMCs stimulated with exogenously supplemented D1 produced increased amounts of tropoelastin and crosslinked matrix elastin [31]. This upregulatory phenomenon was maintained when the oligomers were presented to SMCs as a surface-immobilized substrate wherein HA was chemically derivatized, but not crosslinked (chapter 4). In addition, we reported successful synthesis and recruitment of elastin by SMCs seeded

atop bio-activated HA hydrogels containing a surface-mixture of bioinert HMW HA and shorter, more bioactive HA fragments and oligomers [220] generated by UV-induced scission of the HMW HA. However, since the effects of UV light can be difficult to control, and potentially cause random ionizations that can be structurally disruptive, a better approach is to create 'bio-activated' gels containing bio-inert long-chain HA, necessary to maintain mechanical integrity and potentially provide a high degree of biocompatibility, and smaller, more cell-interactive HA oligomers of defined sizes, that would specifically evoke the desired cell responses. Therefore, in this study we sought to explore the concept of incorporating bio-active HA oligomers into photo-crosslinked mixtures of GM-derivatized long-chain HA, to create standalone biomaterials for use as vascular regenerative scaffolds capable of directing encapsulated SMCs to exhuberantly synthesize mimics of native elastic matrix structures.

The synthesis of GM-HA relied on the reaction of glycidyl methacrylate (GM) with HA in the presence of a catalyst, triethylamine. An excess of GM relative to HA was also used because of the limited solubility and hydrolysis of GM in aqueous medium.For the same reason, tetrabutyl ammonium bromide was used to facilitate the transfer of GM into the aqueous phase and thus enhance it's reactivity with HA. It has been suggested that during this derivatization, two reactions occur simultaneously at pH 7.4. The first is a reversible trans-esterification that occurs through the primary hydroxyl group and the second, an irreversible ring-opening conjugation that occurs through the carboxylic acid group toward the highest substituted carbon of the epoxide [348]. However, as the reaction proceeds, there is a decline in the amount of trans-esterification products and a parallel

increase in the concentration of ring-opening products. This suggests that the reaction of HA with GM requires a long reaction time (5-10 days) to promote ring-opening vs. generation of trans-esterification products. Due to the relatively short reaction time (18 h) utilized in this study, we believe the GM-HA produced primarily included the trans-esterification product (Figure 6.1). In addition, the initial derivatization of HA by GM was conducted in a solution that was highly viscous due to the presence of HMW HA, and was therefore less-conducive to reaction between GM and HA. Thus, the amount of crosslinking induced with GM-HA gels (apparent crosslinking density) was lower (1-2%) than that of DVS-HA (10-20%; chapter 5).

FTIR analysis was unable to confirm the primary mechanism of the reaction between HA and GM but it was able to show the presence of the carbon-carbon double bond of the methacrylate group (absorption bands 936 and 1492 cm^{-1}) indicating the successful derivatization of HA with GM. The main difference registered between the FTIR spectra performed before and after UV irradiation was the disappearance of the absorption bands (936 and 1492 cm^{-1}) corresponding to the of the carbon-carbon double bonds in the irradiated polymer. The disappearance of these bands suggests that the crosslinking reaction was complete following UV irradiation of HA for 1.11 min/ mg HA. After UV irradiation, the infrared spectrographs of GM-HA were indistinguishable from HA implying that GM-HA retained the basic structure of HA and hence its function.

In this study, we hoped that GM crosslinking of HA would decelerate and possibly inhibit its natural breakdown. However, we found GM-HA to still be susceptible to degradation. Therefore, we investigated the impact of incorporated oligomer content

on the rate of degradation of GM-HA gels when exposed to a super-physiologic concentration of *testicular hyaluronidase in vitro*. The degradation rates of these gels were influenced by the hydrogel swelling capacity (and thereby enzyme concentration within the gels). Hydrogels containing a higher D1 content exhibited a slightly higher capacity for hydration, and thus, higher swelling ratios, which allowed greater entry of enzymes from the bulk solution into the gel interior. The degradation rates of GM-HA gels were much higher than that observed for DVS-HA gels; likely due to the decreased apparent crosslinking density and higher swelling ratios.

Rheological analysis provided a quantitative evaluation of the viscous and elastic responses of GM-HA. Both the storage moduli (G') and loss moduli (G") were independent of frequency and G' values were always higher than G", which is typical of a "strong hydrogel", whose response to oscillating frequency more closely resembles a solid than a liquid. The G' and G" values of GM-HA gels that did not incorporate any D1 oligomers were similar to that exhibited by other commercially available HA hydrogel products for soft tissue augmentation; the G' and G" of Hylaform (a dermal filler) are 185 Pa and 21 Pa, respectively, at 3.0 Hz [321]. However, vascular regenerative applications demand far more resilient biomaterials then does skin due to the dynamic and strenuous nature of blood vessels. A completely esterified form of HA (HYAFF), which has shown potential as a regenerative vascular grafting material (but yet not shown to be conducive to elastogenesis of SMCs), possesses G' and G" values on the order of 420 kPa and 17 kPa, respectively, at 1 Hz [256,326]. The high strength of this and other successful vascular grafting materials indicates that our GM-HA hydrogels would not by themselves be

suitable for use as a vascular scaffolding materials, but rather must be composited with other existing natural or synthetic graft materials, at least from the standpoint of surviving the forces experienced in a vascular environment.

SEM was used to evaluate the changes in interior morphology of dehydrated hydrogels as a function of D1 concentration. Dehydration itself caused the gels to shrink, drawing the HMW HA strand toward one-another resulting in the appearance of very solid non-porous material in the absence of HA oligomers. The addition of D1 resulted in the emergence of a more porous gel containing a higher quantity and more uniformly-sized pores. The addition of HA oligomers into GM-HA gels decreased their apparent crosslinking density and enhanced their swelling capacity. This, likely, resulted in a looser polymer matrix with greater porosity. Dehydration reduced the degree of porosity of the GM-HA gels from that of the hydrated state, however, it is evident that the increase in porosity of gels with a greater HA oligomer content was maintained. This increase in porosity could provide opportunities for encapsulated cells to adhere, spread and migrate within these gels.

Acetone precipitation, to remove excess GM, a known cytotoxic chemical, from the GM-HA conjugates, was used since dialysis procedures used in other methods tended to be lengthy and laborious [195]. The subcutaneous implant studies show the GM involved in the crosslinking of GM-HA to be exceedingly biocompatible. Very few inflammatory cells surrounded the implant-tissue interface suggesting GM-HA elicited a much lower inflammatory response than DVS-HA. The collagen density in the region around the implants and further afield appeared uniform, indicating the lack of exaggerated fibrous

capsule formation. The primary cell types that respond to subcutaneous implants are typically fibroblasts and inflammatory cells. Fibroblast attempt to isolate the implant by surrounding it with a collagen I-rich fibrous capsule, while inflammatory cells degrade/ digest the implant. The lack of an accumulation of collagen I and inflammatory cell adjacent to the D1 oligomer-free GM-HA gels indicates a very biocompatible material. The addition of D1 oligomers into GM-HA stimulated a moderate increase in inflammatory cell recruitment, though still much lower than DVS-HA with the same content of D1. The only difference between GM-HA and DVS-HA was the amount and type of crosslinker; therefore, we can conclude that the toxicity observed in DVS-HA (chapter 5) was due to the DVS content. In addition, similar to the matrigel control, a greater amount of tissue infiltration was observed within GM-HA, as compared to the DVS-HA. Tissue projections into the defect site were observed for all formulations possibly due to the lower crosslinking density (lowered stiffness) as compared to DVS-HA, which enables cells to readily infiltrate.

The goal of this work was to incorporate HA oligomers into photo-crosslinked GM-HA gels containing predominantly HMW HA, in order to provide greater bioactivity, and specifically enhance elastogenesis of encapsulated SMCs. It is possible that photo-initiator concentration, duration of UV exposure for crosslinking, and HA oligomer concentration may affect the viability of cells encapsulated within the photopolymerized hydrogels [349]. Therefore we used calcein AM to determine whether SMCs survived the encapsulation process, under these conditions to fabricate GM-HA. We found that the SMCs were able to endure UV exposure times that were twice the dosage we deemed

necessary for gel solidification via crosslinking (2.22 vs. 1.11 min/ mg HA) and remained viable in the presence of 0.01% w/v I2959 photo-initiator. After 3 weeks of culture of encapsulated SMCs, elastin was detected within the GM-HA gels; the presence of HA oligomers doubled elastin matrix deposition. SMCs do produce enzymes that degrade HA; therefore, it is possible that in the absence of D1 oligomers encapsulated SMCs were stimulated to produce elastin by the HA fragments generated by cellular degradation of long-chain HA within the gels. However, given the increase in elastin production observed with exogenous and immobilized HA oligomers (see chapters 3, 4), and GM-HA gels incorporating D1, it must be concluded that the presence of HA oligomers is primarily responsible for the increase in elastin production. One way in which HA impacts cellular events is through interaction with cell surface receptors that, in turn, transduce intracellular signals. One such receptor is CD44, a widely distributed cell surface glycoprotein that is expressed as numerous iso-forms that are, however, not active on all cell types [350]. The intracellular domain of CD44 interacts with cytoskeletal proteins and regulates signaling, thereby providing a direct link between extracellular HA and the cell cytoskeleton [351]. HA oligomers are capable of binding to cell surface receptors in a monovalent manner, possibly allowing HA–bound receptors to cluster and/or multiple HA molecules to bind to a single receptor resulting in the stimulation of specific cell signaling cascades [233]. Binding of HA oligomers to CD44 has been shown to activate intracellular signaling pathways that significantly alter cell proliferation and motility [351] and may also promote the production of elastin. HA plays a prominent role in the synthesis and organization of microfibrils (fibrillin), a precursor for elastic fiber

deposition [27-29]. HA has also been implicated to play key roles in the synthesis [352], organization, and stabilization [353] of elastin by SMCs. In addition, HA has been suggested to play an indirect role in elastogenesis through its intimate binding of versican, which in turn interacts with microfibrillar proteins (fibulin-1, 2) and elastin-associated proteins to form higher-order macromolecular structures important for elastic fiber assembly [27-29]. Recent studies provide evidence that some GAGs (e.g., HA) coacervate soluble tropoelastin molecules on their highly anionic surfaces, to facilitate LOX- mediated crosslinking into an insoluble matrix [354], and stabilize elastin fibers against degradation by elastases. Therefore, both HMW HA and HA oligomers may play significant roles in the production of elastin within GM-HA.

6.5 Conclusions

In this study, we successfully developed hydrogels composed of HMW HA and its oligomers, derivatized with UV-crosslinkable glycidyl methacrylate, as potential biomaterials for regeneration of the elastin-rich *tunica media* layer of blood vessels. We showed the mechanical (degradation, viscoelasticity) and physical (crosslinking density, surface structure, swelling) properties of these hydrogels can be modulated by varying the oligomer content within. However, the overall strength of these hydrogels is too low for them to be used as stand-alone biomaterials/cell scaffolding for *in vivo* tissue regeneration, and therefore, must be composited with other more robust biomaterials with a proven record of survival in the rigorous mechanical environment exhibited by blood vessels. Using this crosslinking scheme we were able to encapsulate SMCs directly into

the gel forming a 3-D cellularized scaffold. The embedded cells survived the UV-induced crosslinking process, and extended culture periods (3 weeks). The presence of oligomers within GM-HA enhanced elastin matrix deposition, supporting the notion that HA oligomers are more conducive to SMC elastogenesis than other forms of HA. Upon subcutaneous implantation, GM-HA gels appeared very biocompatible, eliciting a very mild inflammatory cell responses and minimal fibrous capsule formation. Overall, we have demonstrated that HA oligomers are a useful tool to incorporate within crosslinked HA gels and quite possibly other synthetic or natural biomaterials for the purpose of upregulating elastogenesis by vascular SMCs encapsulated in a 3-D space. Though these stand-alone materials do not fulfill the requirements for vascular implantation from a mechanical standpoint, they may be certainly used for in vitro vascular and other tissue regeneration using tissue engineering principles, and quite possibly composited with other more mechanically robust biomaterials to provide greater bioactivity and elastogenic cues for vascular matrix regeneration *in situ* and disease blood vessels *in vivo*.

CHAPTER 7

CONCLUSIONS, STUDY LIMITATIONS, AND FUTURE DIRECTIONS

7.1 Conclusions

Over the past 6 years, our lab has reported extensively on the use of HA as a biomolecular agent for the regenerative repair of vascular tissue. HA has been shown to beneficially impact two key aspects of vascular regeneration, namely functional endothelialization and elastin matrix repair/ regeneration, both of which are crucial to restore vascular homeostasis following trauma or disease. Our previous efforts showed the elastogenic effects of exogenous HA fragments on SMCs to be depend on HA size [31,32]. Only supplements of broad HA oligomer mixtures (D1), containing a lower concentration of 6mers and 12mers, up-regulated elastin synthesis by adult SMCs, and enhanced the formation of an elastin fiber-rich matrix. This project was initiated to investigate the ability of HA to promote surface endothelialization of intravascular implants/ grafts, and thereafter apply this, and previously acquired information on the HA-induced elastogenesis of vascular SMCs, to the development of HA biomaterials, in the form of surface coatings and hydrogels, for vascular tissue engineering. To achieve this goal, the project was divided into four modules. Module 1, investigated the size-specific effects of exogenous HA on EC behavior, and used this information to identify the HA fragment sizes or combination thereof , which would be needed to be presented at biomaterial surfaces to elicit complete and functional endothelialization when implanted intra-vascular. In module 2, we immobilized different-sized HA fragments onto culture

surfaces to determine if the immobilization process, which involved derivatization of HA without incorporation of a crosslinker, would altered the size-specific responses of ECs and SMCs to HA, as identified in module 1. Such a culture model also simulated the use of HA as a scaffold coating material. Modules 3 and 4 involved the development of 3-D HA scaffolds and their ability to promote endothelialization and SMC elastogenesis, respectively, and also permitted assessment of the effects of incorporated crosslinks and HA oligomers on the physical, chemical and biologic properties of the formulated hydrogels.

The initial objective of module 1 was to generate enzymatic digests of HMW HA containing low (D1) and high (D2) concentrations of HA oligomers, and to further test EC responses to these digests, HMW HA, and larger commercially available pure oligomer preparations. In this manner, we demonstrated that both HA oligomers (D2) and HMW HA interact with ECs in a positive manner; D2 enhanced EC proliferation, and angiogenesis, while HMW HA significantly alternated platelet attachment to ECs and their futher aggregation and activation. However, D2 also stimulated modest inflammatory cytokine production and CAM expression, while HMW HA, in general, limited this effect. From this data we concluded that HA oligomers are capable of stimulating an angiogenic response by ECs but may also elicit mild inflammatory reaction in vivo or cell activation in vivo, while HMW HA can act as a protective barrier to exclude potentially harmful blood components from interacting with the ECs. These studies thus stressed on the importance of including both forms of HA within HA biomaterials so as to achieve optimal biocompatibility and biologic responses.

In module 2, we investigated the utility of HA fragments/ oligomers as bioactive surface coatings for biomaterials that would enhance their recruitment, sustenance, and functional guidance of a confluent layer of ECs. To do this, we immobilized the fragments/ oligomers onto a culture substrate via a strategy that involved chemical derivatization of HA, but not crosslinking. We then investigated if these HA fragements/ oligomers stimulated EC function and SMC elastogenesis as did their exogenously-supplemented counterparts. We found that we were able to successfully chemically bind a wide size range of HA fragment onto glass slides. When ECs were seeded on these surfaces, the cells only attached to those surfaces immobilized with a highly concentrated digest of HA oligomers (D2) containing predominantly HA 6mers and 12mers; the larger-sized HA fragments detered cell adherence and/or spreading. The D2-tethered surfaces also stimulated EC proliferation and slightly enhanced CAM expression similar to what we observed with exogenous D2. SMCs cultured on substrates of a differently composed HA oligomers digest (D1), which contained a lower concentration of HA 6mers and 12mers, enhanced cellular tropoelastin synthesis and deposition of crosslinked matrix elastin similar to that induced by exogenous D1 mixtures [31]; however, surface-tethered D1 was more effective in enhancing in desmosine crosslinking and elastic fiber organization. These results attest to the utility of HA oligomers as coatings on the surface or within the interior lattices of various vascular regenerative scaffolding materials, natural or synthetic, for the purpose of modulating behavior and matrix production by cell seeded thereupon. However, the enhanced CAM expression elicited by both exogenous and immobilized HA oligomers is of concern. Therefore, the next step in this project was

to incorporate these bioactive HA oligomers into scaffolds composed predominantly of relatively bioinert HMW HA, to temper EC CAM expression, and create a biomaterial with good handling properties. However, in order to ensure the benefits of HA oligomers were not lost and that the physical and mechanical properties of the composite gel scaffolds were not compromised, we deemed it necessary to determine the optimal content of bioactive HA oligomers within these gel scaffolds. Moreover, creation of such a gel would necessitate the use of chemical crosslinking which could by themselves alter cell response to HA/ oligomers or compromise biocompatibility. We thus sought to assess the impact of crosslinker content on gel biocompatibility and physical properties.

In module 3, we successfully developed hydrogels composed of DVS-crosslinked HMW HA and HA oligomers, as potential biomaterials for the regeneration of the vascular endothelium. We showed the mechanical (degradation, viscoelasticity) and physical (crosslinking density, surface structure, swelling) properties of these hydrogels can be adjusted by varying the crosslinker and oligomer densities within them. However, the overall strength of these hydrogels was too low for their use as standalone materials for vascular applications. Therefore, our study recommends that these DVS-crosslinked gels, composed of relatively bioinert HMW and bioactive HA oligomers, be composited with other existing and mechanically appropriately vascular graft/ implant materials to modulate vascular cell behavior to achieve a faithful regenerative response. The presence of HA oligomers within DVS-HA seemed to enhance EC attachment and proliferation, supporting our hypothesis that crosslinked HA oligomers would retain the biologic signaling characteristics of uncrosslinked HA oligomers, and they would be more

conducive to EC growth than longer sized fragments of HA. However, the high concentration of DVS, required to impart good handling properties to these gels, appeared to stimulate mild inflammation in vivo and EC activation in vitro. Therefore, another crosslinker may be more appropriate to use, which could result in better mechanics and improved biocompatibility. To investigate this, we altered the mechanism of crosslinking within the hydrogels, focusing on the development of UV-photocrosslinked gels based on glycidyl methacrylate-derivatized HMW HA and HA oligomers. Since this crosslinking mechanism was amenable to encapsulating and sustaining cells, we investigated the impact of incorporated GM-derivatized HA oligomer mixtures on elastogenesis by encapsulated SMCs.

Thus, in module 4, we continued with our idea of combining HMW HA and its oligomers into biomaterials but changed the crosslinking scheme (UV crosslinkable glycidyl methacrylate) and the cell type investigated. As with DVS-HA, the mechanical (degradation, viscoelasticity) and physical (crosslinking density, surface structure, swelling) properties of GM-HA could also be modulated by varying oligomer densities within them. However, the overall strength of GM-HA was even lower than DVS-HA, suggesting that the formulation also be necessarily composited with existing scaffolding biomaterials (synthetic or natural) that would be mechanically compliant with the vascular tissue material for vascular applications. The role of oligomer-containing GM-HA within these composite scaffolds would be to recruit and sustain SMCs within, and elastogenically upregulate these cell types that are poorly capable of synthesizing elastin, to regenerate a functional elastic tissue as the scaffold degrades.

Using this photocrosslinking scheme we were able to encapsulate SMCs directly into the gel to form a 3D cellularized scaffold. The embedded cells survived extended periods of UV exposure necessary to initiate crosslinking of GM-HA. The presence of oligomers within GM-HA enhanced elastin matrix deposition by SMCs, supporting our hypothesis that GM-HA oligomers would retain the pro-elastogenic properties of uncrosslinked HA oligomers. GM-HA gels were more biocompatible/ less inflammatory than DVS-HA when implanted subcutaneously in rats. Overall, we showed that HA oligomers are useful to incorporate within existing, mechanically appropriate vascular biomaterial scaffold, either as surface-immobilized coatings or as hydrogels composited with the scaffolds, to promote endothelialization and elastic tissue regeneration. Our studies also indicate that incorporation of HMW HA is also necessary to temper adverse cell responses to HA oligomers (e.g., CAM expression) and provide mechanical stability/ ease of handling to the gels. Therefore, future studies will focus on the development of other more mechanically appropriate materials with known cell adhesive or elastogenic properties that may benefit from the incorporation of HA oligomers.

7.2 Study Limitations

Despite the perceived potential advantages of developing vascular biomaterials with HA oligomers for the promotion of endothelialization and SMCs elastogenesis, limitations pertaining to this study must be addressed prior to their application to tissue engineering systems. These limitations are outlined below.

1. All hydrogels were produced in cylindrical molds composed of polystyrene or plexiglass, which resulted in surface tension-induced liquid migration along the mold-hydrogel interface prior to crosslinking. This produced hydrogels that possessed concave surfaces. Somewhat crude Caliper measurements were use to determine the dimensions of the hydrogels and did not take this concavity into account. Therefore, the surface area and protein deposition calculations may not be exact. It is to be noted however, that concavity was not extreme and was only percieved when attempting to image cells on the hydrogel surface. Therefore, we believe our methods were adequate for the purposes of this study.
2. The HA oligomers used in this study were obtained by enzymatic digestion of HMW HA, using optimized protocols developed in our lab. These oligomeric mixtures contained predominantly 6mers and 12mers, with other oligomers forming the balance. However, any changes in digestion conditions (time, concentrations, temperature, source of HMW HA, etc) can alter the composition of the HA oligomer mixtures, which might significantly alter the cellular response to these mixtures. Thus, high level of quality control in the preparation of these oligomer mixtures is warranted.
3. We used a protein assay to determine the amount of matrigel deposited onto DVS-HA. The accuracy of measurement using the Dc Bio-Rad protein assay is greatest for standards and sample concentrations within the range of 0.2-1.5 μg/ ml. In our studies, the protein concentrations often were lower than 0.2 μg/ ml. This brings the accuracy of our results into question. However, the calibration

curves generated with standards within our concentration range of interest, continued to be linear, as with standards within the recommended range. We also measured a significant decrease of protein within the applied bulk protein solution, following incubation with the gel surfaces. Therefore, the results strongly suggest that this assay is useful for measuring protein concentration outside the range recommended by the manufacturer.

4. For study of interior pore-structures, GM-HA hydrogels were dehydrated prior to imaging by SEM. Therefore, the images generated do not necessarily represent the interior structure of the hydrated hydrogels. Nevertheless, since our interest lies not in elucidating the actual interior morphology of GM-HA, but rather, determining the effects of HA oligomer incorporation on the morphology, the inferences we have drawn by a comparison of the images obtained for each of the gel formulation are likely reliable. However, to investigate the true interior topography of the gels in a hydrated state, in the future, using freezing drying or osmium tetroxide methods is recommended.
5. Neonatal vascular SMCs were embedded within the GM-HA gels as opposed to adult SMCs used in the exogenous and surface tethered studies. Neonatal cells inherently produce a much more exuberant amount of matrix (including elastin) than adult cells. We found that elastin production of these neonatal cells is upregulated when encapsulated within GM-HA containing HA oligomers. However, this may differ from adult SMCs and must be investigated in the future.
6. Upon explanting the hydrogels from subcutaneous implantation, only a small

amount of the tissue surrounding the implant was removed with the implant. Therefore, only a minimal view of the tissue reaction to the implant was observed. In the future a greater amount of the tissue surrounding the implant must be explanted in order to compare the conditions near and distant from the implant and fully diagnose the tissue reaction at the biomatial interface.

7. Most studies use a constant gap distance between the parallel plates of the rheometer when performing a frequency sweep. However, due to the malleability of our gels we decided to utilize a constant normal force. During the application of the normal force, the rheometer constantly recalculated the plate gap involved in the calculation of G' and G". Therefore, we believe the numbers we obtained are accurate.
8. The sterilization process of GM-HA prior to SMC encapsulation required syringe filtration of an extremely viscous solution using a very high back pressure. HA, though solubilized, may have been lost during this process reducing the amount of HA within each gel and hence may have limited its toxicity.
9. Many rheology analysis techniques exists, however, we had to limit our studies to simple frequency sweeps using a very small deformation angle (1 mrad) due to the limited contact between the HA hydrogels and the parallel plates of the rheometer. These hydrogels were composed of a very hydrophilic molecule and high water content and, even with the use of sandpaper on the plate face, contorting the gels was very difficult due to slippage. However, this technique has been published as a valid analytical tool for HA hydrogels and therefore, we

believe our results are both meaningful and useful in the design of HA materials.

7.3 Future Directions

Despite the numerous positive outcomes listed above, the long-term realization of the project objectives is contingent on elucidating several unknowns, which have not yet been explored in this project and will be addressed by others in our group. Thus, future studies can investigate:

Endothelial Cell Studies

1. Response of ECs to HA oligomers incorporated within a known cell adhesive base material with appropriate mechanical properties.
2. Response of ECs to HA oligomers immobilized on a known vascular grafting materials (i.e. ePTFE, Dacron).
3. Effects of dynamic-conditioning (i.e. shear force) of ECs seeded on HA oligomer-incorporating scaffolds.

Smooth Muscle Cell Studies

4. Elastogenesis of *adult* vascular SMCs encapsulated within GM-HA incorporating HA oligomers (D1).
5. Overall production of elastin precursors, and the yield, stability, and organization of elastin matrix generated by SMCs encapsulated within GM-HA, incorporating HA oligomers.

6. Effects of dynamic-conditioning (i.e. cyclic distension) of SMC-ecapsulated GM-HA scaffolds incorporating HA oligomers on elastin gene expression, precursor synthesis, matrix deposition and maturation, and fiber organization.
7. Identification of cell signaling pathways of SMC elastogenesis modulated by HA oligomers.
8. Generation of a functional elastic tissue in tissue culture, that can meet the mechanical and biologic requirements for implantation *in vivo*.

Other Studies

9. Generation of a fully functional blood vessel *in vitro* by encapsulating SMCs within GM-HA loaded with HA oligomers, growth factors and adhesive molecules and seeding ECs on the surface.
10. Utility of HA oligomer-containing GM-HA gels in other relevant areas of tissue engineering such as wound healing, cosmetic/ dermal regeneration.
11. Development of a biodegradable oligomer/ growth factor-loaded scaffold capable of delivering properly sized HA oligomers and specific growth factors to an elastin deficient tissue (i.e. damaged skin, aneurismal blood vessel) at an optimized rate.
12. The mechanical and biological properties of HA oligomer-embedded GM-HA with an added synthetic polymer to enhance mechanical strength and cellular interaction.
13. Mesenchymal stem cell differentiation/ *in vivo* delivery within GM-HA gels

containing HA oligomers for soft tissue (i.e. dermal, etc.) regeneration applications.

14. Generation of photocrosslinkable HA microspheres for the injectable local delivery of drugs/ growth factors/ cells.

APPENDIX

1. Molecular Content of HA-Immobilized Surfaces

In Chapter 4, we immobilized HA onto culture surfaces in order to determine their capacity for regenerating the vascular endothelium and vascular SMC elastogenesis. Upon quantifying the amount of HA on all surfaces we found that the content of HA 1500 was much higher than HA 200, HA 20 and D1. However, converting the HA content to a molecule basis revealed many more molecules of low MW HA (HA 20, D1) attached to the surface than higher MW HA (HA 1500, HA 200). We believe this is due to steric hindrance of the larger molecules preventing further HA deposition near the area of their attachment. The immunofluorescence images showed higher MW HA to deposit on the APTMS functionalized glass surfaces in a less uniform manner and high resolution XPS indicated less efficient binding of high MW HA to the amines of APTMS. This data confirms the isolated and less efficient binding of higher MW HA to the glass surfaces. The molecular weight of D1 was approximated based on the FACE data in chapter 3 and found to contain an average MW of 6709 g/ mol.

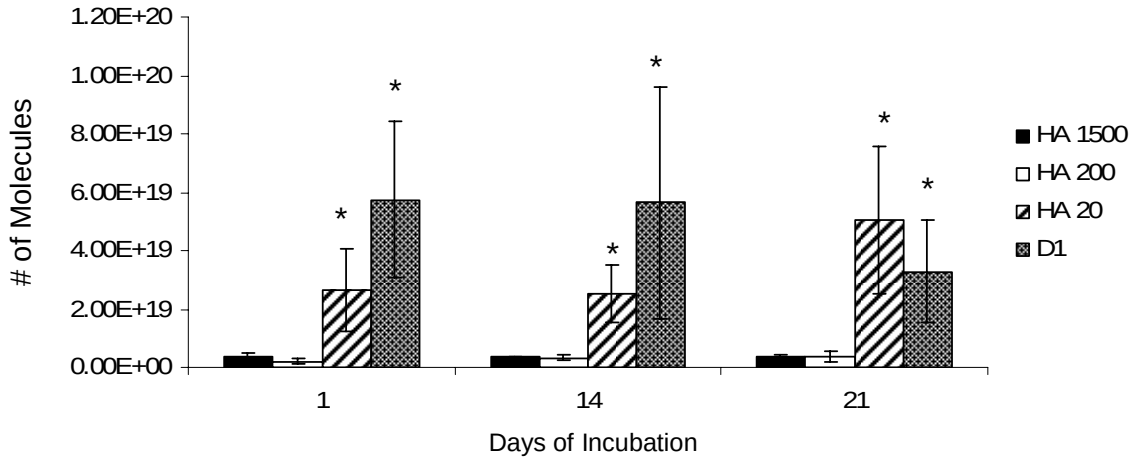

Figure App 1. FACE analysis of HA surfaces on a molecule basis. More molecules of HA 1500 and HA 200 were present on the surface than the lower molecular weights of HA. The amount of HA 1500 and HA 200 was similar, while the content of HA 20 and D1 was approximately the same. In all cases, the amount of HA was stable on the surfaces throughout the 21 days. [* denotes a p-value < 0.05 in comparison to day 1]

REFERENCES

1. www.wikipedia.org.
2. Mitchell SL, Niklason LE. Requirements for growing tissue-engineered vascular grafts. Cardiovasc Pathol 2003;12(2):59-64.
3. Debelle L, Alix AJ. The structures of elastins and their function. Biochimie 1999;81(10):981-94.
4. Hedin U, Roy J, Tran PK, Lundmark K, Rahman A. Control of smooth muscle cell proliferation--the role of the basement membrane. Thromb Haemost 1999;82 Suppl 1:23-6.
5. Raines EW. The extracellular matrix can regulate vascular cell migration, proliferation, and survival: relationships to vascular disease. Int J Exp Pathol 2000;81(3):173-82.
6. Spofford CM, Chilian WM. The elastin-laminin receptor functions as a mechanotransducer in vascular smooth muscle. Am J Physiol Heart Circ Physiol 2001;280(3):H1354-60.
7. Spofford CM, Chilian WM. Mechanotransduction via the elastin-laminin receptor (ELR) in resistance arteries. J Biomech 2003;36(5):645-52.
8. Karnik SK, Brooke BS, Bayes-Genis A, Sorensen L, Wythe JD, Schwartz RS, Keating MT, Li DY. A critical role for elastin signaling in vascular morphogenesis and disease. Development 2003;130(2):411-23.

9. Ahanchi SS, Tsihlis ND, Kibbe MR. The role of nitric oxide in the pathophysiology of intimal hyperplasia. J Vasc Surg 2007;45 Suppl A:A64-73.

10. Pearce WH, Shively VP. Abdominal aortic aneurysm as a complex multifactorial disease: interactions of polymorphisms of inflammatory genes, features of autoimmunity, and current status of MMPs. Ann N Y Acad Sci 2006;1085:117-32.

11. Association AH. Heart Disease and Stroke Statistics - 2006 Update: American Heart Association; 2006.

12. Miller D. The practice of coronary artery bypass surgery. New York: Plenum Medical; 1977.

13. Suma H. Arterial grafts in coronary bypass surgery. Ann Thorac Cardiovasc Surg 1999;5(3):141-5.

14. Doucet S, Schalij MJ, Vrolix MC, Hilton D, Chenu P, de Bruyne B, Udayachalerm W, Seth A, Bilodeau L, Reiber JH and others. Stent placement to prevent restenosis after angioplasty in small coronary arteries. Circulation 2001;104(17):2029-33.

15. Foley DP, Melkert R, Serruys PW. Influence of coronary vessel size on renarrowing process and late angiographic outcome after successful balloon angioplasty. Circulation 1994;90(3):1239-51.

16. Kastrati A, Schuhlen H, Schomig A. Stenting for small coronary vessels: a contestable winner. J Am Coll Cardiol 2001;38(6):1604-7.

17. Tan SW, Johns MR, Greenfield PF. Hyaluronic acid--a versatile biopolymer. Aust J Biotechnol 1990;4(1):38-43.

18. Chen WY, Abatangelo G. Functions of hyaluronan in wound repair. Wound Repair Regen 1999;7(2):79-89.

19. Morra M. Engineering of biomaterials surfaces by hyaluronan. Biomacromolecules 2005;6(3):1205-23.

20. Pavesio A, Abatangelo G, Borrione A, Brocchetta D, Hollander AP, Kon E, Torasso F, Zanasi S, Marcacci M. Hyaluronan-based scaffolds (Hyalograft C) in the treatment of knee cartilage defects: preliminary clinical findings. Novartis Found Symp 2003;249:203-17; discussion 229-33, 234-8, 239-41.

21. Price RD, Myers S, Leigh IM, Navsaria HA. The role of hyaluronic acid in wound healing: assessment of clinical evidence. Am J Clin Dermatol 2005;6(6):393-402.

22. Murata K, Yokoyama Y. High hyaluronic acid and low dermatan sulfate contents in human pulmonary arteries compared to in the aorta. Blood Vessels 1988;25(1):1-11.

23. West DC, Kumar S. The effect of hyaluronate and its oligosaccharides on endothelial cell proliferation and monolayer integrity. Exp Cell Res 1989;183(1):179-96.

24. West DC C, H. Is hyaluronan degradation an angiogenic/metastatic switch? In: Kennedy JF PGO, Williams P. A., Hascall V., editor. Hyaluronan. Cambridge, U.K.: Woodhead Publishing Ltd; 2002. p 165- 172.

25. Feinberg RN, Beebe DC. Hyaluronate in vasculogenesis. Science 1983;220(4602):1177-9.

26. Murphy JF, Lennon F, Steele C, Kelleher D, Fitzgerald D, Long AC. Engagement of CD44 modulates cyclooxygenase induction, VEGF generation, and proliferation in human vascular endothelial cells. Faseb J 2005;19(3):446-8.

27. Isogai Z, Aspberg A, Keene DR, Ono RN, Reinhardt DP, Sakai LY. Versican interacts with fibrillin-1 and links extracellular microfibrils to other connective tissue networks. J Biol Chem 2002;277(6):4565-72.

28. Olin AI, Morgelin M, Sasaki T, Timpl R, Heinegard D, Aspberg A. The proteoglycans aggrecan and Versican form networks with fibulin-2 through their lectin domain binding. J Biol Chem 2001;276(2):1253-61.

29. Zimmermann DR, Dours-Zimmermann MT, Schubert M, Bruckner-Tuderman L. Versican is expressed in the proliferating zone in the epidermis and in association with the elastic network of the dermis. J Cell Biol 1994;124(5):817-25.

30. Laurent S, Boutouyrie P, Lacolley P. Structural and genetic bases of arterial stiffness. Hypertension 2005;45(6):1050-5.

31. Joddar B, Ramamurthi A. Elastogenic effects of exogenous hyaluronan oligosaccharides on vascular smooth muscle cells. Biomaterials 2006;27(33):5698-707.

32. Joddar B, Ramamurthi A. Fragment size- and dose-specific effects of hyaluronan on matrix synthesis by vascular smooth muscle cells. Biomaterials 2006;27(15):2994-3004.

33. Carson DD. Extracellular matrix: forum introduction. Reprod Biol Endocrinol 2004;2:1.

34. Chang J. Textbook of Angiology. New York: Springer; 2000.

35. Junquiera L, Carniero J. Basic Histology Text & Atlas. New York: McGraw Hill; 2005.

36. www.merck.com/mmhe/sec03/ch032/ch032a.html.

37. Gulati R, Lerman A, Simari RD. Therapeutic uses of autologous endothelial cells for vascular disease. Clin Sci (Lond) 2005;109(1):27-37.

38. Brandes RP, Fleming I, Busse R. Endothelial aging. Cardiovasc Res 2005;66(2):286-94.

39. Landmesser U, Drexler H. The clinical significance of endothelial dysfunction. Curr Opin Cardiol 2005;20(6):547-51.

40. Shimokawa H. Primary endothelial dysfunction: atherosclerosis. J Mol Cell Cardiol 1999;31(1):23-37.

41. Ross R. The pathogenesis of atherosclerosis--an update. N Engl J Med 1986;314(8):488-500.

42. Raines EW, Ross R. Smooth muscle cells and the pathogenesis of the lesions of atherosclerosis. Br Heart J 1993;69(1 Suppl):S30-7.

43. Lusis AJ. Atherosclerosis. Nature 2000;407(6801):233-41.

44. http://www.caseychristy.com/HealthWellnessWebsite/cardiovascular.

45. http://healthgate.partners.org/images/si55551781_ma.jpg.

46. Serruys PW, Unger F, Sousa JE, Jatene A, Bonnier HJ, Schonberger JP, Buller N, Bonser R, van den Brand MJ, van Herwerden LA and others. Comparison of coronary-artery bypass surgery and stenting for the treatment of multivessel disease. N Engl J Med 2001;344(15):1117-24.

47. Dietl CA, Benoit CH. Radial artery graft for coronary revascularization: technical considerations. Ann Thorac Surg 1995;60(1):102-9; discussion 109-10.

48. Loscalzo J CM, Dzau VJ. Vascular Medicine: a textbook of vascular biology and diseases. Boston: Little, Brown and Company; 1992.

49. http://www.enh.org/uploadedimages/ir_balloon.jpg.

50. http://hvlib.integris-health.com/library/healthguide/en-us/images/media/medical/hw/nr551659.jpg.

51. http://hvlib.integris-health.com/library/healthguide/en-us/support/topic.asp?hwid=zm2309.

52. http://www.edaya.com/aboutus/qualific/prodexp/lacath/lacath640.jpg.

53. Moore W, Ahn S. Endovascular Surgery. Philidelphia: Saunders; 1989.

54. Karsch K, Haase K. Coronary laser angioplasty : an update. New York: Springer-Verglag; 1991.

55. Gusic RJ, Myung R, Petko M, Gaynor JW, Gooch KJ. Shear stress and pressure modulate saphenous vein remodeling ex vivo. J Biomech 2005;38(9):1760-9.

56. Cooper GJ, Underwood MJ, Deverall PB. Arterial and venous conduits for coronary artery bypass. A current review. Eur J Cardiothorac Surg 1996;10(2):129-40.

57. Motwani JG, Topol EJ. Aortocoronary saphenous vein graft disease: pathogenesis, predisposition, and prevention. Circulation 1998;97(9):916-31.

58. Kannan RY, Salacinski HJ, Butler PE, Hamilton G, Seifalian AM. Current status of prosthetic bypass grafts: a review. J Biomed Mater Res B Appl Biomater 2005;74(1):570-81.

59. Nunn DB, Carter MM, Donohue MT, Hudgins PC. Postoperative dilation of knitted Dacron aortic bifurcation graft. J Vasc Surg 1990;12(3):291-7.

60. http://www.enh.org/healthandwellness/clinicalservices/ir/procedures/default.aspx?id=1773.

61. Sallam M, Spanos V, Briguori C, Di Mario C, Tzifos V, Dharmadhikari A, Albiero R, Colombo A. Predictors of re-occlusion after successful recanalization of chronic total occlusion. J Invasive Cardiol 2001;13(7):511-5.

62. Stephen M, Loewenthal J, Little JM, May J, Sheil AG. Autogenous veins and velour dacron in femoropopliteal arterial bypass. Surgery 1977;81(3):314-8.

63. O'Donnell TF, Jr., Mackey W, McCullough JL, Jr., Maxwell SL, Jr., Farber SP, Deterling RA, Callow AD. Correlation of operative findings with angiographic and noninvasive hemodynamic factors associated with failure of polytetrafluoroethylene grafts. J Vasc Surg 1984;1(1):136-48.

64. Stitzel J, Liu J, Lee SJ, Komura M, Berry J, Soker S, Lim G, Van Dyke M, Czerw R, Yoo JJ and others. Controlled fabrication of a biological vascular substitute. Biomaterials 2006;27(7):1088-94.

65. Rodriguez AE, Palacios IF, Fernandez MA, Larribau M, Giraudo M, Ambrose JA. Time course and mechanism of early luminal diameter loss after percutaneous transluminal coronary angioplasty. Am J Cardiol 1995;76(16):1131-4.

66. Jain M, He Q, Lee WS, Kashiki S, Foster LC, Tsai JC, Lee ME, Haber E. Role of CD44 in the reaction of vascular smooth muscle cells to arterial wall injury. J Clin Invest 1996;98(3):877.

67. Kornowski R, Hong MK, Tio FO, Bramwell O, Wu H, Leon MB. In-stent restenosis: contributions of inflammatory responses and arterial injury to neointimal hyperplasia. J Am Coll Cardiol 1998;31(1):224-30.

68. Komatsu R, Ueda M, Naruko T, Kojima A, Becker AE. Neointimal tissue response at sites of coronary stenting in humans: macroscopic, histological, and immunohistochemical analyses. Circulation 1998;98(3):224-33.

69. Hoffmann R, Mintz GS, Dussaillant GR, Popma JJ, Pichard AD, Satler LF, Kent KM, Griffin J, Leon MB. Patterns and mechanisms of in-stent restenosis. A serial intravascular ultrasound study. Circulation 1996;94(6):1247-54.

70. Farb A, Burke AP, Kolodgie FD, Virmani R. Pathological mechanisms of fatal late coronary stent thrombosis in humans. Circulation 2003;108(14):1701-6.

71. Farb A, Weber DK, Kolodgie FD, Burke AP, Virmani R. Morphological predictors of restenosis after coronary stenting in humans. Circulation 2002;105(25):2974-80.

72. L'Heureux N, Paquet S, Labbe R, Germain L, Auger FA. A completely biological tissue-engineered human blood vessel. Faseb J 1998;12(1):47-56.

73. Tiwari A, Salacinski H, Seifalian AM, Hamilton G. New prostheses for use in bypass grafts with special emphasis on polyurethanes. Cardiovasc Surg 2002;10(3):191-7.

74. Friedman SG, Lazzaro RS, Spier LN, Moccio C, Tortolani AJ. A prospective randomized comparison of Dacron and polytetrafluoroethylene aortic bifurcation grafts. Surgery 1995;117(1):7-10.

75. Devine C, McCollum C. Heparin-bonded Dacron or polytetrafluorethylene for femoropopliteal bypass: five-year results of a prospective randomized multicenter clinical trial. J Vasc Surg 2004;40(5):924-31.

76. Karrer L, Duwe J, Zisch AH, Khabiri E, Cikirikcioglu M, Napoli A, Goessl A, Schaffner T, Hess OM, Carrel T and others. PPS-PEG surface coating to reduce thrombogenicity of small diameter ePTFE vascular grafts. Int J Artif Organs 2005;28(10):993-1002.

77. Prager M, Polterauer P, Bohmig HJ, Wagner O, Fugl A, Kretschmer G, Plohner M, Nanobashvili J, Huk I. Collagen versus gelatin-coated Dacron versus stretch polytetrafluoroethylene in abdominal aortic bifurcation graft surgery: results of a seven-year prospective, randomized multicenter trial. Surgery 2001;130(3):408-14.

78. Elezi S, Kastrati A, Neumann FJ, Hadamitzky M, Dirschinger J, Schomig A. Vessel size and long-term outcome after coronary stent placement. Circulation 1998;98(18):1875-80.

79. Dobesh PP, Stacy ZA, Ansara AJ, Enders JM. Drug-eluting stents: a mechanical and pharmacologic approach to coronary artery disease. Pharmacotherapy 2004;24(11):1554-77.

80. Sakiyama SE, Schense JC, Hubbell JA. Incorporation of heparin-binding peptides into fibrin gels enhances neurite extension: an example of designer matrices in tissue engineering. Faseb J 1999;13(15):2214-24.

81. Kimura Y, Okuda H. Inhibitory effects of soluble elastin on intraplatelet free calcium concentration. Thromb Res 1988;52(1):61-4.

82. Stock UA, Wiederschain D, Kilroy SM, Shum-Tim D, Khalil PN, Vacanti JP, Mayer JE, Jr., Moses MA. Dynamics of extracellular matrix production and turnover in tissue engineered cardiovascular structures. J Cell Biochem 2001;81(2):220-8.

83. Rabkin E, Hoerstrup SP, Aikawa M, Mayer JE, Jr., Schoen FJ. Evolution of cell phenotype and extracellular matrix in tissue-engineered heart valves during in-vitro maturation and in-vivo remodeling. J Heart Valve Dis 2002;11(3):308-14; discussion 314.

84. Shin'oka T, Imai Y, Ikada Y. Transplantation of a tissue-engineered pulmonary artery. N Engl J Med 2001;344(7):532-3.

85. Wake MC, Gupta PK, Mikos AG. Fabrication of pliable biodegradable polymer foams to engineer soft tissues. Cell Transplant 1996;5(4):465-73.

86. Fittkau MH, Zilla P, Bezuidenhout D, Lutolf MP, Human P, Hubbell JA, Davies N. The selective modulation of endothelial cell mobility on RGD peptide containing surfaces by YIGSR peptides. Biomaterials 2005;26(2):167-74.

87. Matsumura G, Hibino N, Ikada Y, Kurosawa H, Shin'oka T. Successful application of tissue engineered vascular autografts: clinical experience. Biomaterials 2003;24(13):2303-8.

88. Hoerstrup SP, Sodian R, Daebritz S, Wang J, Bacha EA, Martin DP, Moran AM, Guleserian KJ, Sperling JS, Kaushal S and others. Functional living trileaflet heart valves grown in vitro. Circulation 2000;102(19 Suppl 3):III44-9.

89. Walles T, Herden T, Haverich A, Mertsching H. Influence of scaffold thickness and scaffold composition on bioartificial graft survival. Biomaterials 2003;24(7):1233-9.

90. http://www.echoincontext.com/doppler01/doppler01_05.asp.

91. Gilbert TW, Sellaro TL, Badylak SF. Decellularization of tissues and organs. Biomaterials 2006;27(19):3675-83.

92. Courtman DW, Pereira CA, Kashef V, McComb D, Lee JM, Wilson GJ. Development of a pericardial acellular matrix biomaterial: biochemical and mechanical effects of cell extraction. J Biomed Mater Res 1994;28(6):655-66.

93. Dahl SL, Koh J, Prabhakar V, LE N. Decellularized native and engineered arterial scaffolds for transplantation. Cell Transplantation 2003;12:659 - 666.

94. Teebken OE, Bader A, Steinhoff G, Haverich A. Tissue engineering of vascular grafts: human cell seeding of decellularised porcine matrix. Eur J Vasc Endovasc Surg 2000;19(4):381-6.

95. Giglia JS, Ollerenshaw JD, Dawson PE, Black KS, Abbott WM. Cryopreservation prevents arterial allograft dilation. Ann Vasc Surg 2002;16(6):762-7.

96. Schaner PJ, Martin ND, Tulenko TN, Shapiro IM, Tarola NA, Leichter RF, Carabasi RA, Dimuzio PJ. Decellularized vein as a potential scaffold for vascular tissue engineering. J Vasc Surg 2004;40(1):146-53.

97. Badylak SF, Record R, Lindberg K, Hodde J, Park K. Small intestinal submucosa: a substrate for in vitro cell growth. J Biomater Sci Polym Ed 1998;9(8):863-78.

98. Sandusky GE, Jr., Badylak SF, Morff RJ, Johnson WD, Lantz G. Histologic findings after in vivo placement of small intestine submucosal vascular grafts and saphenous vein grafts in the carotid artery in dogs. Am J Pathol 1992;140(2):317-24.

99. Chamley-Campbell J, Campbell GR, Ross R. The smooth muscle cell in culture. Physiol Rev 1979;59(1):1-61.

100. Herring M, Baughman S, Glover J, Kesler K, Jesseph J, Campbell J, Dilley R, Evan A, Gardner A. Endothelial seeding of Dacron and polytetrafluoroethylene grafts: the cellular events of healing. Surgery 1984;96(4):745-55.

101. Thomas AC, Campbell JH. Smooth muscle cells of injured rat and rabbit arteries in culture: contractile and cytoskeletal proteins. Atherosclerosis 2001;154(2):291-9.

102. Weinberg CB, Bell E. A blood vessel model constructed from collagen and cultured vascular cells. Science 1986;231(4736):397-400.

103. Buttemeyer R, Mall JW, Paulitschke M, Rademacher A, Philipp AW. In a pig model ePTFE grafts will sustain for 6 weeks a confluent endothelial cell layer formed in vitro under shear stress conditions. Eur J Vasc Endovasc Surg 2003;26(2):156-60.

104. Hirai J, Kanda K, Oka T, Matsuda T. Highly oriented, tubular hybrid vascular tissue for a low pressure circulatory system. Asaio J 1994;40(3):M383-8.

105. Kobashi T, Matsuda T. Fabrication of branched hybrid vascular prostheses. Tissue Eng 1999;5(6):515-24.

106. Clark DP, Hanke CW, Swanson NA. Dermal implants: safety of products injected for soft tissue augmentation. J Am Acad Dermatol 1989;21(5 Pt 1):992-8.

107. Karp JM, Sarraf F, Shoichet MS, Davies JE. Fibrin-filled scaffolds for bone-tissue engineering: An in vivo study. J Biomed Mater Res A 2004;71(1):162-71.

108. Koob TJ, Hernandez DJ. Material properties of polymerized NDGA-collagen composite fibers: development of biologically based tendon constructs. Biomaterials 2002;23(1):203-12.

109. Girton TS, Oegema TR, Grassl ED, Isenberg BC, Tranquillo RT. Mechanisms of stiffening and strengthening in media-equivalents fabricated using glycation. J Biomech Eng 2000;122(3):216-23.

110. Elbjeirami WM, Yonter EO, Starcher BC, West JL. Enhancing mechanical properties of tissue-engineered constructs via lysyl oxidase crosslinking activity. J Biomed Mater Res A 2003;66(3):513-21.

111. Naito M, Nomura H, Iguchi A, Thompson WD, Smith EB. Effect of crosslinking by factor XIIIa on the migration of vascular smooth muscle cells into fibrin gels. Thromb Res 1998;90(3):111-6.

112. Berglund JD, Nerem RM, Sambanis A. Incorporation of intact elastin scaffolds in tissue-engineered collagen-based vascular grafts. Tissue Eng 2004;10(9-10):1526-35.

113. Seliktar D, Black RA, Vito RP, Nerem RM. Dynamic mechanical conditioning of collagen-gel blood vessel constructs induces remodeling in vitro. Ann Biomed Eng 2000;28(4):351-62.

114. Long JL, Tranquillo RT. Elastic fiber production in cardiovascular tissue-equivalents. Matrix Biol 2003;22(4):339-50.

115. Barocas VH, Girton TS, Tranquillo RT. Engineered alignment in media equivalents: magnetic prealignment and mandrel compaction. J Biomech Eng 1998;120(5):660-6.

116. Thie M, Schlumberger W, Semich R, Rauterberg J, Robenek H. Aortic smooth muscle cells in collagen lattice culture: effects on ultrastructure, proliferation and collagen synthesis. Eur J Cell Biol 1991;55(2):295-304.

117. Clark RA, Nielsen LD, Welch MP, McPherson JM. Collagen matrices attenuate the collagen-synthetic response of cultured fibroblasts to TGF-beta. J Cell Sci 1995;108 (Pt 3):1251-61.

118. Grassl ED, Oegema TR, Tranquillo RT. A fibrin-based arterial media equivalent. J Biomed Mater Res A 2003;66(3):550-61.

119. Swartz DD, Russell JA, Andreadis ST. Engineering of fibrin-based functional and implantable small-diameter blood vessels. Am J Physiol Heart Circ Physiol 2005;288(3):H1451-60.

120. Matthews JA, Wnek GE, Simpson DG, Bowlin GL. Electrospinning of collagen nanofibers. Biomacromolecules 2002;3(2):232-8.

121. McManus MC, Boland ED, Koo HP, Barnes CP, Pawlowski KJ, Wnek GE, Simpson DG, Bowlin GL. Mechanical properties of electrospun fibrinogen structures. Acta Biomater 2006;2(1):19-28.

122. Peppas NA, Huang Y, Torres-Lugo M, Ward JH, Zhang J. Physicochemical foundations and structural design of hydrogels in medicine and biology. Annu Rev Biomed Eng 2000;2:9-29.

123. Davies PF. Flow-mediated endothelial mechanotransduction. Physiol Rev 1995;75(3):519-60.

124. Osol G. Mechanotransduction by vascular smooth muscle. J Vasc Res 1995;32(5):275-92.

125. Kakisis JD, Liapis CD, Sumpio BE. Effects of cyclic strain on vascular cells. Endothelium 2004;11(1):17-28.

126. Birukov KG, Shirinsky VP, Stepanova OV, Tkachuk VA, Hahn AW, Resink TJ, Smirnov VN. Stretch affects phenotype and proliferation of vascular smooth muscle cells. Mol Cell Biochem 1995;144(2):131-9.

127. Dartsch PC, Hammerle H, Betz E. Orientation of cultured arterial smooth muscle cells growing on cyclically stretched substrates. Acta Anat (Basel) 1986;125(2):108-13.

128. Parks WC, Pierce RA, Lee KA, Mecham R. Elastin. Advances in Cell Molecular Biology 1993;6:133-182.

129. Sudhir K, Hashimura K, Bobik A, Dilley RJ, Jennings GL, Little PJ. Mechanical strain stimulates a mitogenic response in coronary vascular smooth muscle cells via release of basic fibroblast growth factor. Am J Hypertens 2001;14(11 Pt 1):1128-34.

130. Chapman GB, Durante W, Hellums JD, Schafer AI. Physiological cyclic stretch causes cell cycle arrest in cultured vascular smooth muscle cells. Am J Physiol Heart Circ Physiol 2000;278(3):H748-54.

131. Zeidan A, Nordstrom I, Dreja K, Malmqvist U, Hellstrand P. Stretch-dependent modulation of contractility and growth in smooth muscle of rat portal vein. Circ Res 2000;87(3):228-34.

132. Kanda K, Matsuda T, Oka T. Mechanical stress induced cellular orientation and phenotypic modulation of 3-D cultured smooth muscle cells. Asaio J 1993;39(3):M686-90.

133. Niklason LE, Gao J, Abbott WM, Hirschi KK, Houser S, Marini R, Langer R. Functional arteries grown in vitro. Science 1999;284(5413):489-93.

134. Davies PF, Remuzzi A, Gordon EJ, Dewey CF, Jr., Gimbrone MA, Jr. Turbulent fluid shear stress induces vascular endothelial cell turnover in vitro. Proc Natl Acad Sci U S A 1986;83(7):2114-7.

135. Wechezak AR, Wight TN, Viggers RF, Sauvage LR. Endothelial adherence under shear stress is dependent upon microfilament reorganization. J Cell Physiol 1989;139(1):136-46.

136. Thoumine O, Nerem RM, Girard PR. Changes in organization and composition of the extracellular matrix underlying cultured endothelial cells exposed to laminar steady shear stress. Lab Invest 1995;73(4):565-76.

137. Jo H, Dull RO, Hollis TM, Tarbell JM. Endothelial albumin permeability is shear dependent, time dependent, and reversible. Am J Physiol 1991;260(6 Pt 2):H1992-6.

138. Bazzoni G. Endothelial tight junctions: permeable barriers of the vessel wall. Thromb Haemost 2006;95(1):36-42.

139. Alexander DB, Goldberg GS. Transfer of biologically important molecules between cells through gap junction channels. Curr Med Chem 2003;10(19):2045-58.

140. Lampugnani MG, Corada M, Caveda L, Breviario F, Ayalon O, Geiger B, Dejana E. The molecular organization of endothelial cell to cell junctions: differential association of plakoglobin, beta-catenin, and alpha-catenin with vascular endothelial cadherin (VE-cadherin). J Cell Biol 1995;129(1):203-17.

141. Siflinger-Birnboim A, Malik AB. Regulation of endothelial permeability by second messengers. New Horiz 1996;4(1):87-98.

142. Wheelock MJ, Johnson KR. Cadherins as modulators of cellular phenotype. Annu Rev Cell Dev Biol 2003;19:207-35.

143. Staehelin LA. Structure and function of intercellular junctions. Int Rev Cytol 1974;39:191-283.

144. Lampugnani MG, Caveda L, Breviario F, Del Maschio A, Dejana E. Endothelial cell-to-cell junctions. Structural characteristics and functional role in the regulation of vascular permeability and leukocyte extravasation. Baillieres Clin Haematol 1993;6(3):539-58.

145. Blann AD, Lip GY. Virchow's triad revisited: the importance of soluble coagulation factors, the endothelium, and platelets. Thromb Res 2001;101(4):321-7.

146. Mulivor AW, Lipowsky HH. Role of glycocalyx in leukocyte-endothelial cell adhesion. Am J Physiol Heart Circ Physiol 2002;283(4):H1282-91.

147. Radomski MW, Palmer RM, Moncada S. Endogenous nitric oxide inhibits human platelet adhesion to vascular endothelium. Lancet 1987;2(8567):1057-8.

148. Sneddon JM, Vane JR. Endothelium-derived relaxing factor reduces platelet adhesion to bovine endothelial cells. Proc Natl Acad Sci U S A 1988;85(8):2800-4.

149. Azuma H, Ishikawa M, Sekizaki S. Endothelium-dependent inhibition of platelet aggregation. Br J Pharmacol 1986;88(2):411-5.

150. Radomski MW, Palmer RM, Moncada S. Comparative pharmacology of endothelium-derived relaxing factor, nitric oxide and prostacyclin in platelets. Br J Pharmacol 1987;92(1):181-7.

151. Bunting S, Simmons PM, Moncada S. Inhibition of platelet activation by prostacyclin: possible consequences in coagulation and anticoagulation. Thromb Res 1981;21(1-2):89-102.

152. Moncada S, Gryglewski R, Bunting S, Vane JR. An enzyme isolated from arteries transforms prostaglandin endoperoxides to an unstable substance that inhibits platelet aggregation. Nature 1976;263(5579):663-5.

153. Tateson JE, Moncada S, Vane JR. Effects of prostacyclin (PGX) on cyclic AMP concentrations in human platelets. Prostaglandins 1977;13(3):389-97.

154. Pearson JD, Carleton JS, Gordon JL. Metabolism of adenine nucleotides by ectoenzymes of vascular endothelial and smooth-muscle cells in culture. Biochem J 1980;190(2):421-9.

155. Lollar P, Owen WG. Clearance of thrombin from circulation in rabbits by high-affinity binding sites on endothelium. Possible role in the inactivation of thrombin by antithrombin III. J Clin Invest 1980;66(6):1222-30.

156. Marcum JA, McKenney JB, Rosenberg RD. Acceleration of thrombin-antithrombin complex formation in rat hindquarters via heparinlike molecules bound to the endothelium. J Clin Invest 1984;74(2):341-50.

157. Stern D, Nawroth P, Marcum J, Handley D, Kisiel W, Rosenberg R, Stern K. Interaction of antithrombin III with bovine aortic segments. Role of heparin in binding and enhanced anticoagulant activity. J Clin Invest 1985;75(1):272-9.

158. Esmon CT. The roles of protein C and thrombomodulin in the regulation of blood coagulation. J Biol Chem 1989;264(9):4743-6.

159. Solymoss S, Tucker MM, Tracy PB. Kinetics of inactivation of membrane-bound factor Va by activated protein C. Protein S modulates factor Xa protection. J Biol Chem 1988;263(29):14884-90.

160. Knauer DJ, Thompson JA, Cunningham DD. Protease nexins: cell-secreted proteins that mediate the binding, internalization, and degradation of regulatory serine proteases. J Cell Physiol 1983;117(3):385-96.

161. Lijnen HR. Elements of the fibrinolytic system. Ann N Y Acad Sci 2001;936:226-36.

162. http://depts.washington.edu/labweb/dept/staff/bios/hemostas/images/introfibsys_figure_1.jpg.

163. Reidy MA, Schwartz SM. Endothelial regeneration. III. Time course of intimal changes after small defined injury to rat aortic endothelium. Lab Invest 1981;44(4):301-8.

164. Hannan RL, Kourembanas S, Flanders KC, Rogelj SJ, Roberts AB, Faller DV, Klagsbrun M. Endothelial cells synthesize basic fibroblast growth factor and transforming growth factor beta. Growth Factors 1988;1(1):7-17.

165. Beitz JG, Kim IS, Calabresi P, Frackelton AR, Jr. Human microvascular endothelial cells express receptors for platelet-derived growth factor. Proc Natl Acad Sci U S A 1991;88(5):2021-5.

166. Zerwes HG, Risau W. Polarized secretion of a platelet-derived growth factor-like chemotactic factor by endothelial cells in vitro. J Cell Biol 1987;105(5):2037-41.

167. Heimark RL, Twardzik DR, Schwartz SM. Inhibition of endothelial regeneration by type-beta transforming growth factor from platelets. Science 1986;233(4768):1078-80.

168. Castellot JJ, Jr., Addonizio ML, Rosenberg R, Karnovsky MJ. Cultured endothelial cells produce a heparinlike inhibitor of smooth muscle cell growth. J Cell Biol 1981;90(2):372-9.

169. Bevilacqua MP, Stengelin S, Gimbrone MA, Jr., Seed B. Endothelial leukocyte adhesion molecule 1: an inducible receptor for neutrophils related to complement regulatory proteins and lectins. Science 1989;243(4895):1160-5.

170. Elices MJ, Osborn L, Takada Y, Crouse C, Luhowskyj S, Hemler ME, Lobb RR. VCAM-1 on activated endothelium interacts with the leukocyte integrin VLA-4 at a site distinct from the VLA-4/fibronectin binding site. Cell 1990;60(4):577-84.

171. Deed R, Rooney P, Kumar P, Norton JD, Smith J, Freemont AJ, Kumar S. Early-response gene signalling is induced by angiogenic oligosaccharides of hyaluronan in endothelial cells. Inhibition by non-angiogenic, high-molecular-weight hyaluronan. Int J Cancer 1997;71(2):251-6.

172. Lammle B, Griffin JH. Formation of the fibrin clot: the balance of procoagulant and inhibitory factors. Clin Haematol 1985;14(2):281-342.

173. Kawamoto Y, Nakao A, Ito Y, Wada N, Kaibara M. Endothelial cells on plasma-treated segmented-polyurethane: adhesion strength, antithrombogenicity and cultivation in tubes. J Mater Sci Mater Med 1997;8(9):551-7.

174. Mackman N. Role of tissue factor in hemostasis and thrombosis. Blood Cells Mol Dis 2006;36(2):104-7.

175. van Hinsbergh VW. Regulation of the synthesis and secretion of plasminogen activators by endothelial cells. Haemostasis 1988;18(4-6):307-27.

176. Brenner BM, Troy JL, Ballermann BJ. Endothelium-dependent vascular responses. Mediators and mechanisms. J Clin Invest 1989;84(5):1373-8.

177. Gryglewski RJ, Botting RM, Vane JR. Mediators produced by the endothelial cell. Hypertension 1988;12(6):530-48.

178. Clarke JG, Benjamin N, Larkin SW, Webb DJ, Davies GJ, Maseri A. Endothelin is a potent long-lasting vasoconstrictor in men. Am J Physiol 1989;257(6 Pt 2):H2033-5.

179. Pu FR, Williams RL, Markkula TK, Hunt JA. Effects of plasma treated PET and PTFE on expression of adhesion molecules by human endothelial cells in vitro. Biomaterials 2002;23(11):2411-28.

180. Yuan Y, Liu C, Yin M. Plasma polymerized n-butyl methacrylate coating with potential for re-endothelialization of intravascular stent devices. J Mater Sci Mater Med 2008;19(5):2187-96.

181. Baquey CH, Palumbo F, Porte-Durrieu MC, Legeay G, Tressaud A, R dA. Plasma treatment of expanded PTFE offers a way to a biofunctionalization of its surface. Nuclear Instruments and Methods in Physics Research Section B 1999;151:255-262.

182. Dekker A, Poot AA, van Mourik JA, Workel MP, Beugeling T, Bantjes A, Feijen J, van Aken WG. Improved adhesion and proliferation of human endothelial cells on polyethylene precoated with monoclonal antibodies directed against cell membrane antigens and extracellular matrix proteins. Thromb Haemost 1991;66(6):715-24.

183. Bhatia SN, Balis UJ, Yarmush ML, Toner M. Probing heterotypic cell interactions: hepatocyte function in microfabricated co-cultures. J Biomater Sci Polym Ed 1998;9(11):1137-60.

184. Norde W, Lyklema J. Why proteins prefer interfaces. J Biomater Sci Polym Ed 1991;2(3):183-202.

185. van Wachem PB, Beugeling T, Feijen J, Bantjes A, Detmers JP, van Aken WG. Interaction of cultured human endothelial cells with polymeric surfaces of different wettabilities. Biomaterials 1985;6(6):403-8.

186. Dekker A, Reitsma K, Beugeling T, Bantjes A, Feijen J, van Aken WG. Adhesion of endothelial cells and adsorption of serum proteins on gas plasma-treated polytetrafluoroethylene. Biomaterials 1991;12(2):130-8.

187. Iuliano DJ, Saavedra SS, Truskey GA. Effect of the conformation and orientation of adsorbed fibronectin on endothelial cell spreading and the strength of adhesion. J Biomed Mater Res 1993;27(8):1103-13.

188. Poole-Warren LA, Schindhelm K, Graham AR, Slowiaczek PR, Noble KR. Performance of small diameter synthetic vascular prostheses with confluent autologous endothelial cell linings. J Biomed Mater Res 1996;30(2):221-29.

189. Graham LM, Burkel WE, Ford JW, Vinter DW, Kahn RH, Stanley JC. Immediate seeding of enzymatically derived endothelium in Dacron vascular grafts. Early experimental studies with autologous canine cells. Arch Surg 1980;115(11):1289-94.

190. Shimizu M, Suzuki S, Takaya S, Satoh K. Replacement of the canine inferior vena cava with a seeded graft. Surg Today 2001;31(5):421-7.

191. Meinhart J, Deutsch M, Zilla P. Eight years of clinical endothelial cell transplantation. Closing the gap between prosthetic grafts and vein grafts. Asaio J 1997;43(5):M515-21.

192. Meinhart JG, Deutsch M, Fischlein T, Howanietz N, Froschl A, Zilla P. Clinical autologous in vitro endothelialization of 153 infrainguinal ePTFE grafts. Ann Thorac Surg 2001;71(5 Suppl):S327-31.

193. Mould AP, Komoriya A, Yamada KM, Humphries MJ. The CS5 peptide is a second site in the IIICS region of fibronectin recognized by the integrin alpha 4 beta 1. Inhibition of alpha 4 beta 1 function by RGD peptide homologues. J Biol Chem 1991;266(6):3579-85.

194. Graf J, Ogle RC, Robey FA, Sasaki M, Martin GR, Yamada Y, Kleinman HK. A pentapeptide from the laminin B1 chain mediates cell adhesion and binds the 67,000 laminin receptor. Biochemistry 1987;26(22):6896-900.

195. Trudel J, Massia SP. Assessment of the cytotoxicity of photocrosslinked dextran and hyaluronan-based hydrogels to vascular smooth muscle cells. Biomaterials 2002;23(16):3299-307.

196. Walluscheck KP, Steinhoff G, Kelm S, Haverich A. Improved endothelial cell attachment on ePTFE vascular grafts pretreated with synthetic RGD-containing peptides. Eur J Vasc Endovasc Surg 1996;12(3):321-30.

197. Walluscheck KP, Steinhoff G, Haverich A. Endothelial cell seeding of de-endothelialised human arteries: improvement by adhesion molecule induction and flow-seeding technology. Eur J Vasc Endovasc Surg 1996;12(1):46-53.

198. Desgranges P, Tardieu M, Loisance D, Barritault D. Extracellular matrix covered biomaterials for human endothelial cell growth. Int J Artif Organs 1992;15(12):722-6.

199. Hay ED. Cell Biology of Extracellular Matrix. New York: Plenum Press; 1991.

200. Balazs EA. Chemistry and Molecular Biology of the Intercellular Matrix: Academic Press; 1970.

201. Dingemans KP, Teeling P, Lagendijk JH, Becker AE. Extracellular matrix of the human aortic media: an ultrastructural histochemical and immunohistochemical study of the adult aortic media. Anat Rec 2000;258(1):1-14.

202. Raffetto JD, Khalil RA. Matrix Metalloproteinases and their Inhibitors in Vascular Remodeling and Vascular Disease. Biochemical Pharmacology 2007;75(2):346-359.

203. Kielty CM. Elastic fibres in health and disease. Expert Rev Mol Med 2006;8(19):1-23.

204. Kingwell B, Boutouyrie P. Genetic influences on the arterial wall. Clin Exp Pharmacol Physiol 2007;34(7):652-7.

205. Robert AM, Robert L. Biology and Pathology of Elastic Tissues: S Karger; 1980.

206. Hinek A, Mecham RP, Keeley F, Rabinovitch M. Impaired elastin fiber assembly related to reduced 67-kD elastin-binding protein in fetal lamb ductus arteriosus and in cultured aortic smooth muscle cells treated with chondroitin sulfate. J Clin Invest 1991;88(6):2083-94.

207. Mecham RP. Elastin synthesis and fiber assembly. Ann N Y Acad Sci 1991;624:137-46.

208. Gundiah N, M BR, L AP. Determination of strain energy function for arterial elastin: Experiments using histology and mechanical tests. J Biomech 2007;40(3):586-94.

209. http://biochemistry.utoronto.ca/keeley/bch.html.

210. Keeling WB, Armstrong PA, Stone PA, Bandyk DF, Shames ML. An overview of matrix metalloproteinases in the pathogenesis and treatment of abdominal aortic aneurysms. Vasc Endovascular Surg 2005;39(6):457-64.

211. Brooke BS, Bayes-Genis A, Li DY. New insights into elastin and vascular disease. Trends Cardiovasc Med 2003;13(5):176-81.

212. Bank AJ, Wang H, Holte JE, Mullen K, Shammas R, Kubo SH. Contribution of collagen, elastin, and smooth muscle to in vivo human brachial artery wall stress and elastic modulus. Circulation 1996;94(12):3263-70.

213. Krettek A, Sukhova GK, Libby P. Elastogenesis in human arterial disease: a role for macrophages in disordered elastin synthesis. Arterioscler Thromb Vasc Biol 2003;23(4):582-7.

214. Wolinsky H, Glagov S. A lamellar unit of aortic medial structure and function in mammals. Circ Res 1967;20(1):99-111.

215. Urban Z, Riazi S, Seidl TL, Katahira J, Smoot LB, Chitayat D, Boyd CD, Hinek A. Connection between elastin haploinsufficiency and increased cell proliferation in patients with supravalvular aortic stenosis and Williams-Beuren syndrome. Am J Hum Genet 2002;71(1):30-44.

216. Patel A, Fine B, Sandig M, Mequanint K. Elastin biosynthesis: The missing link in tissue-engineered blood vessels. Cardiovasc Res 2006;71(1):40-9.

217. Swee MH, Parks WC, Pierce RA. Developmental regulation of elastin production. Expression of tropoelastin pre-mRNA persists after down-regulation of steady-state mRNA levels. J Biol Chem 1995;270(25):14899-906.

218. Chen P, Marsilio E, Goldstein RH, Yannas IV, Spector M. Formation of lung alveolar-like structures in collagen-glycosaminoglycan scaffolds in vitro. Tissue Eng 2005;11(9-10):1436-48.

219. Lee SH, Kim BS, Kim SH, Choi SW, Jeong SI, Kwon IK, Kang SW, Nikolovski J, Mooney DJ, Han YK and others. Elastic biodegradable poly(glycolide-co-caprolactone) scaffold for tissue engineering. J Biomed Mater Res A 2003;66(1):29-37.

220. Ramamurthi A, Vesely I. Evaluation of the matrix-synthesis potential of crosslinked hyaluronan gels for tissue engineering of aortic heart valves. Biomaterials 2005;26(9):999-1010.

221. Viglio S, Iadarola P, Lupi A, Trisolini R, Tinelli C, Balbi B, Grassi V, Worlitzsch D, Doring G, Meloni F and others. MEKC of desmosine and isodesmosine in urine of chronic destructive lung disease patients. Eur Respir J 2000;15(6):1039-45.

222. Toole BP. Hyaluronan in morphogenesis. Semin Cell Dev Biol 2001;12(2):79-87.

223. Weigel PH, Hascall VC, Tammi M. Hyaluronan synthases. J Biol Chem 1997;272(22):13997-4000.

224. Tammi M, Tammi R. Hyaluronan in the epidermis. Glycoforum; 2006.

225. Deguine V, Menasche M, Ferrari P, Fraisse L, Pouliquen Y, Robert L. Free radical depolymerization of hyaluronan by Maillard reaction products: role in liquefaction of aging vitreous. Int J Biol Macromol 1998;22(1):17-22.

226. Yamazaki K, Fukuda K, Matsukawa M, Hara F, Yoshida K, Akagi M, Munakata H, Hamanishi C. Reactive oxygen species depolymerize hyaluronan: involvement of the hydroxyl radical. Pathophysiology 2003;9(4):215-220.

227. Day AJ, Prestwich GD. Hyaluronan-binding proteins: tying up the giant. J Biol Chem 2002;277(7):4585-8.

228. Seyfried NT, Day AJ, Almond A. Experimental evidence for all-or-none cooperative interactions between the G1-domain of versican and multivalent hyaluronan oligosaccharides. Matrix Biol 2006;25(1):14-9.

229. Spicer AP, Tien JY. Hyaluronan and morphogenesis. Birth Defects Res C Embryo Today 2004;72(1):89-108.

230. Blundell C, Seyfried N, Day A. Structural and functional diversity of hyaluronan binding protiens. In: Garg H, Hales C, editors. Chemistry and biology of hyaluronan. Amsterdam: Elsevier Press; 2004. p 184-204.

231. Rauch U, Karthikeyan L, Maurel P, Margolis RU, Margolis RK. Cloning and primary structure of neurocan, a developmentally regulated, aggregating chondroitin sulfate proteoglycan of brain. J Biol Chem 1992;267(27):19536-47.

232. Aruffo A, Stamenkovic I, Melnick M, Underhill CB, Seed B. CD44 is the principal cell surface receptor for hyaluronate. Cell 1990;61(7):1303-13.

233. Ponta H, Wainwright D, Herrlich P. The CD44 protein family. Int J Biochem Cell Biol 1998;30(3):299-305.

234. Knudson CB, Knudson W. Hyaluronan and CD44: modulators of chondrocyte metabolism. Clin Orthop Relat Res 2004(427 Suppl):S152-62.

235. Ponta H, Sherman L, Herrlich PA. CD44: from adhesion molecules to signalling regulators. Nat Rev Mol Cell Biol 2003;4(1):33-45.

236. Burdick JA, Mason MN, Hinman AD, Thorne K, Anseth KS. Delivery of osteoinductive growth factors from degradable PEG hydrogels influences osteoblast differentiation and mineralization. J Control Release 2002;83(1):53-63.

237. Evanko SP, Raines EW, Ross R, Gold LI, Wight TN. Proteoglycan distribution in lesions of atherosclerosis depends on lesion severity, structural characteristics, and the proximity of platelet-derived growth factor and transforming growth factor-beta. Am J Pathol 1998;152(2):533-46.

238. Wight TN. Versican: a versatile extracellular matrix proteoglycan in cell biology. Curr Opin Cell Biol 2002;14(5):617-23.

239. Knudson W, Chow G, Knudson CB. CD44-mediated uptake and degradation of hyaluronan. Matrix Biol 2002;21(1):15-23.

240. Toole BP. Hyaluronan: from extracellular glue to pericellular cue. Nat Rev Cancer 2004;4(7):528-39.

241. Toole BP, Wight TN, Tammi MI. Hyaluronan-cell interactions in cancer and vascular disease. J Biol Chem 2002;277(7):4593-6.

242. Knudson CB. Hyaluronan and CD44: strategic players for cell-matrix interactions during chondrogenesis and matrix assembly. Birth Defects Res C Embryo Today 2003;69(2):174-96.

243. Fieber C, Plug R, Sleeman J, Dall P, Ponta H, Hofmann M. Characterisation of the murine gene encoding the intracellular hyaluronan receptor IHABP (RHAMM). Gene 1999;226(1):41-50.

244. Milner CM, Higman VA, Day AJ. TSG-6: a pluripotent inflammatory mediator? Biochem Soc Trans 2006;34(Pt 3):446-50.

245. Politz O, Gratchev A, McCourt PA, Schledzewski K, Guillot P, Johansson S, Svineng G, Franke P, Kannicht C, Kzhyshkowska J and others. Stabilin-1 and -2 constitute a novel family of fasciclin-like hyaluronan receptor homologues. Biochem J 2002;362(Pt 1):155-64.

246. Banerji S, Ni J, Wang SX, Clasper S, Su J, Tammi R, Jones M, Jackson DG. LYVE-1, a new homologue of the CD44 glycoprotein, is a lymph-specific receptor for hyaluronan. J Cell Biol 1999;144(4):789-801.

247. Bono P, Rubin K, Higgins JM, Hynes RO. Layilin, a novel integral membrane protein, is a hyaluronan receptor. Mol Biol Cell 2001;12(4):891-900.

248. Nguyen KT, West JL. Photopolymerizable hydrogels for tissue engineering applications. Biomaterials 2002;23(22):4307-14.

249. Murai T, Miyazaki Y, Nishinakamura H, Sugahara KN, Miyauchi T, Sako Y, Yanagida T, Miyasaka M. Engagement of CD44 promotes Rac activation and CD44 cleavage during tumor cell migration. J Biol Chem 2004;279(6):4541-50.

250. Rossler A, Hinghofer-Szalkay H. Hyaluronan fragments: an information-carrying system? Horm Metab Res 2003;35(2):67-8.

251. Taylor PM. Biological matrices and bionanotechnology. Philos Trans R Soc Lond B Biol Sci 2007;362(1484):1313-20.

252. Termeer C, Benedix F, Sleeman J, Fieber C, Voith U, Ahrens T, Miyake K, Freudenberg M, Galanos C, Simon JC. Oligosaccharides of Hyaluronan activate dendritic cells via toll-like receptor 4. J Exp Med 2002;195(1):99-111.

253. Segura T, Anderson BC, Chung PH, Webber RE, Shull KR, Shea LD. Crosslinked hyaluronic acid hydrogels: a strategy to functionalize and pattern. Biomaterials 2005;26(4):359-71.

254. Park YD, Tirelli N, Hubbell JA. Photopolymerized hyaluronic acid-based hydrogels and interpenetrating networks. Biomaterials 2003;24(6):893-900.

255. Liu Y, Shu XZ, Gray SD, Prestwich GD. Disulfide-crosslinked hyaluronan-gelatin sponge: growth of fibrous tissue in vivo. J Biomed Mater Res A 2004;68(1):142-9.

256. Lepidi S, Abatangelo G, Vindigni V, Deriu GP, Zavan B, Tonello C, Cortivo R. In vivo regeneration of small-diameter (2 mm) arteries using a polymer scaffold. Faseb J 2006;20(1):103-5.

257. Luo Y, Ziebell MR, Prestwich GD. A hyaluronic acid-taxol antitumor bioconjugate targeted to cancer cells. Biomacromolecules 2000;1(2):208-18.

258. Prestwich G. Biomaterials from chemically modified hyaluronan. Glycoforum; 2001.

259. Tomihata K, Ikada Y. Crosslinking of hyaluronic acid with water-soluble carbodiimide. J Biomed Mater Res 1997;37(2):243-51.

260. Vercruysse KP, Marecak DM, Marecek JF, Prestwich GD. Synthesis and in vitro degradation of new polyvalent hydrazide cross-linked hydrogels of hyaluronic acid. Bioconjug Chem 1997;8(5):686-94.

261. Malson T, Lindqvist B; Biomatrix, Inc, assignee. Crosslinked hyaluronate gels, their use and methods for producing them. USA. 1998.

262. Band P. Hyaluronan derivatives: Chemistry and clinical applications. In: Laurent T, editor. The chemistry, biology and medical applications of hyaluronan and its derivatives. London, UK: Portland Press; 1998. p 33-42.

263. Daley WP, Peters SB, Larsen M. Extracellular matrix dynamics in development and regenerative medicine. J Cell Sci 2008;121(Pt 3):255-64.

264. Baier Leach J, Bivens KA, Patrick CW, Jr., Schmidt CE. Photocrosslinked hyaluronic acid hydrogels: natural, biodegradable tissue engineering scaffolds. Biotechnol Bioeng 2003;82(5):578-89.

265. Denlinger J. Hyaluronan and its derivatives as viscoelastics in medicine. In: Laurent T, editor. The chemistry, biology and medical Applications of hyaluronan and its derivatives. London: Portland Press Ldt; 1998. p 235 - 242.

266. Gerwin N, Hops C, Lucke A. Intraarticular drug delivery in osteoarthritis. Adv Drug Deliv Rev 2006;58(2):226-42.

267. Liao YH, Jones SA, Forbes B, Martin GP, Brown MB. Hyaluronan: pharmaceutical characterization and drug delivery. Drug Deliv 2005;12(6):327-42.

268. Scott D, Coleman PJ, Mason RM, Levick JR. Direct evidence for the partial reflection of hyaluronan molecules by the lining of rabbit knee joints during trans-synovial flow. J Physiol 1998;508 (Pt 2):619-23.

269. Miller EH. Viscosupplementation: therapeutic mechanisms and clinical potential in osteoarthritis of the knee. J Am Acad Orthop Surg 2001;9(2):146-7.

270. Hoekstra D. Hyaluronan-Modified Surfaces for Medical Devices. MD&DI 1999;February:48.

271. Xue L, Greisler HP. Biomaterials in the development and future of vascular grafts. J Vasc Surg 2003;37(2):472-80.

272. Siegelman MH, DeGrendele HC, Estess P. Activation and interaction of CD44 and hyaluronan in immunological systems. J Leukoc Biol 1999;66(2):315-21.

273. Pure E, Cuff CA. A crucial role for CD44 in inflammation. Trends Mol Med 2001;7(5):213-21.

274. Pries AR, Kuebler WM. Normal endothelium. Handb Exp Pharmacol 2006(176 Pt 1):1-40.

275. Al'Qteishat A, Gaffney J, Krupinski J, Rubio F, West D, Kumar S, Kumar P, Mitsios N, Slevin M. Changes in hyaluronan production and metabolism following ischaemic stroke in man. Brain 2006;129(Pt 8):2158-76.

276. Camenisch TD, Schroeder JA, Bradley J, Klewer SE, McDonald JA. Heart-valve mesenchyme formation is dependent on hyaluronan-augmented activation of ErbB2-ErbB3 receptors. Nat Med 2002;8(8):850-5.

277. Amarnath LP, Srinivas A, Ramamurthi A. In vitro hemocompatibility testing of UV-modified hyaluronan hydrogels. Biomaterials 2006;27(8):1416-24.

278. Vercruysse KP, Prestwich GD. Hyaluronate derivatives in drug delivery. Crit Rev Ther Drug Carrier Syst 1998;15(5):513-55.

279. Yow KH, Ingram J, Korossis SA, Ingham E, Homer-Vanniasinkam S. Tissue engineering of vascular conduits. Br J Surg 2006;93(6):652-61.

280. Sattar A, Rooney P, Kumar S, Pye D, West DC, Scott I, Ledger P. Application of angiogenic oligosaccharides of hyaluronan increases blood vessel numbers in rat skin. J Invest Dermatol 1994;103(4):576-9.

281. Slevin M, Krupinski J, Gaffney J, Matou S, West D, Delisser H, Savani RC, Kumar S. Hyaluronan-mediated angiogenesis in vascular disease: Uncovering RHAMM and CD44 receptor signaling pathways. Matrix Biol 2006.

282. Camenisch TD, Spicer AP, Brehm-Gibson T, Biesterfeldt J, Augustine ML, Calabro A, Jr., Kubalak S, Klewer SE, McDonald JA. Disruption of hyaluronan synthase-2 abrogates normal cardiac morphogenesis and hyaluronan-mediated transformation of epithelium to mesenchyme. J Clin Invest 2000;106(3):349-60.

283. Box G, Hunter W, Hunter J, editors. Statistics for experimenters: an introduction to design, data analysis, and model building Somerset, NJ: Wiley; 1978.

284. Licht M. Multiple regression and correlation. In: Grims L, Yarnold P, editors. Reading and understanding multivariate statistics. Washington, DC: American Psychological Association; 1995. p 19–64.

285. Montgomery D, Peck E. Introduction to Linear Regression Analysis. New York: Wiley; 1992. p 210.

286. Labarca C, Paigen K. A simple, rapid, and sensitive DNA assay procedure. Anal Biochem 1980;102(2):344-52.

287. Alberti S, Fornaro M. Higher transfection efficiency of genomic DNA purified with a guanidinium thiocyanate-based procedure. Nucleic Acids Res 1990;18(2):351-3.

288. Moore KL, Andreoli SP, Esmon NL, Esmon CT, Bang NU. Endotoxin enhances tissue factor and suppresses thrombomodulin expression of human vascular endothelium in vitro. J Clin Invest 1987;79(1):124-30.

289. Ibrahim S, Joddar B, Craps M, Ramamurthi A. A surface-tethered model to assess size-specific effects of hyaluronan (HA) on endothelial cells. Biomaterials 2007;28(5):825-35.

290. Gao F, Cao M, Yang C, He Y, Liu Y. Preparation and characterization of hyaluronan oligosaccharides for angiogenesis study. J Biomed Mater Res B Appl Biomater 2006;78(2):385-92.

291. Akhtar S, V B. Streptococcus pneumoniae hyaluronate lyase: An Overview. Current Science 2004;86(25):285-295.

292. Tung JS, Mark GE, Hollis GF. A microplate assay for hyaluronidase and hyaluronidase inhibitors. Anal Biochem 1994;223(1):149-52.

293. Liu D, Liu T, Li R, Sy MS. Mechanisms regulating the binding activity of CD44 to hyaluronic acid. Front Biosci 1998;3:d631-6.

294. Bandman O, Coleman RT, Loring JF, Seilhamer JJ, Cocks BG. Complexity of inflammatory responses in endothelial cells and vascular smooth muscle cells determined by microarray analysis. Ann N Y Acad Sci 2002;975:77-90.

295. Dolle JP, Rezvan A, Allen FD, Lazarovici P, Lelkes PI. Nerve growth factor-induced migration of endothelial cells. J Pharmacol Exp Ther 2005;315(3):1220-7.

296. Jiang H, Movsesyan V, Fink DW, Jr., Fasler M, Whalin M, Katagiri Y, Monshipouri M, Dickens G, Lelkes PI, Guroff G and others. Expression of human p140trk receptors in p140trk-deficient, PC12/endothelial cells results in nerve growth factor-induced signal transduction and DNA synthesis. J Cell Biochem 1997;66(2):229-44.

297. Chirco R, Liu XW, Jung KK, Kim HR. Novel functions of TIMPs in cell signaling. Cancer Metastasis Rev 2006;25(1):99-113.

298. Moncada S, Higgs EA. Nitric oxide and the vascular endothelium. Handb Exp Pharmacol 2006(176 Pt 1):213-54.

299. Siegel-Axel DI, Gawaz M. Platelets and endothelial cells. Semin Thromb Hemost 2007;33(2):128-35.

300. Imaizumi T, Albertine KH, Jicha DL, McIntyre TM, Prescott SM, Zimmerman GA. Human endothelial cells synthesize ENA-78: relationship to IL-8 and to signaling of PMN adhesion. Am J Respir Cell Mol Biol 1997;17(2):181-92.

301. Rollins BJ. Chemokines. Blood 1997;90(3):909-28.

302. Gasson JC. Molecular physiology of granulocyte-macrophage colony-stimulating factor. Blood 1991;77(6):1131-45.

303. McKee CM, Penno MB, Cowman M, Burdick MD, Strieter RM, Bao C, Noble PW. Hyaluronan (HA) fragments induce chemokine gene expression in alveolar macrophages. The role of HA size and CD44. J Clin Invest 1996;98(10):2403-13.

304. Kasama T, Strieter RM, Lukacs NW, Lincoln PM, Burdick MD, Kunkel SL. Interferon gamma modulates the expression of neutrophil-derived chemokines. J Investig Med 1995;43(1):58-67.

305. Umehara H, Bloom ET, Okazaki T, Nagano Y, Yoshie O, Imai T. Fractalkine in vascular biology: from basic research to clinical disease. Arterioscler Thromb Vasc Biol 2004;24(1):34-40.

306. Ramamurthi A, Vesely I. Ultraviolet light-induced modification of crosslinked hyaluronan gels. J Biomed Mater Res A 2003;66(2):317-29.

307. Saltzman WM, Parkhurst MR, Parsons-Wingerter P, Zhu WH. Three-dimensional cell cultures mimic tissues. Ann N Y Acad Sci 1992;665:259-73.

308. Stile RA, Barber TA, Castner DG, Healy KE. Sequential robust design methodology and X-ray photoelectron spectroscopy to analyze the grafting of hyaluronic acid to glass substrates. J Biomed Mater Res 2002;61(3):391-8.

309. Matinlinna JP, Lassila LV, Ozcan M, Yli-Urpo A, Vallittu PK. An introduction to silanes and their clinical applications in dentistry. Int J Prosthodont 2004;17(2):155-64.

310. Staros JV, Wright RW, Swingle DM. Enhancement by N-hydroxysulfosuccinimide of water-soluble carbodiimide-mediated coupling reactions. Anal Biochem 1986;156(1):220-2.

311. Johnston JB. A simple, nondestructive assay for bound hyaluronan. J Biomed Mater Res 2000;53(2):188-91.

312. Chung TW, Liu DZ, Wang SY, Wang SS. Enhancement of the growth of human endothelial cells by surface roughness at nanometer scale. Biomaterials 2003;24(25):4655-61.

313. Lee JH, Lee JW, Khang G, Lee HB. Interaction of cells on chargeable functional group gradient surfaces. Biomaterials 1997;18(4):351-8.

314. Savani RC, Cao G, Pooler PM, Zaman A, Zhou Z, DeLisser HM. Differential involvement of the hyaluronan (HA) receptors CD44 and receptor for HA-mediated motility in endothelial cell function and angiogenesis. J Biol Chem 2001;276(39):36770-8.

315. Bressan GM, Pasquali-Ronchetti I, Fornieri C, Mattioli F, Castellani I, Volpin D. Relevance of aggregation properties of tropoelastin to the assembly and structure of elastic fibers. J Ultrastruct Mol Struct Res 1986;94(3):209-16.

316. Wei YT, Tian WM, Yu X, Cui FZ, Hou SP, Xu QY, Lee IS. Hyaluronic acid hydrogels with IKVAV peptides for tissue repair and axonal regeneration in an injured rat brain. Biomed Mater 2007;2(3):S142-6.

317. Srinivas A, Ramamurthi A. Effects of gamma-irradiation on physical and biologic properties of crosslinked hyaluronan tissue engineering scaffolds. Tissue Eng 2007;13(3):447-59.

318. Flory P. Principles of polymer chemistry. Ithica, NY: Cornell University Press; 1953.

319. Denizot F, Lang R. Rapid colorimetric assay for cell growth and survival. Modifications to the tetrazolium dye procedure giving improved sensitivity and reliability. J Immunol Methods 1986;89(2):271-7.

320. Griffiths P, de Haseth J. Fourier Transform Infrared Spectroscopy. New Jersey: John Wiley & Sons Inc.; 2007.

321. Manna F, Dentini M, Desideri P, De Pita O, Mortilla E, Maras B. Comparative chemical evaluation of two commercially available derivatives of hyaluronic acid (hylaform from rooster combs and restylane from streptococcus) used for soft tissue augmentation. J Eur Acad Dermatol Venereol 1999;13(3):183-92.

322. Arshinoff S. The use of ophthalmic viscosurgical devices in cataract surgery. In: Kennedy J, Phillips G, Williams P, Hascall V, editors. Hyaluronan: Biomedical, Medical, and Clinical Aspects. Cambridge, UK: Woodhead Publishing Limited; 2002. p 119-128.

323. Weiss C. Hyaluronan and hylan in the treatment of osteoarthritis. In: Kennedy J, Phillipps G, Williams P, Hascall V, editors. Hyaluronan: Biomedical, Medical, and Clinical Aspects. Cambridge, UK: Woodhead Publishing Limited; 2002. p 467-482.

324. Ramamurthi A, Vesely I. Smooth muscle cell adhesion on crosslinked hyaluronan gels. J Biomed Mater Res 2002;60(1):195-205.

325. Prestwich G, Luo Y, Kirker K, Ziebell M, Shelby J. Hyaluronan biomaterials for targeted drug delivery and wound healing. In: Kennedy J, Phillipps G, Williams P, Hascall V, editors. Hyaluronan: Biomedical, Medical, and Clinical Aspects. Cambridge, UK: Woodhead Publishing Limited; 2002. p 277-284.

326. Borzacchiello A, Mayol L, Ramires PA, Pastorello A, Di Bartolo C, Ambrosio L, Milella E. Structural and rheological characterization of hyaluronic acid-based scaffolds for adipose tissue engineering. Biomaterials 2007;28(30):4399-408.

327. Zingg W, Neumann AW, Strong AB, Hum OS, Absolom DR. Effect of surface roughness on platelet adhesion under static and under flow conditions. Can J Surg 1982;25(1):16-9.

328. Monheit GD. Hylaform: a new hyaluronic acid filler. Facial Plast Surg 2004;20(2):153-5.

329. Koyano T, Minoura N, Nagura M, Kobayashi K. Attachment and growth of cultured fibroblast cells on PVA/chitosan-blended hydrogels. J Biomed Mater Res 1998;39(3):486-90.

330. Rowley JA, Madlambayan G, Mooney DJ. Alginate hydrogels as synthetic extracellular matrix materials. Biomaterials 1999;20(1):45-53.

331. Lapcik LJaL, Lapcik L, De Smedt S, Demeester J, Chabrecek P. Hyaluronan: Preparation, Structure, Properties, and Applications. Chem Rev 1998;98(8):2663-2684.

332. Shu XZ, Ghosh K, Liu Y, Palumbo FS, Luo Y, Clark RA, Prestwich GD. Attachment and spreading of fibroblasts on an RGD peptide-modified injectable hyaluronan hydrogel. J Biomed Mater Res A 2004;68(2):365-75.

333. Davidson J, Giro M. Regulation of Matrix Accumulation. New York: Academic Press; 1986.

334. Ross R, Bornstein P. The elastic fiber. I. The separation and partial characterization of its macromolecular components. J Cell Biol 1969;40(2):366-81.

335. Rosenbloom J, Abrams WR, Mecham R. Extracellular matrix 4: the elastic fiber. Faseb J 1993;7(13):1208-18.

336. Li DY, Brooke B, Davis EC, Mecham RP, Sorensen LK, Boak BB, Eichwald E, Keating MT. Elastin is an essential determinant of arterial morphogenesis. Nature 1998;393(6682):276-80.

337. Sandberg LB, Soskel NT, Leslie JG. Elastin structure, biosynthesis, and relation to disease states. N Engl J Med 1981;304(10):566-79.

338. Keating MT. Elastin and vascular disease. Trends Cardiovasc Med 1994;4:165-169.

339. Tsang VL, Bhatia SN. Three-dimensional tissue fabrication. Adv Drug Deliv Rev 2004;56(11):1635-47.

340. Oakes BW, Batty AC, Handley CJ, Sandberg LB. The synthesis of elastin, collagen, and glycosaminoglycans by high density primary cultures of neonatal rat aortic smooth muscle. An ultrastructural and biochemical study. Eur J Cell Biol 1982;27(1):34-46.

341. Mengher LS, Pandher KS, Bron AJ, Davey CC. Effect of sodium hyaluronate (0.1%) on break-up time (NIBUT) in patients with dry eyes. Br J Ophthalmol 1986;70(6):442-7.

342. Vlodavsky I, Bar-Shavit R, Ishai-Michaeli R, Bashkin P, Fuks Z. Extracellular sequestration and release of fibroblast growth factor: a regulatory mechanism? Trends Biochem Sci 1991;16(7):268-71.

343. Bulpitt P, Aeschlimann D. New strategy for chemical modification of hyaluronic acid: preparation of functionalized derivatives and their use in the formation of novel biocompatible hydrogels. J Biomed Mater Res 1999;47(2):152-69.

344. Grigolo B, Roseti L, Fiorini M, Fini M, Giavaresi G, Aldini NN, Giardino R, Facchini A. Transplantation of chondrocytes seeded on a hyaluronan derivative (hyaff-11) into cartilage defects in rabbits. Biomaterials 2001;22(17):2417-24.

345. Radice M, Brun P, Cortivo R, Scapinelli R, Battaliard C, Abatangelo G. Hyaluronan-based biopolymers as delivery vehicles for bone-marrow-derived mesenchymal progenitors. J Biomed Mater Res 2000;50(2):101-9.

346. Anseth K, Burdick J. New directions in photopolymerizable biomaterials. Mat Rec Soc Bull 2002;27:130-136.

347. Pathak C, Sawhney A, Hubbell J. Rapid photopolymerization of immunoprotective gels in contact with cells and tissue. J Am Chem Soc 1992;114:8311-8312.

348. Li Q, Wang D, Elisseeff J. Heterogeneous-phase reaction of glycidyl methacrylate and chondroitin sulfate: mechanism of ring-opening-transesterification competition. Macromolecules 2003;36:2556-2562.

349. Burdick JA, Chung C, Jia X, Randolph MA, Langer R. Controlled degradation and mechanical behavior of photopolymerized hyaluronic acid networks. Biomacromolecules 2005;6(1):386-91.

350. Goodison S, Urquidi V, Tarin D. CD44 cell adhesion molecules. Mol Pathol 1999;52(4):189-96.

351. Turley EA, Noble PW, Bourguignon LY. Signaling properties of hyaluronan receptors. J Biol Chem 2002;277(7):4589-92.

352. Merrilees MJ, Lemire JM, Fischer JW, Kinsella MG, Braun KR, Clowes AW, Wight TN. Retrovirally mediated overexpression of versican v3 by arterial smooth muscle cells induces tropoelastin synthesis and elastic fiber formation in vitro and in neointima after vascular injury. Circ Res 2002;90(4):481-7.

353. Baccarani-Contri M, Vincenzi D, Cicchetti F, Mori G, Pasquali-Ronchetti I. Immunocytochemical localization of proteoglycans within normal elastin fibers. Eur J Cell Biol 1990;53(2):305-12.

354. Fornieri C, Baccarani-Contri M, Quaglino D, Jr., Pasquali-Ronchetti I. Lysyl oxidase activity and elastin/glycosaminoglycan interactions in growing chick and rat aortas. J Cell Biol 1987;105(3):1463-9.